IN-03
46769

NASA Contractor Report 4398
DOT/FAA/RD-91/14

P.200

Synthetic Aperture Radar Imagery of Airports and Surrounding Areas

Study of Clutter at Grazing Angles and Their Polarimetric Properties

Robert G. Onstott, Denise J. Gineris, and James T. Clinthorne

CONTRACT NAS1-18465
OCTOBER 1991

NASA

NASA Contractor Report 4398
DOT/FAA/RD-91/14

Synthetic Aperture Radar Imagery of Airports and Surrounding Areas

Study of Clutter at Grazing Angles and Their Polarimetric Properties

Robert G. Onstott, Denise J. Gineris,
and James T. Clinthorne
Environmental Research Institute of Michigan
Ann Arbor, Michigan

Prepared for
Langley Research Center
under Contract NAS1-18465

NASA

National Aeronautics and
Space Administration
Office of Management
Scientific and Technical
Information Program
1991

FOREWORD

This is the final report of the Phase III Extension for Contract NAS1-18465 (Processed Synthetic Aperture Radar (SAR) Data), sponsored by National Aeronautics and Space Administration (NASA) Langley Research Center (LaRC). This report is the last in a four report series. The thrust of the overall effort is the statistical description of ground clutter at airports and in the surrounding areas. In Phase I of this activity, SAR data of airports which existed in the Environmental Research Institute of Michigan (ERIM) SAR data archive were examined for utility to this program. Eight calibrated digital images at high resolution and coarse resolution were created. The coarse resolution images were provided to NASA LaRC for use in their Microburst/Clutter/Radar Simulation programs whereas the high resolution images underwent a statistical clutter analysis at ERIM. In Phase II of this program, SAR data were collected on an opportunity basis at the Philadelphia Airport using a set of radar parameters which more closely matched those which are anticipated to be encountered by an aircraft on its approach to an airport. One calibrated digital image each at high resolution and coarse resolution was generated. During Phase III, a dedicated SAR mission was flown over the Denver Stapleton International Airport and surrounding area. A wide variety of geometries and scene contents were acquired and these data and study results were presented. An extension to Phase III was made for additional processing and analysis of SAR data to address collections with small grazing angles, collections which included mountains in the far range to document sources of possible range ambiguity, and the polarimetric properties of ground clutter with emphasis on determining what is the ground backscatter response for polarizations which enhance microburst features.

The work reported here was performed by members of the Center for Earth Sciences, Advanced Concepts Division, Environmental Research Institute, under the direction of Dr. S.R. Robinson. The principal investigator for this project was Dr. R.G. Onstott. The contract was

monitored by E.M. Bracalente, NASA Langley Research Center, Hampton, Virginia.

The authors gratefully acknowledge the support of the Center for Earth Science Staff during the project. In particular, Ms. Janice Anquetil, Ms. Marsha Allen, and Mr. Patrick Hayes.

TABLE OF CONTENTS

LIST OF TABLES

LIST OF FIGURES

LIST OF FIGURES (CONT.)

LIST OF FIGURES (cont.)

I. INTRODUCTION

Low altitude microburst windshear represents a significant hazard to aircraft, particularly during take-off and landing. The intense down drafts and the resultant divergent outflow can have a significant effect on the lift characteristics of the endangered aircraft. When encountered at low altitude, the pilot has little time to react correctly to maintain safe flight. The Federal Aviation Administration (FAA), jointly with the National Aeronautics and Space Administration (NASA), has sponsored an investigation into the development of airborne sensors to detect microburst windshear. One sensor of interest is a microwave Doppler radar operating at X-band or higher frequencies. Critical to the analysis of the capability of such a sensor to perform this detection is the microwave backscatter description of both the microburst event and the clutter background, especially during the approach and departure from an airport.

NASA Langley Research Center (LaRC) has developed a Microburst/Clutter/Radar simulation program to assess the performance of Doppler radar as it views a low-level microburst along an approach to an airport. Inputs to this simulator include the airport ground clutter database, a simulated microburst database, the operating parameters of the proposed weather radar, and candidate signal processing software for use in detection. In the operation of the simulation program the received signal amplitude level for each range bin is calculated. Each range bin may include contributions from both the microburst and the ground clutter.

To date the Environmental Research Institute of Michigan has provided NASA LaRC with seventeen synthetic aperture radar (SAR) images of selected airport scenes for use in their Microburst/Clutter/Radar Simulator and for the characterization of the ground clutter surrounding airports. Eight of the images were archival data, one was of a target-of-opportunity airport, and eight were taken from a dedicated collection over the Denver Stapleton International Airport on 16 November 1988. In addition, statistical analyses of these airport environments have been performed by ERIM to describe the range of scattering conditions encountered. Clutter types, mean backscatter intensities, probability distributions, and areal extent of the clutter types in the image were determined.

The Denver Stapleton International Airport was chosen by NASA LaRC as the focus of the dedicated data collection for a number of reasons. This airport has had a history of windshear events, many of which have been documented by the National Oceanographic and Atmospheric Administration. Additionally, it is located near the center of Denver, a large metropolitan area, and experiences heavy air traffic. As a clutter scene it is therefore representative of other airports which serve large urban areas. Finally, the airport is located near the Rocky Mountains, which allows the examination of the ambiguity effects of mountain clutter which have the potential to mask microburst targets. This report presents the results of additional processing and analysis performed on the SAR data obtained of the Denver Stapleton International Airport during Phase III of the contract work. This additional work encompassed three analyses: 1) the analysis of an image of the front range of the Rocky Mountains to obtain data on mountain clutter, 2) the analysis of airport clutter collected at small grazing angles, and 3) an examination of the polarization properties of airport clutter and heavy rain.

II. DATA COLLECTION

The NASA Denver collection consisted of one mission flown on 16 November 1988. Twenty-seven data passes were made with the purpose of collecting SAR data which would represent the radar clutter field which an aircraft would experience when landing at this airport. In simulating this flight geometry, a series of low altitude passes were utilized to image the ground scene at very large incidence angles. This configuration is illustrated in Figures 1a through 1d.

The location of the flight lines and pass identification of the images used in this analysis are provided in Table 1. A flight (Pass 14) was made parallel to the front range of the Rocky Mountains with an altitude of 5500 feet above ground level (AGL). The resultant image was named the Rocky Mountain X-HH image. The low-altitude X-HH and X-VV pair of images was taken from Pass 43, a north heading and west-looking flight track with an altitude of 2900 feet AGL. The polarimetric set of data came from Pass 37, an east heading and north-looking flight track with an altitude of 5600 feet AGL.

The radar used during this collection was the NADC/ERIM P-3 SAR . This radar operated at a frequency of 9.375 GHz (X-band) and at VV, HH, VH and HV polarizations. For the low altitude and Rocky Mountain passes VV and HH polarizations were used in a double swath mode. For the polarimetric images VV, HH, VH, and HV polarizations were collected in single swath mode. Low resolution, with an azimuth resolution of 2.8 m and a slant range resolution of 3.0 m, was used in order to maximize the coverage of the images. Operation in this mode was recommended since the final images would be digitally processed to a coarser resolution of 20 m.

III. CLUTTER FROM MOUNTAIN TERRAIN

The clutter scene used in this analysis is a west looking image of the front range of the Rocky Mountains. Ground area coverage is illustrated in Figure 2 and the image is provided in Figure 3. The image subtends incidence angles from 0° to 85°. The ground range coverage is 19.6 km and extends from Harriman Lake on the east to Evergreen, Colorado in the west. The image covers an area in azimuth of approximately 10.1 km, which extends from just south of Hine Lake to the south side of Green Mountain. Approximately 65% of the image is occupied by the front range of the Rocky Mountains. The most prominent feature of the range is the Hogback, an uplift thrust feature which juts up at a steep angle. Behind the Hogback is the north end of the Rampart Range. The other 35% of the image contains an assortment of standard clutter features. The area has several lakes, reservoirs, and scattered residential suburbs, but the primary clutter type is grassland. Just south of Green Mountain is the city of Lakewood, Colorado.

The clutter content of the Rocky Mountains image is presented in Table 2. Easily three-fourths of the image is occupied by either the hogback thrust feature or the foothills of the Rockies. Of the remaining area of the image approximately one-third is residential, one twenty-fifth is water, and the rest is grassland. Table 3, Figure 4, and Appendix A present the statistics of the clutter sub-regions which were used in this analysis. A map of the selected clutter regions is presented in Figure A-1 for reference.

The results of a threshold analysis of the image are presented in Figures 5 and 6. The image in Figure 5 presents a comparison of radar scattering coefficient images thresholded at -30 dB, -20 dB, -10 dB, 0 dB, and 10 dB. The most prominent feature in the series of images is the lack of returns at far range. Only the hogback feature at the front of the range stands out significantly. A few returns from the Rocky mountains can be seen in the -30 dB threshold, but only from the front of the range. Some grassy areas and all water areas have backscattering coefficients of less than -30 dB, but most returns in the near range of the image are brighter than -30 dB. At the -20 dB threshold the Rocky

Mountains are not visible and the hogback returns have also been diminished, although they still represent the dominant geological feature of the scene. Other prominent returns in this backscattering coefficient bin are residential areas, the south end of Green Mountain, and specular returns coming from the extreme near range of the image. At the -10 dB threshold, the dominating features are the nearest section of the hogback and specular returns. Only a fraction of the image has radar scattering coefficients (or scattering cross sections) above 0 dB and these returns are mainly specular. Figure 6 presents a distribution of the thresholded returns. Almost 73 percent of the image has returns of -30 dB or less; these values are essentially in the noise. Approximately 25 percent of the returns have values of -30 dB to -10 dB; these values represent those returns from natural targets and residential areas. The remaining 2 percent of the data, which have backscattering coefficient values of -10 dB and higher, represent mostly specular returns and a few returns from the closest areas of the hogback.

The Rocky Mountains image is somewhat different than the other Denver images in that it has comparatively few clutter groups. The image content consists mainly of grassland and geological features, with a few residential, reservoir and lake areas scattered throughout. The incidence angle dependency plots for the clutter subregions in the image and the histograms of the clutter are presented in Figures 7 through 12. The grass clutter, Figure 7c and Figure 8, shows a decrease in the mean scattering coefficient value with increasing incidence angle. This is consistent with theory and previous experimentation. In the incidence angle range of 60° to 64° however, the data appears to cluster around two different scattering coefficient values, one at about -30 dB and one at about -25 dB. The bimodal nature of the data in this angle range can also be seen in the histogram in Figure 8b. This may represent a variation in surface type. In general, the histograms for the grass sub-regions are fairly symmetric and narrow, with means varying from approximately -22 dB at small incidence angles (around 45°) to -30 dB for larger incidence angles (around 79°) and with an average coefficient of variation of 1.35. These histogram shapes, means and coefficients of variation are almost identical to that of the other Denver images and are indicative of the uniformity of the grassland areas.

The residential clutter, Figure 7b and Figure 9, also displays a decrease in the radar scattering coefficient with increasing incidence angle, but the data is less clustered than that of the grass sub-regions. This is due to aspect angle diversity in the residential data caused by variations in street orientation in the residential areas. The histograms for the residential clutter sub-regions are much broader than those of the grassland areas, with means from -5 dB at 40° incidence angle to -19 dB at 74° incidence angle and an average coefficient of variation of 6.62. For all residential clutter histograms, the leading tail is larger than the trailing tail, indicating a skew in the data towards larger radar scattering coefficients. This broad shape and comparatively large rightward skew in the histograms have also appeared in the histograms of other man-made targets in the Denver and Philadelphia areas and appear to be characteristic of man-made targets. The means and coefficient of variations for the residential clutter in the Rocky Mountain image are also on the order of that of residential clutter in other Denver images.

Both the thrust (hogback) feature and the mountains behind them display a decrease in radar scattering coefficient value as the incidence angle is increased. If the data from the two incidence angle plots in Figure 7 is overlain, both sets of data have the same decreasing trends. The mean normalized radar scattering coefficient has values which vary from about -17 dB at 65° incidence angle to -25 dB at 79°. The thrust feature has, for the most part, higher means than the mountains, with -11 dB at 65° and -22 dB at 79°, but has a slightly lower (by 2 dB) mean in the 70° to 74° range. This may be due to the change in aspect angle of the hogback that occurs in the 70° to 74° range of the image. The two clutter groups have similar coefficients of variation, with 1.2 for the mountain data and 1.1 for the thrust feature. The histograms of the clutter data, Figure 10 and Figure 11, for all data subsets except mountain data at 75° to 79°, are symmetric and narrow, much like those of the grass sub-regions. This similarity is to be expected. Both the hogback and the front range of the Rockies are highly eroded and weathered surfaces. The same type of scrub grass which grows on the plains in front of these features grows on the features themselves. In addition, the erosional debris from the mountains has been washed down onto the plains, causing more similarity between the two. The surface of the hogback and the front range behind it are essentially the same surface as the plains before them. Differences in the means between the two are caused by differences in imaging geometry since both the hogback and the front range have a significant slope. The local incidence angle to the hogback varies from 42° to 59°, and that of the front range is significantly smaller than this. The returns from the water areas are presented in Figure 12. They are almost completely in the noise.

Although the mountainous terrain in this image would not be expected to produce severe range ambiguity effects due to moderate backscatter levels, this data may be used to examine the limitations of a radar system when imaging near such geological features. Mountainous terrain in the immediate vicinity of an airport has the potential to be a source of strong returns. If the backscattering cross sections of mountain and airport clutter is known, it is possible, using the ratio of the slant ranges to the clutter areas, to approximate the image slant range at which mountain clutter would significantly interfere with the airport returns. Mathematically, this can be calculated using the following equation:

$$\frac{\sigma^\circ_m}{R^4_m} \geq \frac{\sigma^\circ_a}{R^4_a} \qquad \text{(Eq. 1)}$$

or

$$\frac{\sigma^\circ_m}{\sigma^\circ_a} \quad \frac{R^4_a}{R^4_m} \geq 1 \qquad \text{(Eq. 2)}$$

where σ°_m and σ°_a are the backscattering cross sections of the mountain and airport clutter respectively, and R_m and R_a are the ranges to these features. In calculating a test case the maximum mountain return and minimum airport return will be used to form a worst case scenario. The maximum return from the Rocky Mountain clutter was 1.57 dB at a range of 4779 m. The minimum backscattering cross section of an airport terminal was -9.6 dB. Given these values, the airport must be located at a slant range of 2382 m to make the product of the ratios of the backscattering cross sections and the slant ranges equal to one. As long as the airport is at a distance of at least 2400 m from the mountains, mountain clutter does not provide an additional enhancement.

The distribution of returns for the entire image is presented in Figure 13. The mean of the image is -18.97 dB, which is lower than the image distributions calculated for the other Denver images and is indicative of the less culturally developed nature of the image. On average, returns of -30 dB or less make up approximately 20 percent more of this image than of the other Denver images. The distribution plot of this image is also shaped differently from those of the other Denver images. The Rocky Mountains image displays much less of a skew to the right than the other Denver data analyzed. From past analyses, the rightward skew is indicative of the existence of man-made clutter returns, so the lack of this skew would point to a smaller contribution of man-made returns to the total image distribution.

IV. GROUND CLUTTER AT SMALL GRAZING ANGLES

The clutter scenes used in this analysis are a pair of X-HH and X-VV west looking images of the Denver Stapleton International Airport. The images are illustrated in Figures 14 and 15. The ground area coverage of these images is illustrated in Figure 16. The image subtends incidence angles from 0° to 87.5°. The ground range coverage is 19.6 km and extends from Peoria Street on the east to Sheridan Boulevard in the west. The image covers an area in azimuth of approximately 13.2 km and extends from 80th Avenue in the north to 1st Avenue in the south. In the near range of the image just northeast of the airport is Ladora Lake on the Rocky Mountain Arsenal. The arsenal also extends north of the airport. Directly east of the airport is an area of warehouses and airport storage facilities. Running east and west, and just south of the airport, is Colfax Avenue. Along Colfax, strip malls and other commercial buildings produce bright returns. Off of Colfax to the north and south are urban residential areas. South of Colfax Avenue in the near range is Lowry Air Force Base. Many buildings on the base can be identified. Just northwest of the airport is the Commerce City area. Just off Interstate 85 is the Mile High Kennel Club. It is characterized by a small area of low returns with a bright center. South of this feature are Interstates 270 and 70. Following a track south of Interstate 70 along Colorado Boulevard is the Park Hill Golf Course and the City Park. These rectangular shaped areas produce weak backscatter. Directly west of City Park is an area of bright returns originating from the high rise buildings of the downtown Denver area. North of downtown Denver is a mixed commercial and residential area. In the far range of the two images are some strong returns associated with the cities of Lakewood, Edgewater, Wheatridge, and Arvada.

Table 4 presents the results of the composition analysis of the low altitude images. The majority of the image, about 84 percent, contains clutter of a metropolitan nature in the form of urban, city, residential, or industrial areas. The airport and air force base take up about 10 percent of the images, and rural areas about six percent. Approximately half of the images consists of unclassifiable clutter which is known from ground truth to consist of the metropolitan area of Denver.

The results of the threshold analysis of the data are presented in Figures 17 through 20. Figures 17 and 18 represent the distribution and thresholded images for the X-HH low altitude image and Figures 19 and 20 represent the same for the X-VV image. The threshold distributions indicate that 74 percent of the X-HH image and 62 percent of the X-VV image have scattering coefficient values of -40 db or less. The thresholded images show that areas of weakest backscattering cross sections are primarily located in the far range of the images. The runways at the airport and some of the grassy areas also appear to have values of -40 db or below. In this particular threshold bin the golf course is especially distinguishable in both polarizations and the Denver City Park can be discerned in the VV image. A bright return which stands out in the City Park area may be the Denver Museum of Natural History. Returns from the near range are dominant. Approximately 9.5 percent of the X-VV image and 5.5 percent of the X-HH image have returns between -30 db and -40 db. Areas with normalized scattering coefficients of this value are primarily located in the near range of the images and are represented mostly by the grassy areas at Lowry Air Force Base and the airport, as well as by water and runway returns. Near range returns still dominate the image. Fifteen percent of the VV image and 13 percent of the HH image have returns between -20 dB and -30 dB. Natural clutter areas appear to have the majority of their backscatter values within this range. Returns which are greater than -20 dB appear to arise almost exclusively from hard-target clutter. Neither the remaining returns in the near or far range of the image appear to dominate the scene. For like polarization, returns with values above -20 dB appear to be evenly distributed throughout the scene. Eight percent of the X-VV image and 5 percent of the X-HH image have returns between -10 dB and -20 dB. Sources are located primarily in the near range half of the image and are located in the urban and residential areas with some from the city area of Denver proper. Returns with values greater than -10 dB appear to be strictly associated with buildings in the city of Denver and the occasional strong return at very near range. Three and a half percent of the X-VV image and 1.5 percent of the X-HH image have returns in the -10 dB to 0 db range. These returns are attributed to hard targets and are seen in the mid range of the image. There are approximately 2.2 percent of the X-VV image and 1.1 percent of the X-HH image pixels which have scattering coefficients greater than 0 dB. All are attributed to hard targets and all are located in the mid-to-far range of the image at incidence angles of 80° or greater.

General summaries of the statistical analysis that was performed on the low altitude image set are presented in Tables 5 and 6 and in Figures 21 and 22. Maps of the clutter areas used are presented in Figures A-2 and A-3. Results of the statistical analysis are presented in Tables A-2 and A-3. The results produced at the two like polarization (VV and HH) are very similar. Grass, water, and runway clutter produce the smallest scattering coefficients of all the different clutter types. Mean values of these clutter types were consistent with those of the previously analyzed Denver data and new values for small grazing angles were added. Scattering coefficients of residential and urban areas are consistently larger than those of natural targets, but do not display the amount of separation seen previously. They are, however, within a standard deviation of the residential and urban clutter of the previously analyzed image sets. Returns from hard target clutter areas, such as the city and industrial parks, are consistent with previous data as are the returns from single hard targets, such as terminals, warehouses, and parking lots.

Plots of scattering coefficients versus incidence angle for the image pair are presented in Figures 23 and 24. The most unique feature in this series of plots is the large increase in scattering coefficient values for incidence angles greater than 78° for building clutter at both VV and HH polarizations, Figures 23a and 24a. Backscatter values are constant at about -18 dB for angles up to 78°. Clutter returns rise to a maximum, about 30 dB higher than the baseline values at angles of about 85° to 86°. This sudden increase is attributed to specular scatter from the sides of buildings.

The grass clutter results are presented in Figures 23b and 24b. These plots display the characteristic behavior of terrain clutter; cross sections decrease slowly through incidence angles up to 68°, after which they decrease rapidly. The middle angle portion of the HH and VV responses have mean values of about -25 dB to -26 dB. The values of the grass returns measured for these images are identical to those analyzed in previous analysis, and are also similar to those obtained using scatterometers.

The angular response of urban clutter is presented in Figures 23d and 24d. Both the HH and VV data display trends which have an almost constant value of about -17 dB until 80° after which the range of values increases about 10 dB. This behavior is also representative of the urban clutter data from other areas. The HH and VV backscatter levels are most similar in value to those obtained from the second and third 'step west' images. Data at VV polarization shows a larger spread of values than HH data, an indication of polarization dependent scattering mechanisms.

Residential clutter, presented in Figures 23c and 24c, is also consistent with past analysis results. Both the HH and VV data sets have the same mean value of about -19 dB until about 78°, at which point the VV data remains constant, and the HH data decay with increasing angle. The VV data also shows a greater spread in values than for the HH data, a trend also apparent with urban clutter. The behavior of the residential clutter is most similar to that of the second and third 'step west' images, and about 2 dB lower than the values of the first 'step west' image. In addition, mean VV values are similar to those obtained at VV polarization from the polarimetric image set.

There is only a small range of incidence angle data available for city clutter and is shown in Figures 23f and 24f. The VV data show a mean scattering coefficient of -10 dB, while the HH data has a mean of -13 dB. The HH data is most similar in value to the first and third 'step west' images, but the VV mean values are about 4 dB lower than those obtained in the polarimetric image set. The cluster of city backscatter cross sections for both HH and VV polarizations lie within the clusters for building clutter.

The industrial clutter angular response data, presented in Figures 23e and 24e, also lacks a dense coverage at various incidence angles, but does extend over a wide range of angles. The mean cross section at HH is about -14 dB and at VV about -12 dB. These values are within the range of values obtained from the 'step west' images. As seen for the other hard target categories, cross section enhancements were seen at the small grazing angles as compared to those at the middle angles.

Finally, runway clutter is presented in Figures 23g and 24g, and show the behavior for smooth surfaces. The backscatter at VV and HH decrease with incidence angle, but their fall-off rates differ. The VV data starts out with a higher mean, (about -35 dB) at 70° and then decreases quickly. The HH data has a mean of about -40 dB at this angle and then cluster at a value of -46 dB. These trends are similar to those obtained through scatterometer measurements at VV polarization. Scatterometer data for smooth asphalt shows a higher mean value at VV polarization, by about 6 dB, for angles in the 65° to 75° range, and a slightly quicker fall-off rate.

In Figures 25 through 41 histograms of scattering coefficients for the various clutter types are presented. The incidence angle plots provide the most in depth presentation of the changes in mean value of the scattering coefficient with angle, this analysis will concentrate primarily on differences in the shape of the distributions for different clutter types and on differences in shape within a clutter type due to differences in incidence angle. Distributions for grass clutter are presented in Figures 25 and 26. Distributions are narrow and symmetric, with peak percentage of occurrences decreasing from about 10.5 percent as the incidence angle increases. Returns from grass are very weak at higher angles, where the grass return is at or below the radar system noise floor.

Residential clutter distributions are presented in Figures 27 and 28. These distributions are symmetric and are slightly wider than those of the grass clutter. Some distributions exhibit a slight leading tail (i.e., predominate distribution toward larger σ° to the right of the plot). These distributions are similar to those of the second and third 'step west' images and to those of the polarimetric image set. The returns for the 80° to 84° and VV and HH polarizations show a large spread of values and distribution shapes which are unique and dissimilar to those obtained at the middle angles.

Urban clutter distributions are presented in Figures 29 and 30. These distributions are similar in shape to those of the residential areas but display a prominent leading tail, an indication of strong dominant scattering sources. At angles greater than 65°, a population of the distributions at HH polarization broaden while the distributions at VV polarization maintain similar shapes until about 80°. This difference may imply that more returns, though not necessarily greater returns, could be expected with VV polarization than with HH polarization.

The distributions with the highest content of man-made clutter are presented in Figures 31 through 39. In the distributions for the city clutter, Figure 31, a prominent leading tail is seen in both the HH and VV data. The VV data has a mean which is 5 dB higher than that of the HH data. These distributions are similar in both shape and size to those of the city obtained from the second, third, and fourth 'step west' images. Industrial distributions are presented in Figures 32 and 33. The most prominent feature of the distributions is the large leading tails, which are present whether the distributions are broad or narrow. These distributions have the largest leading tail of all the man-made clutter, and are most similar to the industrial distributions of the third and fourth 'step west' images. Not surprisingly, the distributions for building clutter, Figures 34 and 35, are most similar in shape to those of the industrial clutter. Single buildings are probably most like an industrial area in that the only features present in the clutter area would be many man-made targets and very little of anything else.

Distributions were also created for hard target clutter areas. The parking lot distributions, Figure 36, are generally very broad. A leading tail is present but not prominent; the distributions are reasonably symmetric. The shapes of these distributions are similar to those of the polarimetric image set, and the second and third 'step west' images. Distributions for two terminals, one oriented parallel to the line of flight of the radar (H5) and one oriented perpendicular to the line of flight (H6), are presented in Figure 37. All distributions exhibit a rightward skew, but the mean of the distributions varies. For the X-VV image, orientation appears to make no difference in the mean value. For the HH image, returns from terminal H5 are lower than those from H6 by 10 dB. Figures 38 and 39 present the distributions for some smaller man-made targets in the vicinity of the airport. Both X-VV and X-HH data displays a wide distribution with a strong rightward skew in the distributions for a airplane at the airport. This distribution is similar in shape to that of the airplane distribution in the third 'step west' image as well as similar in mean value. The VV distribution has a secondary peak at higher values. The distributions for a truck and airplane are similar in that the truck distributions also show a secondary peak, but unlike the airplane distributions, the truck distributions are much narrower. The warehouse distributions, Figure 39, are broad and similar to the distributions for building obtained in the 'step west' images but are broader than the building distributions just examined. The VV distribution has a prominent leading tail, whereas the HH distribution is reasonably symmetric.

In summary, the distributions change from being symmetric and narrow to broad and having prominent leading tail as the clutter areas change in content from entirely natural targets to entirely man-made targets. The distributions from the selected man-made features also follow this trend. Additionally, the distributions for the individual hard targets appear to differ depending upon whether the hard target is a building or vehicle.

Whole image clutter distributions are presented in Figures 40 and 41. The general shapes of the clutter distributions at VV and HH polarizations are most similar to those of the 'step west' set of Denver Images. In particular, they are almost identical to the distributions for the second and third 'step west' images. This should be the case in that the low altitude image set cover basically the same ground area as these 'step west' images. The small size of the distributions implies that much of the image content lies at the noise floor or below; most of the pixel values in the images are at the noise threshold level. The mean scattering coefficients of the images are -12.21 dB for X-VV and -9.25 for X-HH and are lower than those obtained from the other metropolitan areas analyzed. The clutter distribution for the VV low altitude image is broader than that of the HH image, implying that the VV image has more non-threshold values than the HH image. This is also noticeable upon visual inspection of the image.

Tables 7 and 8 present the backscattering cross sections for some of the hard targets in the low altitude images. Table 9 presents a comparison of the backscattering cross section values from hard targets in previously analyzed Denver images to those obtained from the low altitude image set. The hard target values in the low altitude images correlate well with similar targets of approximately the same effective areas and located at similar incidence angles.

Figures 42 through 47 display individual targets from the series of Denver images as the targets were imaged at incidence angles from 60° to 84°. Table 10 lists the sources of these sub-images. These figures provide a visual illustration of how the returns change with increasing incidence angle. Natural terrain cross sections decrease quickly as expected. The grass clutter drops into the noise at around 80° and the returns from trees drop off at about 82°. Most hard targets are visible at all incidence angles but the dominant scatterers appear to scintillate and change position. At the middle incidence angles, many returns originate from the roofs of buildings. With increasing angle, fewer returns come from roof tops and the primary reflectors are associated with the fronts of the buildings which face the radar. This is evident in the images of the airport terminal area in Figure 42. In the scene at 68.9° returns arise from almost all locations within the image. Some radar shadowing of the buildings just below the airport is also visible. In the 78.6° and 78.9° images, returns from all areas are still apparent, but returns from the faces of structures which mainly face the radar are enhanced. Returns at 82.8° are limited to the structures which are oriented perpendicular to the radar, although areas of the terminal and of the fence surrounding the terminal which do not face the radar also produced strong backscatterer. Some returns also may originate from the roofline of the back sides of the buildings as evidenced by the warehouse area in Figure 43. It is interesting to note that the returns from the parking lots at the airport, which appear to be quite strong at the incidence angles from 68° to 79°, completely disappear by 82.8°. At even higher incidence angles the urban clutter and city clutter become easily delineated. This is evident in Figure 45 of the Park Hill Golf Course. In the 68.3° image, the city area above and below the golf course visually has a mean similar to the urban area to the right of it. The images observed at 82.2° and 83° are dramatically different, and the city areas are much brighter than the urban areas.

V. POLARIZATION PROPERTIES OF MICROBURST AND GROUND CLUTTER

In this study, circular and elliptical polarized imagery were synthesized from the Pass 37 SAR image. Statistical analysis similar to that conducted on previously analyzed images, including the analysis of returns from various ground targets, were conducted and compared to the results obtained from the horizontal and vertical polarized images previously processed. An examination was made of the polarization properties of rain for conditions which may be encountered during microbursts. SAR data were then synthesized at these polarizations and statistics examined. The goal was to determine what polarizations may maximize the microburst return and minimize the ground clutter returns (i.e. to optimize the microburst-to-clutter ratio).

Methods to enhance the backscatter associated with microbursts for radars operating in the microwave region emphasizes the need to exploit the backscatter characteristics of hydrospheres or rain. Under some conditions, raindrops are spherical in shape. The backscatter cross section for a sphere in the Rayleigh region (drop size is much less than the radar wavelength) varies as the fourth power of the frequency. Hence, higher frequencies may be selected for microburst feature enhancement. A second opportunity also exist. That is to exploit the polarization properties of both the hydrospheres and the ground clutter.

Polarimetric Properties and Radar

The transmitted electromagnetic (EM) wave vector polarization is determined by the antenna structure. The incident EM wave excites currents on the illuminated target and the induced currents re-radiate EM energy, i.e. produce the scattered field. The radar antenna receives only the component of the scattered field that is co-linear to the transmitted wave. Since the direction of the scattered vector EM field is unknown, two antennas are required for completed reception. This is illustrated in Figure 48. The transmitted and received field vectors or incident and scattered fields are uniquely related to the target through a scattering matrix. This is illustrated in Figure 49. A polarimetric radar provides a measure of the scattering matrix of a target. Note that the elements of the scattering matrix are complex. The notation used here is written where the first letter indicates the transmitted polarization and the second letter the received polarization. If the incident field vector is denoted as $\underline{E}^i$ and the scattered field vector by $\underline{E}^s$, then the scattered field is related to the incident field and scattering matrix [S] by

$$\underline{E}^s = e^{jkr} r^{-1} [S] \underline{E}^i \qquad \text{(Eq. 3)}$$

where k is the wave number and r is range. The scattering matrix which includes all transmit-receive combinations is given by

$$[S] = \begin{bmatrix} S_{HH} & S_{HV} \\ S_{VH} & S_{VV} \end{bmatrix} \quad \text{or} \qquad \text{(Eq. 4)}$$

$$[S] = \begin{bmatrix} |S_{HH}| e^{j\Theta HH} & |S_{HV}| e^{j\Theta HV} \\ |S_{VH}| e^{j\Theta VH} & |S_{VV}| e^{j\Theta VV} \end{bmatrix} \qquad \text{(Eq. 5)}$$

where S_{pq} is an element of the scattering matrix, p and q denote transmit-receive polarizations, $|S_{pq}|$ is the magnitude of the scattering matrix element, and $e^{j\Theta pq}$ is the element phase information. A scattering matrix may be normalized with respect to the phase of one of the elements so that relative phase differences are indicated. Therefore, the most often used form is

$$[S] = e^{j\Theta HH} \begin{bmatrix} |S_{HH}| & |S_{HV}|e^{j\Theta HV'} \\ |S_{VH}|e^{j\Theta VH'} & |S_{VV}|e^{j\Theta VV'} \end{bmatrix} \quad \text{(Eq. 6)}$$

The Θ_{VH}' indicates that the phase is measured with respect to the HH polarization.

There are five target types that are of interest in the microburst-clutter problem. These are the flat plate, trihedral, sphere, dihedral and complex target. The scattering matrices for both the linear and circular basis for the four simple target types are summarized in Table 11. The exact nature of these matrices will become important later in this discussion. The scattering matrices for complex man-made targets may take on many forms, oftentimes they are combinations of the simple targets described here. Many complex targets provide backscatter returns at all polarization combinations.

For the general case of elliptical polarization one may use the diagram shown in Figure 50. Here the electric vector traces out an ellipse moving either clockwise (left-hand) or counter clockwise (right-hand). The ellipticity diagram may be used to define the polarization of the wave. There are two angles, the tilt angle τ and ellipticity angle ϵ, in which the electric field may be expressed. The electric field is given by

$$\underline{E} = \sqrt{E_x^2 + E_y^2}\,(\cos\gamma^x + \sin\gamma e^{j\delta y}) \quad \text{(Eq. 7)}$$

where

$$\gamma = 0.5 \cos^{-1}(\cos 2\epsilon \cos 2\tau) \text{ and} \quad \text{(Eq. 8)}$$

$$\delta = \tan^{-1}(\tan 2\epsilon / \sin 2\tau). \quad \text{(Eq. 9)}$$

In the process of polarization synthesis process the orthogonal vectors Z must be defined,

$$Z = \tau \begin{vmatrix} a \\ be^{j\delta} \end{vmatrix} \quad \text{(Eq. 10)}$$

where $\delta = \Theta_V - \Theta_H$, $\tau = P_o^{.5}e^{j\Theta H}$, and $P_o = |Z_H|^2 + |Z_V|^2$.

In the linear basis, the orthogonal vectors are

$$Z_V = \begin{vmatrix} 0 \\ 1 \end{vmatrix} \quad Z_H = \begin{vmatrix} 0 \\ 1 \end{vmatrix} \qquad \text{(Eq. 11)}$$

where in the case of Z_V, a = 0, b = 1, and δ = 0 or π, and Z_H, a = 1, b = 0, and δ = 0 or π. For the circular basis,

$$Z_{LC} = 1/\sqrt{2} \begin{vmatrix} 1 \\ j \end{vmatrix} \quad Z_{RC} = 1/\sqrt{2} \begin{vmatrix} 1 \\ -j \end{vmatrix} \qquad \text{(Eq. 12)}$$

with a = b and $\delta = \pi/2$ for Z_{LC}, and a = b, and $\delta = 3\pi/2$ for Z_{RC}. Elliptical basis is the most general case and

$$Z_{LC} = \tau \begin{vmatrix} a \\ be^{j\delta} \end{vmatrix} \quad Z_{RC} = \tau \begin{vmatrix} a \\ be^{j\delta} \end{vmatrix} \qquad \text{(Eq. 13)}$$

with $a \neq 0$, $b \neq 0$, and $0 < \delta < \pi$ for Z_{LC}, and $a \neq 0$, $b \neq 0$, and $-\pi < \delta < 0$ for Z_{RC}.

Polarization Properties of Rain

For a wide range of meteorological conditions, raindrops are well described as spherical in shape. Backscatter properties of spheres are similar to those of flat plates and a trihedral corner reflectors. For a linearly polarized radar the scattered field orientation is identical to the incident field orientation, and an almost negligible amount of power is returned in the polarization orthogonal to the transmit polarization. This property is represented in the scattering matrix for a sphere in Table 11. For a circularly polarized wave incident on the sphere, a similar response occurs but the reflected wave encounters a change in polarization sense. In other words, the scattered field is reflected in the opposite field rotation direction. If right circular is transmitted then left circular is scattered and is required to receive.

The natural shape for a raindrop is spherical. Depending upon the speed at which it falls to the earth it may take on the shape of an oblate spheroid. Wind forcing may also cause a rotation of raindrop resulting in a canting of the drop about vertical. In Figure 51, three diagrams are provided to illustrate this. To fully characterize a raindrop requires its equivolume diameter, axial ratio, and tilt angle τ formed between the minor axis and the normal to the earth.

Spherical raindrops produce no return in the orthogonal channel if linear polarization is used, or in the same sense, if circular-polarization is used. Even with the influence of the propagating medium and most conditions, the combinations of VV, HH, RL, or LR will provide the greatest backscatter return. However, in very heavy rain and thunderstorms considerable energy has been observed in the orthogonal polarizations (VH, HV, RR, and LL) [1] with depolarization ratios as small as 5 dB possible.

In a case of heavy rain, it has been reported [2], that with the selection of the optimum elliptical polarization that cancellation (i.e. the reduction in depolarization) in some areas of heavy rain may be improved by 12 dB. Using this example and assuming a circular polarization case with a depolarization ratio of 10 dB, the magnitude of the elements of the scattering matrices for circular polarization and the optimum elliptical polarization would be

$$[|S|]_C = \begin{bmatrix} 0.316 & 1.0 \\ 1.0 & 0.316 \end{bmatrix} \quad \text{and} \qquad \text{(Eq. 14)}$$

$$[|S|]_E = \begin{bmatrix} 0.08 & 1.09 \\ 1.09 & 0.08 \end{bmatrix} \qquad \text{(Eq. 15)}$$

This illustration shows that by utilizing the optimum polarization, in this case elliptical polarization, the cross-polarized channels have been enhanced by 0.75 dB.

Polarization Properties for a Canted Oblate Spheroid

As a first case, the polarization properties of a canted oblate spheroid are examined, since the resulting properties are easily understood. The raindrop has unequal major and minor axes and a major axis which is rotated about vertical. Starting with an uncanted spheroid, horizontal polarization aligns with the major axis and vertical polarization aligns with the minor axis. The result is an enhanced horizontal backscatter whose magnitude is dependent on the axial ratio. A polarimetric radar has the important attribute of being orientation insensitive. If the raindrops are canted, the radar may maintain the same backscatter response as in the uncanted case by realigning its transmit-receive field vectors with the major and minor axes of the canted raindrop. In doing so, an elliptical basis results.

Examination of the literature provides a wide array of observations with somewhat variable results. The case of heavy rainfall with rainfall rates were greater than 20 mm/hr and wind speeds greater than 20 m/s were characterized by raindrops with mean diameters of about 2 mm. Drops of this size have been reported to have axial ratios of about 0.95. For this wind speed a tilt angle of about 10° has been observed [3].

For the conditions chosen (axial ratio = 0.95, tilt angle = 10°), the ellipticity angle may be determined from

$$\epsilon = \tan^{-1}(1/\text{axial ratio}). \qquad \text{(Eq. 16)}$$

For right hand circular $\epsilon = -46.5°$ and $\tau = 10°$ resulting in $\gamma = 46.4°$ and $\delta = 88.97°$. For left hand circular $\epsilon = 46.5°$ and $\tau = 10°$ and results in $\gamma = 46.4°$ and $\delta = -88.97°$. A δ of -89° corresponds to a phase shift of 1° and is directly attributable to an axial ratio less than 1. The resulting elliptical basis vectors are

$$Z_{LC} = \begin{vmatrix} 0.6896 \\ 0.7242e^{-j88.97°} \end{vmatrix} \quad Z_{RC} = \begin{vmatrix} 0.6896 \\ 0.7242e^{j88.97°} \end{vmatrix} . \quad \text{(Eq. 17)}$$

SAR clutter scenes were synthesized for this elliptical polarization case.

Propagation Through a Rain Filled Medium

Microbursts can originate from many convective systems. Typical thunderstorms which produce microbursts may be no more than 5 km in diameter at the base [4]. The core of the strong vertical and horizontal wind shear in the thunderstorm, referred to as a microburst, generally extends it influence to less than 4 km [5]. If the core is greater than 4 km, the phenomena is then referred to as a microburst. Heavy rainfall is often present during microburst activity. For a severe thunderstorm rainfall may be as high as 150 mm/hr. During heavy rain, raindrops will distort becoming oblate spheroids. A rain filled medium with these drop shapes may no longer have isotropic propagation properties. As an example, a differential phase shift between horizontal and vertical polarized waves may result [3]. In the case of a rain cell with a rain rate of 76 mm/hr a one-way differential phase shift of 7°/km may be induced.

Average rain rates during a microburst episodes have been estimated at 76.2 mm/hr with maximum rain rates of 165 mm/hr [6]. Observations suggest that most microburst occur in association with narrow precipitation shafts. Intense thunderstorm cells are generally only 3 km to 5 km wide at the base, so the area covered by heavy rain would be less than or equal to the width at the base. For a 3 km cell, a 6 km round-trip path through the cell would result in imaging the rain with a radar, with a 3 km path to the center of the microburst [6]. Under these circumstances a total two-way phase shift of 20° may be expected. Raindrops tend to have an orientation such that their major axis lies along the horizontal plane. Hence, horizontal-polarized returns are often larger than vertically-polarized returns [7,8]. In Figure 52, the ratio between HH and VV returns (ZDR) is shown versus the median drop diameter. This results shows that the difference between VV and HH returns increases, almost linearly, with increasing drop size. The ratio between like and cross-polarized returns (LDR) is also shown. Depolarization increases rapidly from 0 to 1 mm diameters, but for diameters smaller than about 1 mm the absolute magnitude of the depolarization is small (below 30 dB). Depolarization is polarization sensitive, with horizontal polarization depolarized the least by raindrops [9].

Using results provided in [3] we will consider the effects associated with propagation through a rain-filled medium. In summary the parameters are a rainfall rate of 75 mm/hr, a viewing angle of 90° (corresponds to viewing the horizon) and a depolarization of -40 dB [3], a 20° phase shift (HH-VV), and a VV return about 2.5 dB lower than HH [8]. A scattering matrix may then be written as

$$[S] = \begin{bmatrix} 1 & 0.01 \\ 0.01 & 0.75e^{-j20^\circ} \end{bmatrix} \qquad \text{(Eq. 18)}$$

To determine the optimum elliptical polarization, polarization combinations were synthesized creating a polarization signature pair for the two cases where the transmit and receive polarizations are aligned and the case when they are orthogonal. These polarization signatures are provided in Figure 53. They show that HH-polarization provides the peak backscatter cross section of all polarizations (maximum σ of 1.000 at HH). Note that the cross-polarized maximum (σ value of 0.766) is smaller by 1.16 dB and occurs for a set of elliptical polarizations denoted LR_e-Peak and RL_e-Peak. Based on these peaks, the tilt and ellipticity angles were determined and the SAR clutter scenes were then synthesized for this case. The resulting basis vectors are

$$Z_{LC} = \begin{vmatrix} 0.6943 \\ 0.7197e^{j75.1^\circ} \end{vmatrix} \quad Z_{RC} = \begin{vmatrix} 0.6943 \\ 0.7197e^{-j75.1^\circ} \end{vmatrix} \qquad \text{(Eq. 19)}$$

and the SAR clutter scenes were synthesized for this case. Polarization signatures were recalculated for the scattering matrix used above, but with a zero phase difference with the purpose to examine the effect of the phase shift (see Figure 54). Note that the phase difference is responsible in shifting the null in the co-polarized case and the peak in the cross-polarized case from circular to elliptical polarization. This illustrates that the greater the phase shift, the greater is the difference between the optimum elliptical polarization and circular polarization.

VI. DENVER POLARIMETRIC SAR IMAGE SET

Image Set Description

In this analysis a single swath image (about 10 km x 10 km) which contains the Denver Stapleton terminal was selected. The ground coverage of this image is similar to that given in Figure 2 of the Volume III Final Report for the polarimetric image set. Image sets are presented in Figures 59 and 60 for linear and circular polarized. Visual examination allows the qualitative comparison for these simple targets to their ideal scattering matrices. Images at VV, HH, and HV polarizations are provided in Figure 55, 56 and 57. The image for VH is not provided, it is identical to that of HV. For most all classes of targets and clutter reciprocity holds, HV = VH. The image subtends incidence angles from 43° to 82° and the first half of the ground range is from 1593 m to 12047 m. The image covers an area which extends from just south of Lowry Air Force Base (AFB) to almost north of the Denver airport and from the warehouse district to the east of the airport to just west of Lowry AFB, and contains a good variety of ground clutter types. Starting from the south, which is in the image near range, is the Lowry AFB. The residential area just to the east of the base is part of the city of Aurora and the area to the west is part of the city of Denver. In this area streets are generally curvilinear, a characteristic of suburban developments. North of Lowry AFB, and extending in a band which crosses half the image is an urban community. This community, made up of blocks of smaller, closely-spaced, ranch style homes, is centered on Colfax Avenue, a main throughway through Denver, and extends up to the airport on the north side and down to Lowry AFB on the south side.

Further north is Denver Stapleton airport. Terminals, associated buildings, and parking lots west of the runways are easily distinguishable. East of the airport are additional airport buildings and large warehouses. Interstate 70 separates the airport buildings from the warehouse district, goes under the north/south runways, and cuts through part of the city just west of the airport. The city area just to the west of the airport is a conglomeration of office buildings, hotels, and other related facilities. In the most northerly part of the image are the Denver Stapleton airport runways, warehouses and a highly industrialized suburb called Commerce City. The Commerce City area is separated from the business park by Interstate 270.

Calibration Target Array

An array of calibration targets was deployed during the SAR collection to absolutely calibrate the radar imagery according to backscatter levels as well as to permit the amplitude and phase balance between the transmit and receive channels (See Figure 58). The latter is important in polarimetric calibration. Three target types were used: trihedrals, dihedrals with three rotation angles, and active radar calibrators. Scattering matrices for the trihedrals and dihedrals are provided in Table 11. The active radar calibrators were oriented to produce an equal intensity response at each polarization. Scattering matrices were retrieved to quantitatively describe their responses. Examples of scattering matrices for the trihedrals are provided in Appendix E. It is instructive to study these targets and observe their presence or lack of presence at each polarization. Since the radar does have a finite isolation between channels, the zeros of the scattering matrices will be replaced by values similar to the system isolation. The dihedrals are particularly interesting. The rotation at the three difference angles produce three distinct scattering matrices at linear polarization. Dihedrals produce backscatter by a reflection from two conducting surfaces. Trihedrals produces backscatter by reflections off three surfaces. Circular polarized radar has the important property of separating returns into even-bounce origin (see LL or RR) or odd-bounce origin (see LR or RL). Note that the dihedrals are almost totally absent from circular cross-polarization images.

As suggested earlier, man-made targets may produce a wide variety of backscatter responses. As an example, aircraft cross sections have been observed to be less with circular-polarization than with linear-polarization. Experimental results have shown that aircraft illuminated with one sense of circular polarization produced returns which were statistically equally distributed between the right-hand circular and left-hand circular polarizations. Hence, there was no circular polarization preference and a 3 dB reduction in the optimum power return, since the energy is distributed into two channels rather than one. In the linear polarization case, there was only about 0.5 dB reduction in the orthogonal channel. For this example of a man-made target of complex shape, circular polarization results in a 2.5 dB lower reduction in backscatter power (in RL or LR) compared with the use of linear polarization (VV or HH) [10].

VII. POLARIZATION PROPERTIES OF GROUND CLUTTER

Clutter statistics were obtained for the four transmit-receive polarization combinations in the scattering matrices for the linear polarization case, the circular polarization case, the elliptical polarization case for an oblate spheroid, and the elliptical polarization case of a rain filled medium. These tables are provided in Appendix D. Statistics were produced for urban, residential, grass, terminal area, and buildings. Many thousands of pixels were utilized to produce these results. Incidence angles ranged from 50° to 80°. A second set of tables was generated which describe the unique pieces of information a polarimetric radar provides, the polarimetric discriminants. Polarimetric discriminants are defined in Appendix D. These tables provide a compact method to describe the scattering properties of the clutter scenes analyzed.

Synthesis of Circular Polarization

In the synthesis of circular polarization from linear polarization, the following operations are performed:

$$
\begin{aligned}
S_{RR} &= .5[(S_{HH} - S_{VV}) - j(S_{HV} + S_{VH})] \\
S_{RL} &= .5[(S_{HH} + S_{VV}) + j(S_{HV} - S_{VH})] \\
S_{LR} &= .5[(S_{HH} + S_{VV}) - j(S_{HV} - S_{VH})] \\
S_{LL} &= .5[(S_{HH} - S_{VV}) + j(S_{HV} + S_{VH})]
\end{aligned}
\qquad \text{(Eq. 20)}
$$

Note that S_{LR} and S_{RL} are nearly identical whenever S_{VH} and S_{HV} are small compared to S_{VV} and S_{HH}. In addition, it is important to point out that S_{RL} and S_{LR} fall midway between S_{HH} and S_{VV} for this case.

Clutter Responses at Linear and Circular Polarization

Clutter scenes of urban areas, a residential area, an area which contains objects along an airport runway, a plant, and an area about an airport terminal were synthesized at circular polarization. These images are provided in Figures 61 to 66 at both linear and circular polarization, so that a comparison between the two may be made as a function of the different transmit-receive combinations. The sites selected are highlighted in an overlay found on the complete SAR image provided in Figure 56. The images are presented with equal intensity modulation to provide the best visualization of the different sources of scatter. The tables of statistics should be consulted to determine the quantitative differences between backscatter levels.

One of the urban areas is illustrated in Figure 61. The most striking difference in all the different cases is between the linear cross-polarization examples and all the others. The cultural aspect of this scene is most apparent in the linear co-polarized and circular polarization cases. In this case, VV, HH, RR, RL, LR and LL all show similar backscatter responses. The circular polarization cases, however, give the visual impression that the energy is equally spread in all channels. The VV image suggests that there are slightly more scattering points as compared to the response at HH-polarization. The prominent backscatter features in this urban scene are present in all the different polarization cases.

An urban area next to the Lowry Air Force Base is presented in Figure 62. There are three features of particular interest in this scene: the well structured urban area which is observed oriented to the radar look direction, the building complex in the upper right hand corner of the image, and the scatterers associated with a building in the upper left hand corner of the image. The urban area produced a response similar to that described in the example above, except that a greater number of scattering points appear in the HH image than the VV image. The circular polarization response suggests that the scattering centers are complex, dominated by neither single nor double bounce mechanisms, with the effect that the energy is, again, equally distributed among the four different polarization cases. Based upon the building scatter in the upper right hand corner, circular polarization provides the best choice for suppressing building clutter by insuring that features which are particularly polarization sensitive are suppressed slightly. Note that this building is brightest in VV polarization, while HH and the circular polarization cases are similar. Linear cross-polarized returns are typically many dB lower than those of linear polarization. Therefore complex cultural clutter when mapped to circular polarization will be suppressed by spreading the energy into four channels rather than just two.

A residential area, Figure 63, also shows a response similar to that described above. The strong scattering points which dominate the response for the like linear polarization are presented in a similar manner in the circular polarization set. In comparing the differences between VV and HH, it is interesting to note that there are two distinct populations of polarization sensitive scatters. One set is enhanced with VV-polarization, while the second population is enhanced with HH-polarization. It was not determined if these populations were equally distributed. Again, it appears that circular polarization distributed the energy associated with these scatterers throughout all channels.

The scene in Figure 64 was chosen because it provided a linear string of point scatterers in a weak background. In the center is an assembly of points which line the sides and center of the airport runway. In the bottom edge of the image is a string of scatterers which may be a fence. Linear cross-polarization worked well to suppress the scatterers associated with the fence, but the points on the runway are still prominent, though probably reduced in intensity by many dB. The response at VV and HH polarization look reasonably similar, with HH-polarization providing possibly more scattering points, but at a minimum they are more distinct in the clutter background. It is difficult to tell the difference between the circular polarization case and the HH case.

An ensemble of organized scatterers is presented in Figure 65 and are associated with a plant facility. In this case, the most prominent features are observed in the linear cross-polarized scenes, but, in a general sense, there is a good deal of similarity between the responses for all of the polarization cases.

The terminal area at an airport presents a critical problem in that it has been seen to be the primary source of intense scatter within the airport clutter area. In Figure 66, the Denver Stapleton terminal area is presented. Responses are similar in all polarization cases. Linear cross-polarization is reduced from that produced at the like polarizations. The greatest number of scatterers is visible in the VV image when compared to the HH image. The circular polarization cases are interesting in that RR and RL are most similar to the VV case, while LR and LL are more similar to the HH case.

Determination of Target-to-Clutter Ratios

Given that ZDR = $\sigma_{HHr}/\sigma_{VVr}$ (subscript r indicates that these are the radar returns for the rain in a microburst) and Pr = $\sigma_{VVc}/\sigma_{HHc}$ (subscript c indicates that these are the radar returns for the ground clutter), the target-to-clutter ratios (TCR) where the target of interest is the rain in a microburst, may be derived:

$$TCR_{HH} = Kr[|S_{HH}|^2_r]/Kc[|S_{HH}|^2_c], \qquad \text{(Eq. 21)}$$

$$TCR_{VV} = Kr[|S_{VV}|^2_r]/Kc[|S_{VV}|^2_c], \text{ and} \qquad \text{(Eq. 22)}$$

$$TCR_{RLc} = Kr[0.25(S_{HH} + S_{VV})^2_r]/Kc[0.25(S_{HH} + S_{VV})^2_c]. \qquad \text{(Eq. 23)}$$

where Kr and Kc are system gain constants and RLc indicates circular polarization. Ratios of target-to-clutter ratios will be examined because the issue being addressed here is not what are the actual target-to-clutter ratios, but which polarization produces the largest ratio. Hence, by examining all ratios with respect to HH-polarization, the optimum polarization will be determined. Normalizing the TCR with respect to TCR_{HH} and expressing in terms of ZDR and Pr we have

$$TCR_{VV}/TCR_{HH} = ZDR^{-1}Pr^{-1}, \text{ and} \qquad \text{(Eq. 24)}$$

$$TCR_{RLc}/TCR_{HH} \approx (ZDR^{-1} + 1)/(Pr + 1). \qquad \text{(Eq. 25)}$$

Based upon the above, general cases of ZDR and PR were examined. Because raindrops distort in a preferential way, ZDR $\geq$ 1 completely describes the range of ZDR values. For the case of Pr, values may be both smaller and larger than 1. In examining the above there are four cases to consider:

1. If Pr = 1, then HH is the preferred polarization.

2. If ZDR = 1 & Pr < 1, then

   VV is preferred over HH,
   VV is preferred over RLc, and
   RLc is preferred over HH.

3. If ZDR = 1 & Pr > 1, then

   HH is preferred over VV,
   HH is preferred over RLc, and
   RLc is preferred over VV.

4. If the clutter scene is mixed, and cases of both Pr < 1 and Pr > 1 exist, then

   RLc is preferred over VV or HH.

A computer program was written to examine the polarization preference if ZDR = 1 to 3, and Pr = 0.1 to 1. Results indicate that

1. For ZDR = 1 and 0.1 <Pr <1, then VV is preferred.

2. For ZDR = 2, VV is preferred for 0.1 < Pr < 0.5 and HH is preferred when 0.5 < Pr < 1.

3. For ZDR = 3, VV is preferred for 0.1 < Pr < 0.35 and HH is preferred when 0.35 < Pr < 1.

The clutter results obtained from the Denver polarimetric image set indicate that $\sigma^\circ_{HH} > \sigma^\circ_{VV}$ by 4 to 13 dB. Man-made targets such as the terminals and buildings produced polarization ratio values of about -5 dB and urban of about -7 dB. For these cases, $Pr < 1$ and VV is the preferred polarization.

Results

For the rain filled medium case, the matrix of the amplitudes of the scattering cross sections for the linear, circular, and optimum elliptical polarization cases are then

$$[|S|]_L = \begin{bmatrix} 1.0 & 0.01 \\ 0.01 & 0.75 \end{bmatrix}_L , \qquad \text{(Eq. 26)}$$

$$[|S|]_C = \begin{bmatrix} 0.189 & 0.861 \\ 0.861 & 0.189 \end{bmatrix}_C , \text{ and} \qquad \text{(Eq. 27)}$$

$$[|S|]_E = \begin{bmatrix} 0.0 & 0.884 \\ 0.884 & 0.0 \end{bmatrix}_E . \qquad \text{(Eq. 28)}$$

The above provide the following radar scattering cross sections relative to HH-polarization: $|S_{HH}|^2 = 0$ dB, $|S_{VV}|^2 = -2.5$ dB, $|S_{RLc}|^2 = -1.3$ dB, and $|S_{RLe}|^2 = -1.1$ dB. Target-to-clutter ratios (i.e. rain-to-clutter ratios) are derived based on the above and the clutter backscatter responses and are provided in Table 12. Results provided in this table show that the target-to clutter ratios for VV are larger than for HH (on average by about 5.75 dB) or for RLc (on average by about 2.75 dB). However, if the elliptical polarization which maximizes the cross-polarization response (noting that RLe ≈ LRe) is obtained, then TCRs which are a few dB greater than those produced at VV-polarization may be obtained. This was found true for the urban, terminal, or building clutter, but not for the residential clutter.

VIII. CONCLUSIONS

The mountain terrain data obtained from the Rocky Mountain image correlates well with data obtained from the other Denver images. Clutter groups common to all of the Denver data produced similar results. An interesting feature of the mountain terrain data is the similarity in the shape of the backscattering coefficient distributions of the mountain, geological thrust feature, and grass clutter. This is not surprising however, as the vegetation on the surfaces of the grass areas, mountains, and thrust feature was similar. The mean returns from the mountain areas and thrust features are significantly higher than those of the grassy areas due to the local slope of these geological features. An analysis of the returns from these two geological features produced results applicable to the problem of range ambiguity effects potentially associated with mountainous terrain. Although the data in the Rocky Mountain Image did not produce a range ambiguity problem with the SAR, an analysis may be performed using mean backscattering coefficients calculated from the data to determine range ambiguity effects for other systems. In calculating a test case using the maximum mountain return and minimum airport return found in the data, it was determined that as long as an airport is approximately 1.5 miles from steep geological features, mountain clutter may not present this type of a problem.

The analysis of the low altitude images has provided additional data to complement the description of ground clutter in the Denver area, especially that of hard targets at high incidence angles. These data provided excellent angle diversity and the scattering associated with the front sides of buildings at large incidence angles was dramatically illustrated and documented. In general, cultural clutter returns which arise from city buildings and prominent structures may produce backscattering coefficients 30 dB above a background level of -18 dB at 85° to 86°. Other clutter groups correlate well with previously analyzed Denver data. As with other clutter areas, the statistical distributions change from symmetric and narrow to asymetric and broad as the clutter areas change in content from entirely natural targets to entirely man-made targets. Comparisons of selected image features at different incidence angles reveal that the primary scatterers at large incidence angles are the faces of hard-target structures which are perpendicular or nearly perpendicular to the radar. Most other clutter disappear into the noise at angles of 80° and beyond.

The polarization properties of hydrospheres and clutter were examined. The optimum linear polarization was determined by the polarization ratio. If $\sigma^{\circ}_{HHc} > \sigma^{\circ}_{VVc}$, then VV-polarization is the preferred polarization. VV-polarization is preferred over circular polarization (RL or LR), except when the clutter scene has a non-preferential mix of Pr ratios. In this case, circular polarization is anticipated to be the preferred polarization. It was illustrated in this study that elliptical polarization, based on the scattering matrix for a rain-filled medium, produced the optimum target-to-clutter ratio.

These results suggest that the distribution of the polarization ratio of the ground clutter needs to be well-characterized for the imaging geometry of the microburst detection radar. This supports the determination of the optimum polarization. Results also indicate that, at large angles, clutter levels are the greatest at HH-polarization. In addition, characterization of the polarization properties of microbursts may provide a reliable definition of the optimum elliptical polarization. If this polarization can be defined, then the optimum polarization is an elliptical polarization.

REFERENCES

1. Nathanson, F.E., "Adaptive Circular Polarization", IEEE 1975 International Radar Conference, pp. 221-225, April 21-23, 1975.

2. Hendry, A., and G.C. McCormick, "Deterioration of Circular-polarization Clutter Cancellation in Anisotropic Precipitation Media", Electronics Letters, vol. 10, no. 10, pp. 165-166, May 16, 1974.

3. Oguchi, T., "Electromagnetic Wave Propagation and Scattering in Rain and Other Hydrospheres, Proc. of IEEE, Vol. 71, No. 9, September, 1983.

4. Bowles, R.L. and W. Frost, editors, "Wind Shear/Turbulence Inputs to Flight Simulation and System Certification", NASA CP-2474, 1987.

5. Ahrens, D.C., Meteorology Today, West Publishing Co., St. Paul, Minnesota, pp. 428-430, 1988.

6. Compiled by E.M. Bracalente & V.E. Delnore, Wind Shear Detection Forward-Looking Sensor Technology, collected viewgraphs and notes from conference held February 24-25, 1987 at NASA Langely Research Center, Hampton VA; NASA Conference Publication 10004, DOT/FAA/PS-87/2, pg. 89 & 227, October 1987.

7. "Industry Review of Forward Looking Sensor Technology for Detection of Wind Shear", Meeting Notes, pg. 89 and 227, National Aeronautics and Space Administration, Langley Research Center, Hampton, Virginia, 24-25 February 1987.

8. Seliga, T.A., K. Aydin, and V.N. Bringi, "Differential Reflectivity and Circular Depolarization Ratio Radar Signals and Related Drop Oscillations and Propagation Effects in Rainfall", Radio Science, Vol. 19, No. 1, pp. 81-89, January-February, 1984.

9. Bringi, V.N., R.M. Rasmussen, and J. Vivekanandan, "Multiparameter Radar Measurements in Colorado Convective Storms. Part I: Gaupel Melting Studies", J. Atmos. Sci., Vol. 43, pp. 2545 -2563, 1983.

10. Rogers, R.R., "A Review of Multiparameter Radar Observations of Precipitation", Radio Science, Vol. 19, No. 1, pp. 23-36, January-February, 1984.

11. Skolnik, M., "Introduction to Radar Systems", McGraw-Hill Book Co., pp. 504-506, 1980.

Table 1. NASA LaRC Denver Flight Summary

Pass	Beg Lat	Beg Lon	End Lat	End Lon	Comments
2	39:56.51	104:44.43	39:36.49	104:44.43	1st Step West, West-Look
4	39:56.51	104:45.52	39:36.49	104:45.42	Full Pol Airport, West-Look
6	39:36.49	104:59.28	39:56.51	104:59.28	Full Pol Airport, East-Look
8	39:56.51	104:50.35	39:36.49	104:50.35	Full Pol Airpot Mid Angle, West-Look
10	39:36.49	105:03.77	39:56.51	105:03.77	Double Swath Airport, East-Look
12	39:56.51	104:47.43	39:36.49	104:47.43	2nd Step West, West-Look
14	39:32.48	105:06.82	40:14.52	105:06.82	Rocky Mountains, Double Swath
15	39:32.48	105:06.82	40:14.52	105:06.82	Rocky Mountains, Double Swath
16	39:32.48	105:06.82	40:14.52	105:06.82	Rocky Mountains, Double Swath
18	40:14.52	105:08.63	39:32.48	105:08.63	Rocky Mountains, Full Pol
19	40:14.52	105:08.63	39:32.48	105:08.63	Rocky Mountains, Full Pol
20	40:14.52	105:08.63	39:32.48	105:08.63	Rocky Mountains, Full Pol
21	40:14.52	105:08.63	39:32.48	105:08.63	Rocky Mountains, Full Pol
22	40:14.52	105:08.63	39:32.48	105:08.63	Rocky Mountains, Full Pol
23	40:14.52	105:08.63	39:32.48	105:08.63	Rocky Mountains, Full Pol

NASA LaRC Denver Flight Summary (Cont.)

Pass	Beg Lat	Beg Lon	End Lat	End Lon	Comments
25	39:36.49	104:50.43	39:56.51	104:50.43	3rd Step West, West-Look
27	39:56.51	104:41.03	39:36.49	104:41.03	Double Swath Airport, West-Look
29	39:36.49	104:53.43	39:56.51	104:53.43	4th Step West, West-Look
30	39:36.49	104:53.43	39:56.51	104:53.43	4th Step West, West-Look
31	39:55.36	104:44.63	39:55.36	105:11.88	Double Swath Airport, South-Look
33	39:51.79	104:44.23	39:51.79	105:11.47	Full Pol Airport, South-Look
35	39:44.89	104:44.23	39:44.89	105:11.47	Full Pol Airport Mid Angle North-Look
37	39:41.17	104:44.24	39:41.17	105:11.46	Full Pol Airport, North-Look
39	39:37.60	104:44.64	39:37.60	105:11.86	Double Swath Airport, North-Look
41	39:36.49	104:53.43	39:56.51	104:53.43	4th Step West, West-Look
42	39:36.49	104:53.43	39:56.51	104:53.43	4th Step West, West-Look
43	39:40.49	104:53.31	39:52.50	104:53.31	Low Altitude, West-Look
44	39:40.49	104:53.31	39:52.50	104:53.31	Low Altitude, West-Look

Table 2. Image Composition Areal Analysis, Rocky Mountain Image

Clutter Scene	Percent of Total Image Area
Residential	8.0
Rural	19.0
Thrust Feature	7.0
Mountains	66.0

Table 3. Clutter Returns for Targets in the Rocky Mountains Image, X-HH

	Mean (dB)	MIN (dB)	Max (dB)	SDev (MAG)	$\frac{\text{Mean + SDev}}{\text{Mean}}$ (dB)
Grass (45°-49°)	-21.89	-35.48	-12.81	0.59509E-02	2.83
Grass (60°-64°)	-26.11	-35.48	-6.94	0.39100E-02	4.44
Grass (65°-69°)	-27.57	-35.48	-8.68	0.28616E-02	4.21
Grass (70°-74°)	-28.68	-35.48	-14.37	0.16956E-02	3.52
Grass (75°-79°)	-29.81	-35.48	-18.71	0.12856E-02	3.48
Mountain (65°-69°)	-17.23	-35.48	-5.63	0.22962E-01	3.45
Mountain (70°-74°)	-16.17	-35.48	-5.21	0.28489E-01	11.07
Mountain (75°-79°)	-25.57	-35.48	-9.19	0.64210E-02	5.21
Residential (40°-49°)	-5.15	-35.48	20.33	0.20633E+01	8.90
Residential (50°-59°)	-13.14	-35.48	17.10	0.47496E+00	10.33
Residential (60°-64°)	-18.30	-35.48	13.15	0.12981E+00	9.90
Residential (65°-69°)	-12.52	-35.48	21.00	0.11668E+01	13.39
Residential (70°-74°)	-19.08	-35.48	8.17	0.80215E-01	8.74
Thurst (65°-69°)	-11.37	-35.48	1.57	0.78578E-01	3.17
Thurst (70°-74°)	-18.22	-35.48	-5.01	0.16711E-01	3.24
Thurst (75°-79°)	-21.65	-35.48	-9.56	0.71796E-02	3.12
Water (55°-59°)	-35.42	-35.48	-27.46	0.45580E-04	0.64
Water (65°-59°)	-35.23	-35.48	-21.25	0.24487E-03	2.59
Water (70°-74°)	-35.46	-35.48	-29.22	0.32042E-04	0.46

Table 4. Image Composition Areal Analysis, Low Altitude Images

Clutter Scene	Percent of Total Image Area
Rural	7.10
Residential	1.95
Urban	18.71
City	0.22
Airport Grounds	8.12
Lowry AFB	1.62
Recreational Areas	0.64
Warehouses	2.10
Mixed City and Industrial	11.37
Unclassified/City	48.17

RS-90-131-3a

Table 5. Clutter Returns for Targets in the X-HH Low Altitude Image

	Mean (dB)	MIN (dB)	Max (dB)	SDev (MAG)	$\frac{\text{Mean} + \text{SDev}}{\text{Mean}}$ (dB)
Grass (40°-49°)	-23.82	-47.22	-11.25	0.43735×10^{-2}	3.13
Grass (75°-79°)	-30.24	-47.22	-7.13	0.23352×10^{-2}	5.40
Buildings (40°-49°)	-20.58	-43.59	0.50	0.45907×10^{-1}	7.96
Buildings (85°-89°)	4.01	-47.22	33.58	0.36690×10^{2}	11.92
Industrial (80°-84°)	-13.21	-47.22	20.97	0.10742×10^{1}	13.71
City (80°-84°)	-12.46	47.22	20.18	0.92445×10^{0}	12.38
Residential (65°-69°)	-17.62	-40.43	0.98	0.42338×10^{-1}	5.38
Urban (65°-69°)	-18.63	-47.22	5.65	0.48624×10^{-1}	6.58
Water (60°-64°)	-41.00	-47.22	-41.00	0.13275×10^{-3}	4.27
Parking Lot (80°-84°)	-13.79	-47.22	13.84	0.59904×10^{0}	11.86
Runway (60°-64°)	-38.29	-47.22	-28.84	0.16065×10^{-3}	3.29
Terminal (H6)	-5.13	-32.29	19.22	0.29332×10^{1}	10.24
Plane (H73)	-17.15	-32.46	-5.37	0.46675×10^{-1}	5.32
Plane (H75)	-12.85	-30.33	3.15	0.21023×10^{0}	5.05
Truck (H14)	-19.17	-44.90	-8.49	0.29543×10^{-1}	5.37

Table 6. Clutter Returns for Targets in the X-VV Low Altitude Image

	Mean (dB)	MIN (dB)	Max (dB)	SDev (MAG)	$\frac{\text{Mean + SDev}}{\text{Mean}}$ (dB)
Grass (40°-49°)	-24.22	-53.33	-12.50	0.40316×10^{-2}	3.15
Grass (75°-79°)	-31.39	-53.33	-2.00	0.32115×10^{-2}	7.34
Buildings (40°-49°)	-19.24	-40.05	-0.54	0.49171×10^{-1}	7.10
Buildings (85°-89°)	6.35	-53.33	35.33	0.58432×10^{2}	11.63
Industrial (80°-84°)	-9.01	-53.33	21.02	0.16915×10^{1}	11.60
City (80°-84°)	-7.55	-53.33	28.52	$0.39557 \times 10^{+1}$	13.71
Residential (65°-69°)	-17.29	-39.94	2.76	0.63513×10^{-1}	6.44
Urban (65°-69°)	-18.78	-41.80	1.96	0.52876×10^{-1}	6.98
Water (60°-64°)	-38.35	-53.33	-23.13	0.30207×10^{-3}	4.87
Parking Lot (80°-84°)	-9.60	-53.33	14.26	0.98772×10^{0}	10.00
Runway (60°-64°)	-31.43	-53.33	-20.58	0.10600×10^{-2}	3.99
Terminal (H6)	-11.90	-42.40	10.23	0.45606×10^{0}	9.07
Plane (H73)	-20.39	-46.01	-0.52	0.57611×10^{-1}	8.63
Plane (H75)	-15.99	-42.82	3.04	0.17623×10^{0}	9.03
Truck (H14)	-18.07	-39.10	-7.17	0.41057×10^{-1}	5.60

Table 7. Hard Targets Represented as σ, Low Altitude Image, X-HH

Indentifier	Region	θ	σ (dBsm)	Effective Area (m^2)
H1	Building	77.43	28.12	18,102.5
H5	Terminal	78.85	29.82	12,239.42
H6	Terminal	78.09	42.43	57,371.33
H7	Terminal	74.82	13.18	25,194.24
H8	Parking Lot	81.13	34.51	16,236.29
H9	Parking Lot	79.36	27.37	26,842.75
H10	Plane	74.82	-0.77	1,508.54
H11	Plane	77.67	11.03	1,026.43
H12	Plane	75.90	2.56	1,446.34
H13	Parking Lot	77.37	30.30	36,827.14
H15	Truck	66.98	-0.39	373.25
H16	Truck	77.44	2.18	279.94
H17	Parking Lot	79.45	28.35	13,779.07
H19	Plane	77.18	12.75	1,244.16
H20	Plane	77.23	13.11	1,959.55
H21	Plane	77.18	16.65	948.67
H22	Parking Lot	81.13	25.79	6,283.01
H23	Fence	76.44	10.19	12,379.39
H25	Building	64.34	22.30	30,497.47
H26	Building	50.88	21.70	15,552.00
H27	Parking Lot	79.57	32.12	31,555.01
H29	Building	83.81	60.96	6,531.84
H33	Building	82.82	40.71	2,597.18
H34	Building	82.88	20.59	202.18
H54	Building	85.83	33.90	248.83
H56	Building	85.47	41.28	746.50
H59	Building	85.58	47.34	1,026.43
H63	Building	83.92	44.69	1,010.88
H65	Building	86.04	53.09	637.63
H68	Building	86.95	50.06	186.62
H73	Plane	77.40	16.93	2,410.56
H74	Plane	76.87	9.47	1,384.13
H75	Plane	78.12	20.61	2,255.04
H76	Truck	78.12	8.88	2,006.21
H77	Truck	74.62	9.58	2,006.21
H78	Building	49.54	22.13	18,662.40
H79	Building	67.23	23.24	18,646.85
H80	Building	58.30	28.96	18,631.30
H84	Building	79.62	40.04	37,153.73
H87	Building	74.05	17.65	6,236.35
H89	Building	74.36	22.24	30,964.03
H91	Building	76.72	17.62	13,125.89
H94	Building	77.78	28.55	7,185.02
H95	Building	65.70	26.10	9,253.44
H96	Building	65.82	26.59	13,359.17
H97	Building	66.27	21.28	6,454.08
H110	Terminal	78.37	32.74	29,144.45
H111	Structure	58.20	6.60	1,259.71
H112	Structure	58.20	12.08	1,259.71
H114	Structure	71.79	14.88	1,259.71
H115	Structure	73.43	12.04	1,259.71
H117	Structure	75.86	17.78	1,150.85
H124	Structure	80.57	0.51	15.55
H125	Warehouse	46.51	22.39	6,220.80
H126	Warehouse	55.14	24.60	24,883.20
M1	Tree	70.16	10.74	762.05
M2	Tree	55.63	18.83	4,665.60
M3	Tree	66.66	24.24	15,334.27
M4	Tree	51.67	22.59	30,326.40
M5	Tree	74.00	19.31	13,965.70

Table 8. Hard Targets Represented as σ, Low Altitude Image, X-VV

Indentifier	Region	θ	σ (dBsm)	Effective Area (m^2)
H1	Building	77.43	29.72	30,995.14
H5	Terminal	78.85	33.36	30,466.37
H6	Terminal	78.09	36.01	62,208.00
H7	Terminal	74.82	21.32	43,234.56
H8	Parking Lot	81.13	38.03	38,257.92
H9	Parking Lot	79.36	33.32	38,833.34
H10	Plane	74.82	11.43	3,110.40
H11	Plane	77.67	12.85	2,892.67
H12	Plane	75.90	-4.69	2,861.57
H13	Parking Lot	77.37	29.99	38,880.00
H15	Truck	66.98	-0.32	388.80
H16	Truck	77.44	1.28	373.25
H17	Parking Lot	79.45	23.96	18,055.87
H19	Plane	77.18	3.77	3,094.85
H20	Plane	77.23	4.78	3,405.89
H21	Plane	77.18	7.20	1,586.30
H22	Parking Lot	81.13	33.31	34,727.62
H23	Fence	76.44	9.13	17,760.38
H25	Building	64.34	19.12	31,057.34
H26	Building	50.88	24.57	15,552.00
H27	Parking Lot	79.57	34.97	70,621.63
H29	Building	83.81	61.74	11,912.83
H33	Building	82.82	45.51	9,206.78
H34	Building	82.88	-2.45	1,057.54
H54	Building	85.83	36.26	1,073.09
H56	Building	85.47	44.68	2,970.43
H59	Building	85.58	49.59	2,130.62
H63	Building	83.92	28.41	1,026.43
H65	Building	86.04	55.33	2,441.66
H68	Building	86.95	50.48	451.01
H73	Plane	77.40	17.54	6,345.22
H74	Plane	76.87	13.48	6,407.42
H75	Plane	78.12	21.52	5,894.21
H76	Truck	78.12	5.86	2,239.49
H77	Truck	74.62	5.02	2,239.49
H78	Building	49.54	23.46	18,662.40
H79	Building	67.23	26.64	18,662.40
H80	Building	58.30	29.51	18,662.40
H84	Building	79.62	41.42	62,052.48
H87	Building	74.05	20.76	6,298.56
H89	Building	74.36	17.43	31,104.00
H91	Building	76.72	14.54	18,506.88
H94	Building	77.78	29.51	7,776.00
H95	Building	65.70	27.42	9,253.44
H96	Building	65.82	23.92	13,436.93
H97	Building	66.27	25.11	6,469.63
H110	Terminal	78.37	33.83	53,887.68
H111	Structure	58.20	7.88	1,259.71
H112	Structure	58.20	13.22	1,259.71
H114	Structure	71.79	12.52	1,259.71
H115	Structure	73.43	11.69	1,259.71
H117	Structure	75.86	10.48	1,259.71
H124	Structure	80.57	5.19	217.73
H125	Warehouse	46.51	26.26	6,220.80
H126	Warehouse	55.14	27.10	24,883.20
M1	Tree	70.16	14.75	762.05
M2	Tree	55.63	17.98	4,665.60
M3	Tree	66.66	23.09	15,552.00
M4	Tree	51.67	22.17	30,326.40
M5	Tree	74.00	15.30	13,996.80

Table 9. Comparison of Hard Target σ Values

	Low Altitude Image X-VV	Low Altitude Image X-HH	Polarimetric Set X-VV	Polarimetric Set X-HH	1st Step West	2nd Step West	3rd Step West	4th Step West
Planes	-4dB-22dB	-7dB-21dB	---------	--------	10dB-17dB	--------	11dB-20dB	-------
Terminals	21dB-36dB	13dB-43dB	43dB	48dB	32dB-47dB	36dB-45dB	37dB	-------
Buildings	14dB-61dB	17dB-60dB	31dB-41dB	20dB-45dB	20dB-47dB	--------	24dB-33dB	18dB-37dB
Warehouses	27dB	25dB	92dB-34dB	35dB	27dB-33dB	23dB-32dB	25dB	-------

Table 10. Incidence Angles of Sub-Images

Feature	Source Image	Incidence Angle
Terminals	Third 'Step West'	68.9°
Terminals	Low Altitude Image	78.6°
Terminals	Second 'Step West'	78.9°
Terminals	First 'Step West'	82.8°
Golf Course	Fourth 'Step West'	68.3°
Golf Course	Third 'Step West'	78.4°
Golf Course	Second 'Step West'	82.2°
Golf Course	Low Altitude Image	83.9°
Planes	Third 'Step West'	67.4°
Planes	Low Altitude Image	77.7°
Planes	Second 'Step West'	78.1°
Warehouses	Low Altitude Image	67.9°
Warehouses	Second 'Step West'	72.9°
Warehouses	First 'Step West'	80.5°
City Park	Fourth 'Step West'	72.8°
City Park	Third 'Step West'	79.7°
Dog Track	Fourth 'Step West'	63.9°
Dog Track	Third 'Step West'	77.3°
Dog Track	Second 'Step West'	81.7°

Table 11. Scattering Matrices for a Sphere, Flatplate, Trihedral, and Dihedral are Provided for Both the Linear and Circular Basis

RS-90-171a-1

Target Type	Scattering Matrix Linear Basis	Scattering Matrix Circular Basis
Sphere Flatplate Trihedral	$\begin{bmatrix} 1 & 0 \\ 0 & 1 \end{bmatrix}$	$\begin{bmatrix} 0 & 1 \\ 1 & 0 \end{bmatrix}$
Horizontal Dihedral	$\begin{bmatrix} 1 & 0 \\ 0 & -1 \end{bmatrix}$	$\begin{bmatrix} 1 & 0 \\ 0 & 1 \end{bmatrix}$
Vertical Dihedral	$\begin{bmatrix} -1 & 0 \\ 0 & 1 \end{bmatrix}$	$\begin{bmatrix} & 0 \\ 0 & \end{bmatrix}$
Dihedral at 22 1/2°	$\begin{bmatrix} 0.707 & 0.707 \\ 0.707 & -0.707 \end{bmatrix}$	$\begin{bmatrix} e^{j45°} & \\ 0 & e^{-j45°} \end{bmatrix}$
Dihedral at 45°	$\begin{bmatrix} 0 & 1 \\ 1 & 0 \end{bmatrix}$	$\begin{bmatrix} j & 0 \\ 0 & -j \end{bmatrix}$

Table 12. Normalized Radar Scattering Cross-Sections and Rain-to-Clutter Ratio's for Urban, Residential, Terminals, and Buildings

Description		HH dB	VV dB	LR_c dB	Rain Filled LR_e dB	VV/LR_c dB	LR_e/VV dB
Rain RFM/ Normalized		ø	-2.5	-1.3	-1.1	---	---
σ^o's	Urban	-9.64	-16.3	-13.6	-16.54	---	---
	Residential	-7.8	-20.4	-13.4	-13.8	---	---
	Terminals	+5.81	-1.09	+1.57	-.53	---	---
	Buildings	1.89	-4.29	-1.48	-6.05	---	---
σ^o/HH	Urban	0	-6.66	-3.96	-6.90	---	---
	Residential	0	-12.60	-5.6	-6.0	---	---
	Terminals	0	-6.89	-4.23	-6.33	---	---
	Buildings	0	-6.18	-3.37	-7.94	---	---
TCR/HH	Urban	0	4.2	2.7	5.8	1.5	1.6
	Residential	0	10.1	4.3	4.9	5.8	-5.2
	Terminals	0	4.4	2.9	5.0	1.5	.6
	Buildings	0	4.3	2.1	6.6	2.2	2.3

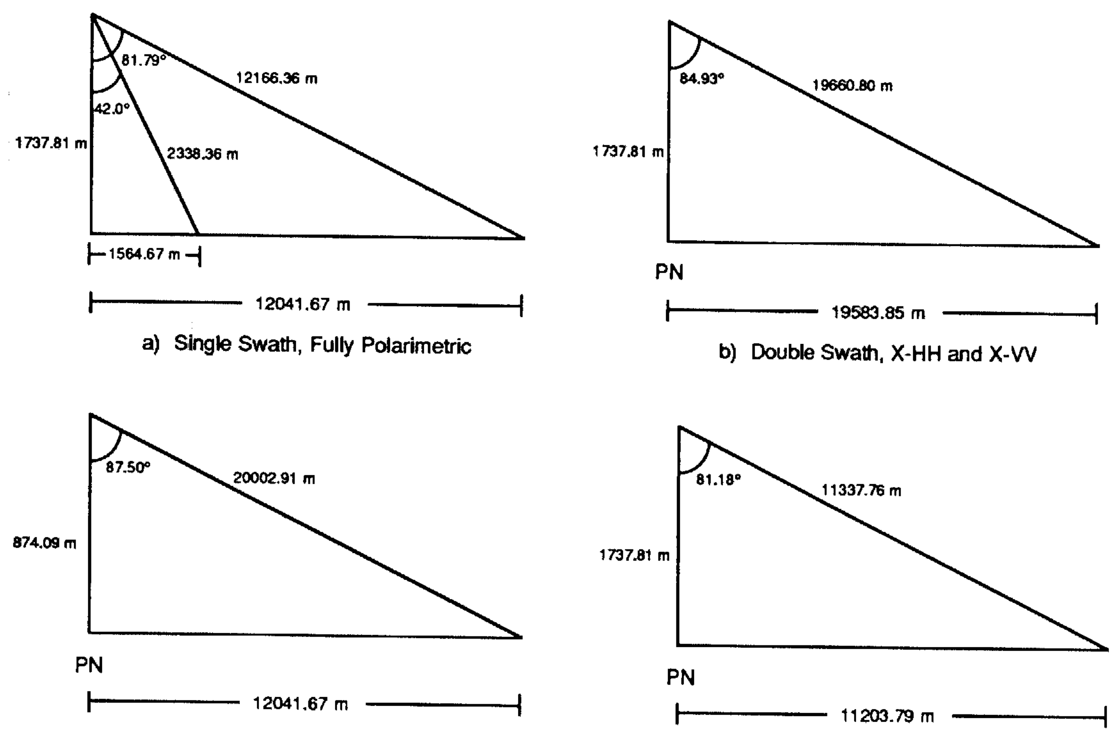

a) Single Swath, Fully Polarimetric

b) Double Swath, X-HH and X-VV

c) Low Altitude Double Swath, X-HH and X-VV

d) Mid-Angle Single Swath, Fully Polarimetric

Figure 1. Image Geometries Used in the Denver Collection
a) Single Swath
b) Double Swath
c) Low Altitude
d) Mid-Angle

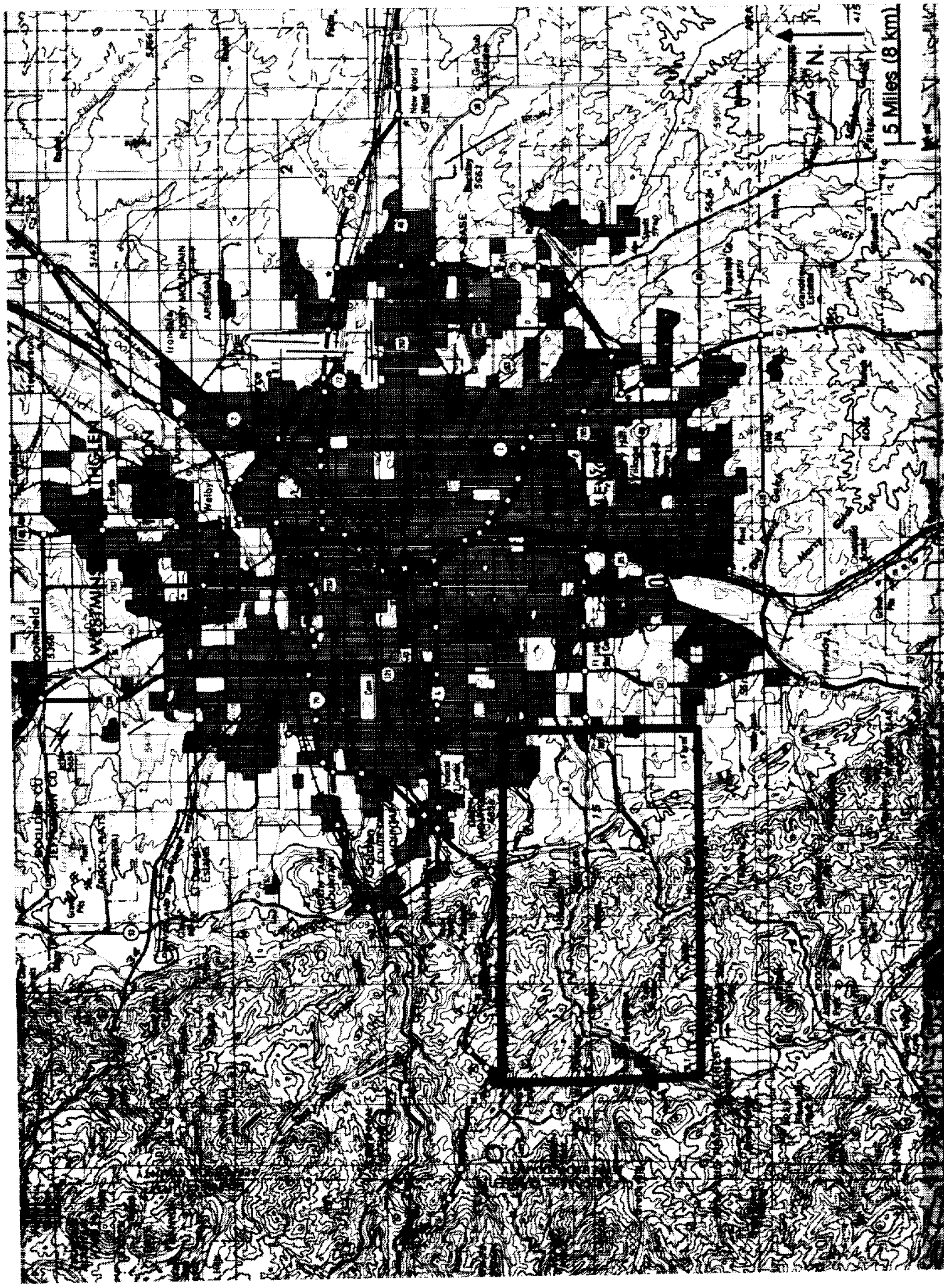

Figure 2. Ground Area Coverage of the Rocky Mountains Image

Figure 3. Rocky Mountains Image, X-HH

ORIGINAL PAGE IS
OF POOR QUALITY

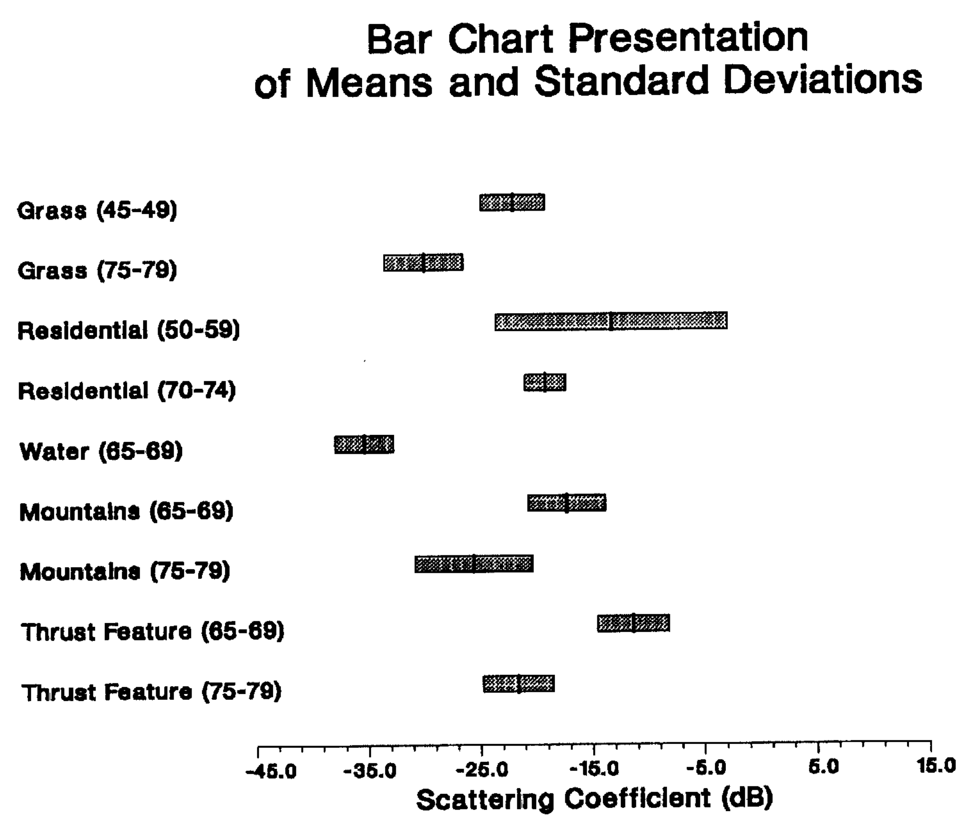

Figure 4. Mean Scattering Coefficient Values, Rocky Mountains Image, X-HH

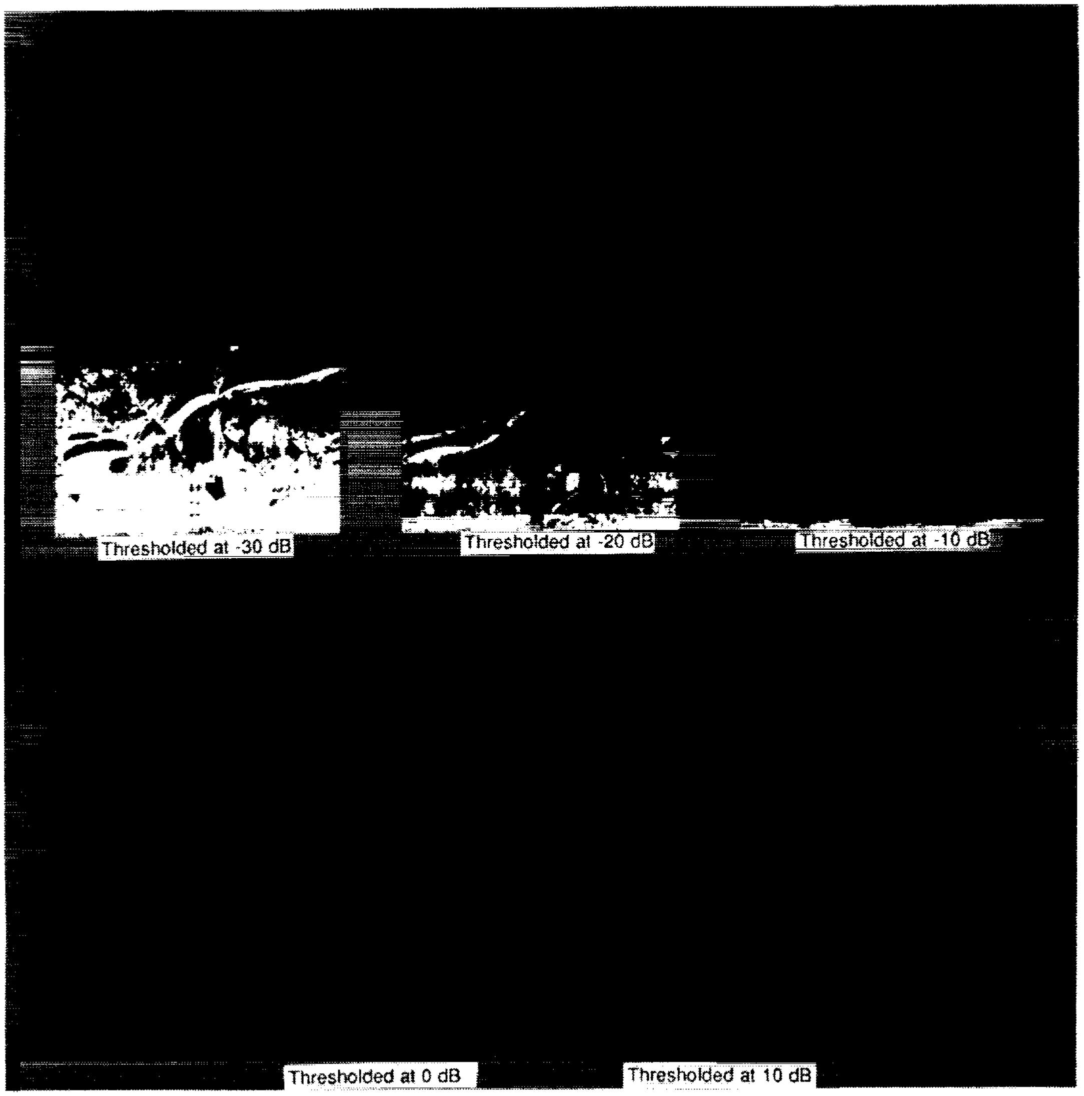

Figure 5. Threshold Images, Rocky Mountains Image, X-HH

ORIGINAL PAGE IS
OF POOR QUALITY

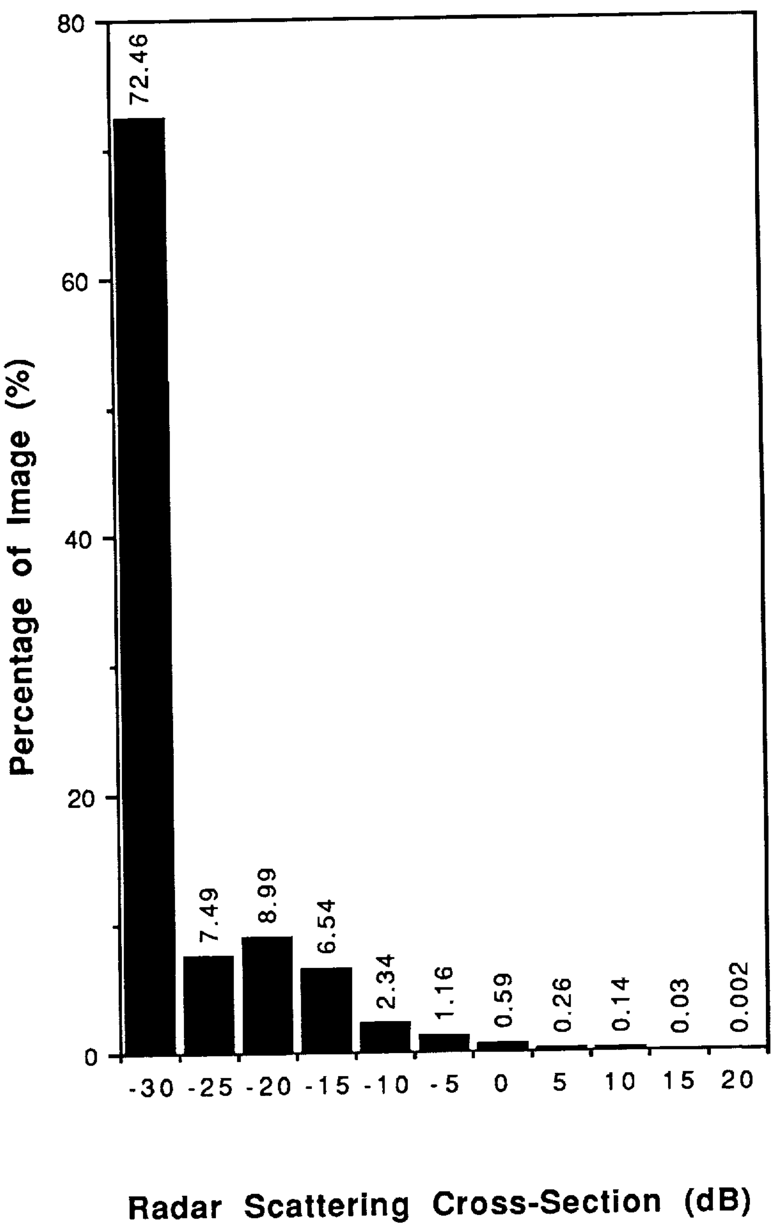

Figure 6. Distribution of Threshold Values, Rocky Mountains Image, X-HH

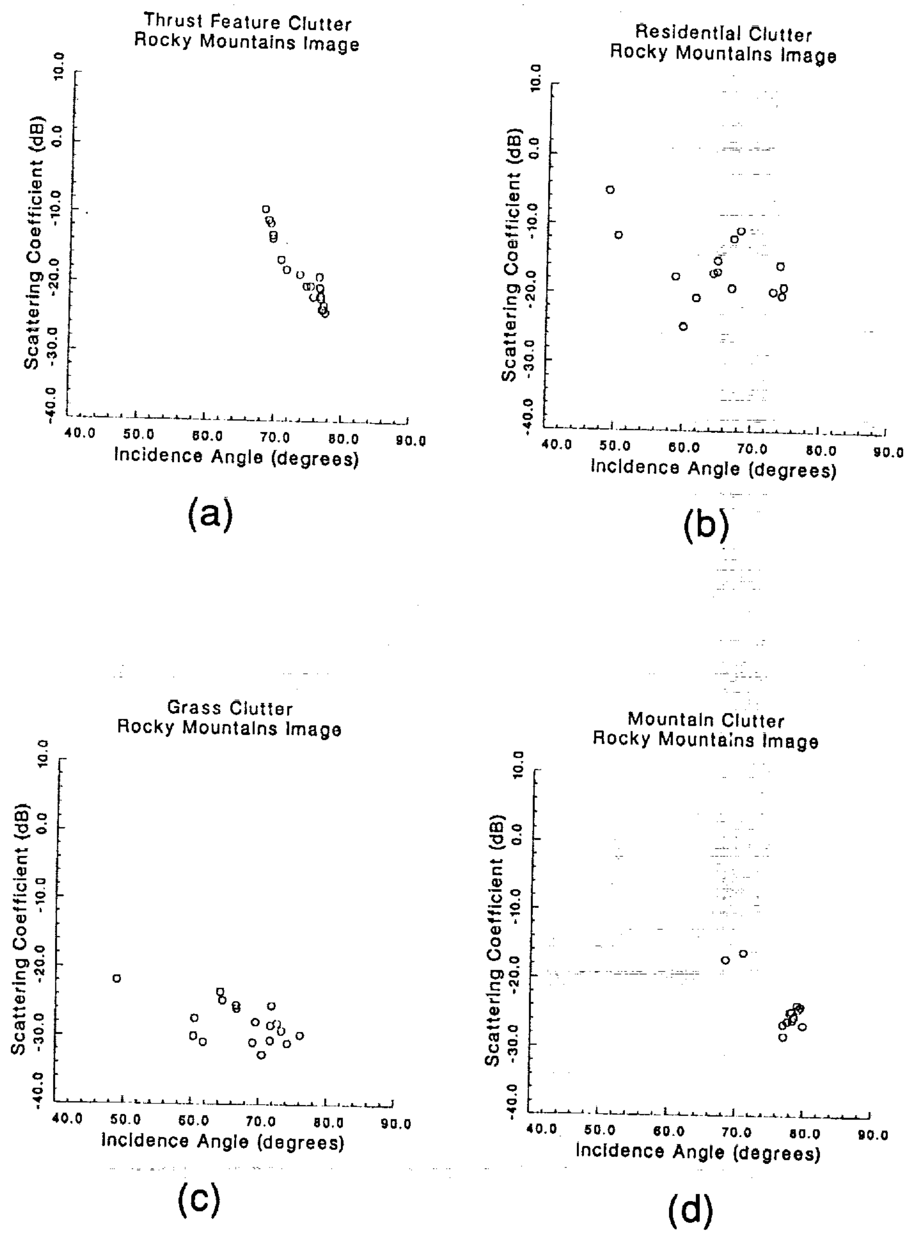

Figure 7. Incidence Angle vs. Scattering Coefficient Plots

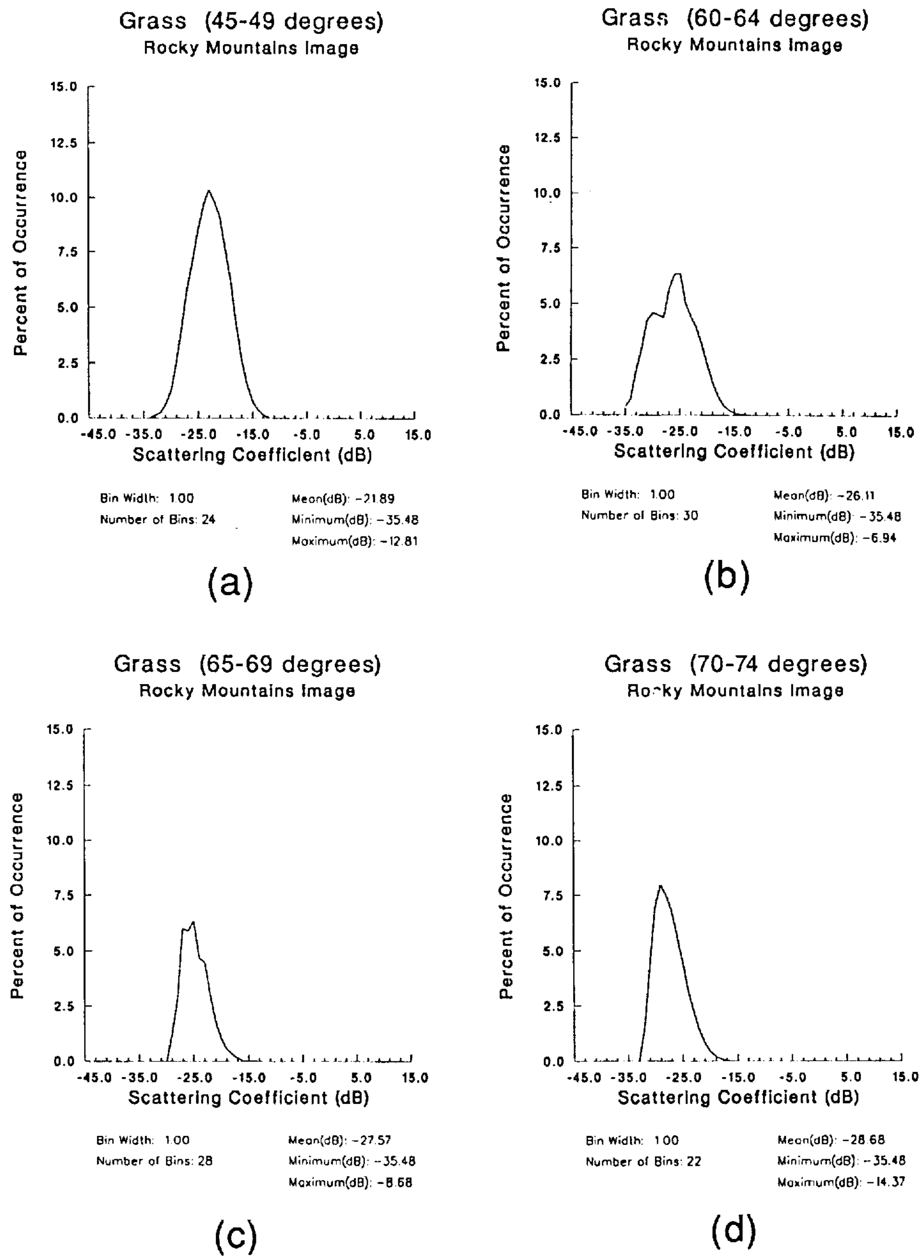

Figure 8. Clutter Distributions of Grass Areas, X-HH

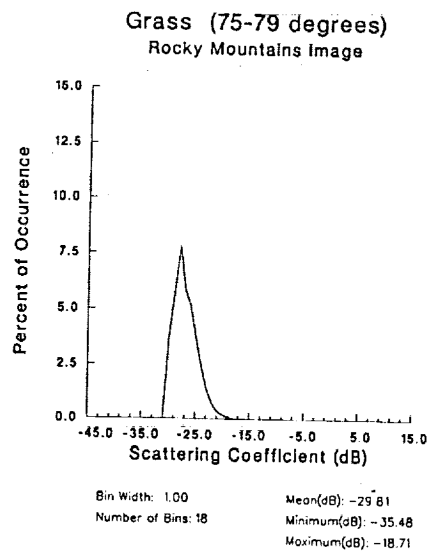

(e)

Figure 8. Clutter Distributions of Grass Areas, X-HH (Cont.)

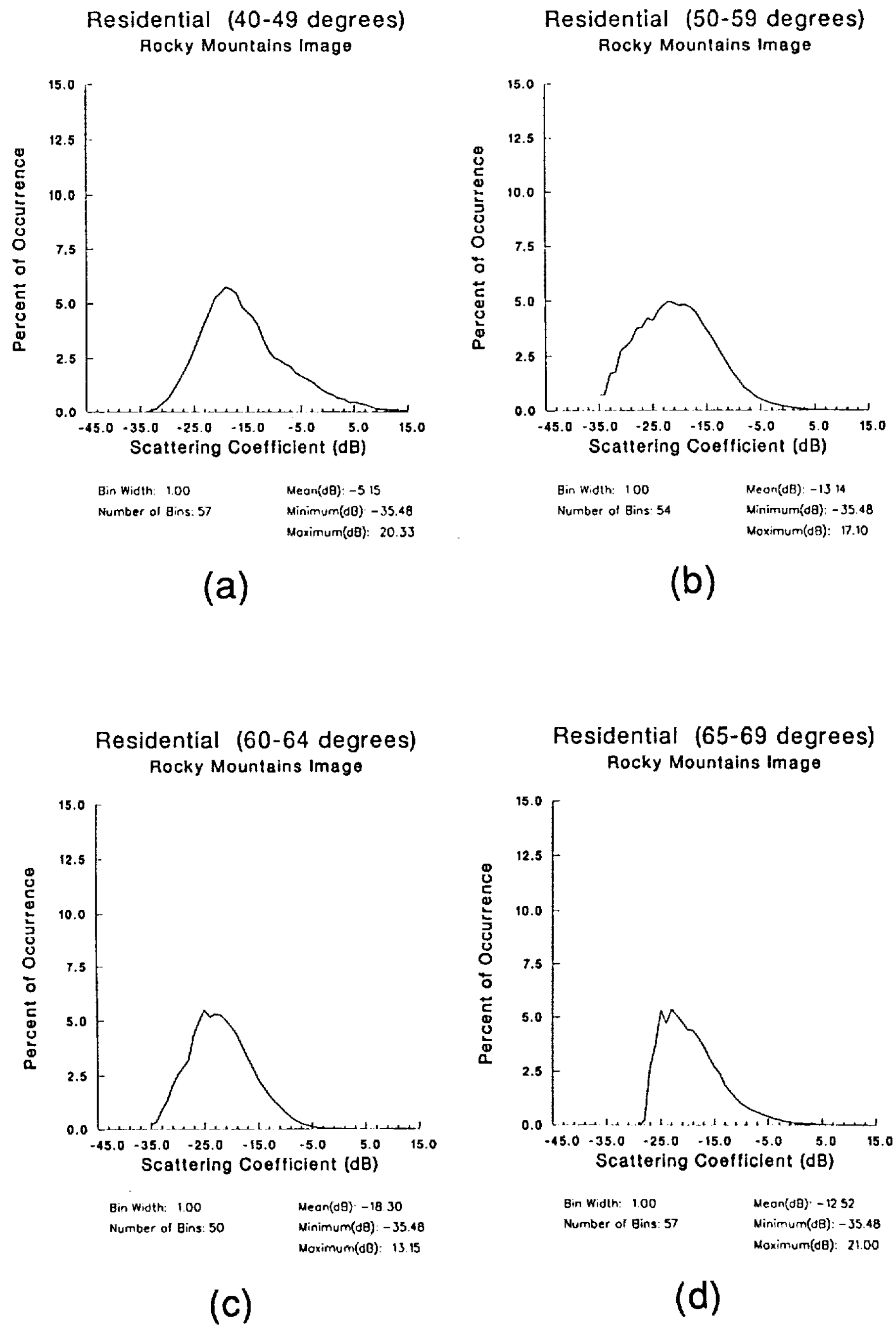

Figure 9. Clutter Distributions of Residential Areas, X-HH

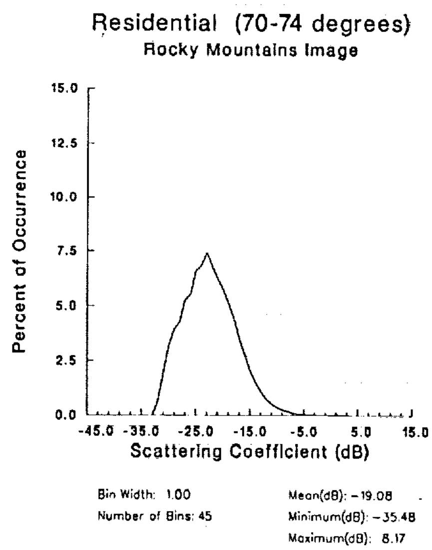

(e)

Figure 9. Clutter Distributions of Residential Areas, X-HH (cont.)

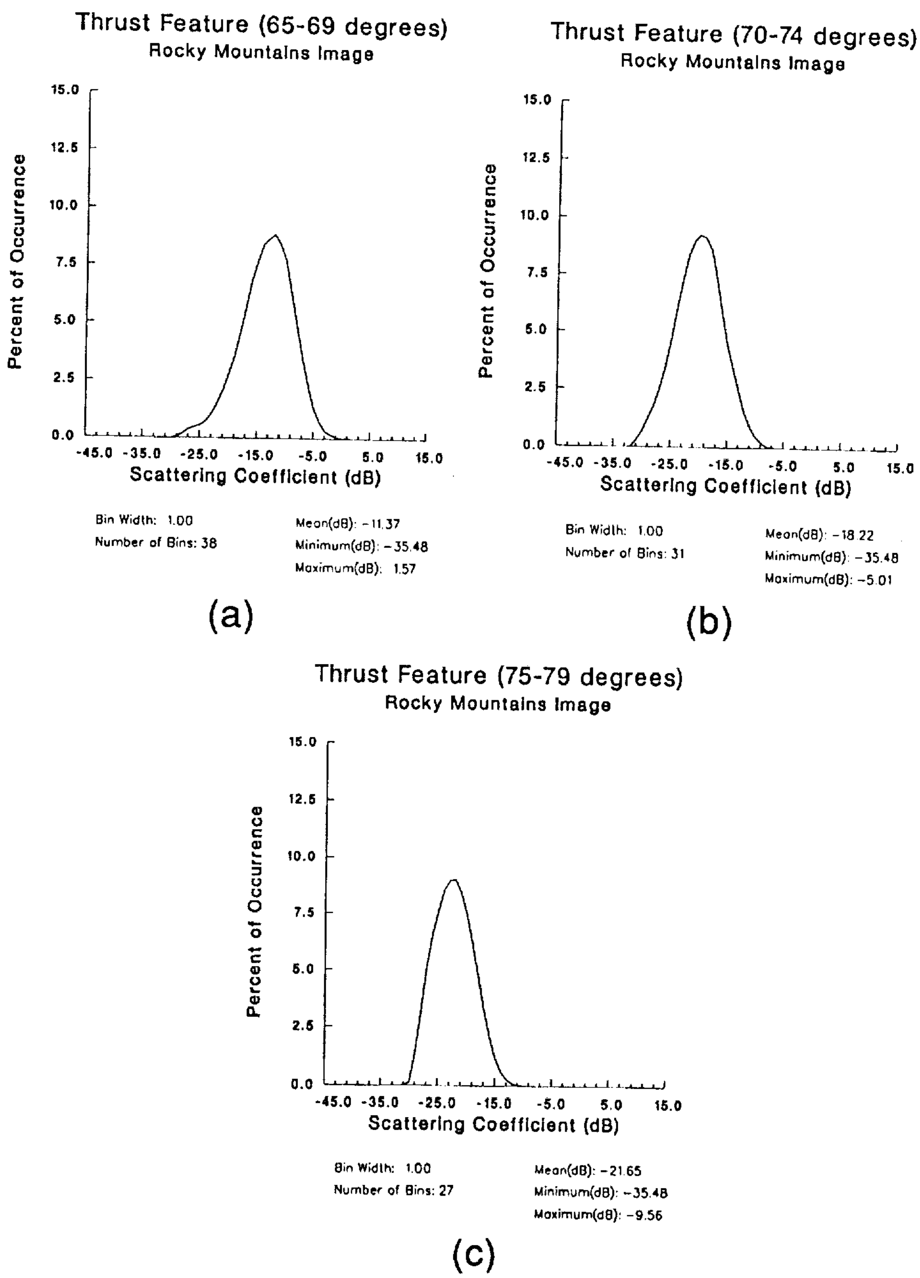

Figure 10. Clutter Distributions of Thrust Feature Areas, X-HH

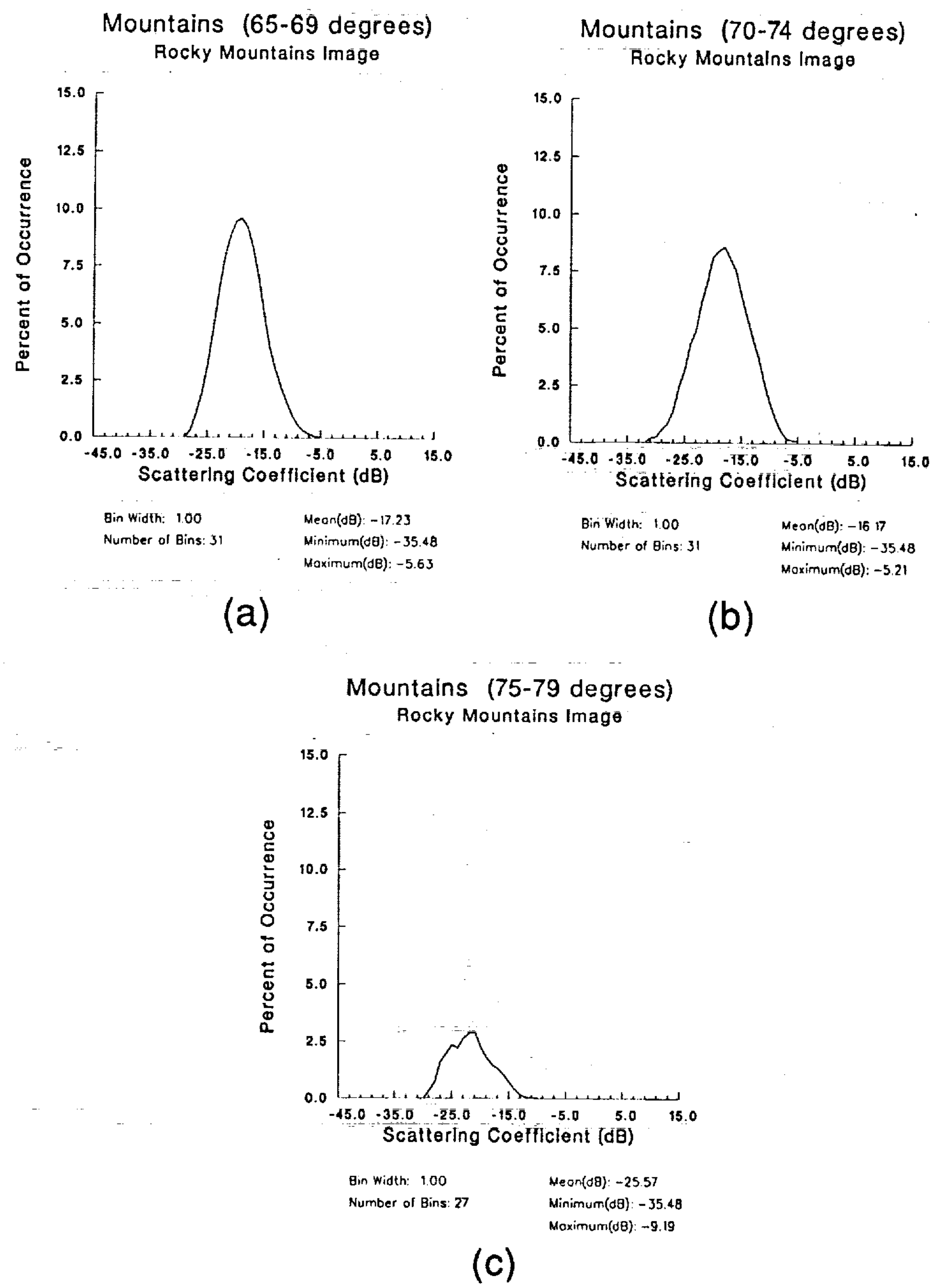

Figure 11. Clutter Distributions of Mountain Areas, X-HH

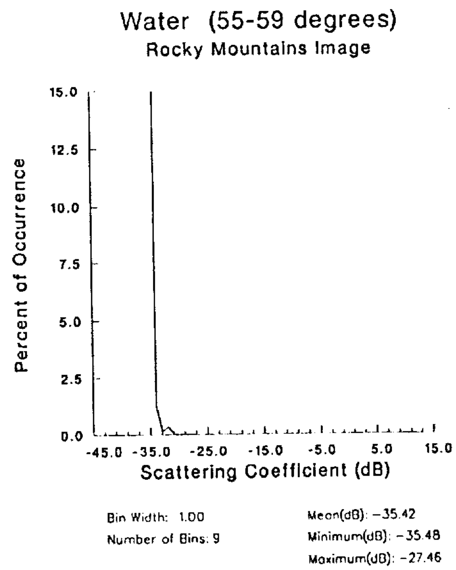

(a)

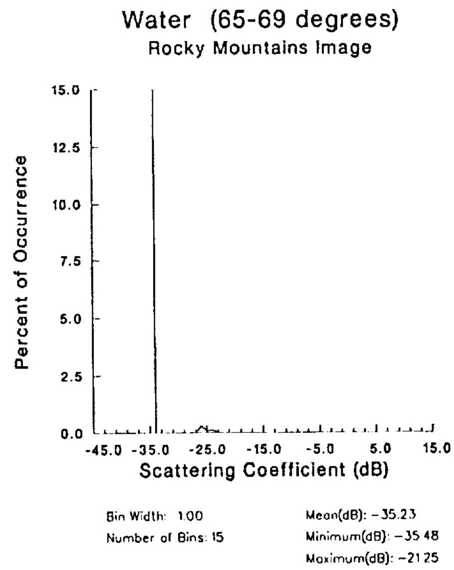

(b)

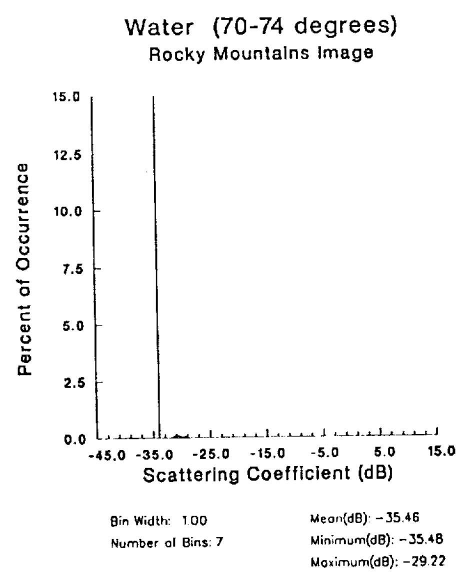

(c)

Figure 12. Clutter Distributions of Water Areas, X-HH

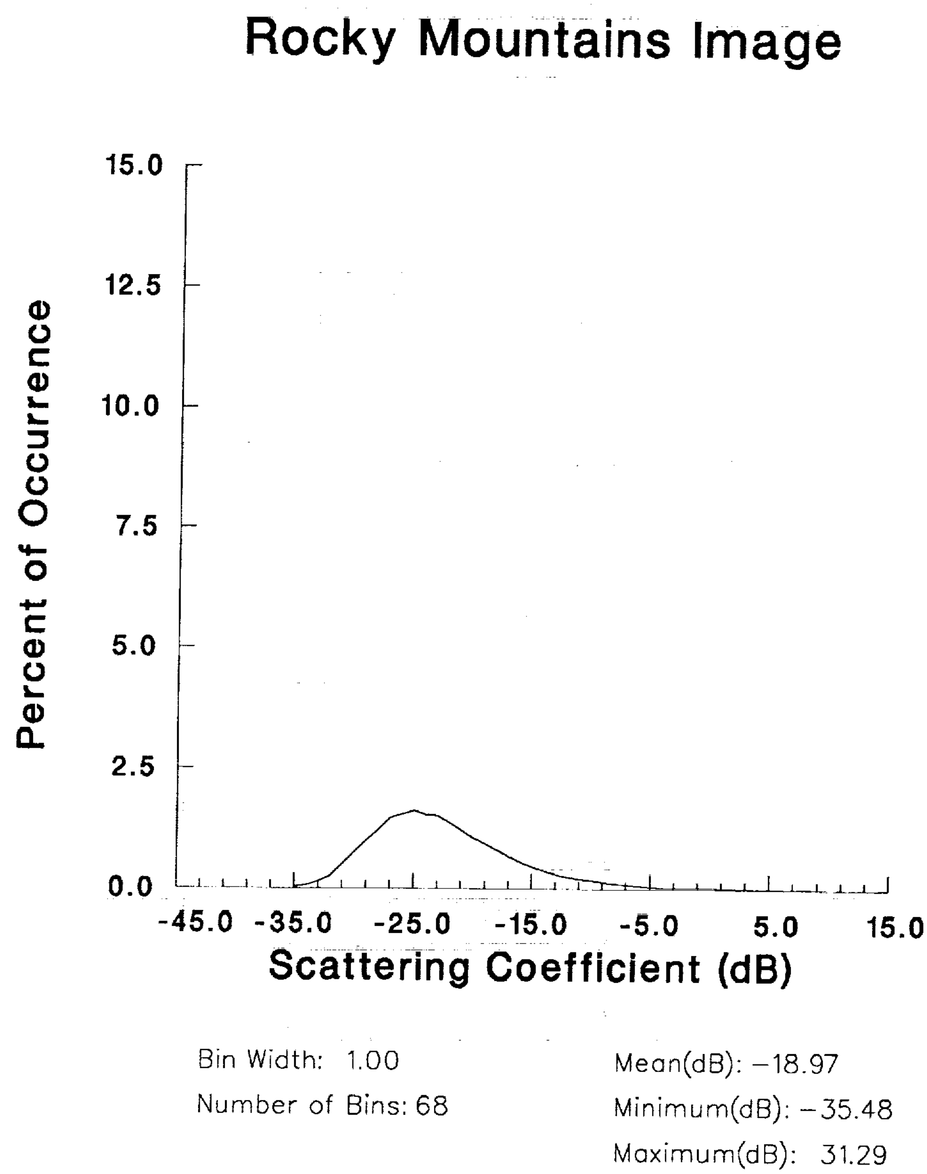

Figure 13. Clutter Distribution, Rocky Mountains Image, X-HH

90-11481

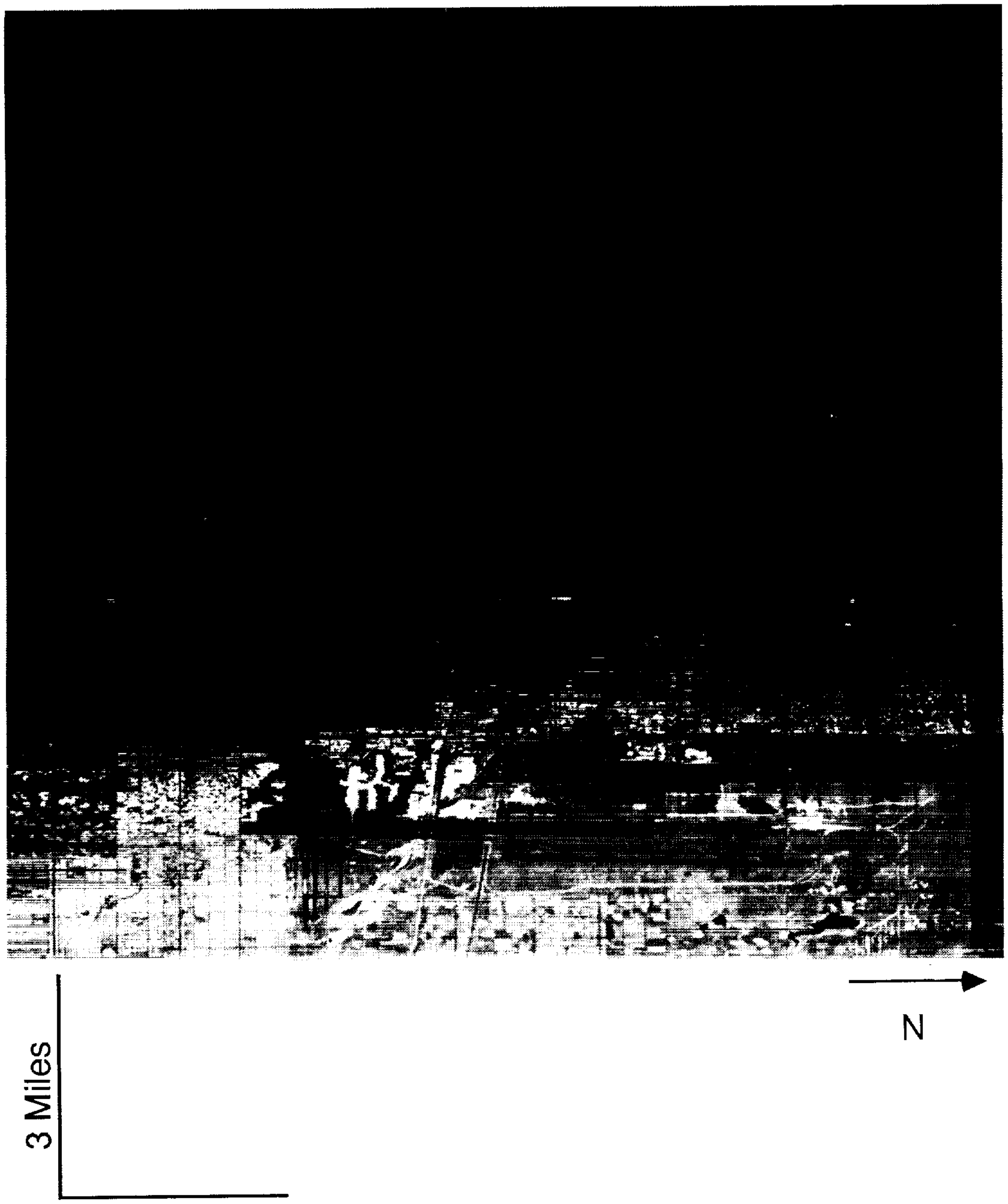

Figure 14. Low Altitude Image, X-HH

90-11482

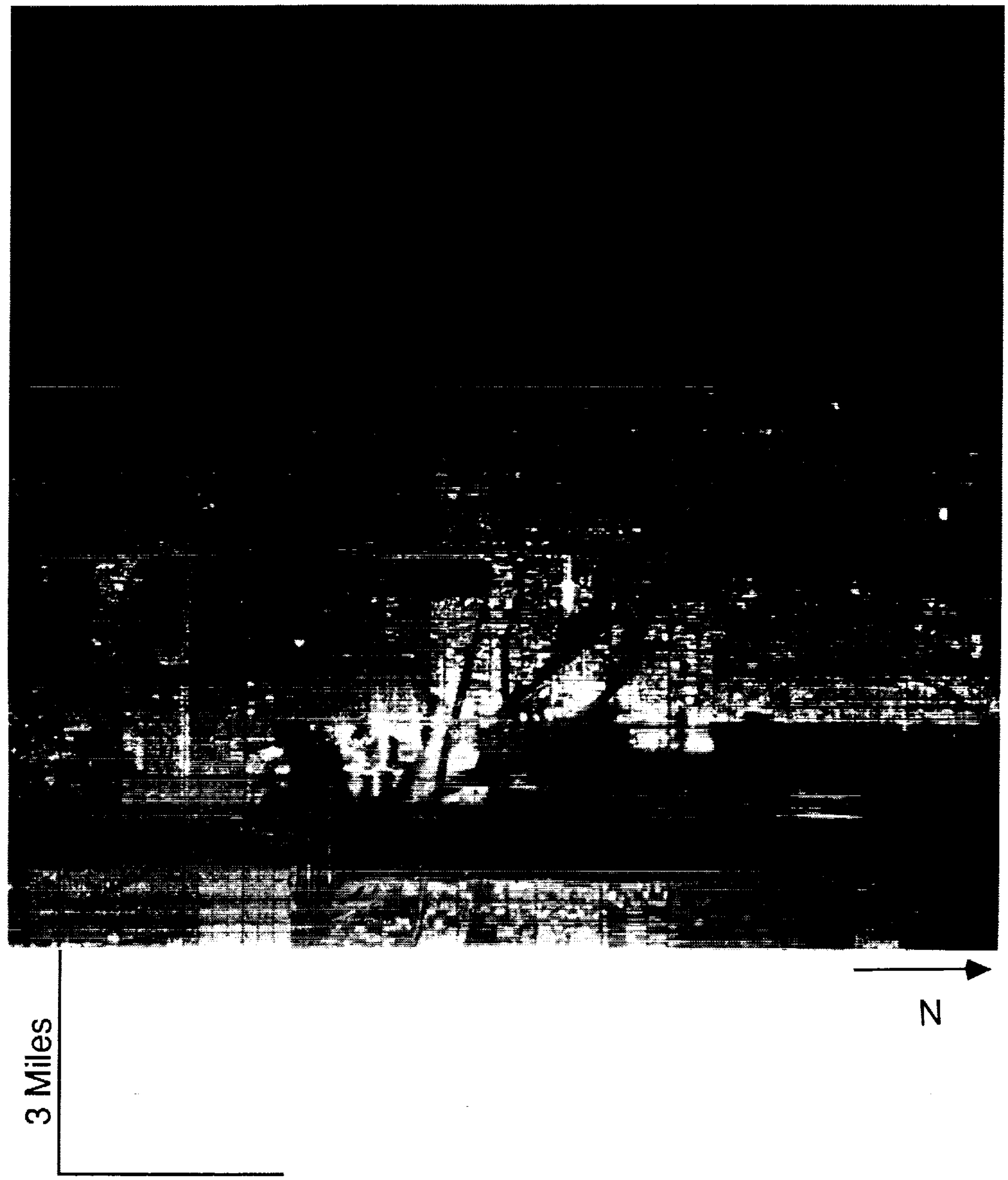

Figure 15. Low Altitude Image, X-VV

ORIGINAL PAGE IS
OF POOR QUALITY

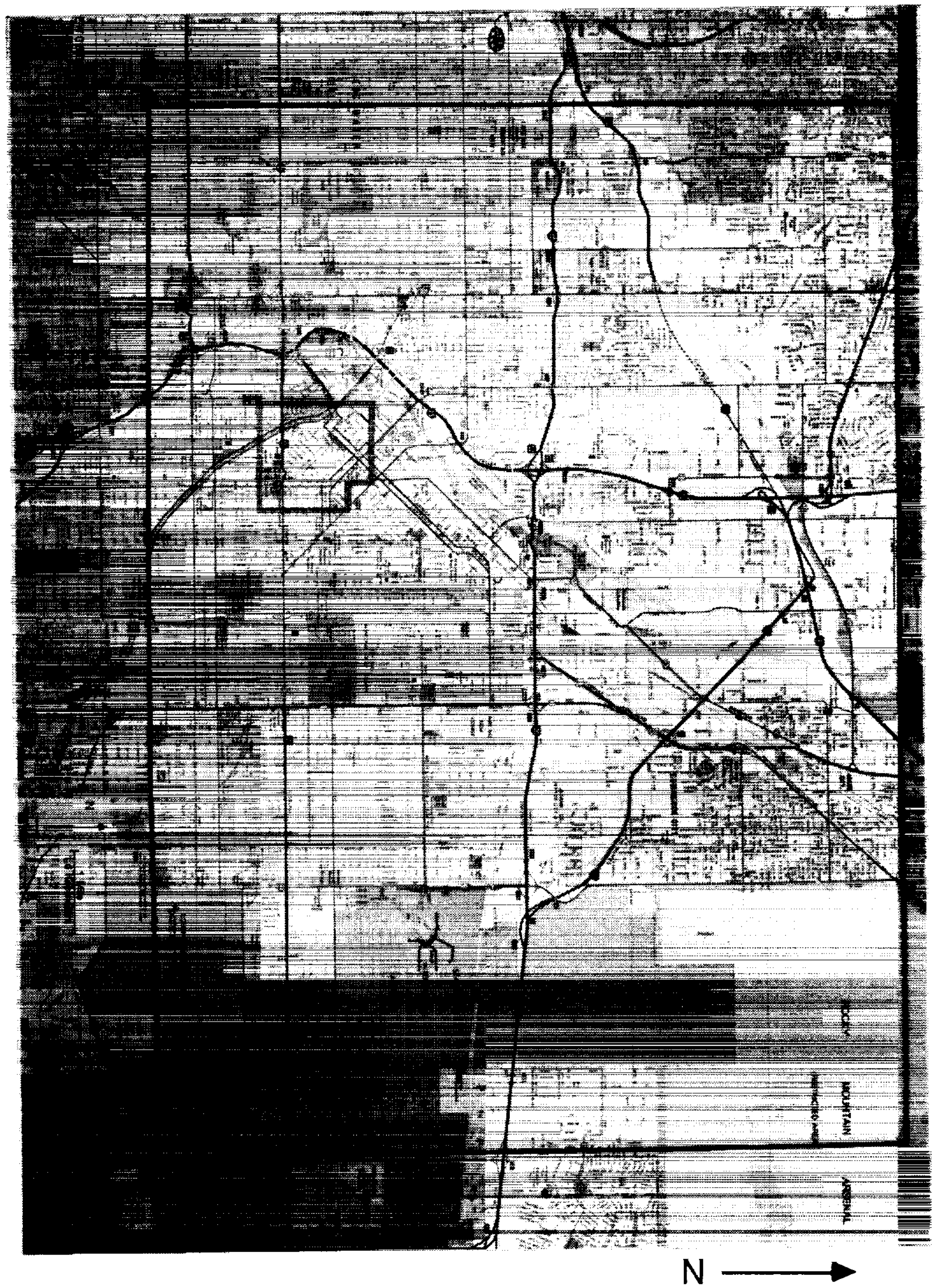

Figure 16. Ground Area Coverage of the Low Altitude Images

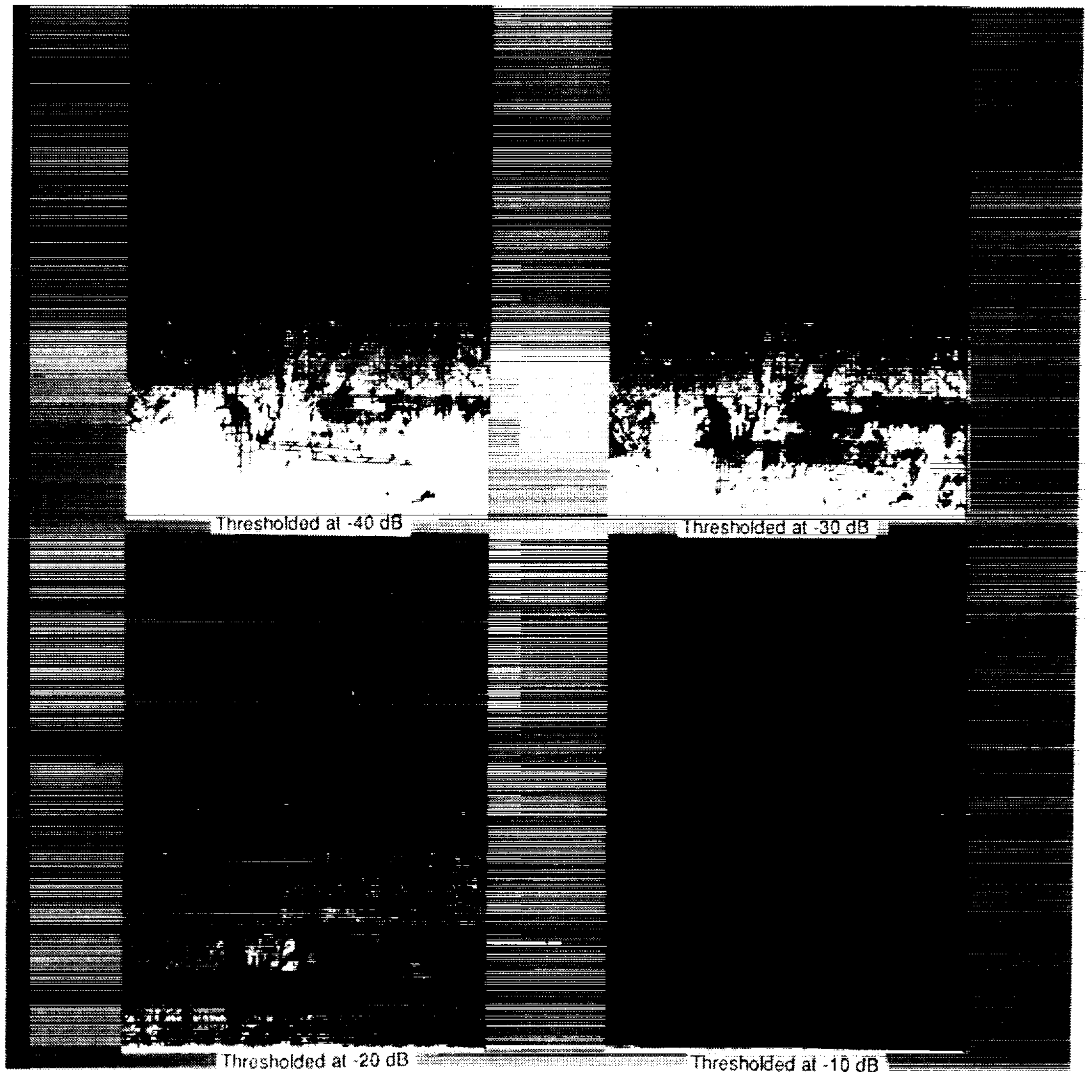

Figure 17. Threshold Images, Low Altitude Image, X-HH

ORIGINAL PAGE IS
OF POOR QUALITY

90-11484

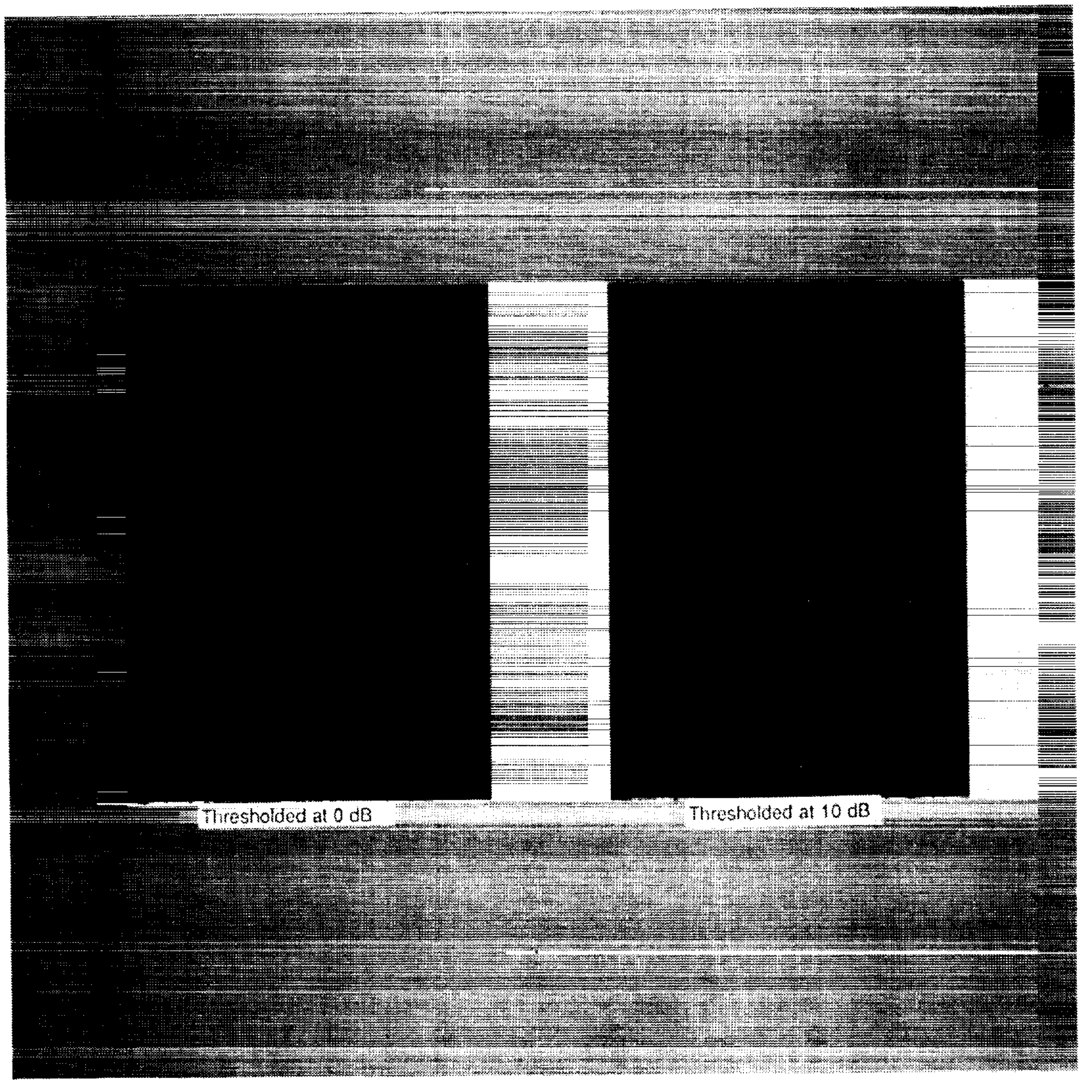

Figure 17. Threshold Images, Low Altitude Image, X-HH (cont.)

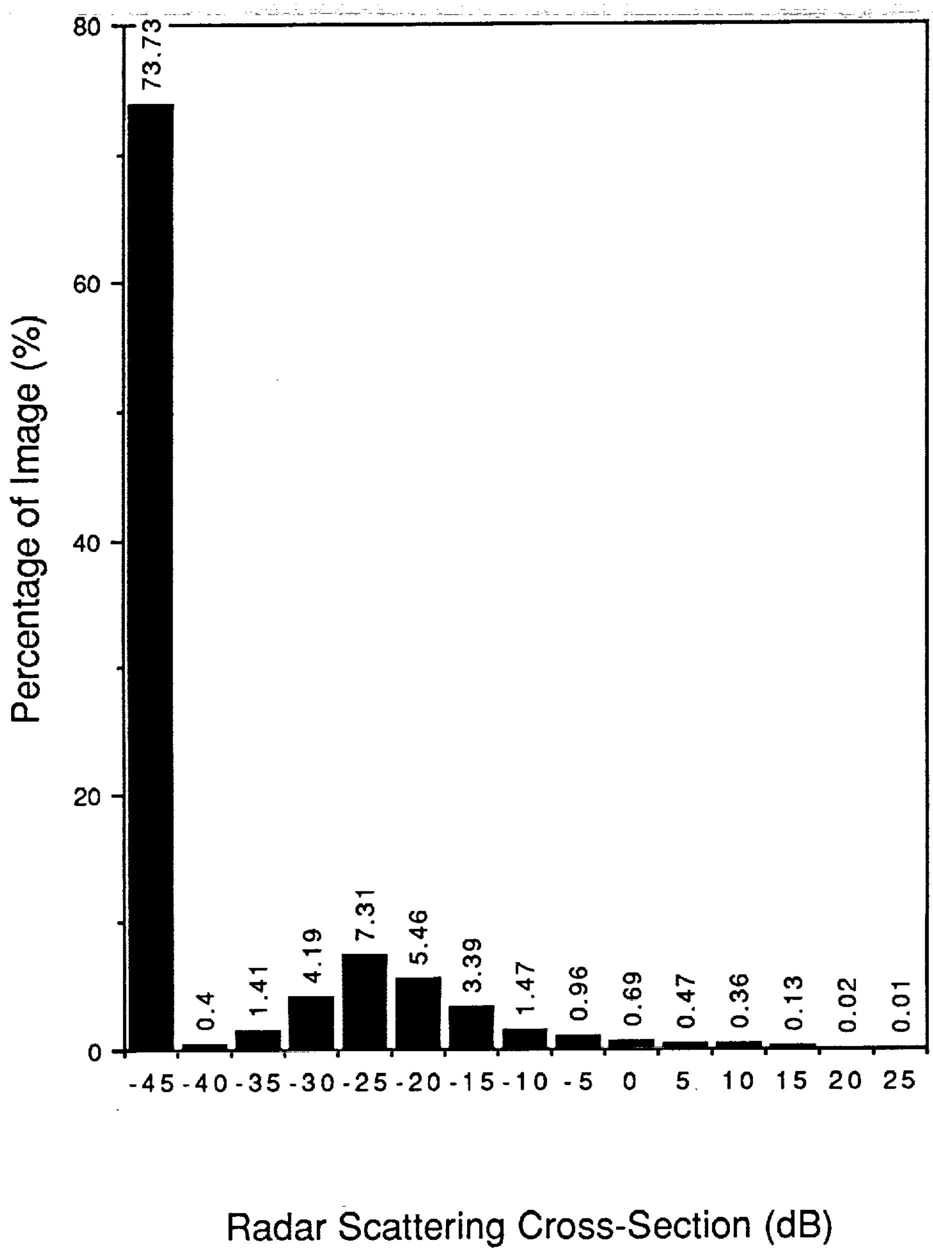

Figure 18. Distribution of Threshold Values, Low Altitude Image, X-HH

90-11485

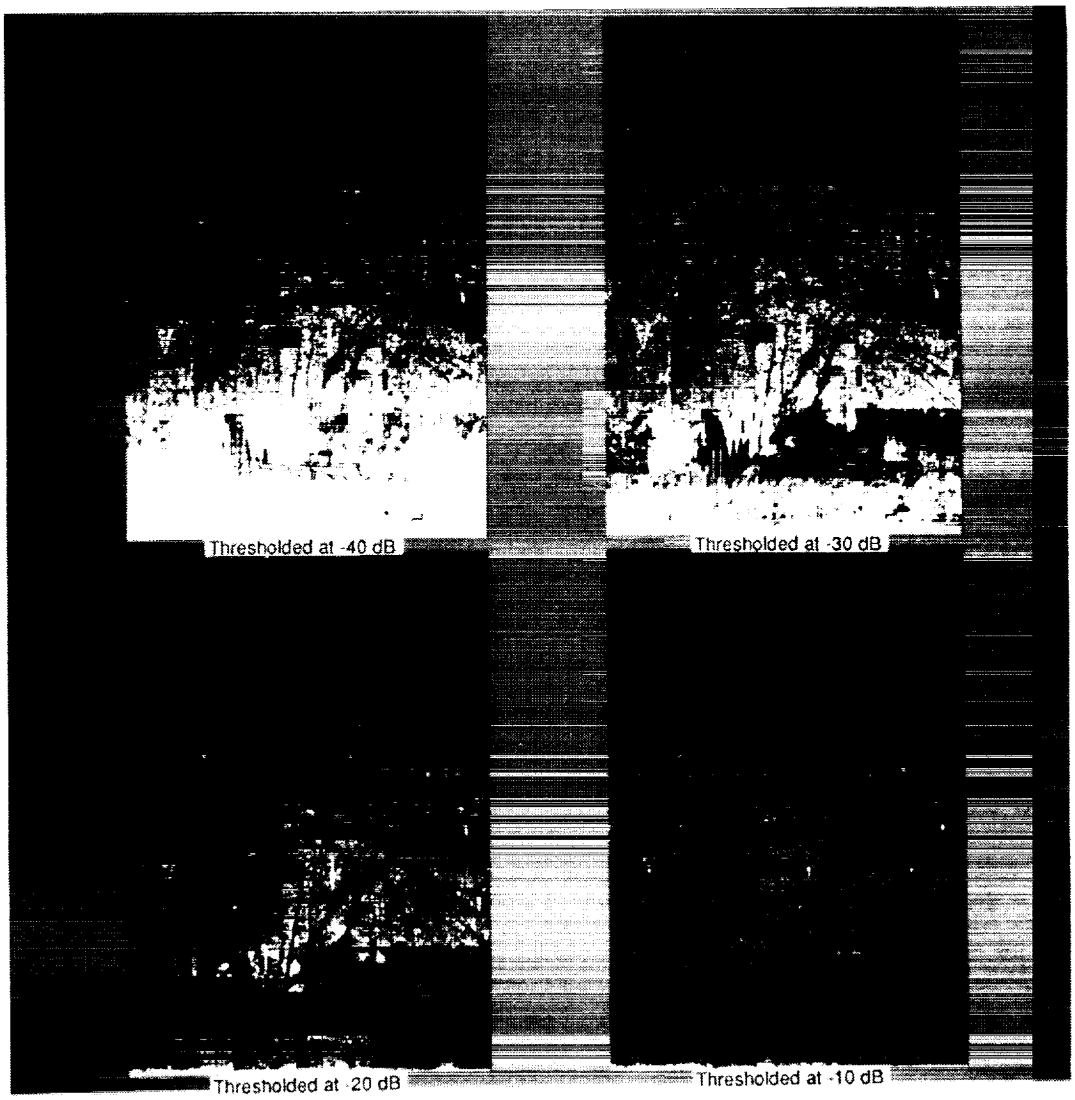

Figure 19. Threshold Images, Low Altitude Image, X-VV

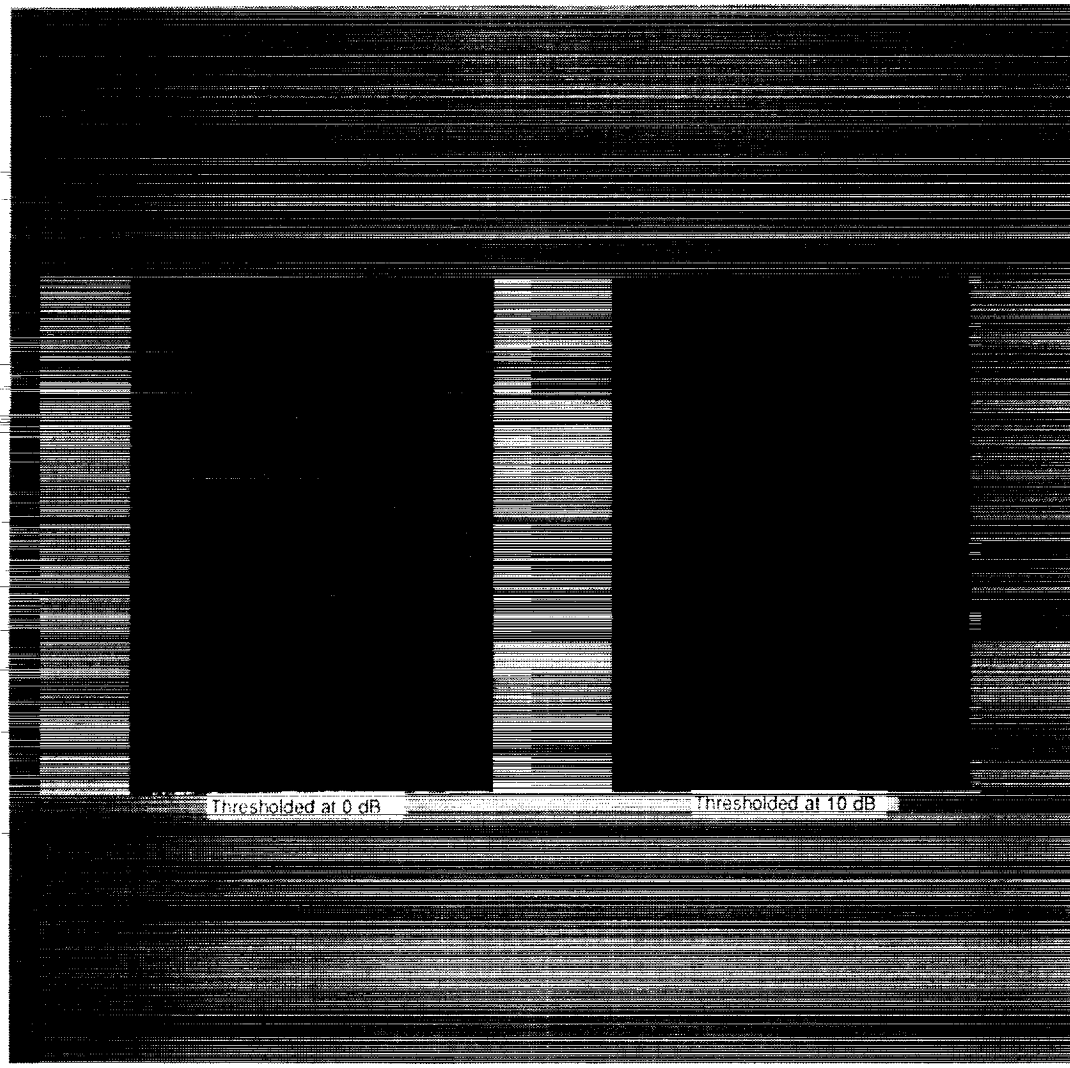

Figure 19. Threshold Images, Low Altitude Image, X-VV (cont.)

ORIGINAL PAGE IS
OF POOR QUALITY

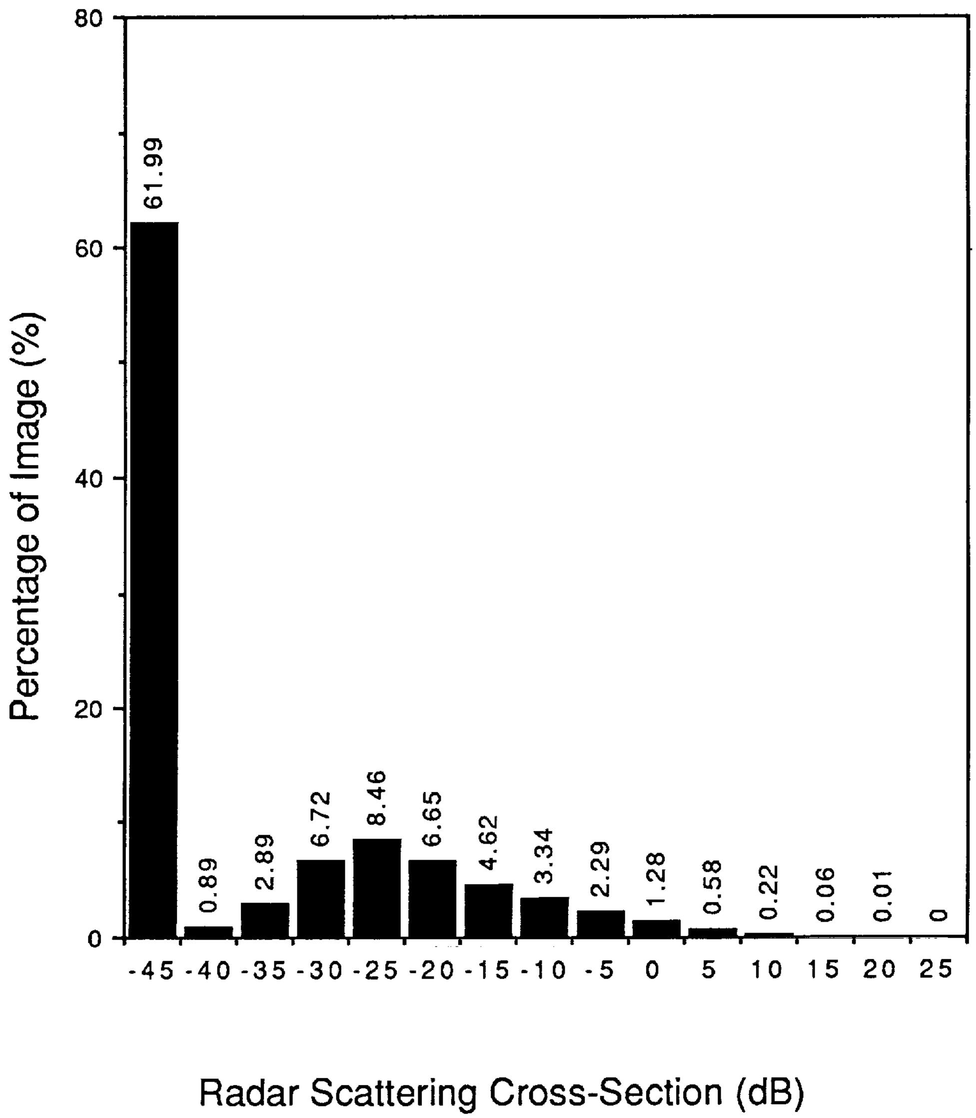

Figure 20. Distribution of Threshold Values, Low Altitude Image, X-VV

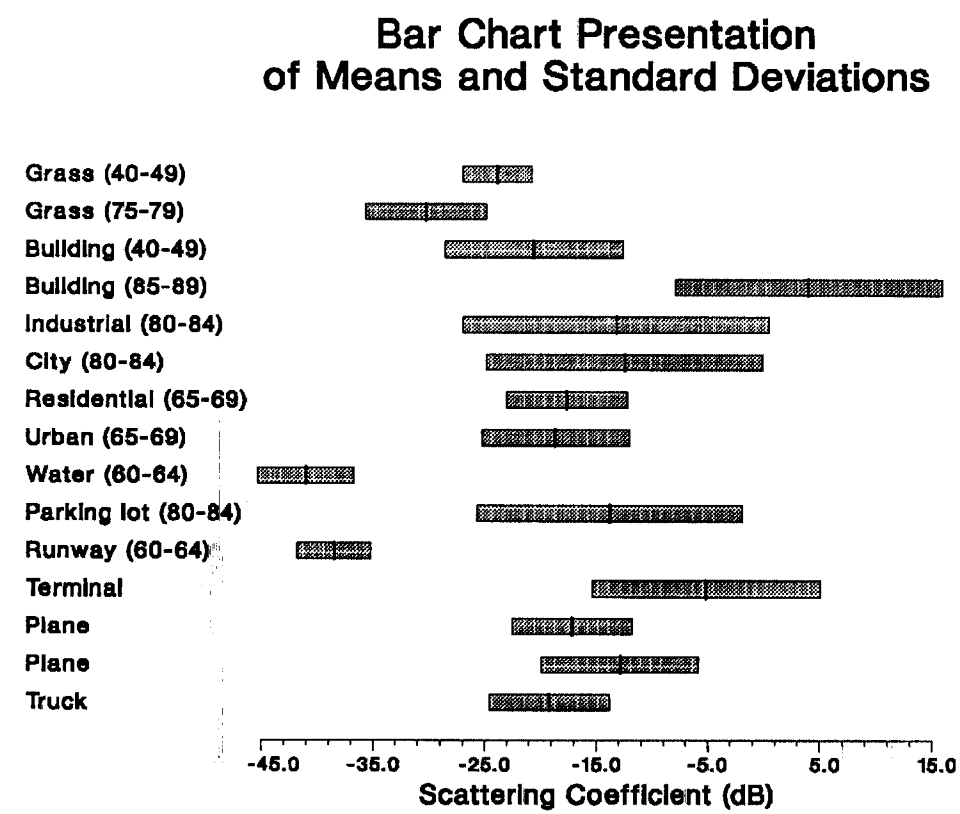

Figure 21. Mean Scattering Coefficient Values, Low Altitude Image, X-HH

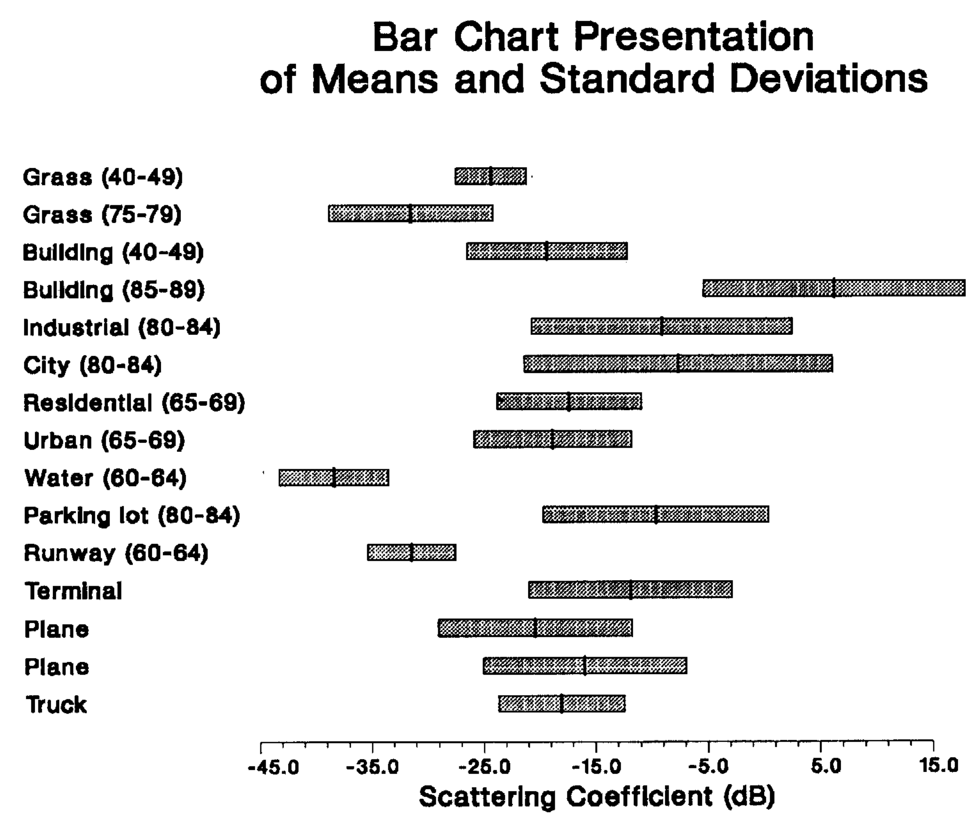

Figure 22. Mean Scattering Coefficient Values, Low Altitude Image, X-VV

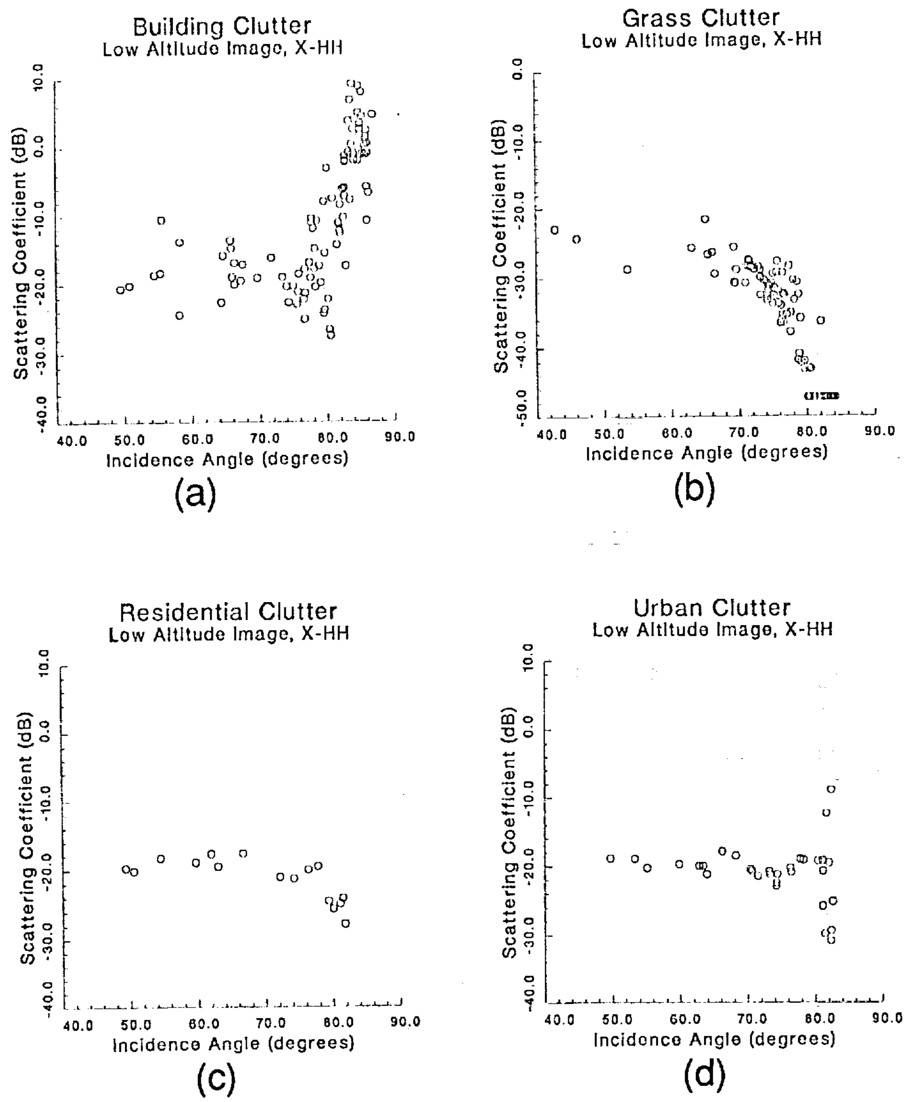

Figure 23. Scattering Coefficient vs. Incidence Angle Plots, X-HH

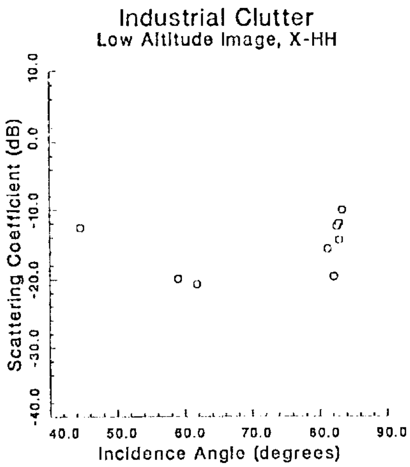

(e)

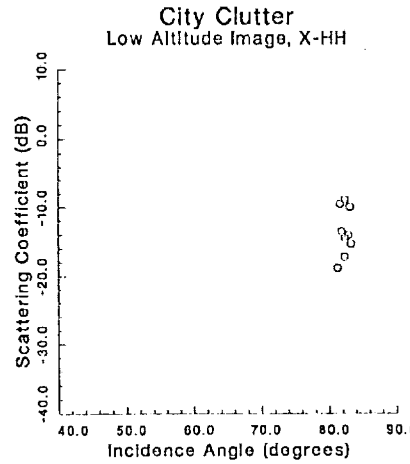

(f)

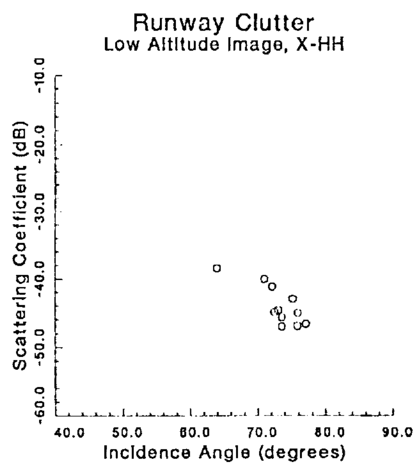

(g)

Figure 23. Scattering Coefficient vs. Incidence Angle Plots, X-HH (cont.)

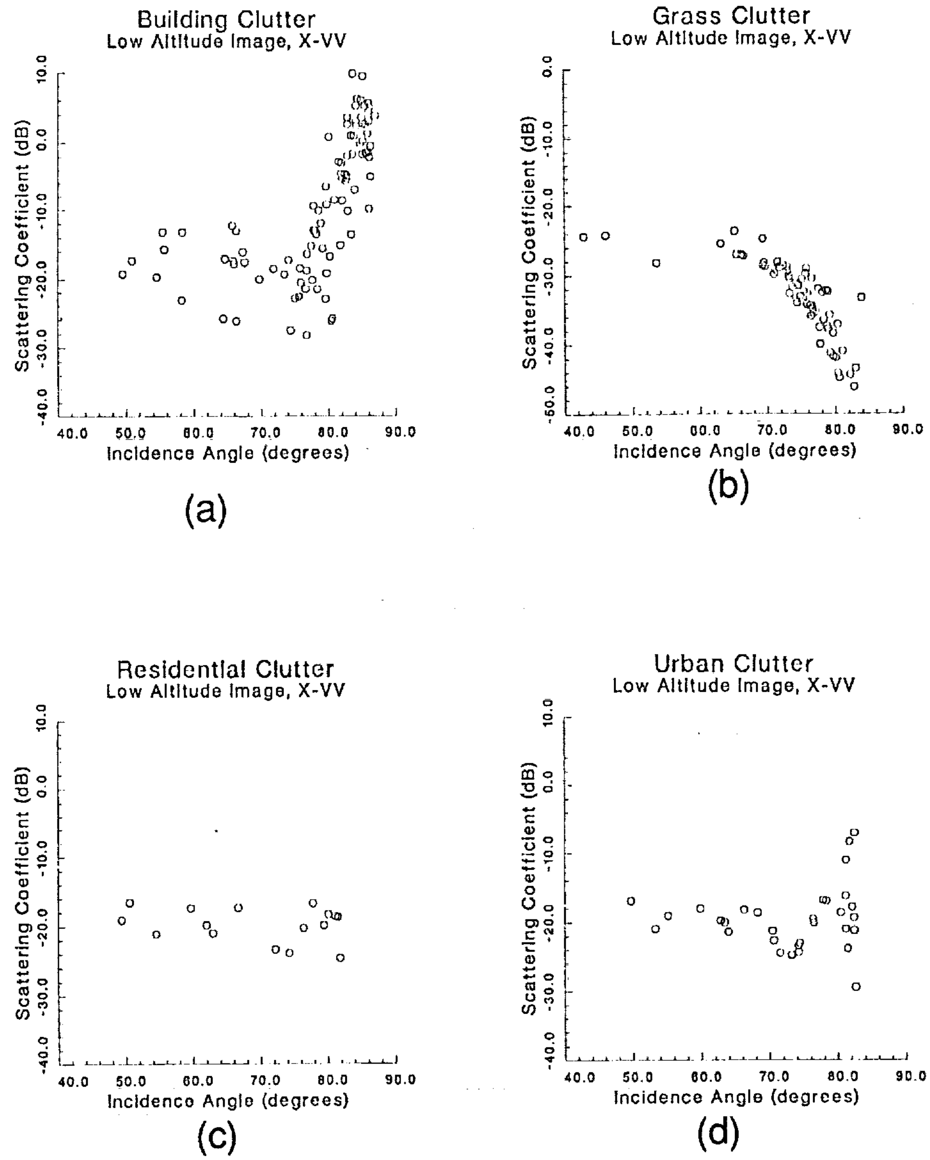

Figure 24. Scattering coefficient vs. Incidence Angle Plots, X-VV

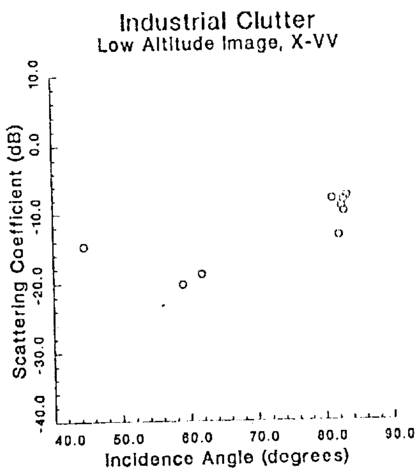

(e)

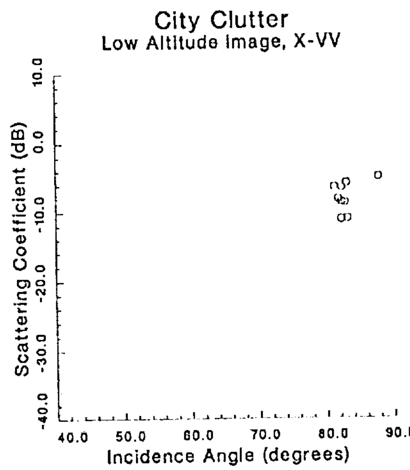

(f)

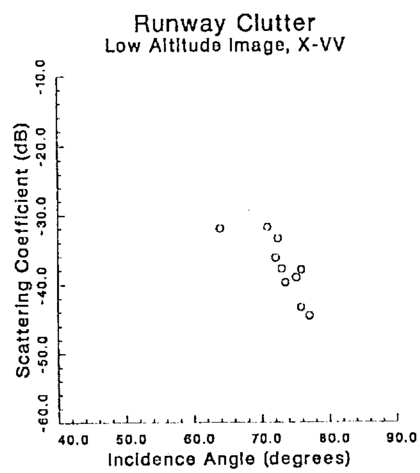

(g)

Figure 24. Scattering Coefficient vs. Incidence Angle Plots, X-VV (cont.)

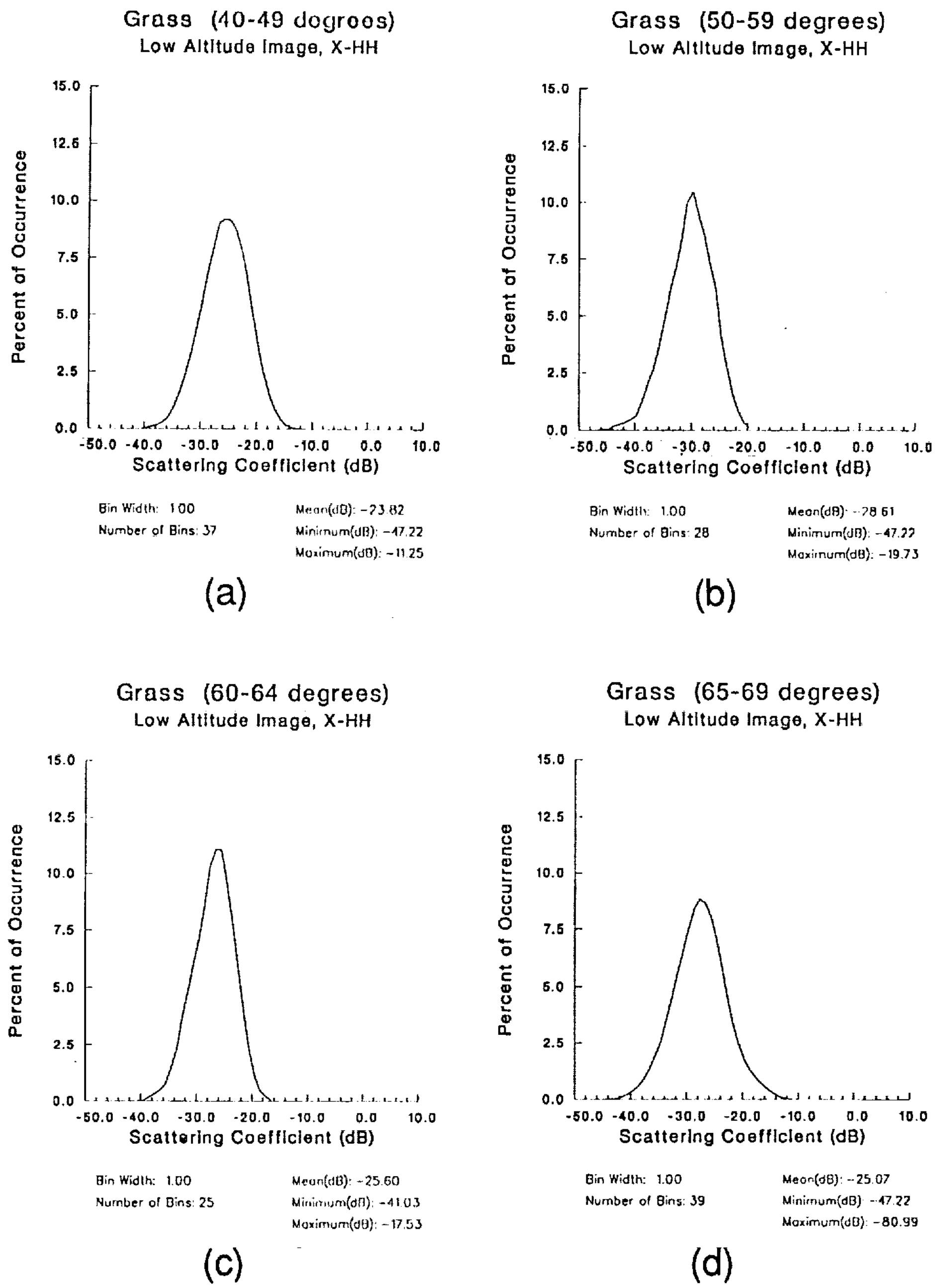

Figure 25. Clutter Distributions of Grass Areas, X-HH

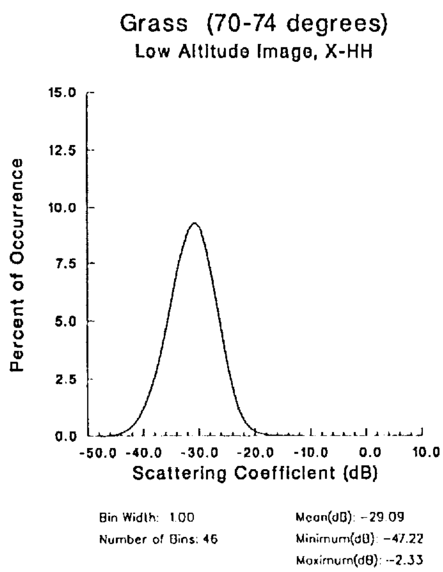

(e)

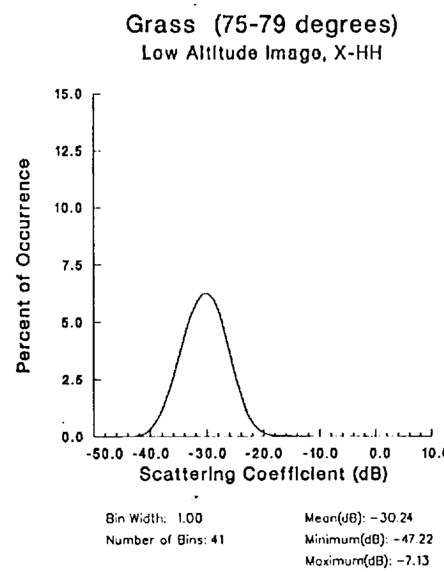

(f)

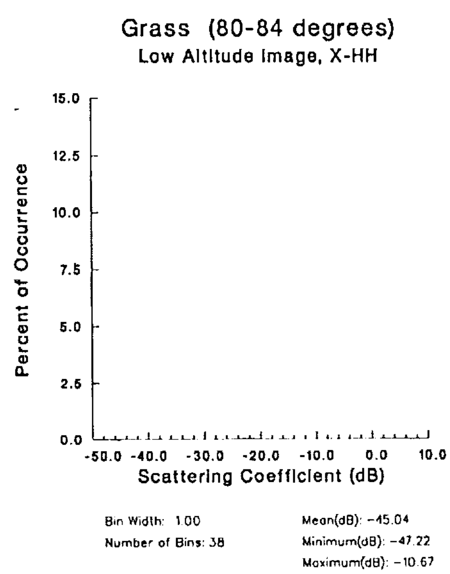

(g)

Figure 25. Clutter Distributions of Grass Areas, X-HH (cont.)

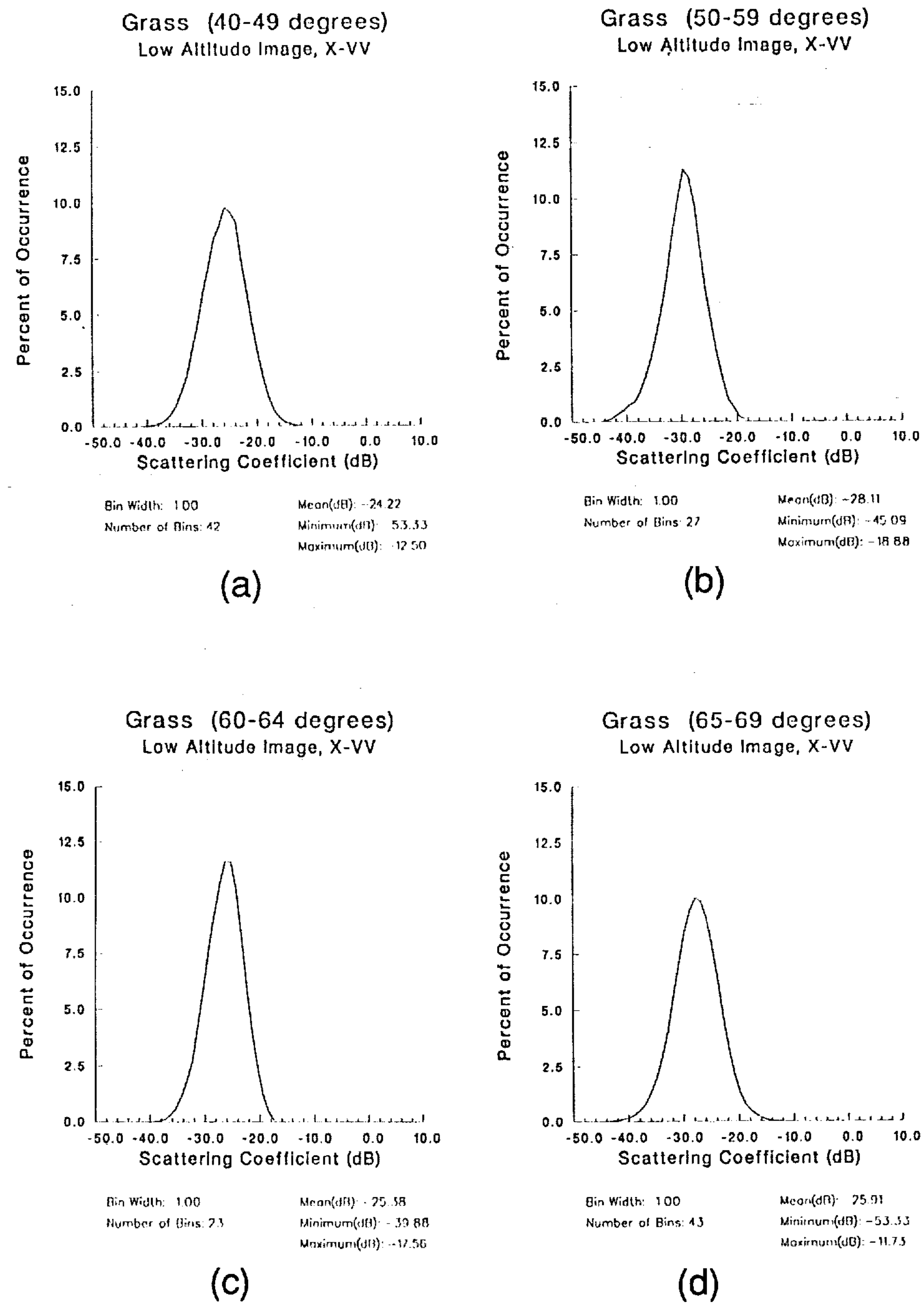

Figure 26. Clutter Distributions of Grass Areas, X-VV

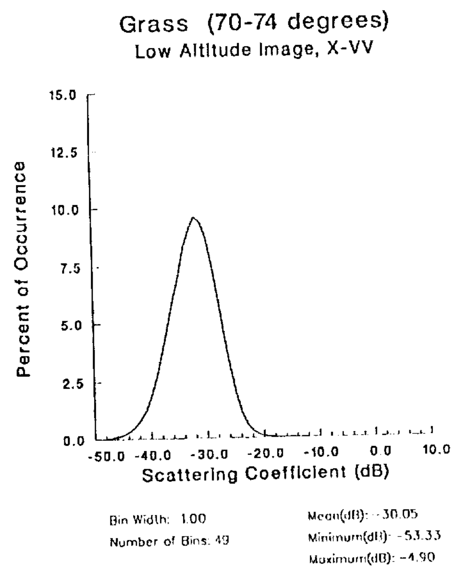

(e)

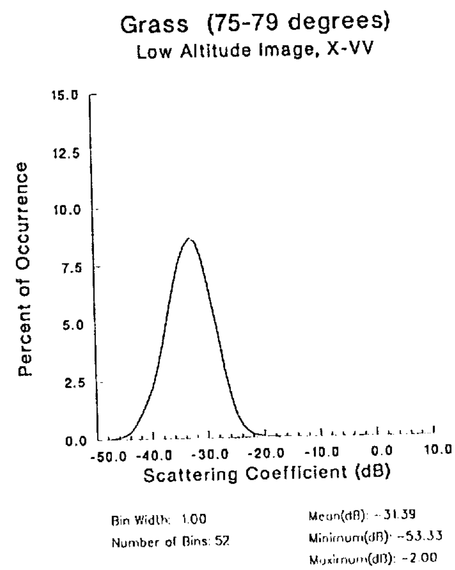

(f)

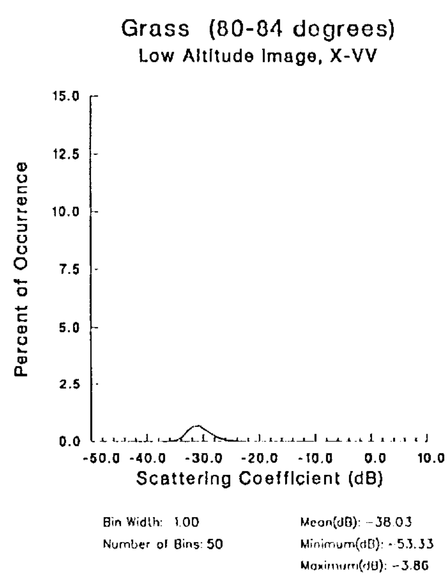

(g)

Figure 26. Clutter Distributions of Grass Areas, X-VV (cont.)

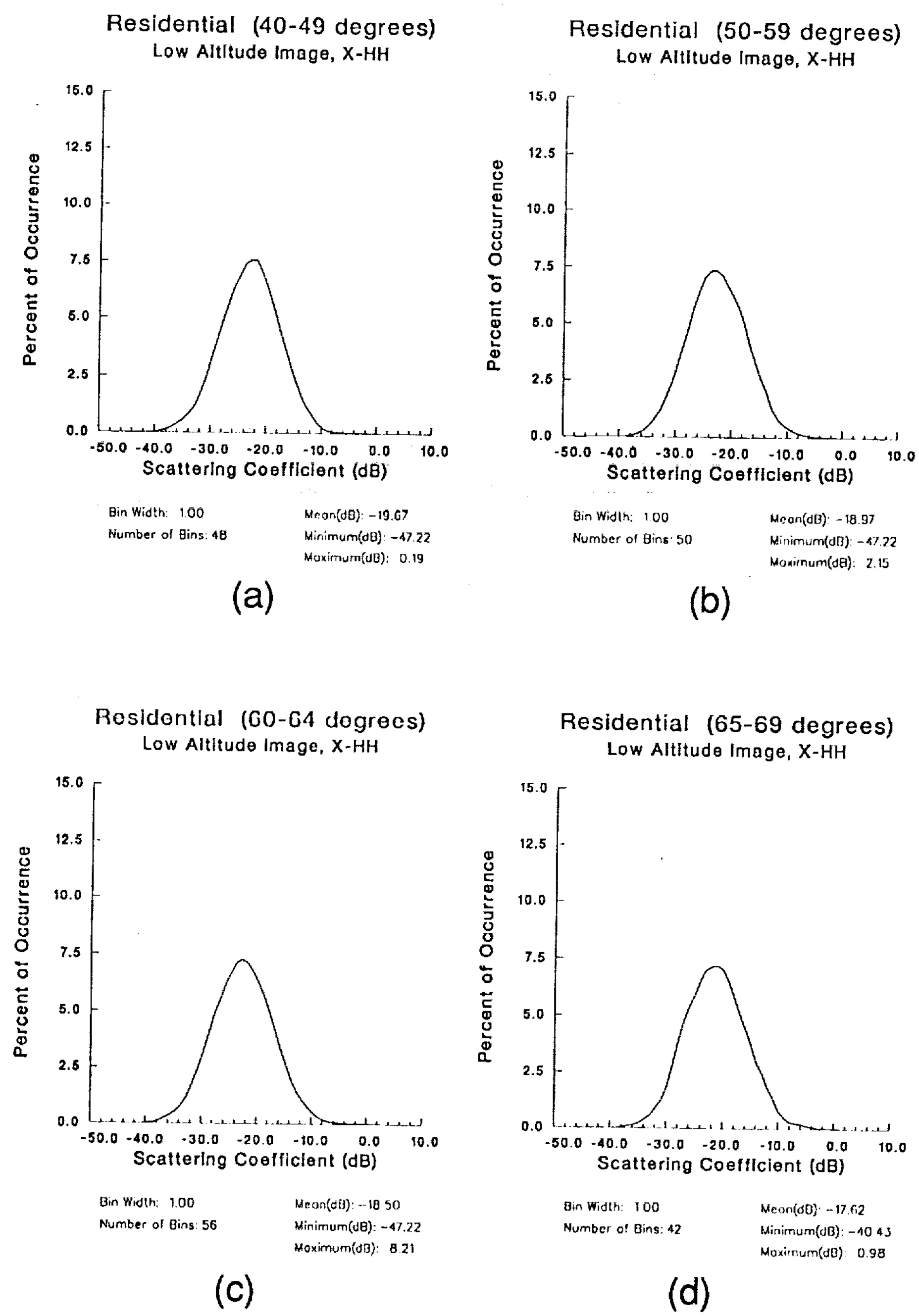

Figure 27. Clutter Distributions of Residential Areas, X-HH

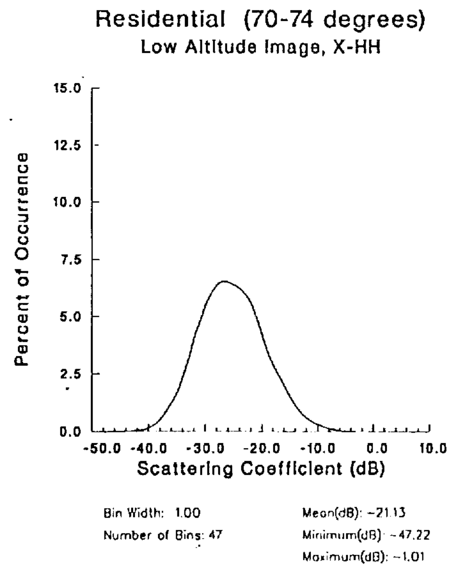

(e)

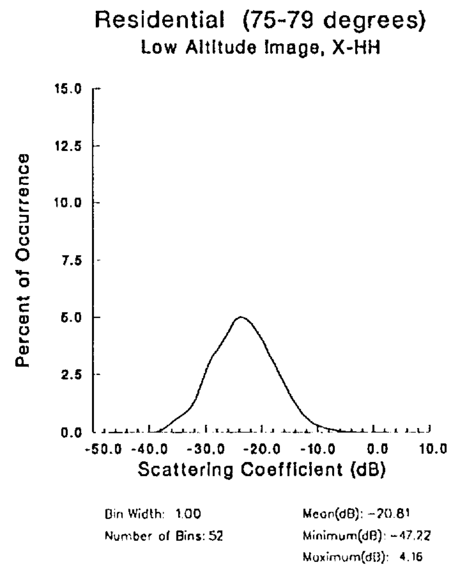

(f)

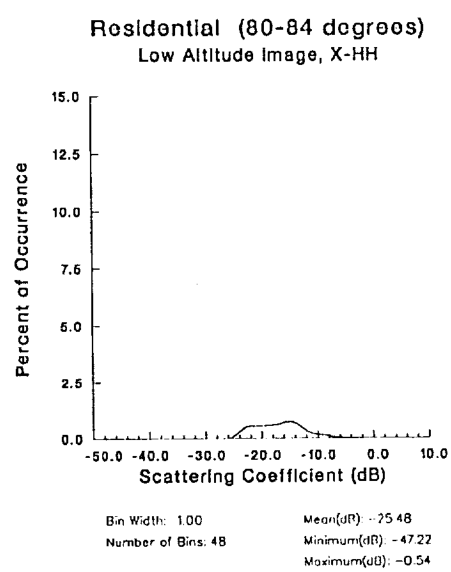

(g)

Figure 27. Clutter Distributions of Residential Areas, X-HH (cont.)

C-2

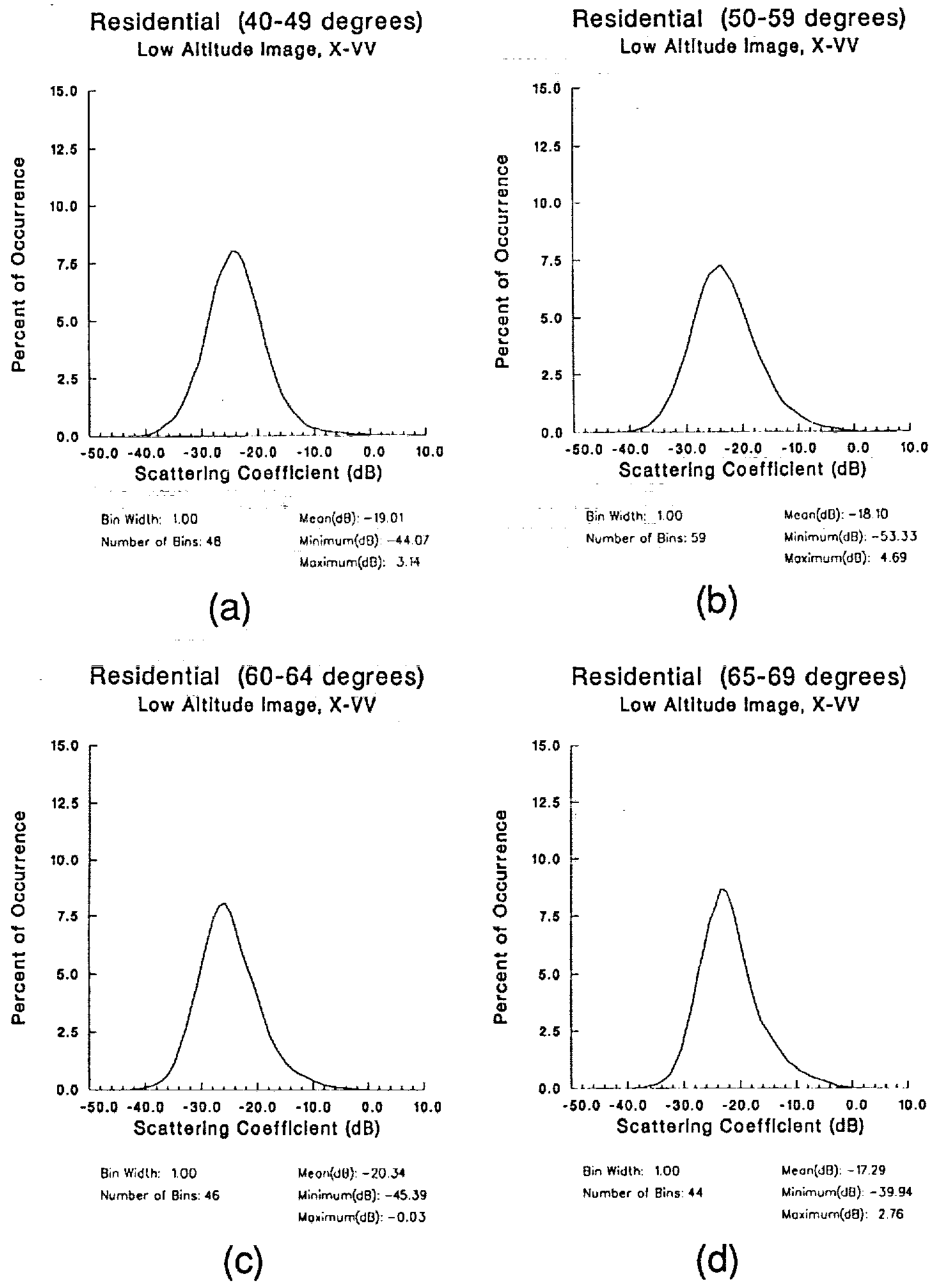

Figure 28. Clutter Distributions of Residential Areas, X-VV

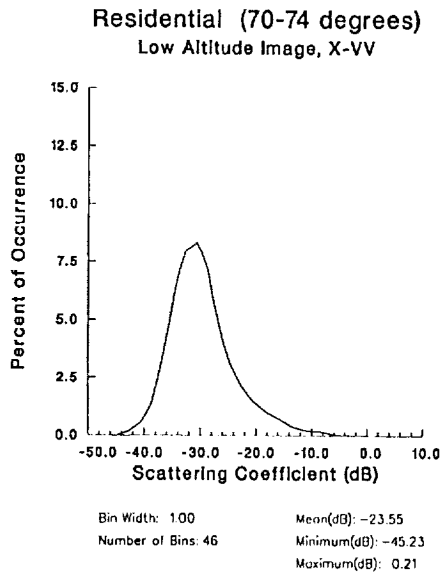

(e)

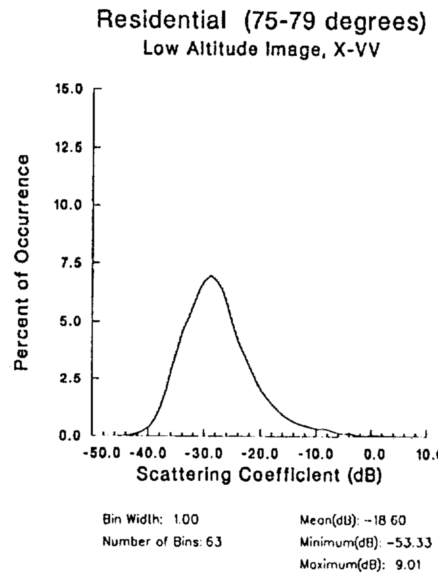

(f)

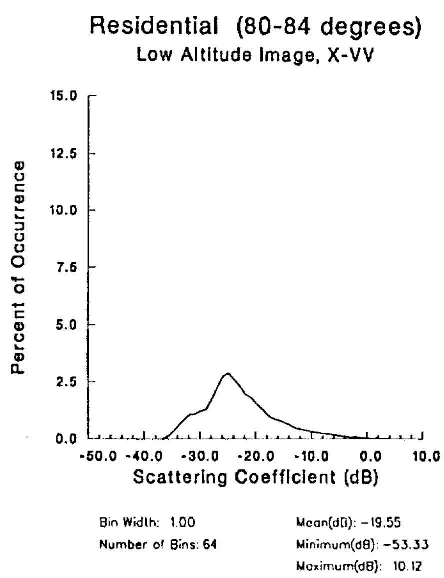

(g)

Figure 28. Clutter Distributions of Residential Areas, X-VV (cont.)

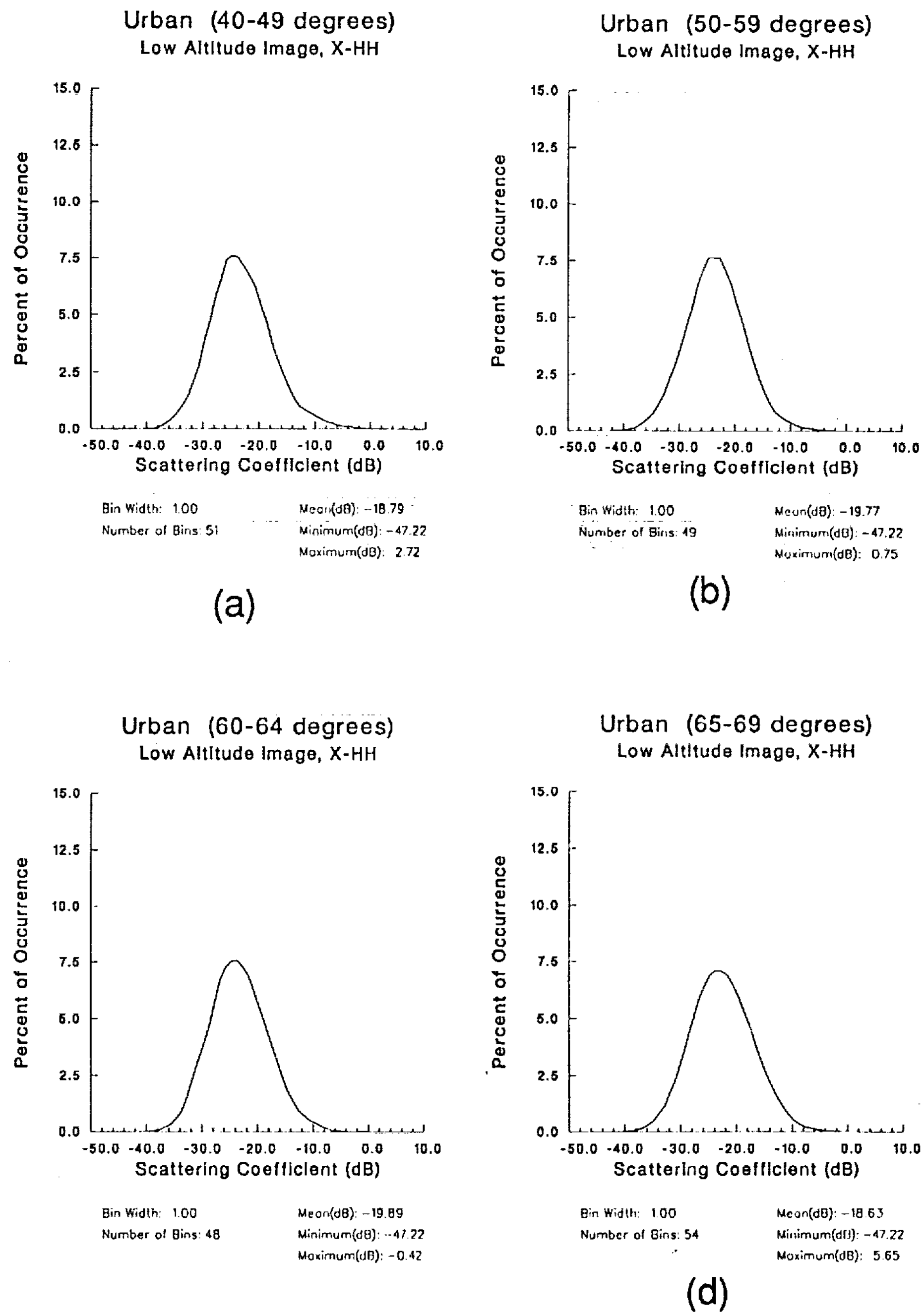

Figure 29. Clutter Distributions of Urban Areas, X-HH

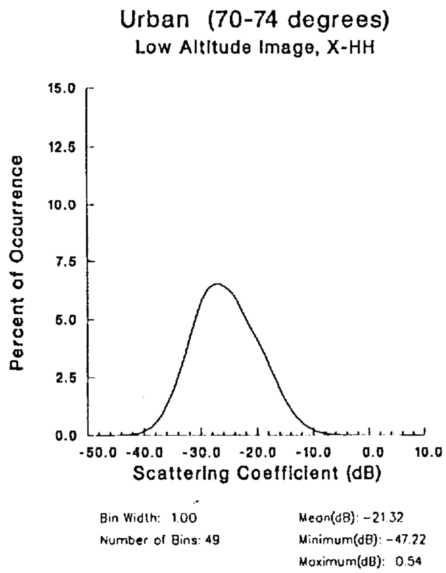

(e)

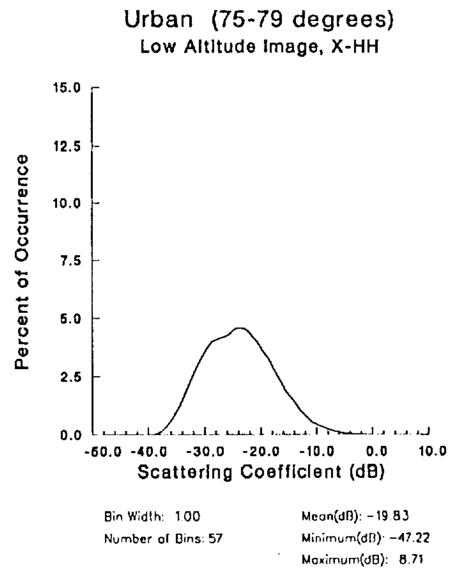

(f)

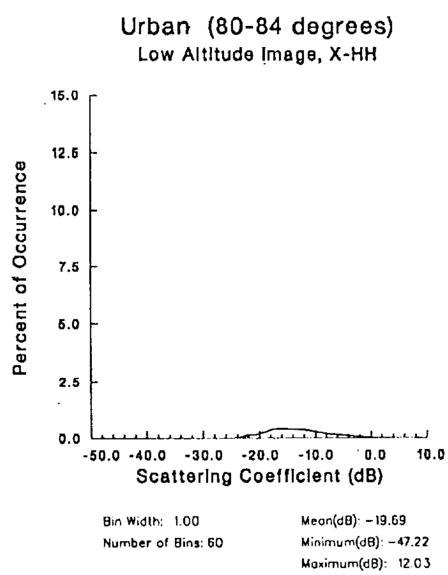

(g)

Figure 29. Clutter Distributions of Residential Areas, X-HH (cont.)

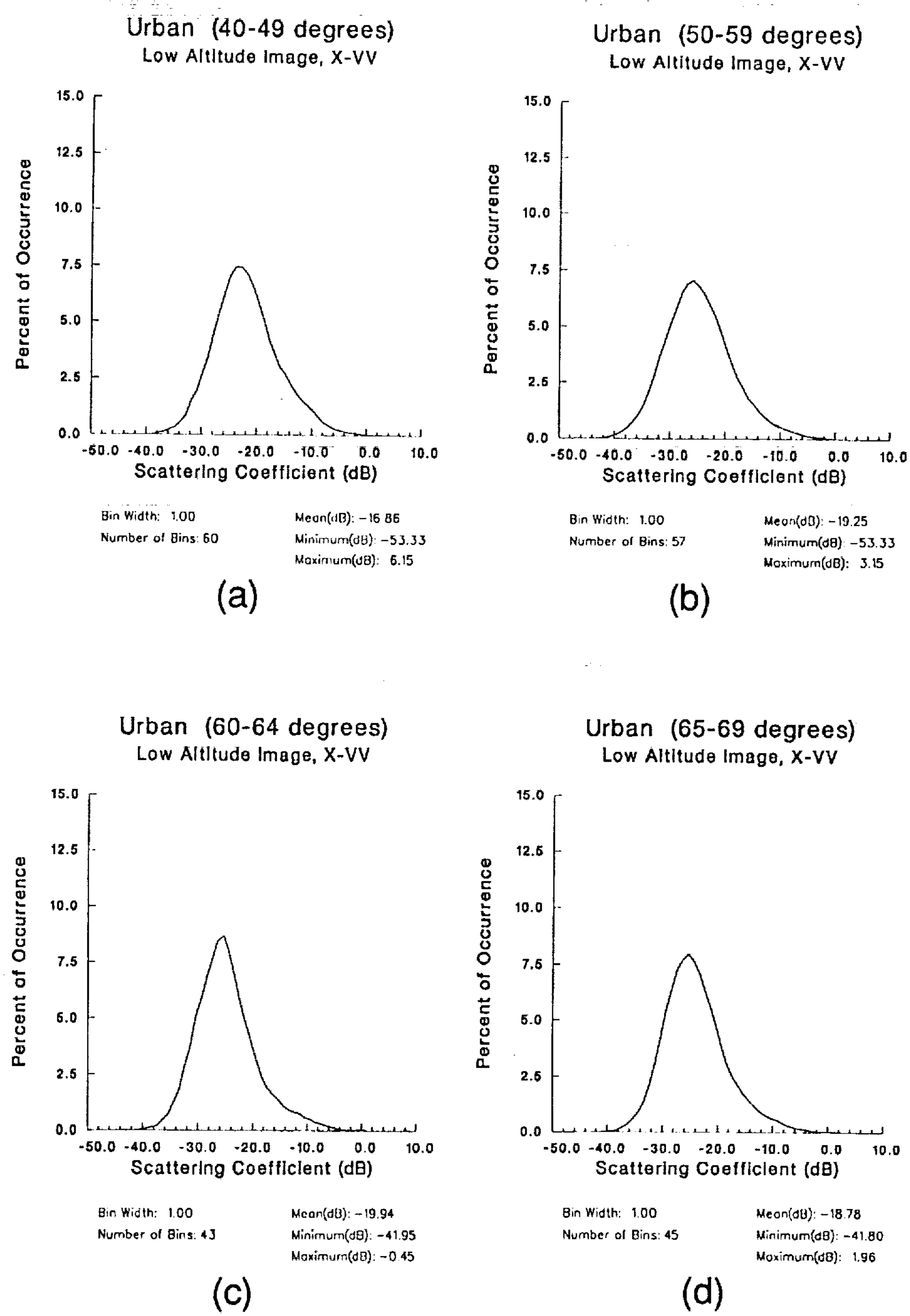

Figure 30. Clutter Distributions of Urban Areas, X-VV

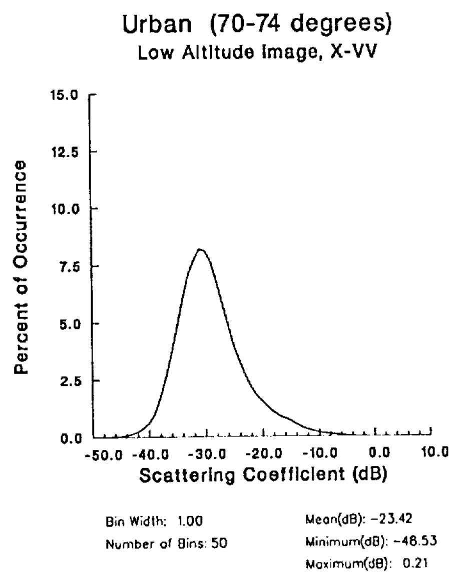

(e)

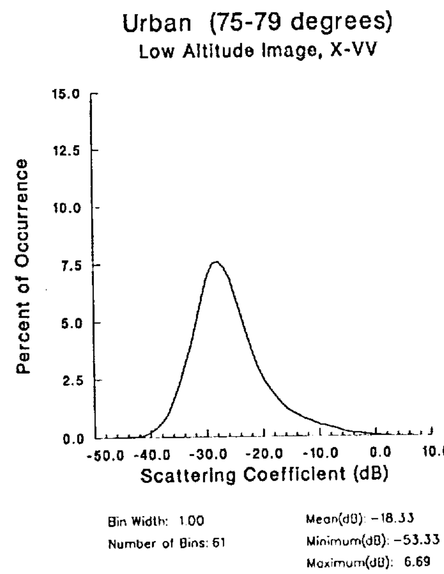

(f)

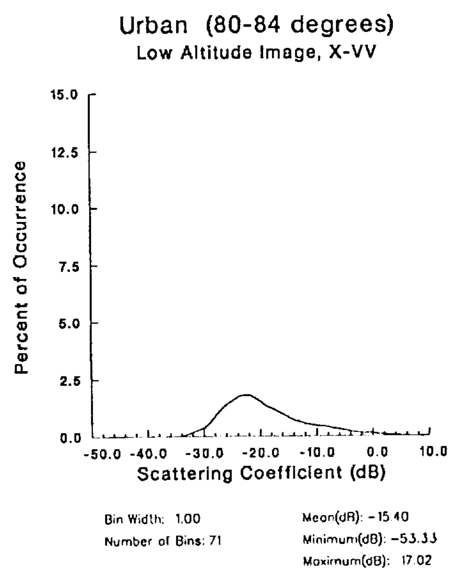

(g)

Figure 30. Clutter Distributions of Residential Areas, X-VV (cont.)

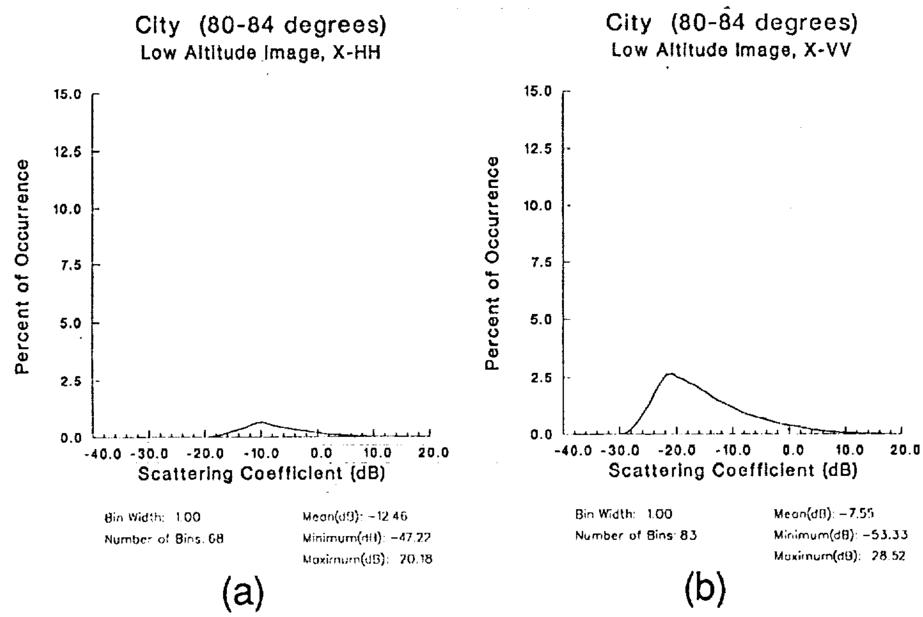

Figure 31. Clutter Distributions of City Areas, X-HH and X-VV

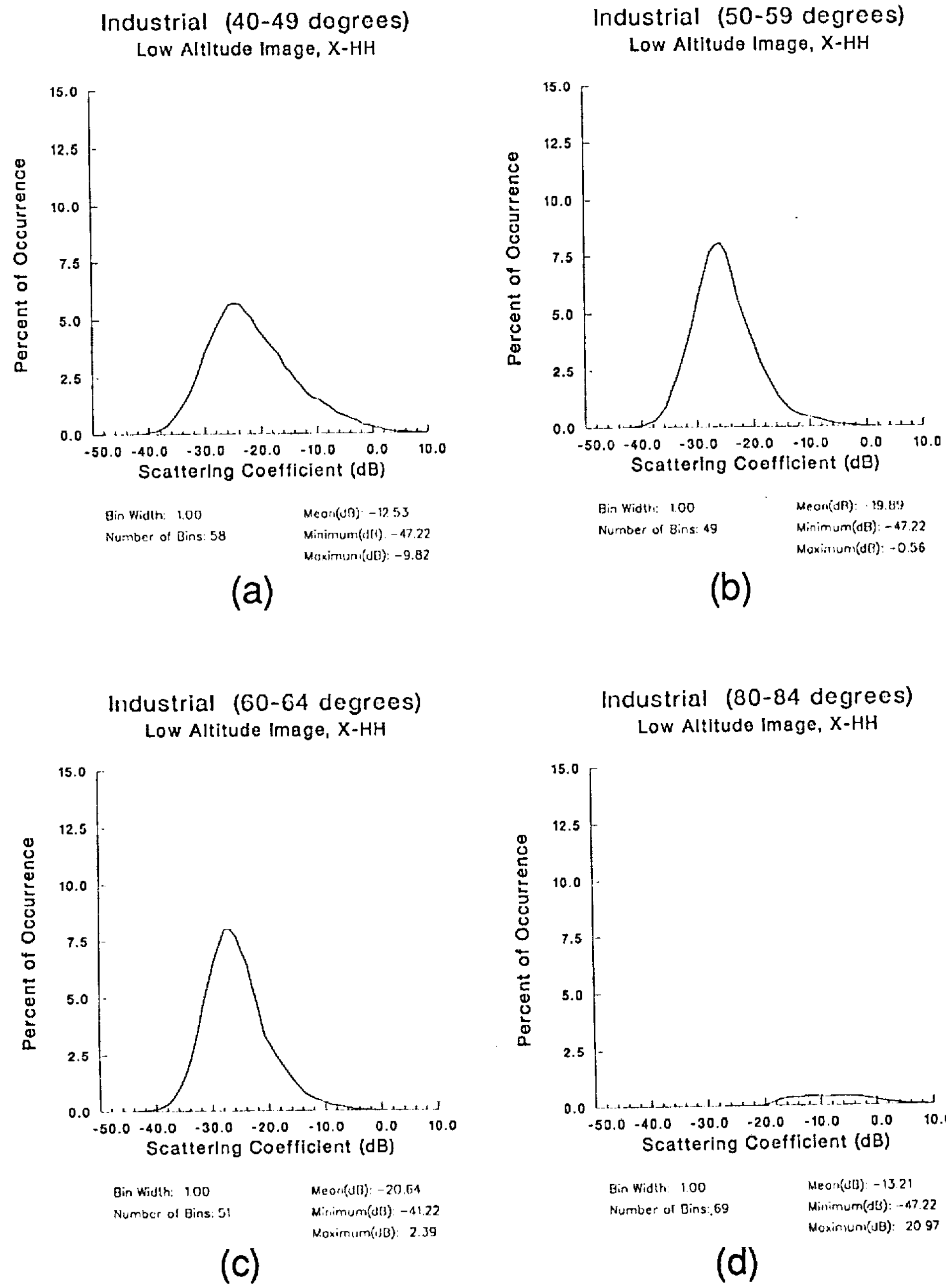

Figure 32. Clutter Distributions of Industrial Areas, X-HH

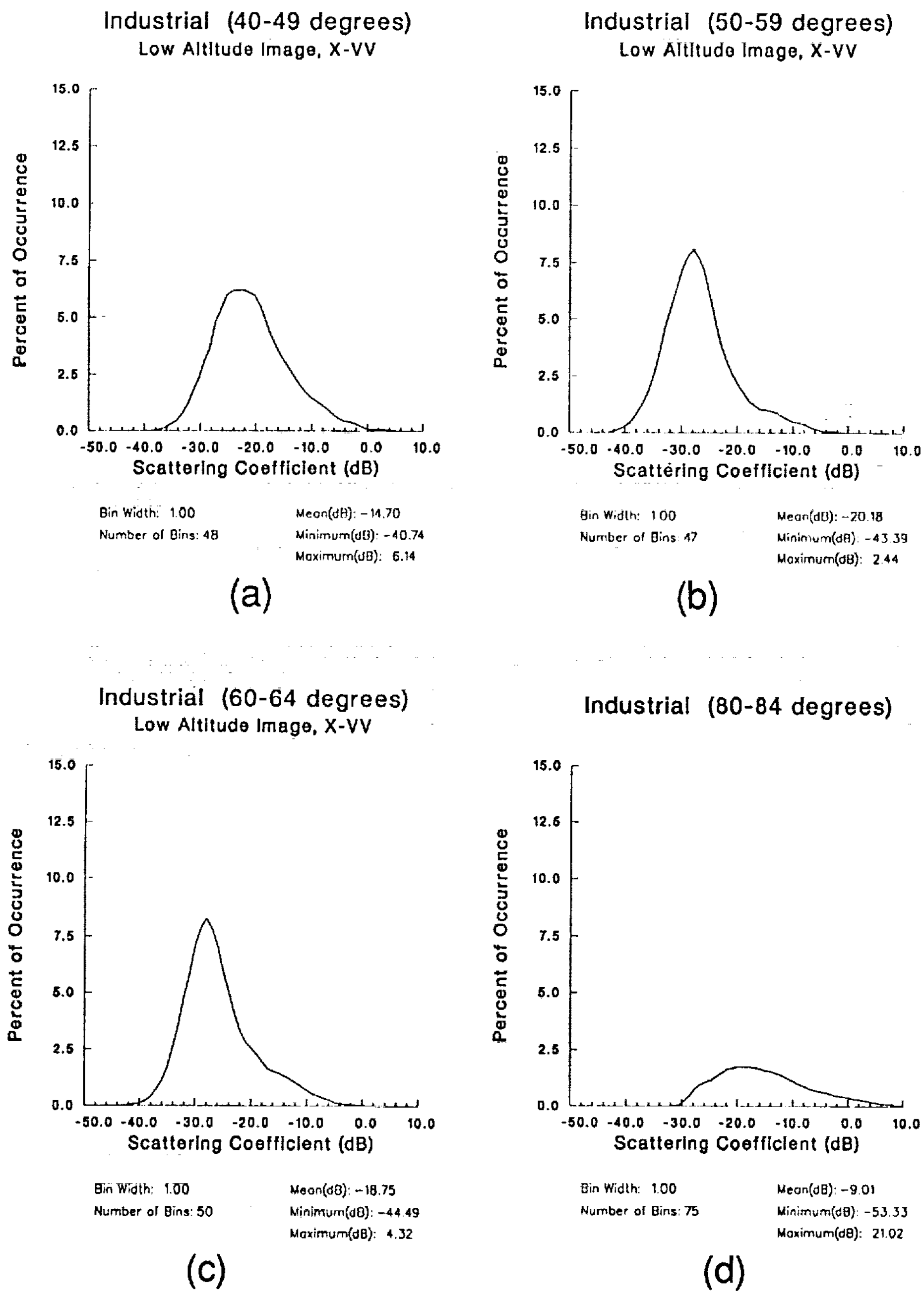

Figure 33. Clutter Distributions of Industrial Areas, X-VV

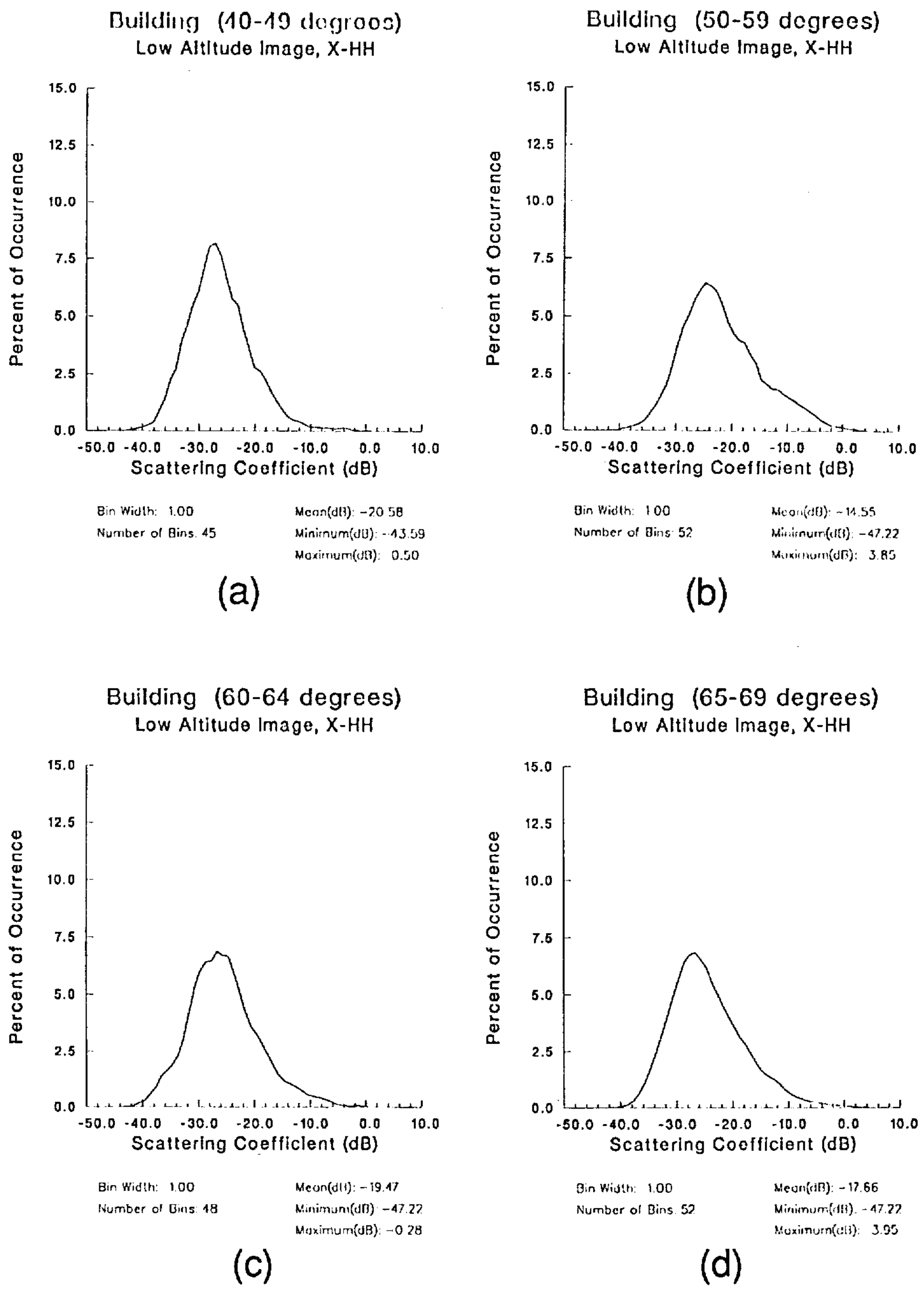

Figure 34. Clutter Distributions of Building Areas, X-HH

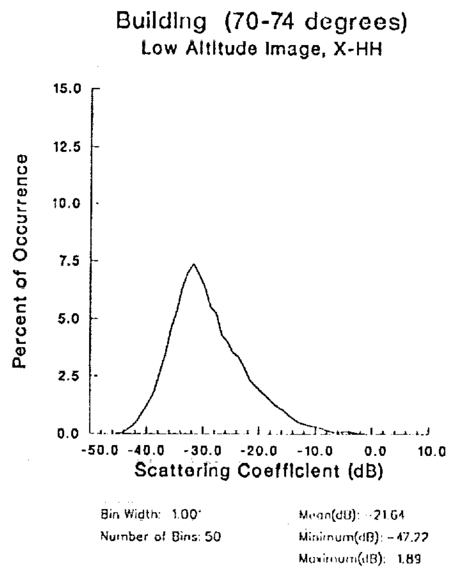

(e)

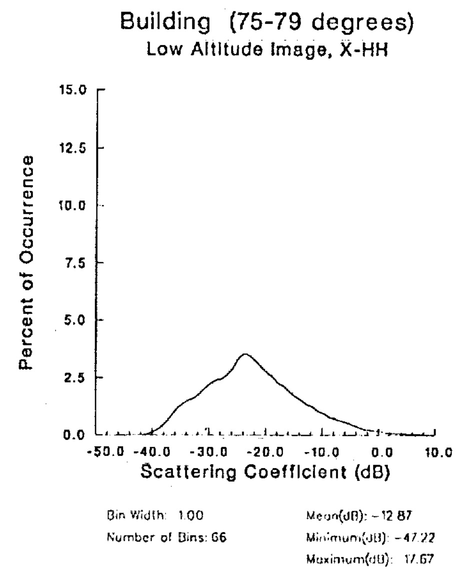

(f)

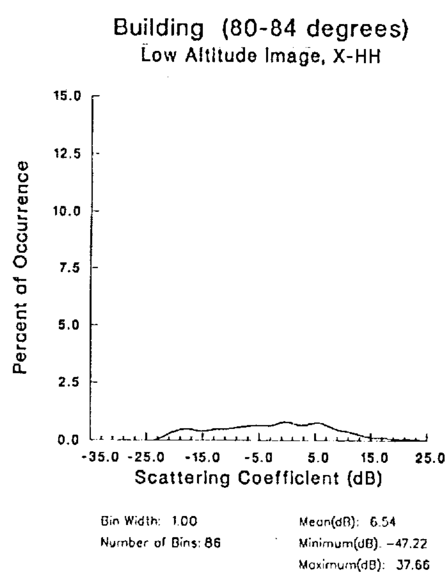

(g)

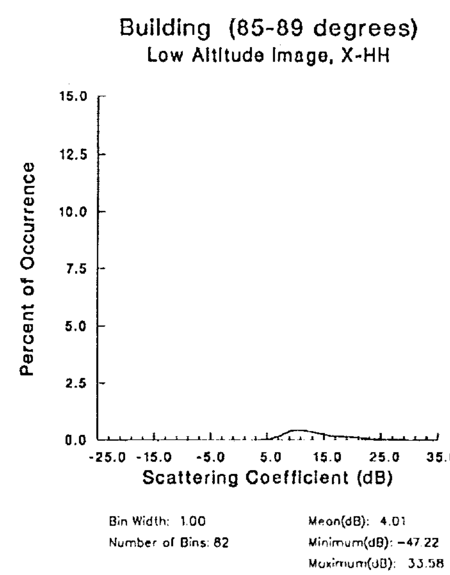

(h)

Figure 34. Clutter Distributions of Building Areas, X-HH (cont.)

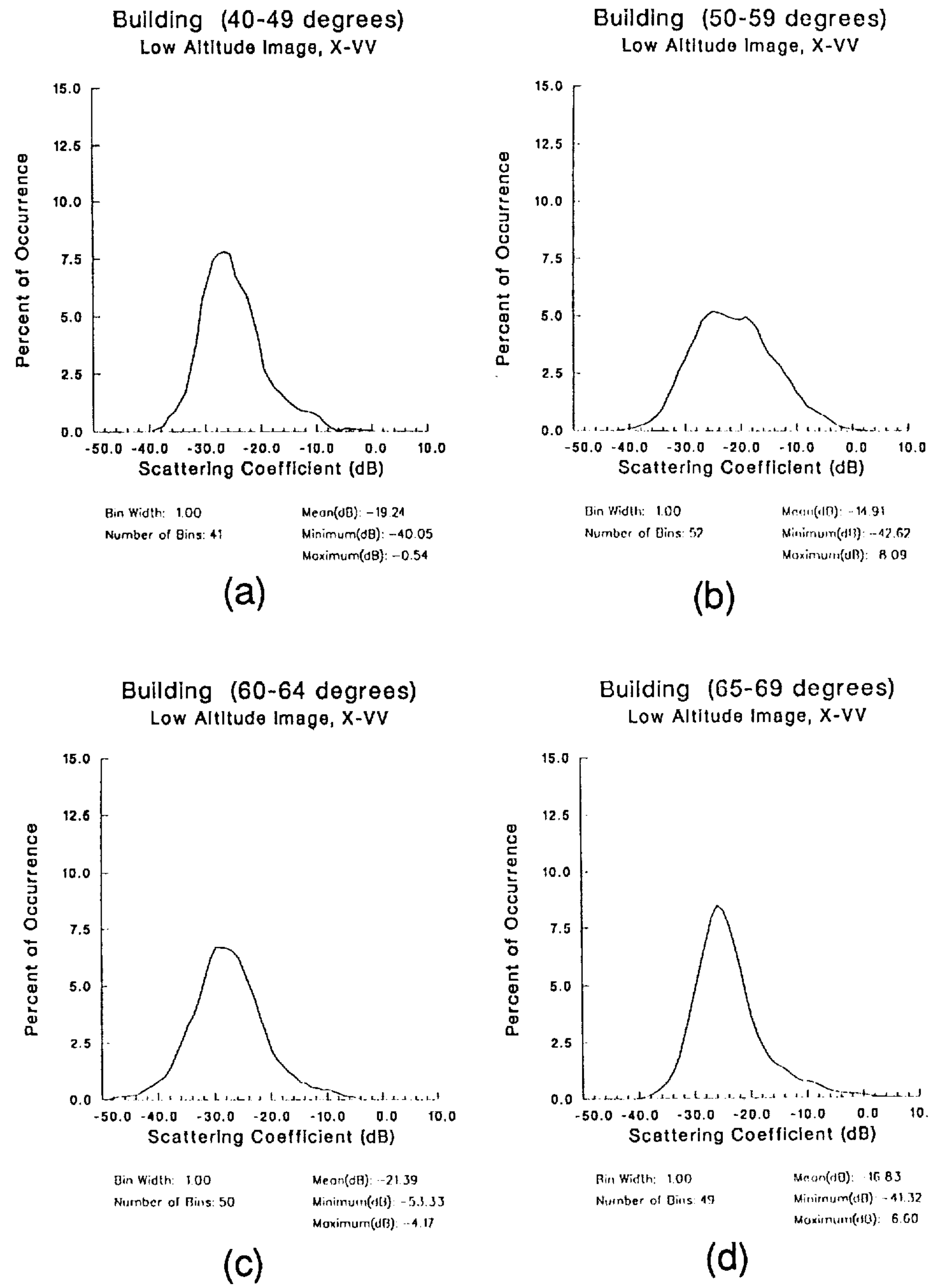

Figure 35. Clutter Distributions of Building Areas, X-VV

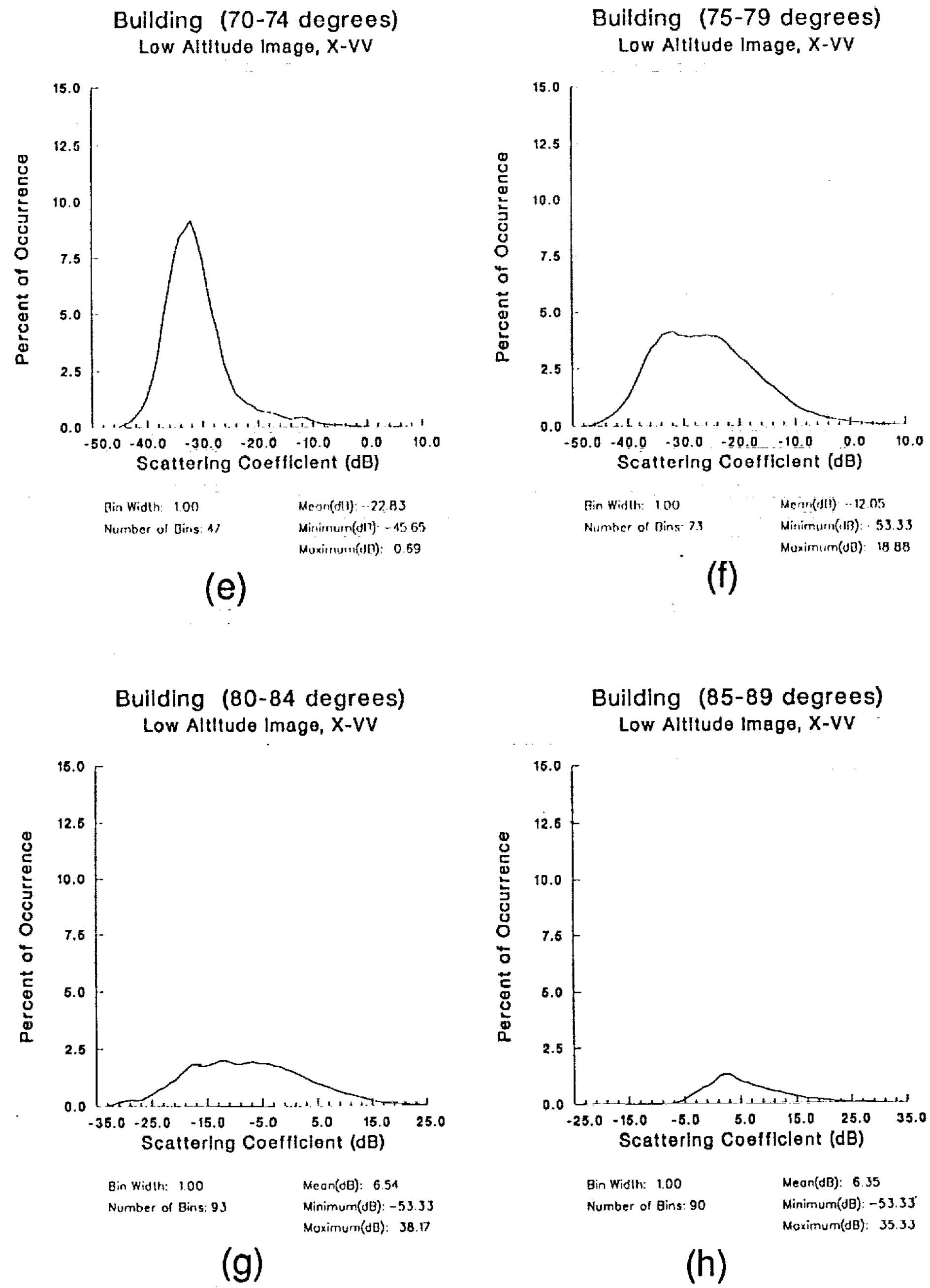

Figure 35. Clutter Distributions of Building Areas, X-VV (cont.)

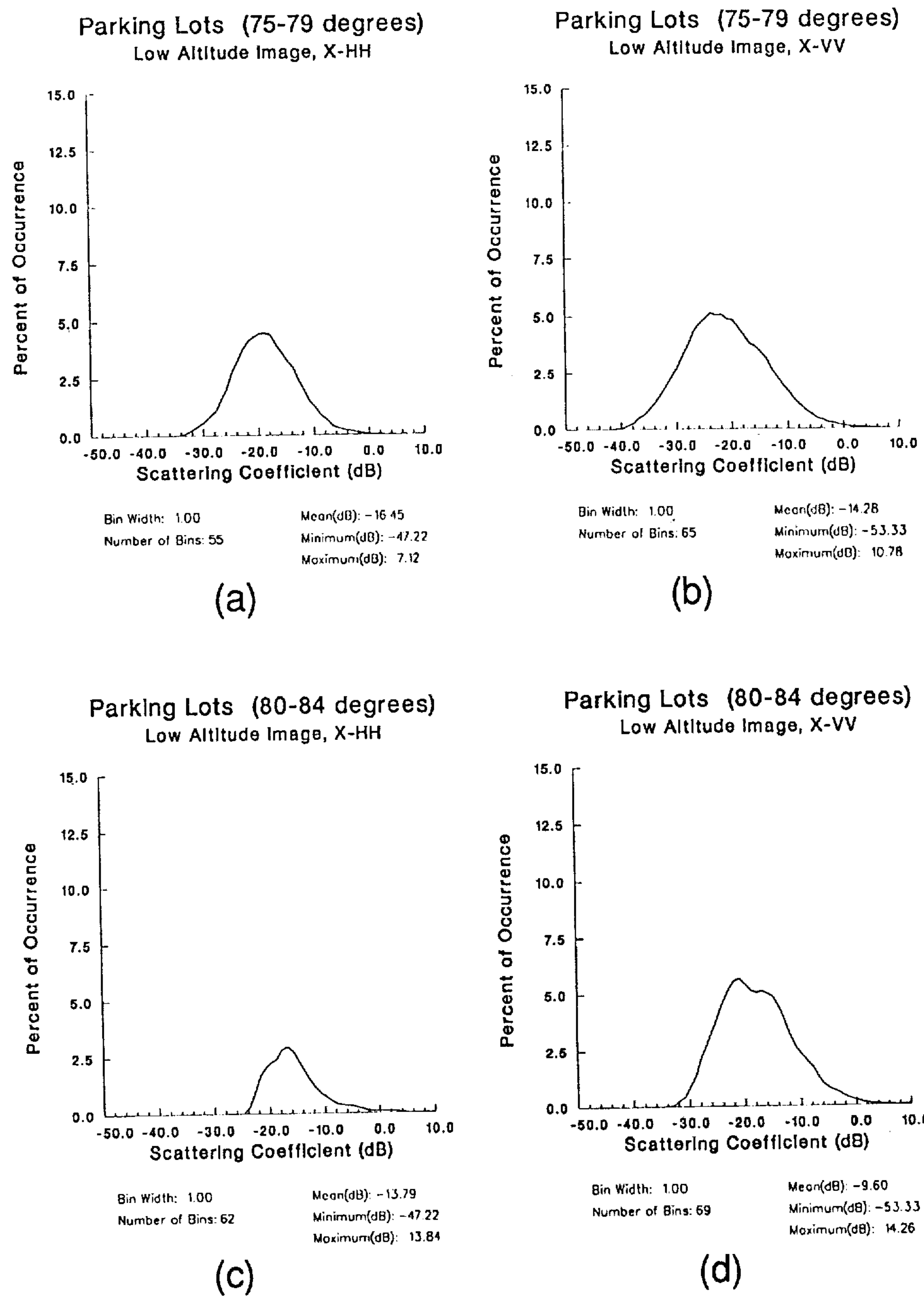

Figure 36. Clutter Distributions of Parking Lots, X-HH and X-VV

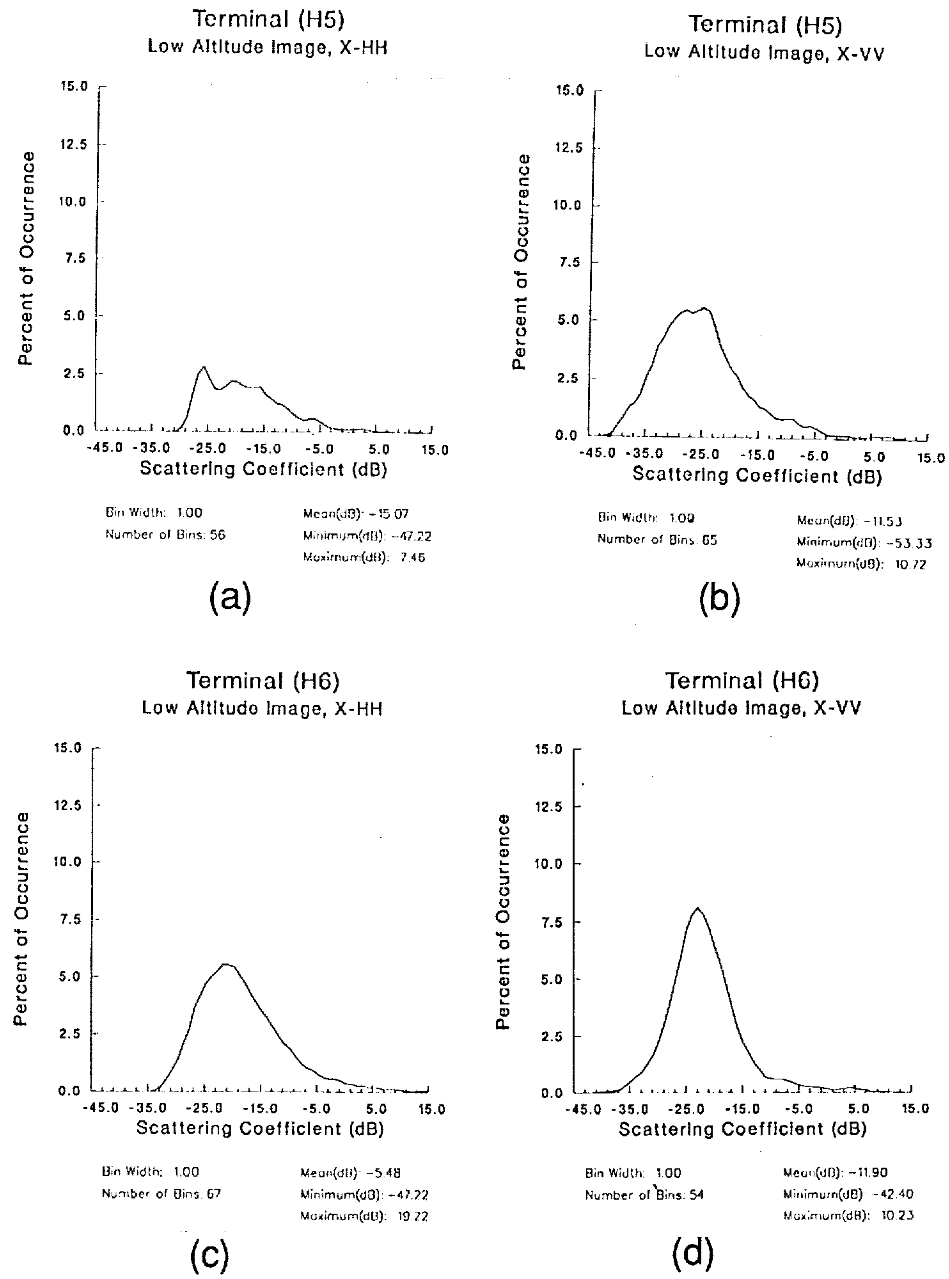

Figure 37. Clutter Distributions of Airport Terminals, X-HH and X-VV. The Orientation of the Terminal to the Line of Flight is Parallel for (a) and (b) and Perpendicular for (c) and (d).

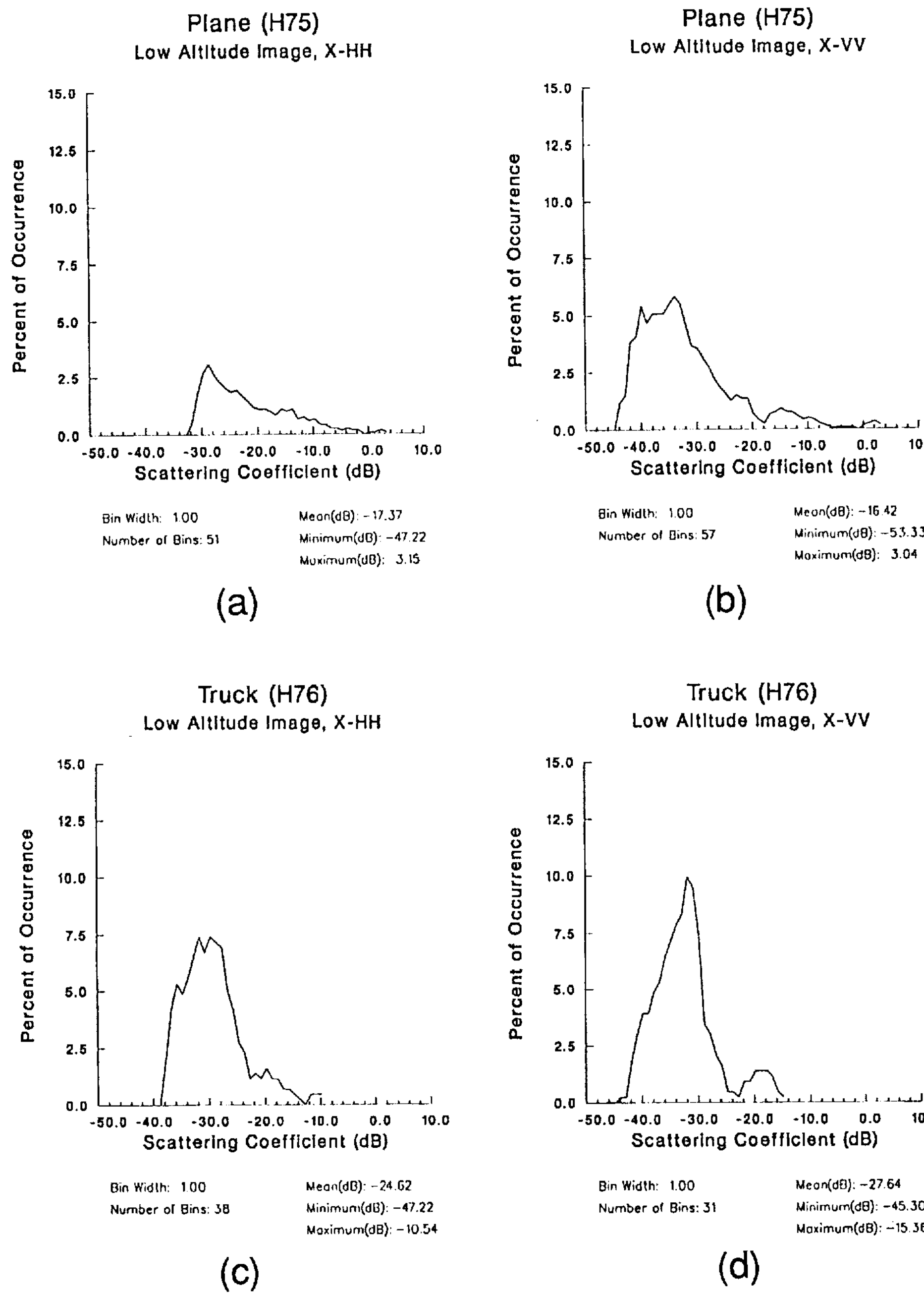

Figure 38. Clutter Distributions of Vehicles, X-HH and X-VV

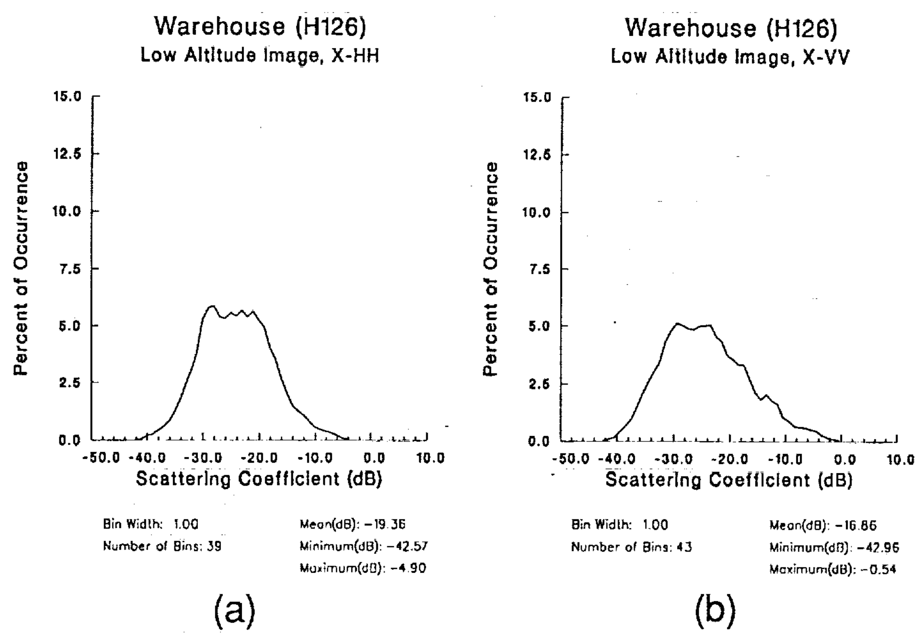

Figure 39. Clutter Distributions of Warehouses, X-HH and X-VV

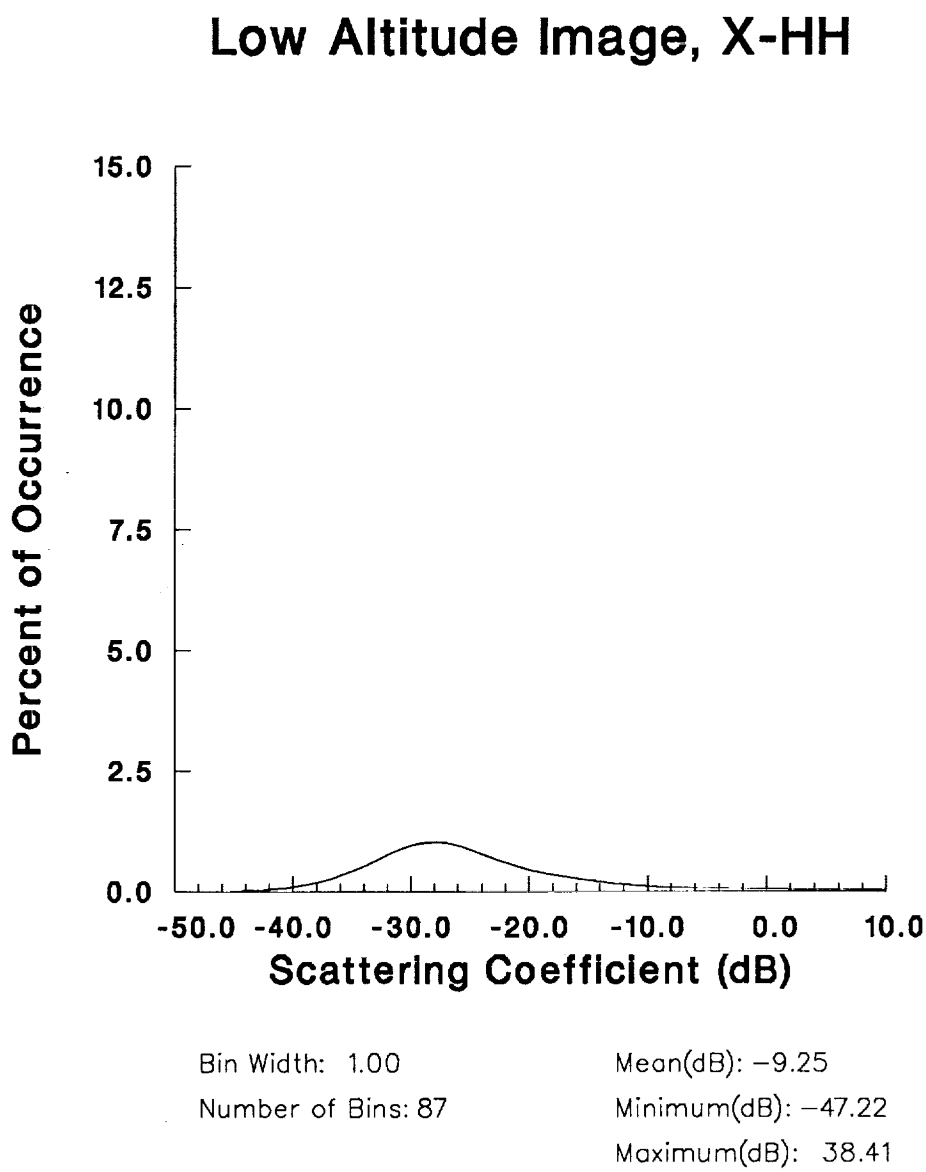

Figure 40. Clutter Distributions, Low Altitude Image, X-HH

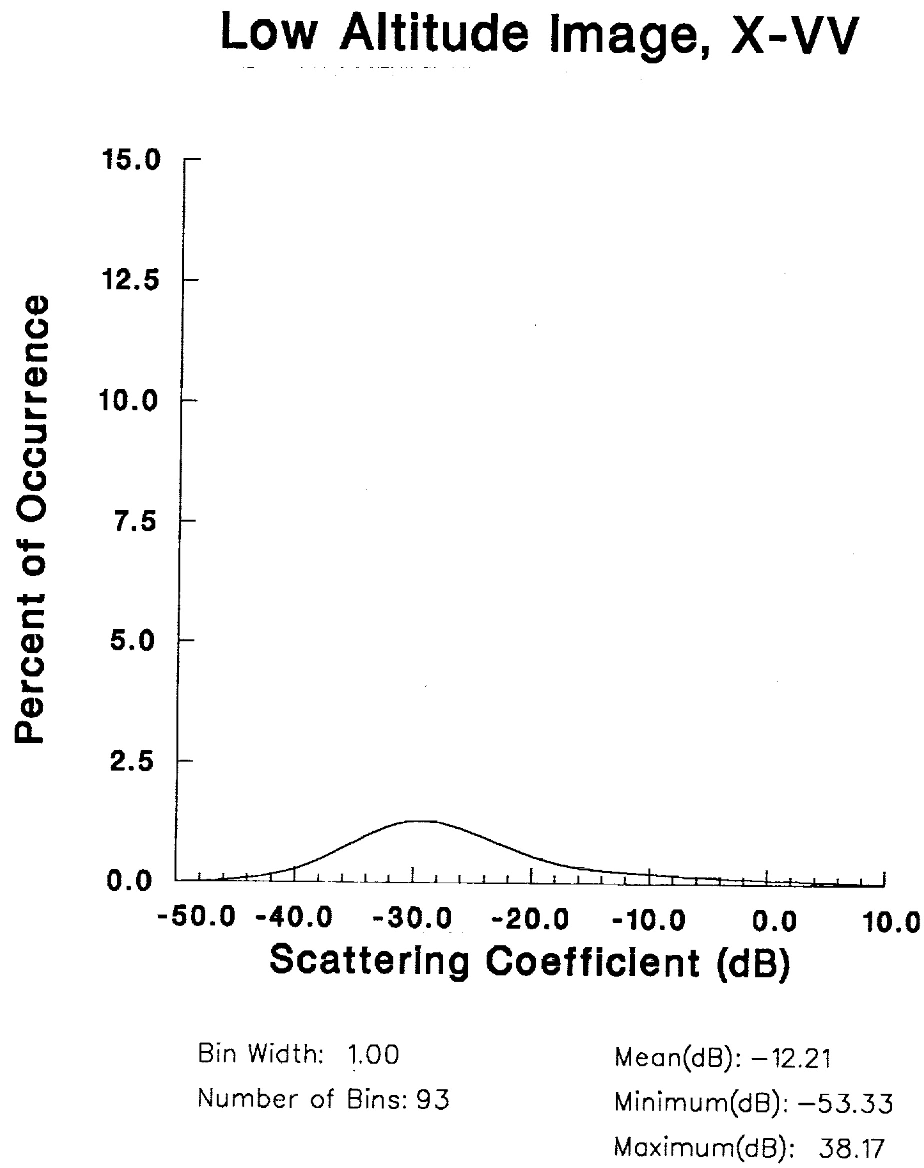

Figure 41. Clutter Distributions, Low Altitude Image, X-VV

ORIGINAL PAGE
BLACK AND WHITE PHOTOGRAPH

90-11465

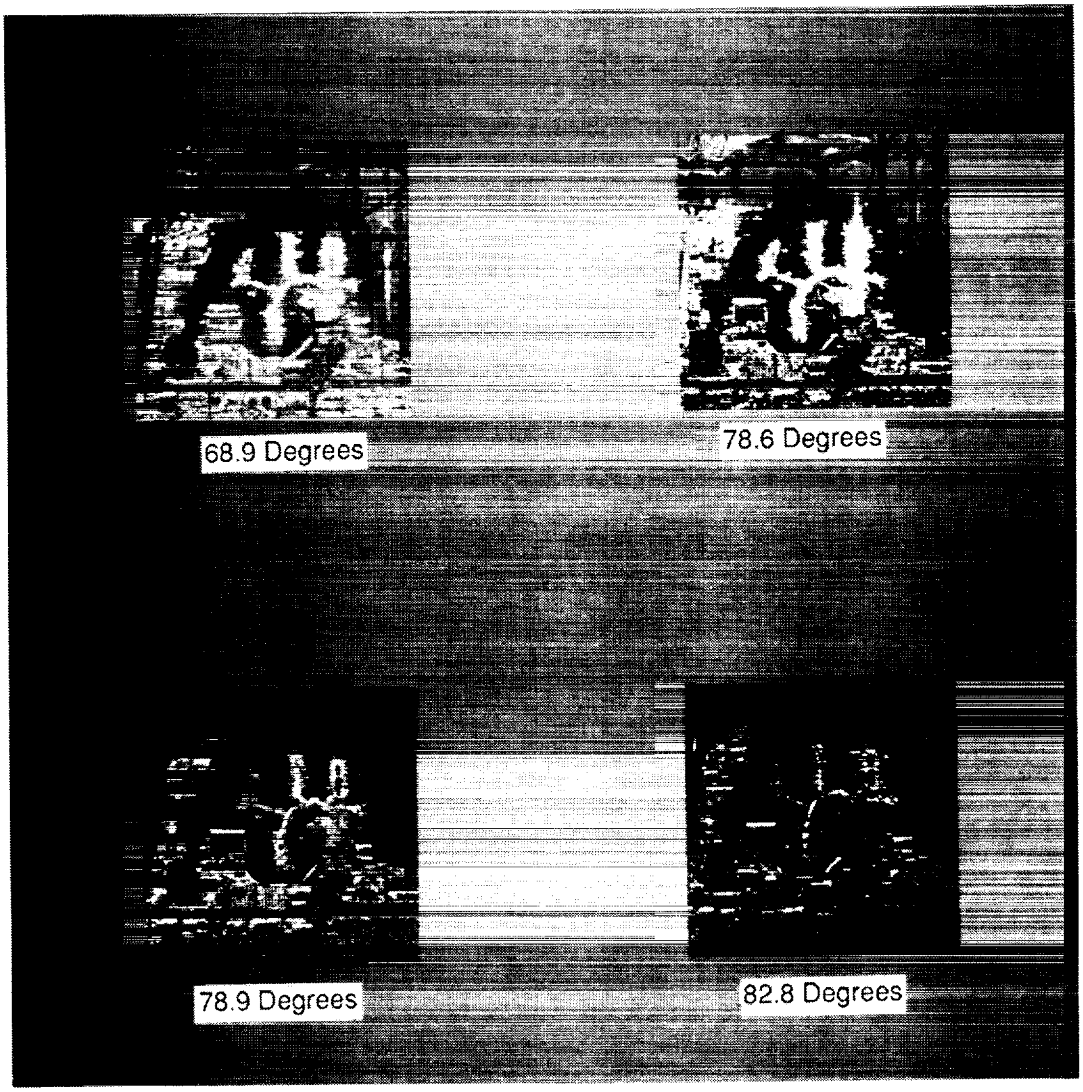

Figure 42. Denver Stapleton International Airport Terminal, Imaged at Successive Incidence Angles, X-HH

ORIGINAL PAGE
BLACK AND WHITE PHOTOGRAPH

90-11464

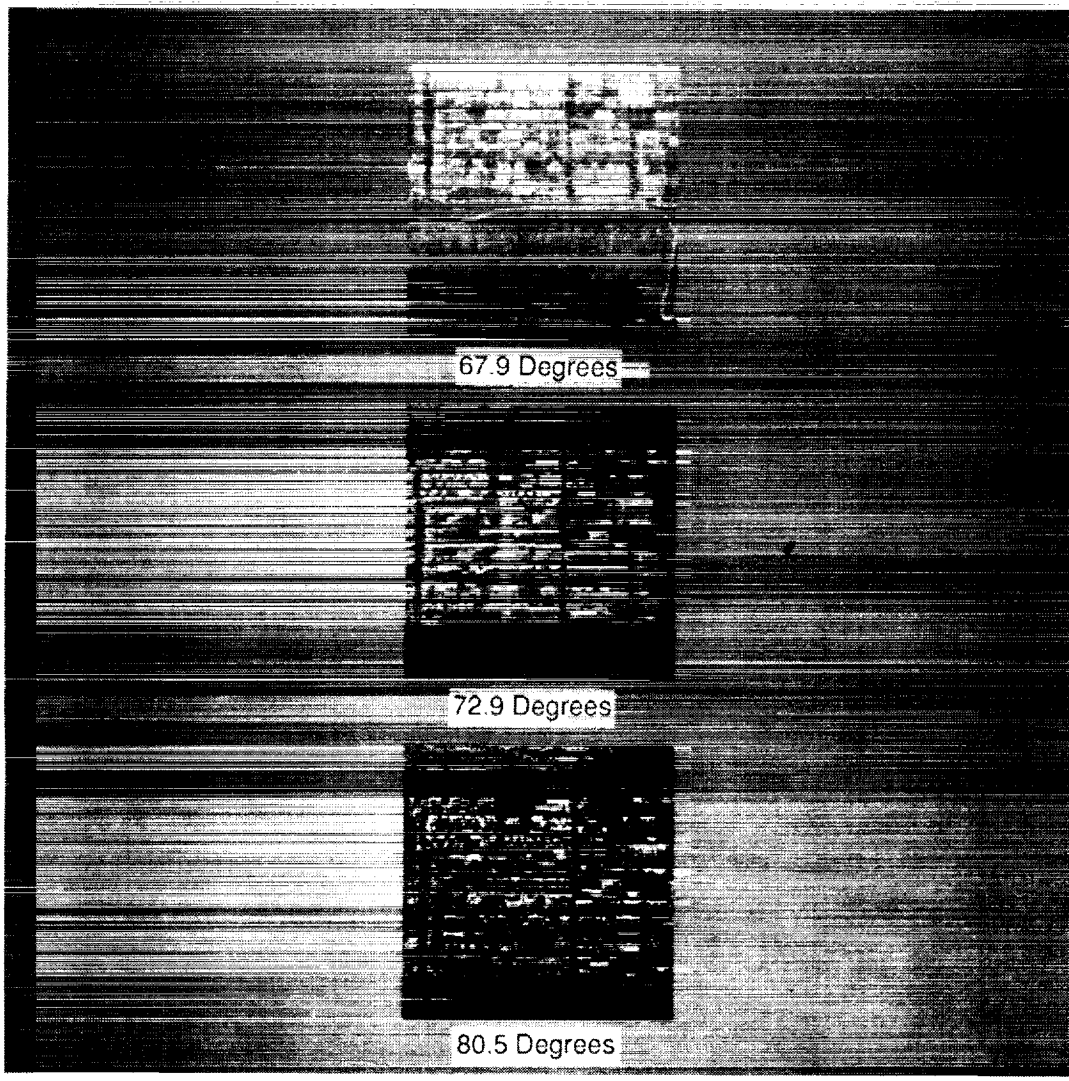

Figure 43. Warehouses at the Airport, Imaged at Successive Incidence Angles, X-HH

ORIGINAL PAGE
BLACK AND WHITE PHOTOGRAPH

90-11463

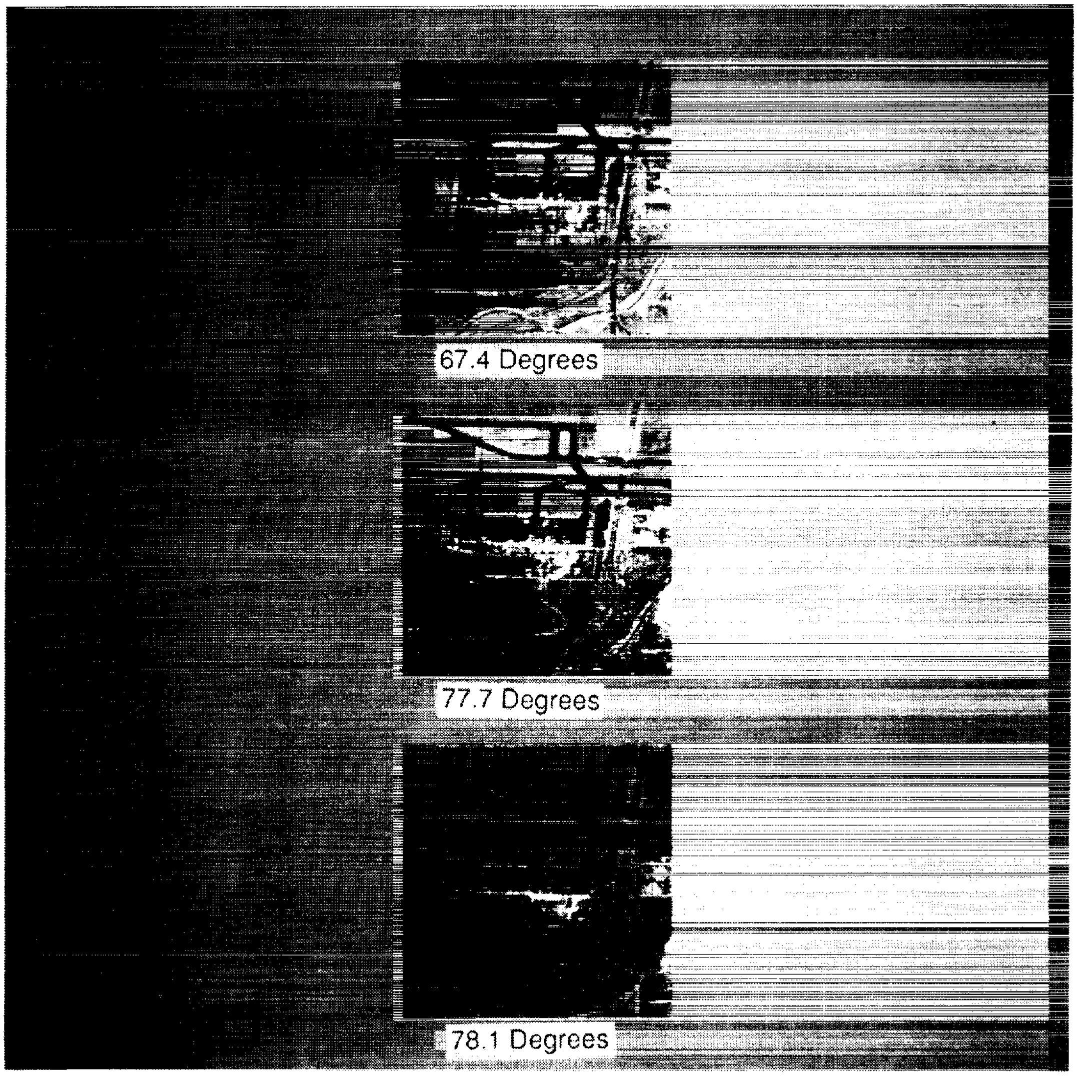

Figure 44. Planes at the Airport, Imaged at Successive Incidence Angles, X-HH

ORIGINAL PAGE
BLACK AND WHITE PHOTOGRAPH

90-11487

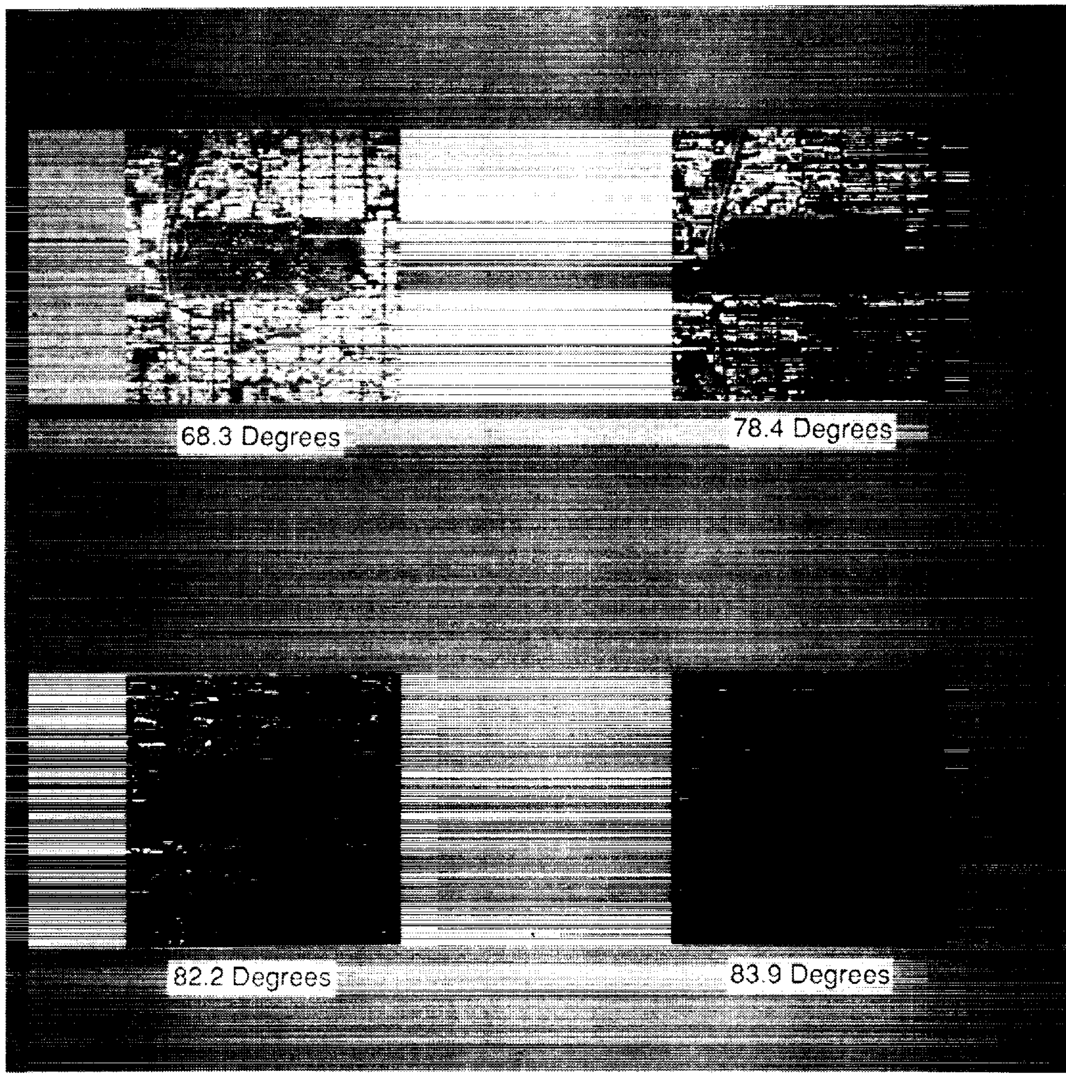

Figure 45. Park Hill Golf Course, Imaged at Successive Incidence Angles, X-HH

ORIGINAL PAGE
BLACK AND WHITE PHOTOGRAPH

90-11462

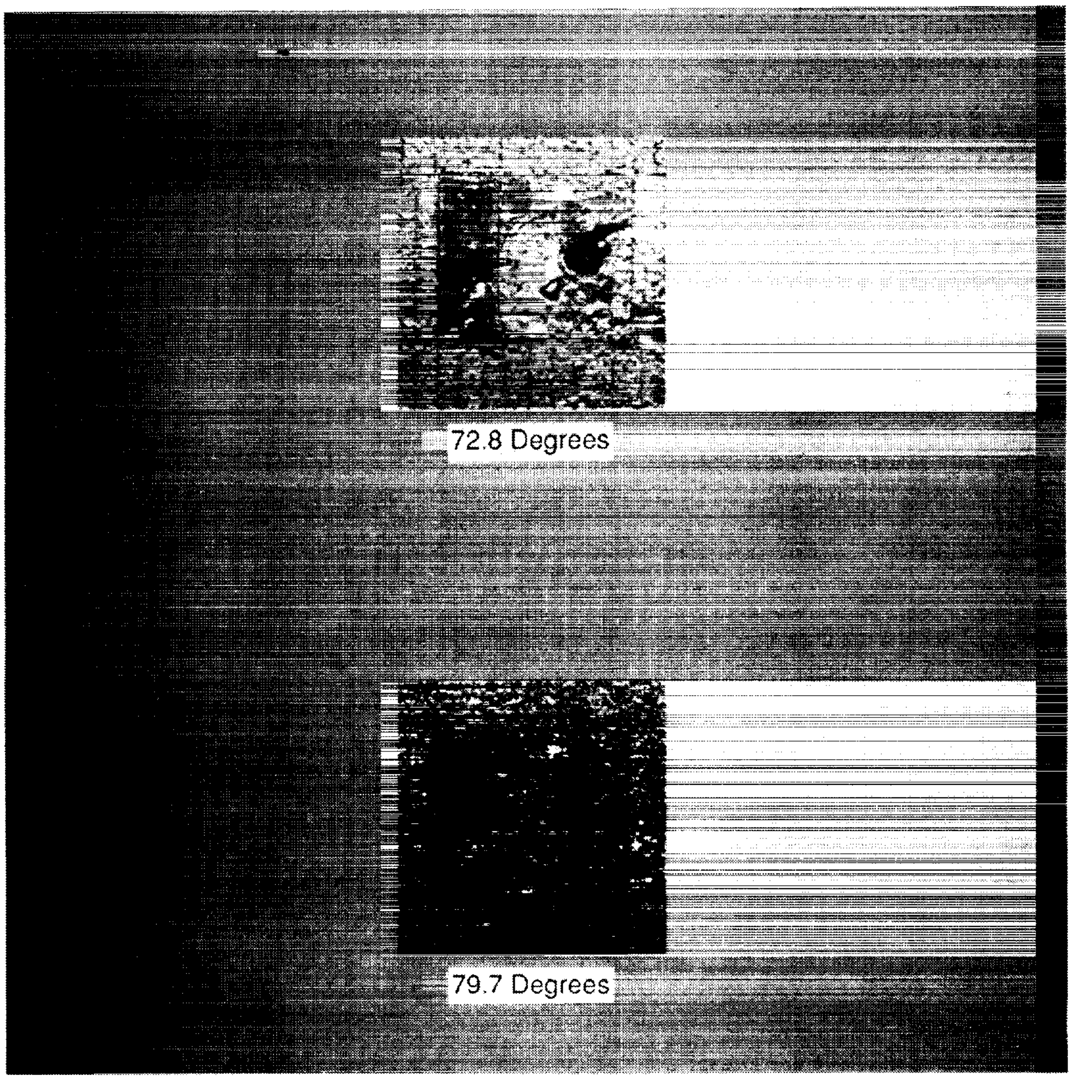

Figure 46. Denver City Park, Imaged at Two Incidence Angles, X-HH

ORIGINAL PAGE
BLACK AND WHITE PHOTOGRAPH

90-11466

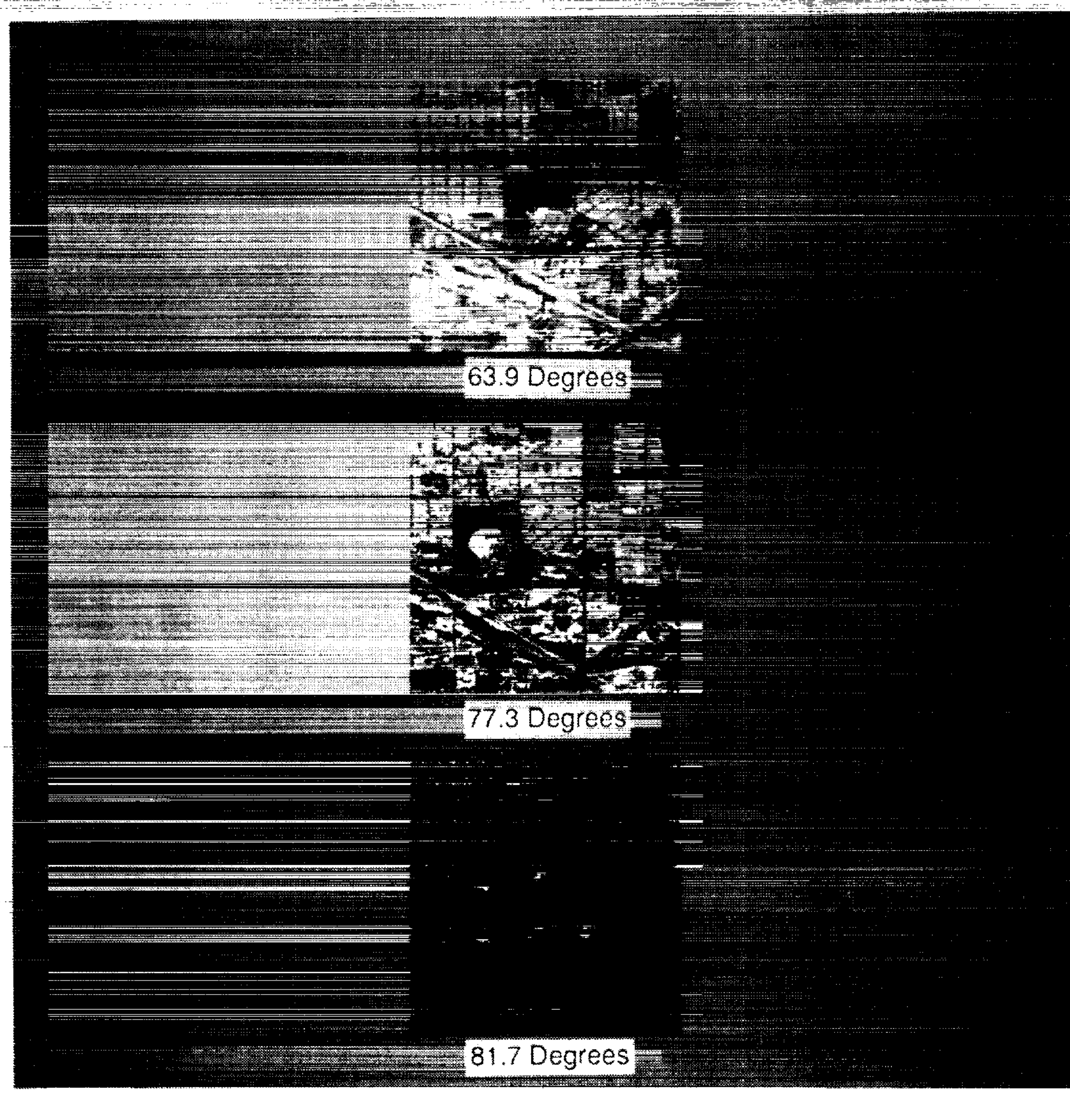

Figure 47. Mile High Kennel Club, Imaged at Successive Incidence Angles

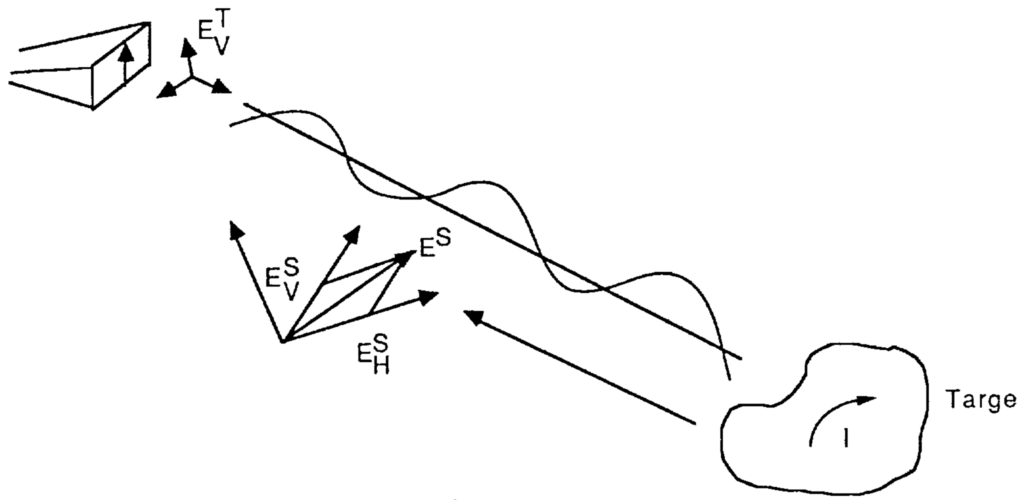

Figure 48. Diagram to Illustrate the Relationship Between the Transmitted and Scattered EM Wave Vector for a Conventional Radar

SCATTERING MATRIX

- Transmitted and Received Field Vectors are Uniquely Related to Target Through Scattering Matrix

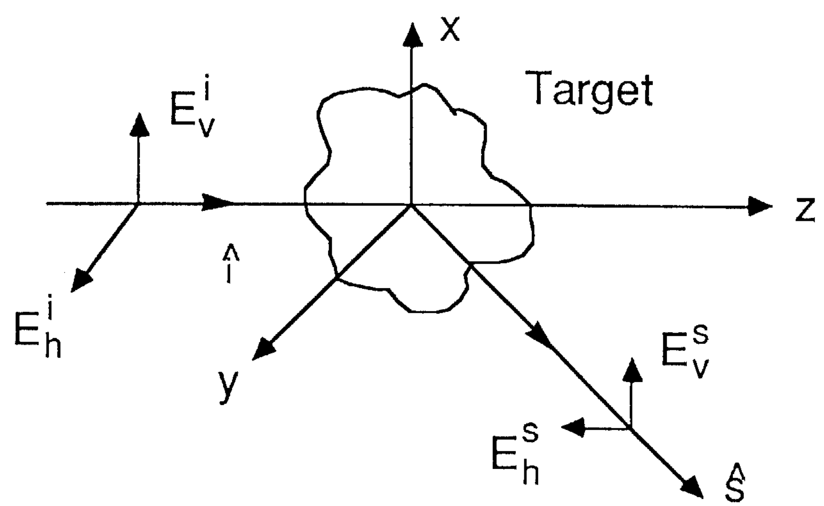

$$\begin{bmatrix} E_h^s \\ E_v^s \end{bmatrix} = \frac{e^{jkr}}{r} \begin{bmatrix} S_{hh} & S_{hv} \\ S_{vh} & S_{vv} \end{bmatrix} \begin{bmatrix} E_h^i \\ E_v^i \end{bmatrix}$$

$$\underline{E}^s = \frac{e^{jkr}}{r} \, S \, \underline{E}^i$$

- Polarimetric Radar Provides the Scattering Matrix of a Target

Figure 49. The Scattered Field Vector $\underline{E}_s$ and Incident Field Vector $\underline{E}_i$ are Uniquely Related by the Target Scattering Matrix S

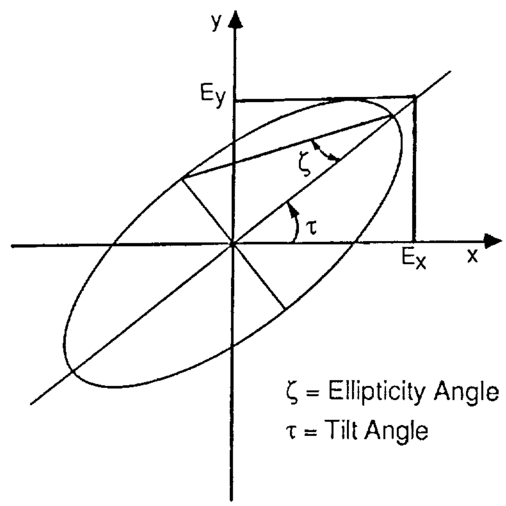

$$\bar{E} = \sqrt{E_x^2 + E_y^2}\ (\cos\gamma\,\hat{x} + \sin\gamma\, e^{j\delta}\,\hat{y})$$

where

$$\gamma = 1/2 \cos^{-1} (\cos 2\zeta \cos 2\tau)$$

$$\delta = \tan^{-1} (\tan 2\varepsilon / \sin 2\tau)$$

	Co-Polarized			Cross-Polarized	
HH	$\tau = 0°, 180°$	$\zeta = 0°$	HV	$\tau = 90°$	$\zeta = 0°$
VV	$\tau = 90°$	$\zeta = 0°$	VH	$\tau = 0°, 180°$	$\zeta = 0°$
RR	$\tau = 0°\text{-}180°$	$\zeta = -45°$	RL	$\tau = 0°\text{-}180°$	$\zeta = +45°$
LL	$\tau = 0°\text{-}180°$	$\zeta = +45°$	LR	$\tau = 0°\text{-}180°$	$\zeta = -45°$

Figure 50. The Ellipticity Diagram for Elliptical Polarization May be Used to Define Polarization

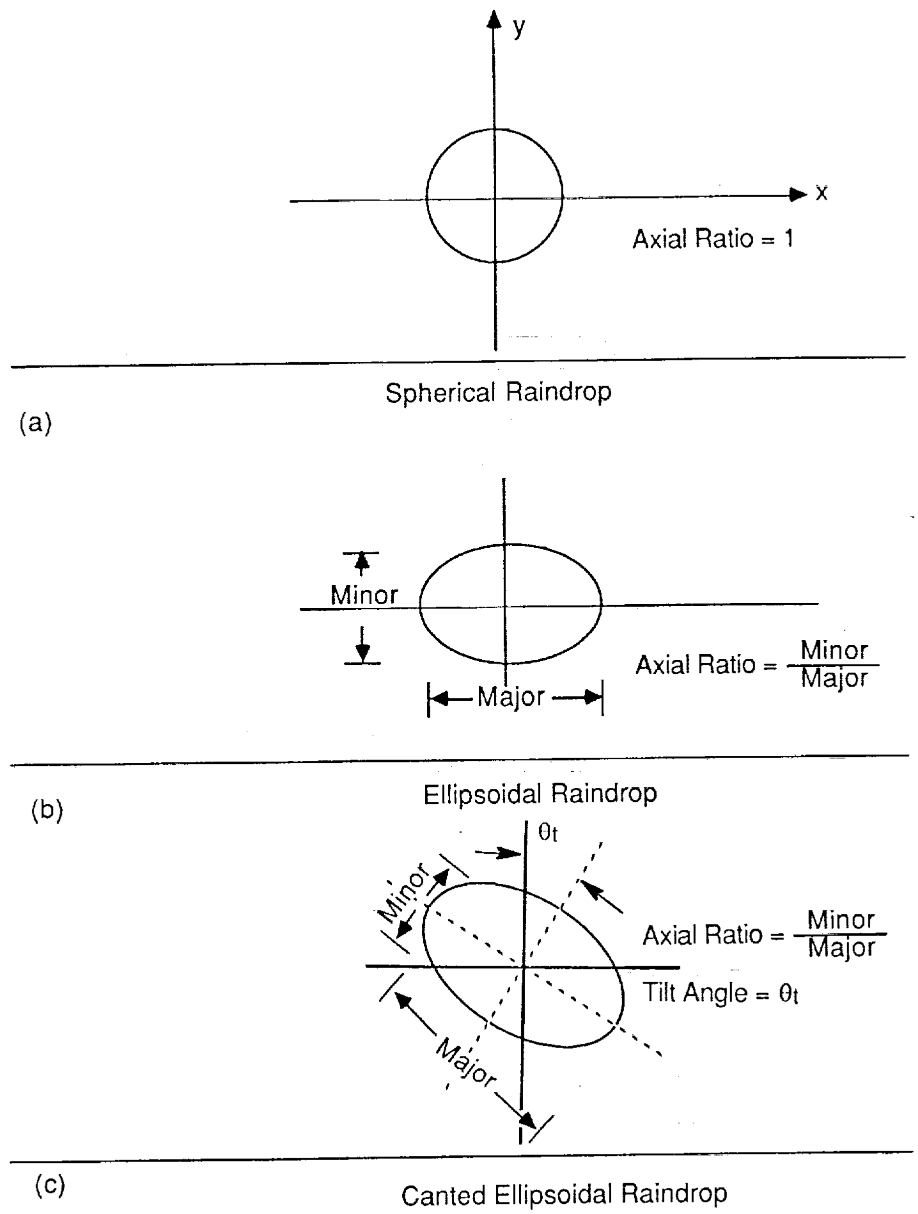

Figure 51. A Raindrop May be Spherical or Ellipsoidal, and May be Rotated to the Axis Normal to the Earth. A Raindrop is Characterized by its Effective Diameter, its Axial Ratio, and a Tilt Angle.

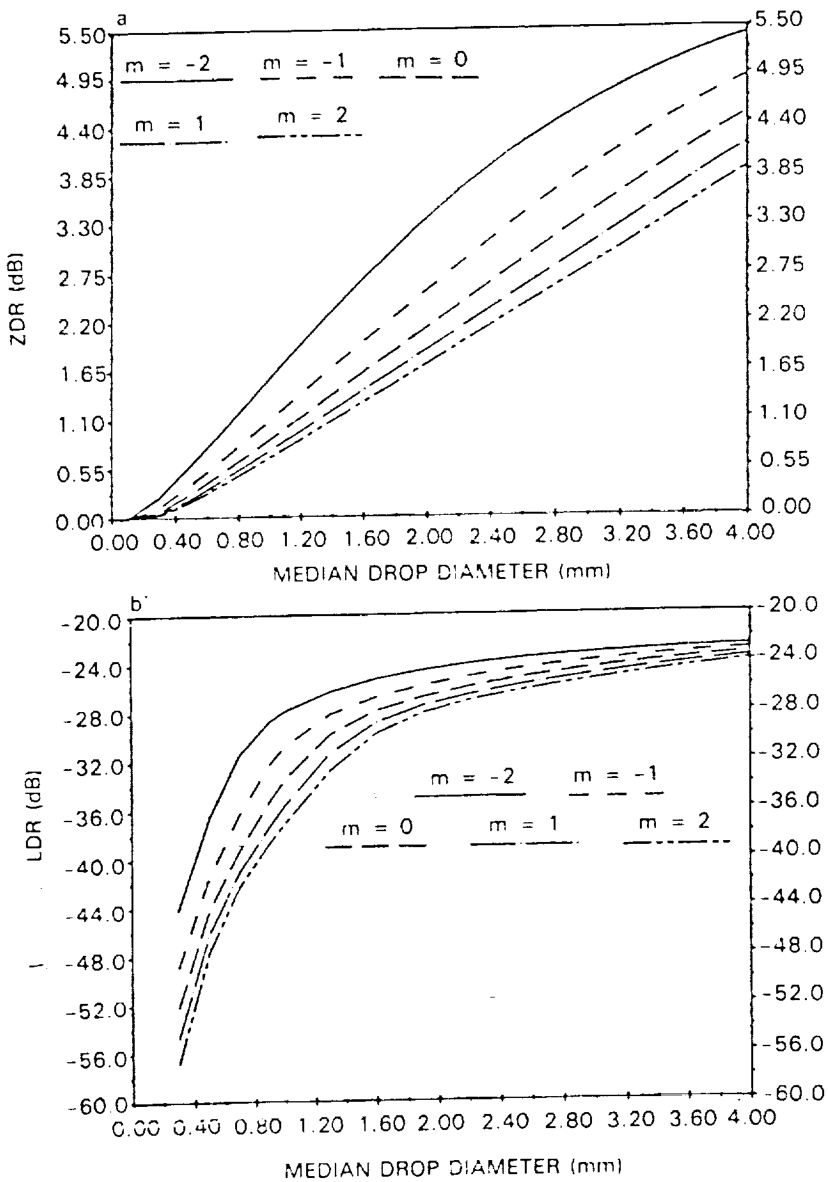

Figure 52. The Ratio Between HH and VV Returns (ZDR) is Shown (a) Versus Median Drop Diameter for 5 Values of the Parameter m in the Gamma Drop Distribution. A Corresponding Comparison Between Like-and-Cross-Polarized Returns (LDR) is Shown in (b). These Results are From Bringi et al. [8].

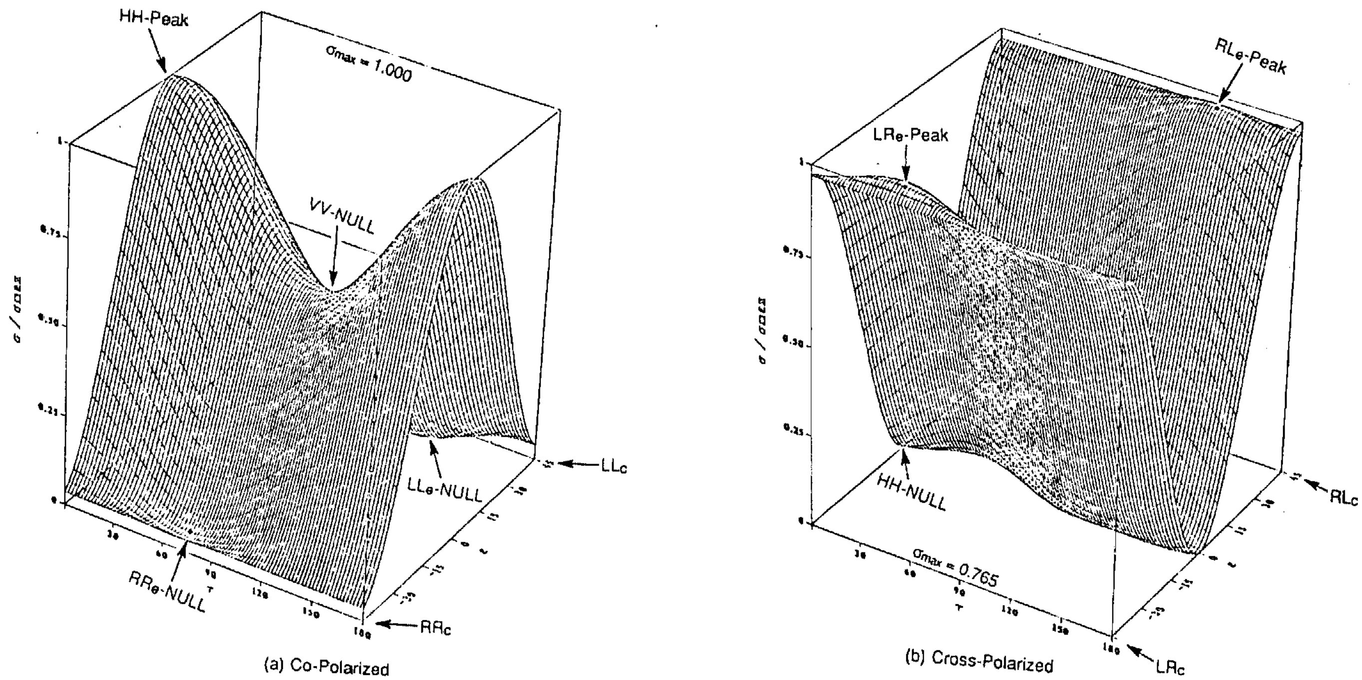

Figure 53. The Co-Polarized (a) and Cross-Polarized (b) Polarimetric Signatures are Shown for the Case of a Wave Propagating Through a Rain Filled Medium Which Produces a Phase Shift of 20° (HH-VV) and 2.5 dB Greater Attenuation in VV-Polarization Than HH-Polarization.

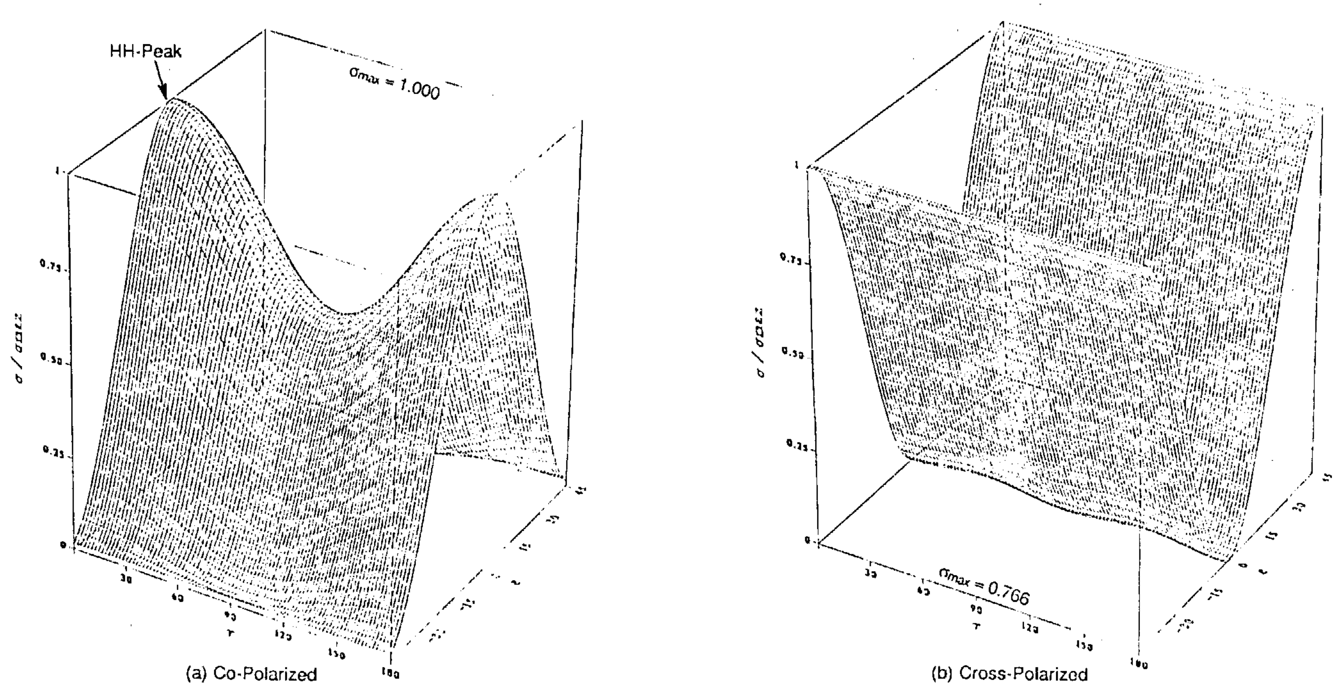

Figure 54. The Co-Polarized (a) and Cross-Polarized (b) Polarization Signatures are Shown for the Case of Wave Propagation Through a Rainfilled Medium Where VV-Polarization Response is 2.5 dB Weaker Than the HH Response. The Phase Shift Between HH and VV Polarization has Been Set to Zero for Illustration Purposes

Figure 55. Denver Stapleton International Airport Polarimetric Set, VV

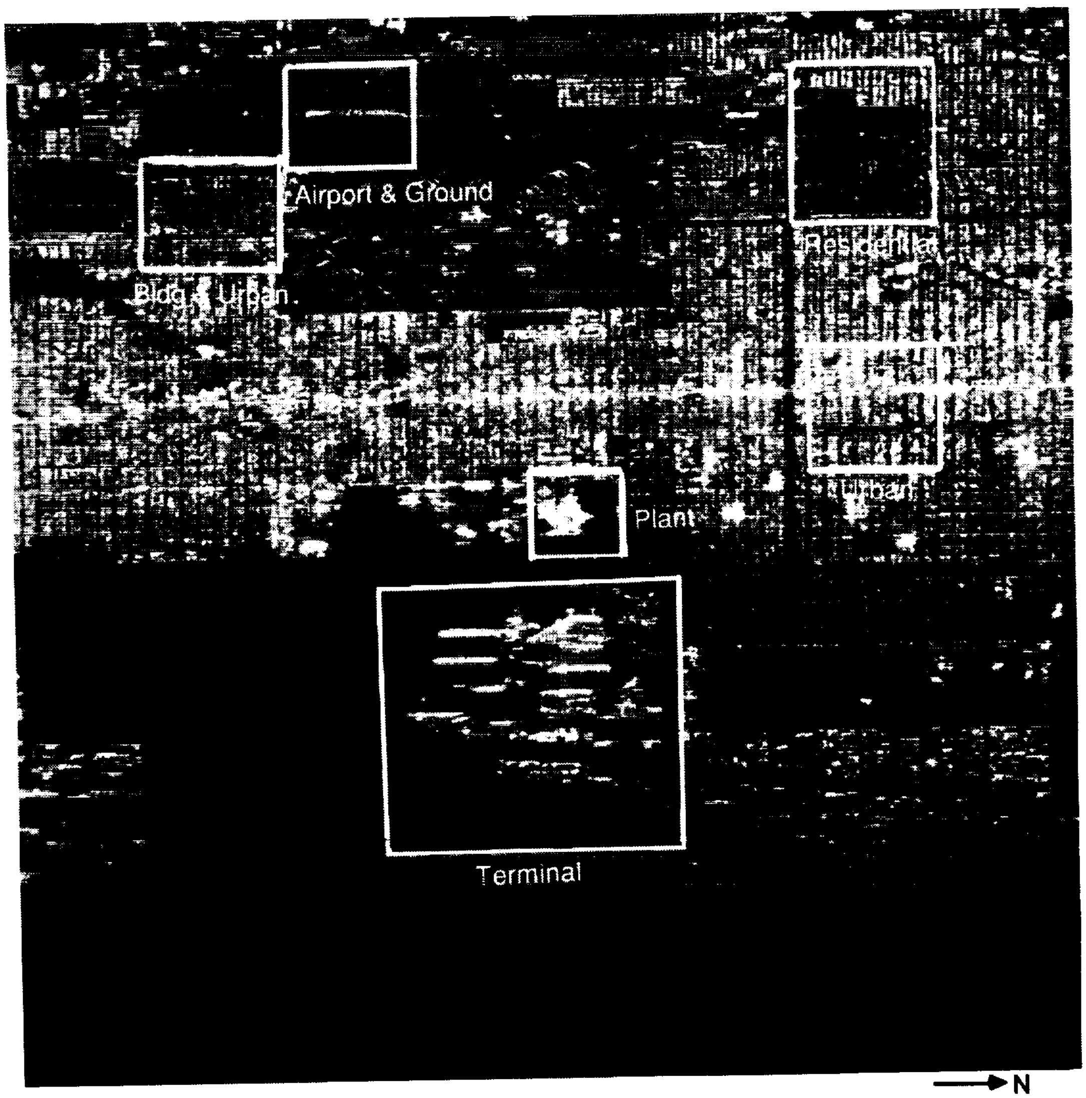

Figure 56. Denver Stapleton International Airport Polarimetric Set, HH. The Location Map for Linear and Circular Polarization Image Sets are Highlighted

Figure 57. Denver Stapleton International Airport Polarimetric Set, HV

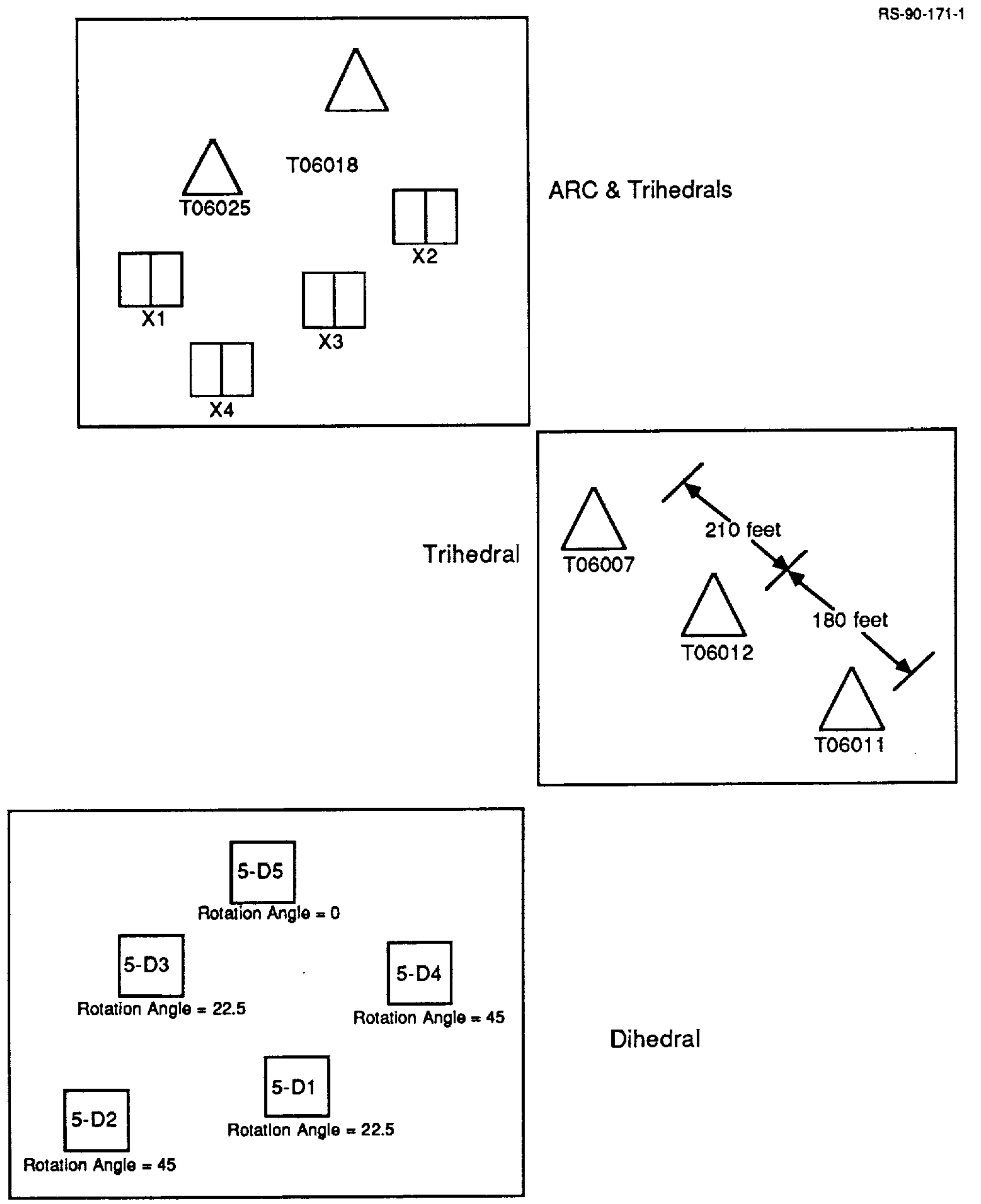

Figure 58. Calibration Target Array Site Plan

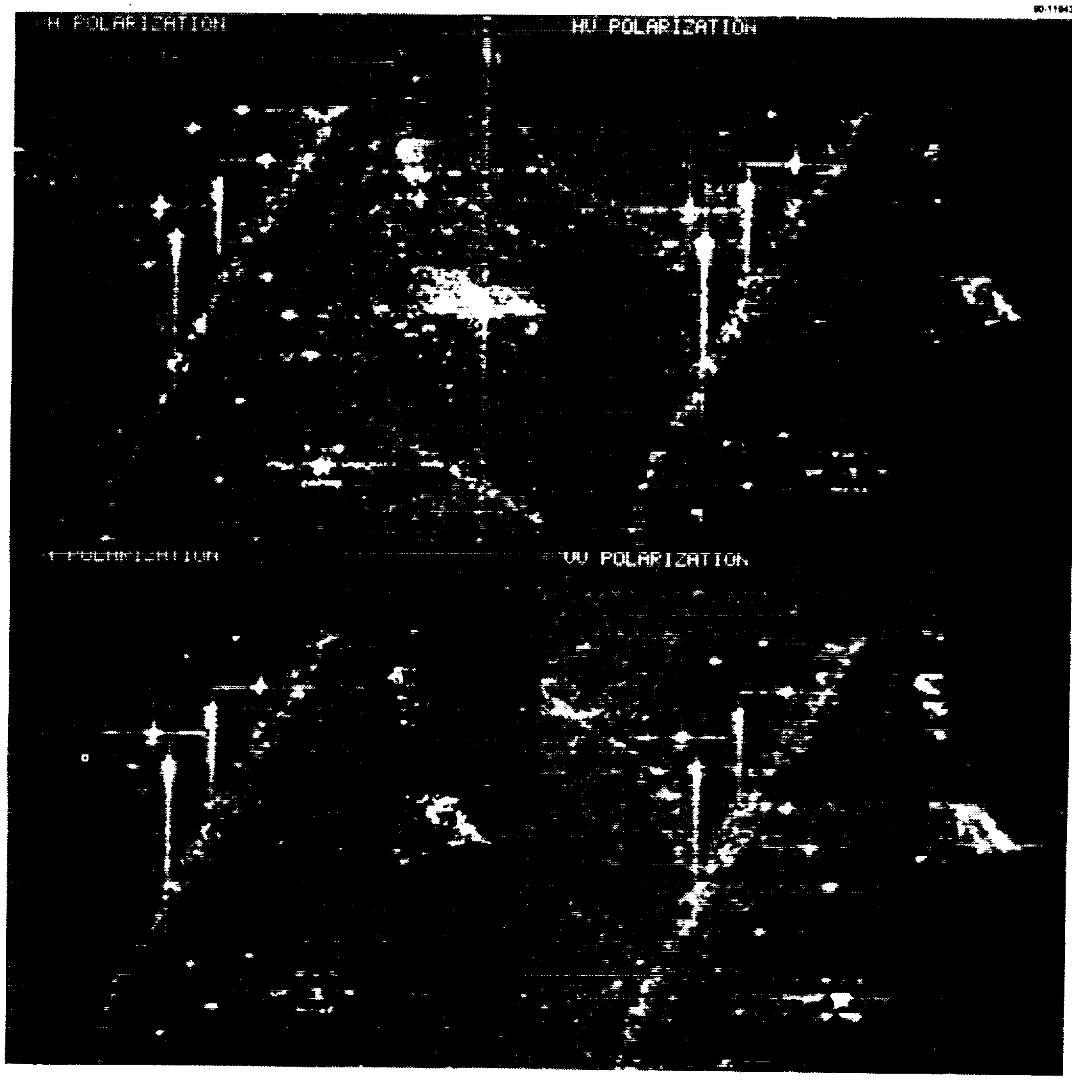

Figure 59. Linear Polarization Image Set of Calibration Target Array

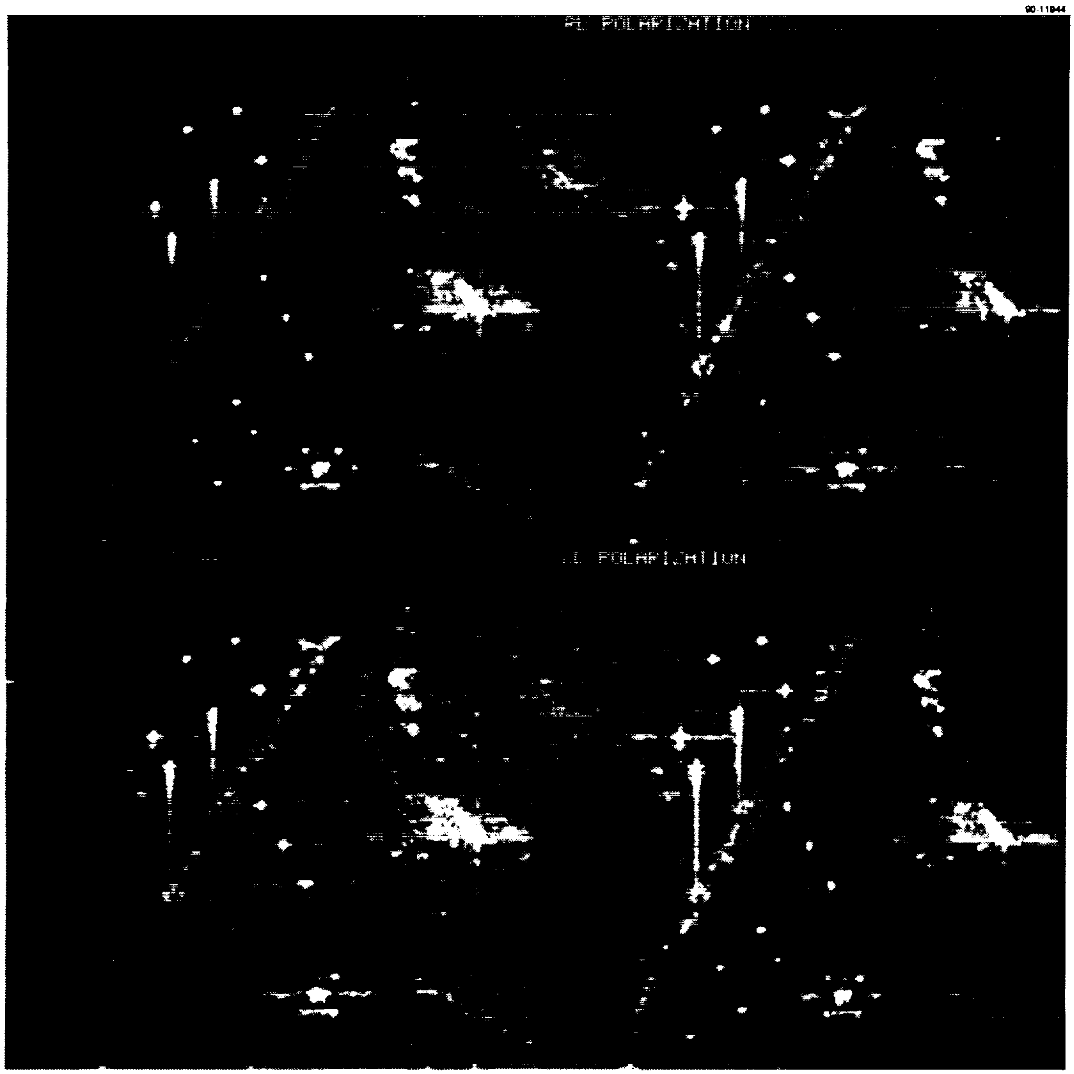

Figure 60. Circular Polarization Image Set of Calibration Targets Array

ORIGINAL PAGE IS
OF POOR QUALITY

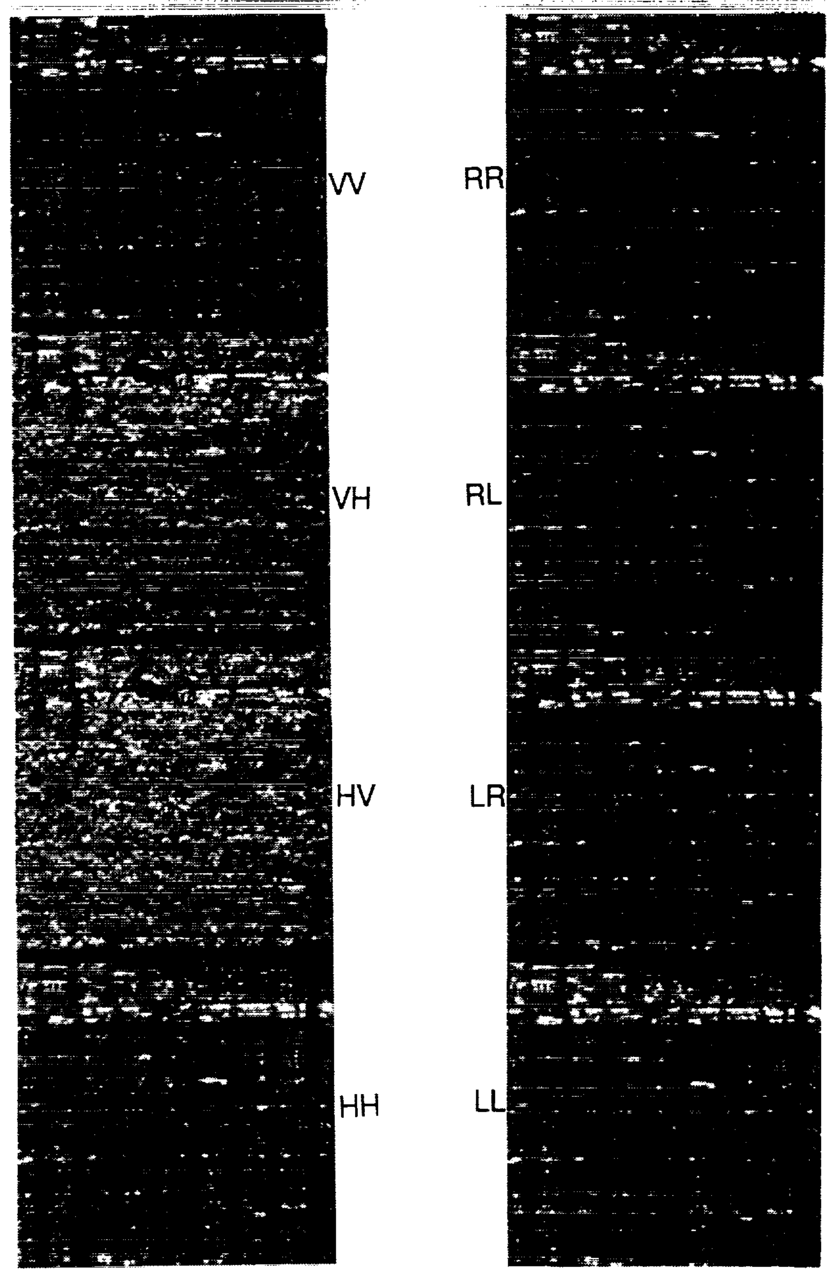

Figure 61. Linear and Circular Polarization Image Set for an Urban Area

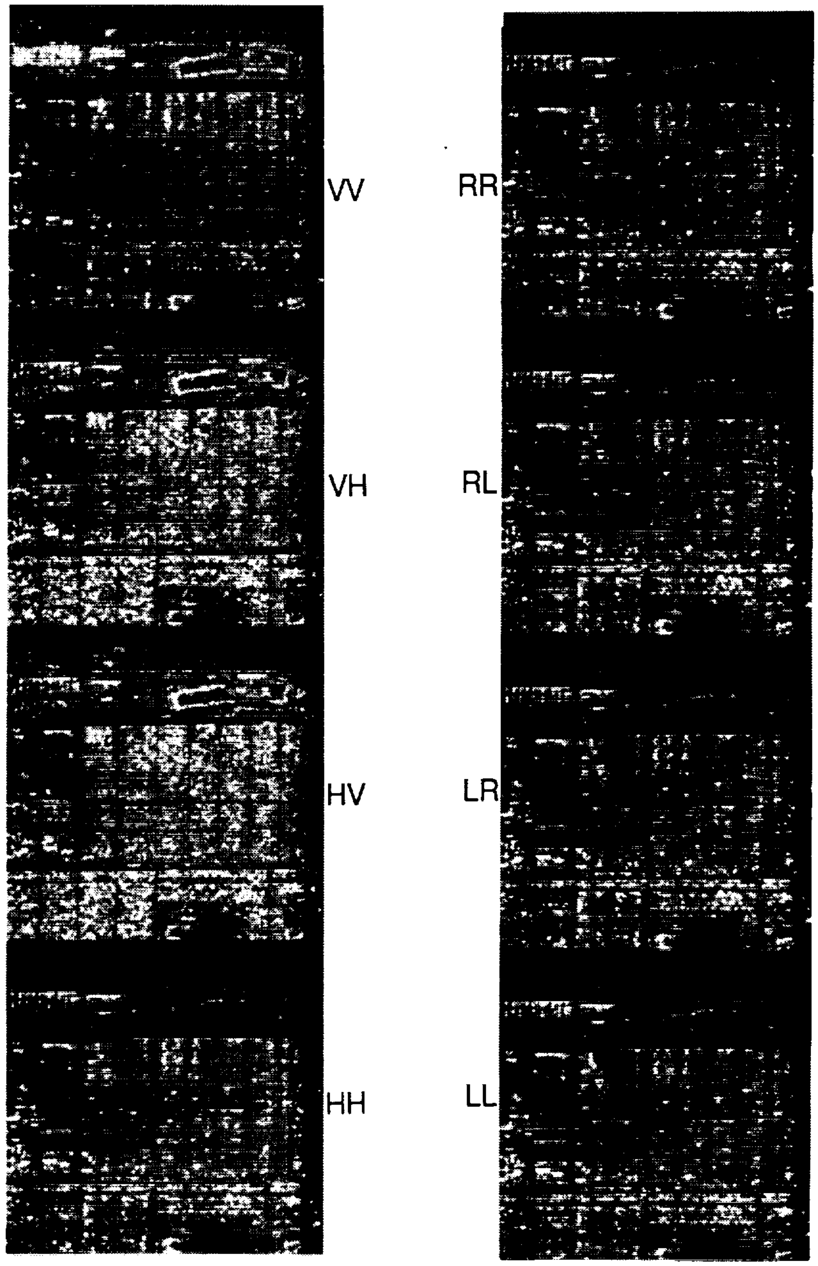

Figure 62. Linear and Circular Polarization Image Set for an Urban Area Next to Airforce Base Area

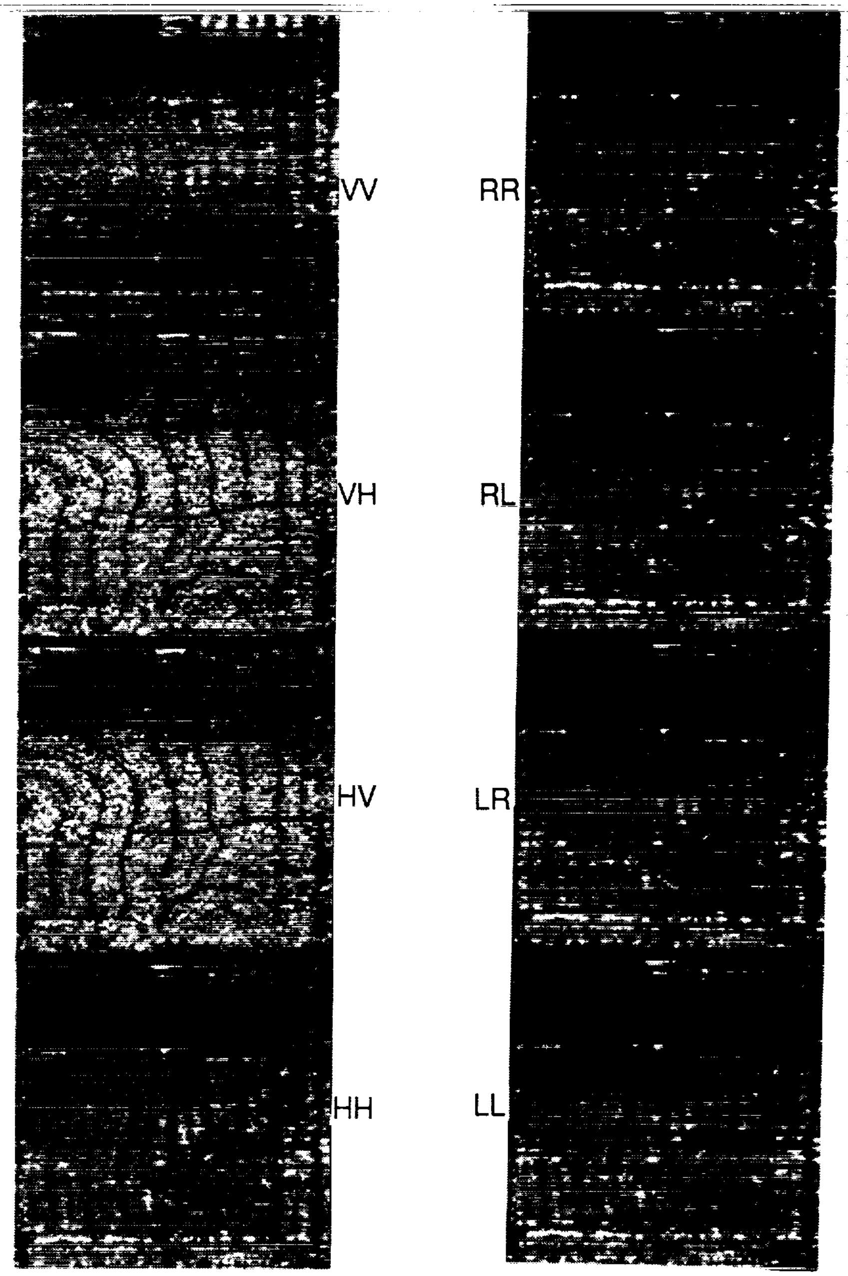

Figure 63. Linear and Circular Polarization Image Set for a Residential Area

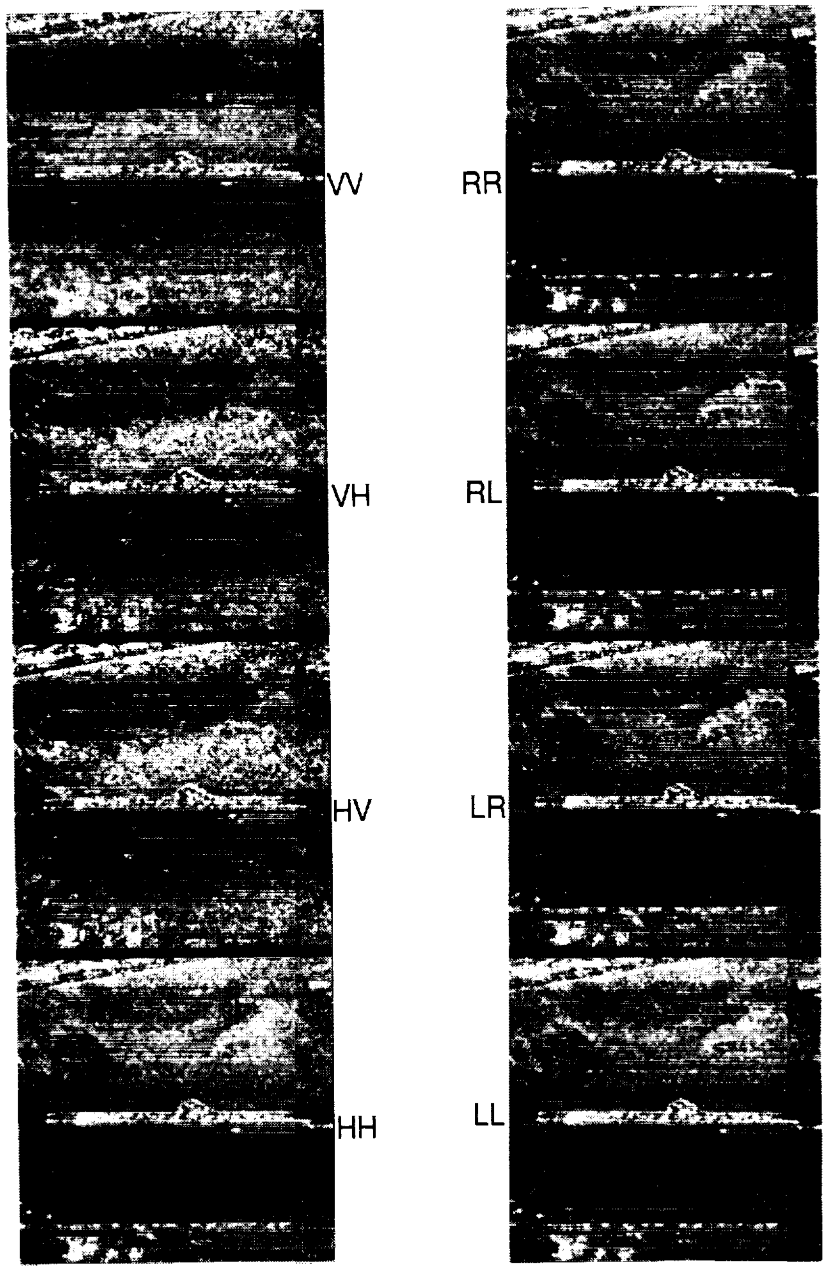

Figure 64. Linear and Circular Polarization Image Set for an Airforce Base Runway Area

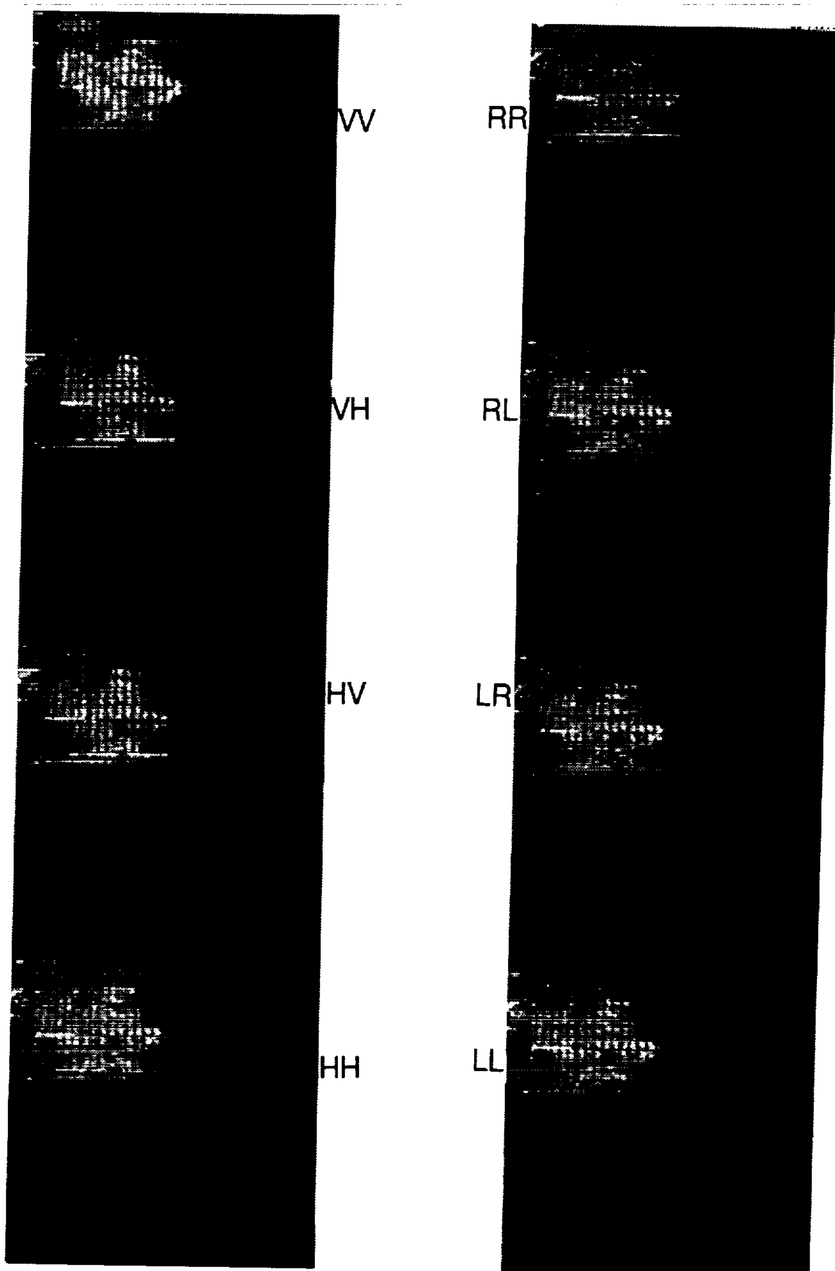

Figure 65. Linear and Circular Polarization Image Set for a Plant Area

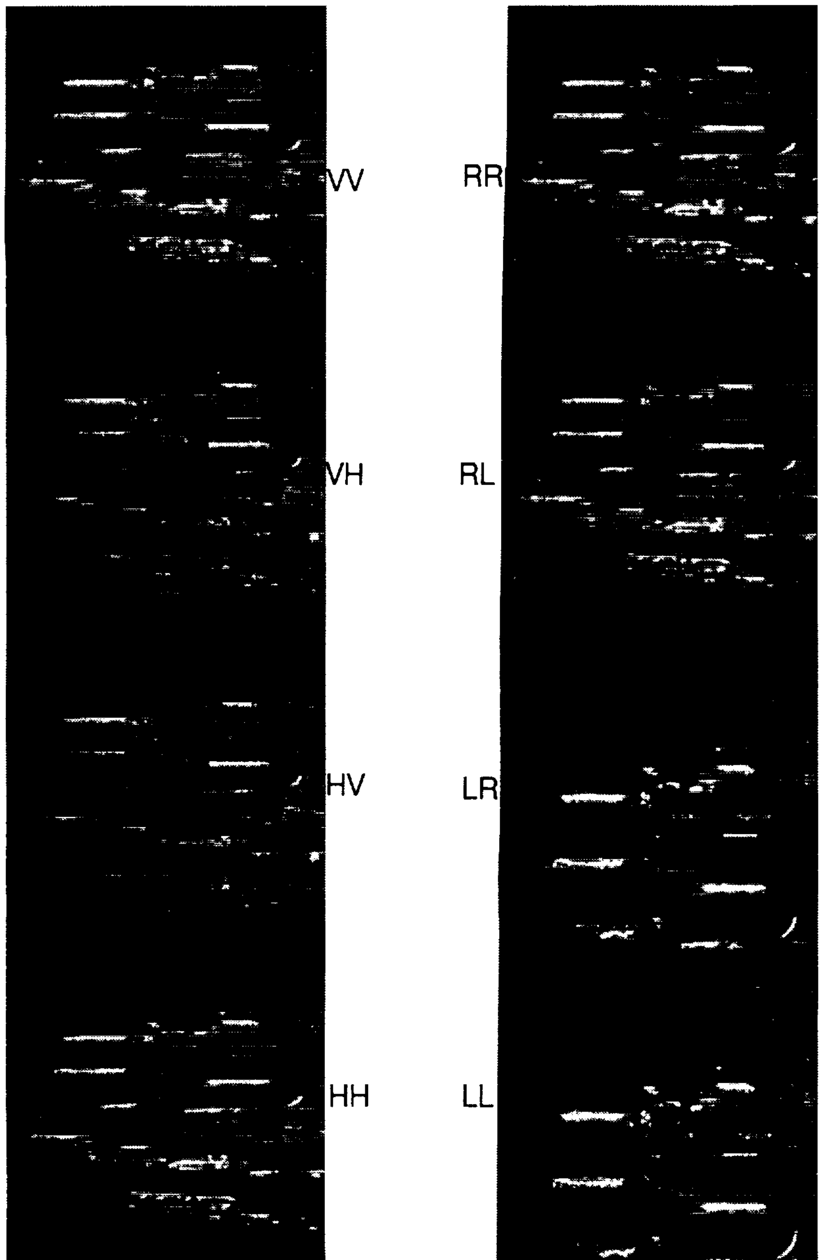

Figure 66. Linear and Circular Polarization Image Set for a Terminal Area

APPENDIX A

Clutter Statistics for Rocky Mountain and Low Altitude Images

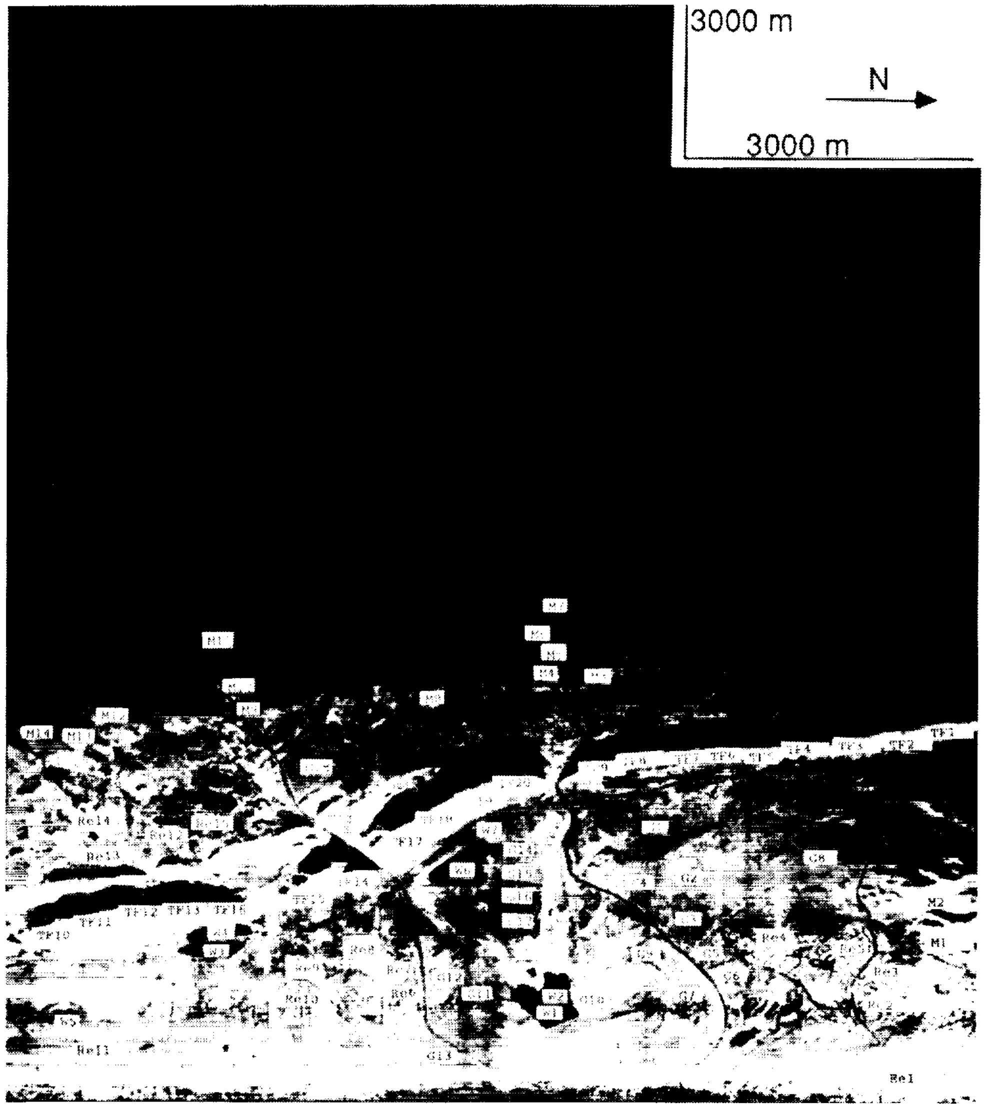

Figure A-1. Map of Clutter Locations, Rocky Mountains Image, X-HH

ORIGINAL PAGE IS
OF POOR QUALITY

PRECEDING PAGE BLANK NOT FILMED

PAGE A-2 INTENTIONALLY BLANK

Table A-1. Clutter Statistics for the Rocky Mountains Image

ID	Region Type	# Pts	Incidence Angle	Min (dB)	Max(dB)	Mean (dB)	Variance	SDEV	Variation
Re1	Residential	12500	50.34	-35.48	17.10	-11.72	0.35435E+00	0.59528E+00	0.88526E-01
Re2	Residential	6250	60.05	-35.48	-3.17	-24.82	0.10403E-03	0.10199E-01	0.30921E-01
Re3	Residential	6250	64.31	-35.48	2.75	-17.07	0.33452E-02	0.57838E-01	0.29467E+01
M1	Mountain	3750	68.45	-35.48	-5.63	-17.25	0.52433E-03	0.22898E-01	0.12147E+01
M2	Mountain	2400	71.01	-35.48	-5.21	-16.22	0.80052E-03	0.28293E-01	0.11839E+01
TF1	Thrust Feature	2400	77.43	-35.48	-14.94	-24.19	0.15688E-04	0.39609E-02	0.10389E+01
TF2	Thrust Feature	2400	77.22	-35.48	-13.94	-23.15	0.21556E-04	0.46428E-02	0.95836E-00
TF3	Thrust Feature	2400	77.11	-35.48	-13.54	-23.75	0.18550E-04	0.43070E-02	0.10215E+01
TF4	Thrust Feature	1000	76.92	-35.48	-15.17	-23.75	0.18952E-04	0.43534E-02	0.10315E+01
TF5	Thrust Feature	2400	76.77	-35.48	-11.57	-22.20	0.35931E-04	0.59943E-02	0.99425E-00
TF6	Thrust Feature	2400	76.75	-35.48	-12.32	-21.85	0.49805E-04	0.70572E-02	0.10807E+01
TF7	Thrust Feature	2400	76.67	-35.48	-10.82	-20.73	0.63368E-04	0.79604E-02	0.94082E-00
TF8	Thrust Feature	2400	76.56	-35.48	-12.05	-20.54	0.63851E-04	0.79907E-02	0.90537E-00
TF9	Thrust Feature	1900	76.48	-35.48	-9.56	-19.01	0.12604E-03	0.11227E-01	0.89319E+00
G1	Grass	10000	74.16	-35.48	-18.72	-31.04	0.85955E-06	0.92712E-03	0.11791E+01
G2	Grass	7500	71.82	-35.48	-15.24	-25.56	0.66122E-05	0.25714E-02	0.92443E-00
G3	Grass	7500	69.50	-35.48	-13.98	-27.99	0.42426E-05	0.20598E-02	0.12977E+01
G4	Grass	5000	71.69	-35.48	-17.59	-28.46	0.19844E-05	0.14087E-02	0.98842E-00
G5	Grass	4500	66.61	-35.48	-8.68	-25.52	0.18707E-04	0.43252E-02	0.15411E+01
G6	Grass	7500	64.24	-35.48	-11.41	-23.51	0.25001E-04	0.50001E-02	0.11222E+01
G7	Grass	6250	60.33	-35.48	-20.80	-30.05	0.71540E-06	0.84581E-03	0.85642E-00
Re4	Residential	8750	68.14	-35.48	21.00	-10.73	0.30085E+01	0.17345E+01	0.20508E+02
Re5	Residential	6250	67.00	-35.48	-1.29	-19.24	0.94536E-03	0.30747E-01	0.25813E+01
G8	Grass	10000	72.67	-35.48	-16.75	-28.15	0.25327E-05	0.15915E-02	0.10402E+01
G9	Grass	1500	66.67	-35.48	-15.95	-25.99	0.94002E-05	0.30660E-02	0.12167E+01
W1	Water	1000	58.07	-35.48	-27.46	-35.37	0.33627E-08	0.57989E-04	0.19990E-00
W2	Water	1000	60.00	-35.48	-29.04	-35.41	0.19806E-08	0.44504E-04	0.15467E-00
G10	Grass	3000	60.47	-35.48	-16.92	-27.47	0.25175E-05	0.15867E-02	0.88547E-00
G11	Grass	5000	61.78	-35.48	-18.68	-30.90	0.84206E-06	0.91764E-03	0.11280E+01
G12	Grass	5000	64.58	-35.48	-6.94	-24.81	0.28689E-04	0.53563E-02	0.16225E+01
G13	Grass	5000	48.98	-35.48	-12.81	-21.90	0.35299E-04	0.59413E-02	0.92056E-00
Re6	Residential	10000	61.66	-35.48	1.98	-20.67	0.10899E-02	0.33013E-01	0.38508E+01
Re7	Residential	5000	64.68	-35.48	6.30	-16.85	0.53325E-02	0.73024E-01	0.35344E+01
Re8	Residential	5000	67.19	-35.48	11.33	-11.94	0.14784E+00	0.38450E+00	0.60125E+01
Re9	Residential	5000	64.88	-35.48	13.15	-15.24	0.97030E-01	0.31150E+00	0.10420E+02
Re10	Residential	7500	58.76	-35.48	3.74	-17.62	0.59934E-02	0.77417E-01	0.44764E+01
W3	Water	1750	66.98	-35.48	-22.81	-35.31	0.34292E-07	0.18518E-03	0.62934E-00
W4	Water	1750	68.33	-35.48	-21.25	-35.14	0.87257E-07	0.29539E-03	0.96374E-00
Re11	Residential	7500	48.98	-35.48	20.33	-5.15	0.42471E+01	0.20609E+01	0.67526E+01
W5	Water	1500	58.61	-35.48	-28.25	-35.45	0.12501E-08	0.35357E-04	0.12391E-00
TF10	Thrust Feature	2400	68.34	-35.48	-0.08	-9.33	0.95748E-02	0.97851E-01	0.83912E-00
TF11	Thrust Feature	2400	68.88	-35.48	-1.07	-10.90	0.49621E-02	0.70442E-01	0.86581E-00
TF12	Thrust Feature	2400	69.19	-35.48	-2.37	-11.38	0.43075E-02	0.65631E-01	0.90095E-00
TF13	Thrust Feature	2400	69.54	-35.48	0.37	-13.59	0.37467E-02	0.61210E-01	0.13994E+01
TF14	Thrust Feature	2400	71.63	-35.48	-6.49	-18.06	0.32805E-03	0.18112E-01	0.11585E+01
TF15	Thrust Feature	2400	70.81	-35.48	-5.01	-16.63	0.52046E-03	0.22814E-01	0.10489E+01
TF16	Thrust Feature	2400	69.52	-35.48	1.57	-13.05	0.49000E-02	0.70000E-01	0.14115E+01
TF17	Thrust Feature	2400	73.61	-35.48	-10.04	-18.70	0.12500E-03	0.11180E-01	0.82805E-00
TF18	Thrust Feature	2400	74.64	-35.48	-11.96	-20.41	0.53635E-04	0.73236E-02	0.80413E+00
TF19	Thrust Feature	2400	75.24	-35.48	-11.28	-20.39	0.62957E-04	0.79345E-02	0.86900E-00
TF20	Thrust Feature	2400	75.66	-35.48	-13.42	-21.92	0.28879E-04	0.53740E-02	0.83597E-00
W6	Water	2400	72.36	-35.48	-29.22	-35.45	0.12699E-08	0.35636E-04	0.12512E-00
W7	Water	600	74.46	-35.48	-35.48	-35.48	0.34079E-14	0.58377E-07	0.20624E-03
G14	Grass	5000	73.30	-35.48	-14.37	-29.22	0.25092E-05	0.15840E-02	0.13224E+01
G15	Grass	5000	71.65	-35.48	-17.83	-30.62	0.94656E-06	0.97291E-03	0.11212E+01
G16	Grass	5000	70.46	-35.48	-22.00	-32.67	0.41286E-06	0.64254E-03	0.11871E+01
G17	Grass	5000	69.10	-35.48	-14.69	-30.93	0.21634E-05	0.14709E-02	0.18209E+01
M3	Mountain	5000	78.68	-35.48	-13.62	-25.48	0.28568E-04	0.53449E-02	0.18898E+01
M4	Mountain	4000	78.53	-35.48	-12.17	-25.48	0.29732E-04	0.54527E-02	0.19276E+01
M5	Mountain	1600	79.06	-35.48	-9.59	-23.77	0.98557E-04	0.99276E-02	0.23646E+01
M6	Mountain	1600	79.29	-35.48	-11.42	-24.32	0.84149E-04	0.91733E-02	0.24815E+01
M7	Mountain	3200	79.92	-35.48	-10.76	-26.72	0.64810E-04	0.80504E-02	0.37835E+01
M8	Mountain	2000	78.01	-35.48	-13.50	-24.81	0.22866E-04	0.47819E-02	0.14475E+01
G18	Grass	5000	76.05	-35.48	-18.71	-29.81	0.16519E-05	0.12853E-02	0.12310E+01
M9	Mountain	400	78.30	-35.48	-15.25	-24.68	0.26715E-04	0.51687E-02	0.15182E+01
M10	Mountain	400	78.39	-35.48	-13.87	-25.95	0.32844E-04	0.57310E-02	0.22572E+01
M11	Mountain	1500	79.58	-35.48	-9.19	-24.00	0.14637E-03	0.12098E-01	0.30398E+01
Re12	Residential	1800	74.00	-35.48	8.17	-15.79	0.36680E-01	0.19152E+00	0.72687E+01
M12	Mountain	2400	77.64	-35.48	-15.32	-26.11	0.90655E-05	0.30109E-02	0.12303E+01
M13	Mountain	2400	77.03	-35.48	-16.94	-26.57	0.60226E-05	0.24541E-02	0.11152E+01
M14	Mountain	2400	77.10	-35.48	-17.97	-28.30	0.34186E-05	0.18489E-02	0.12508E+01
Re13	Residential	7500	73.04	-35.48	4.34	-19.69	0.16248E-02	0.40309E-01	0.37517E+01
Re14	Residential	5000	74.30	-35.48	-4.91	-20.24	0.21731E-03	0.14742E-01	0.15592E+01
Re15	Residential	1800	74.56	-35.48	6.00	-19.01	0.12937E-01	0.11370E+00	0.90528E+01

90-11479

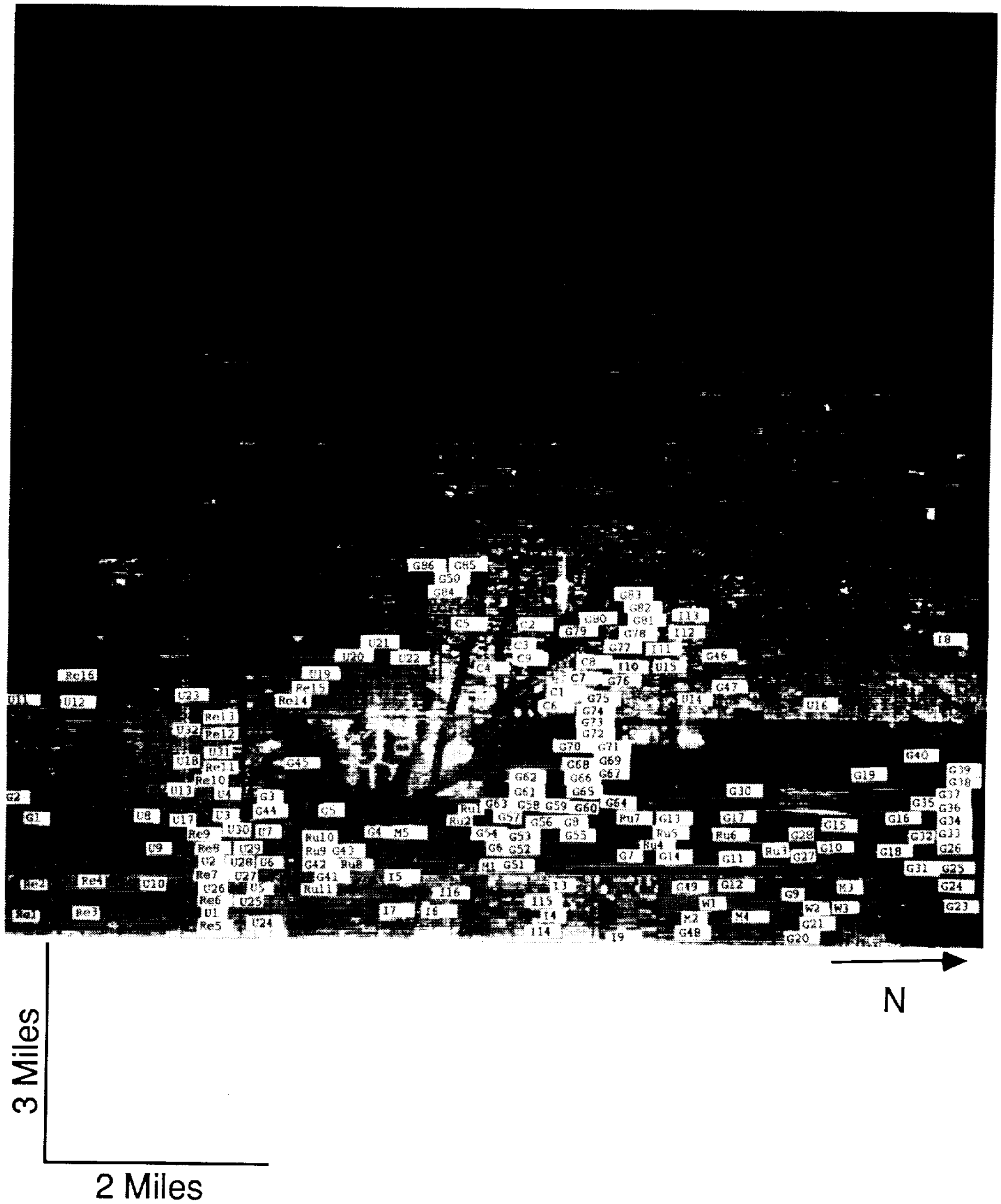

Figure A-2. Map of Clutter Locations, Low Altitude Image

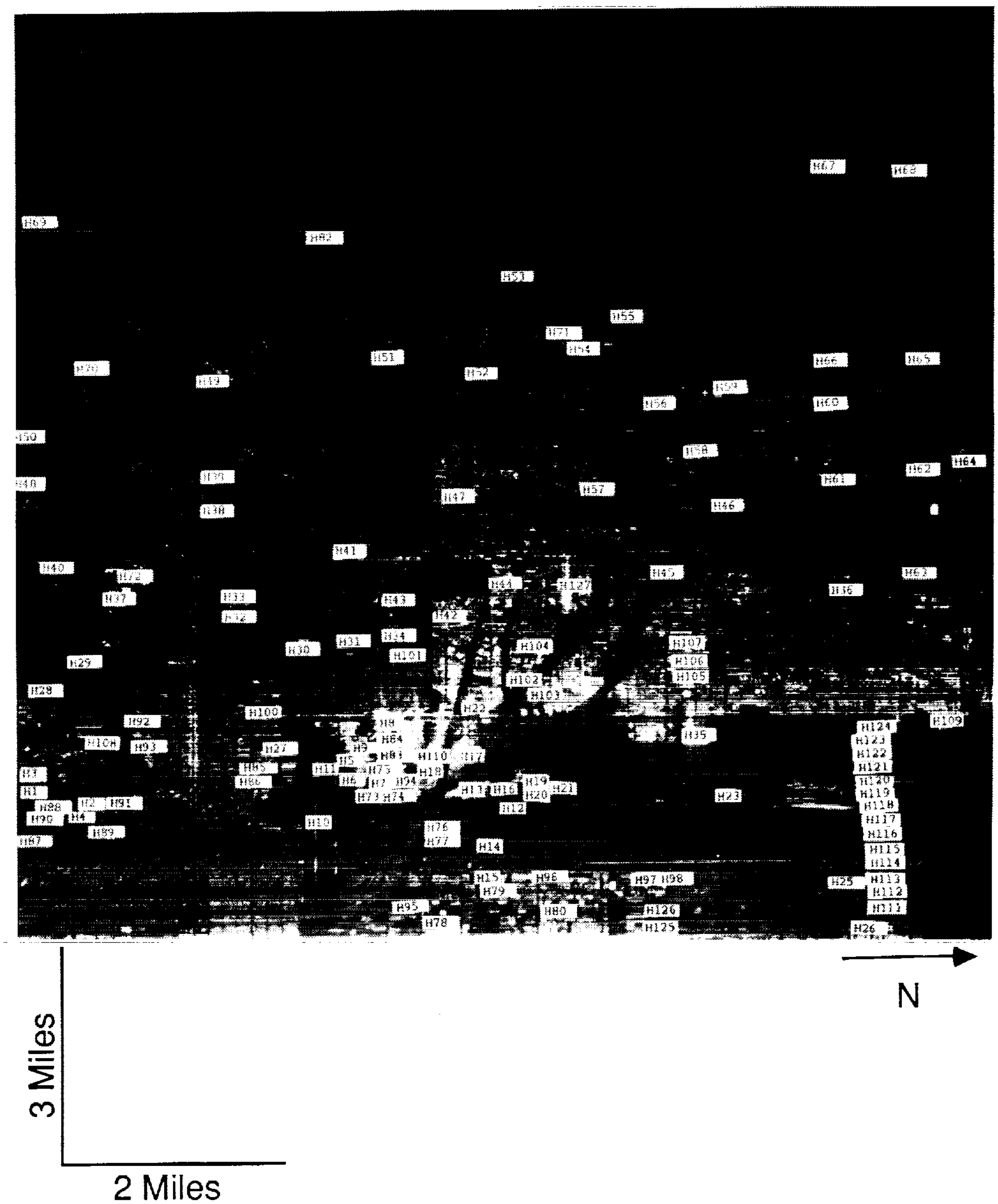

Figure A-3. Map of Clutter Locations, Low Altitude Image

Table A-2. Clutter Statistics for the Denver Low Altitude Image, X-HH

ID	Regional Type	Incidence Angle	# Pts	Min (dB)	Max(dB)	Mean (dB)	Variance	SDEV	Variation
Re1	Residential	49.36	5000	-44.07	3.14	-19.03	0.46119E-02	0.67911E-01	0.54313E+01
Re2	Residential	62.96	5000	-43.22	-0.03	-20.97	0.92351E-03	0.30389E-01	0.37968E+01
Re3	Residential	54.50	5000	-41.84	-2.65	-21.07	0.28637E-03	0.16923E-01	0.21639E+01
Re4	Residential	61.91	5000	-45.39	-1.04	-19.79	0.12638E-02	0.35550E-01	0.33859E+01
G1	Grass	75.11	1000	-46.68	-26.87	-33.79	0.10089E-06	0.31763E-03	0.76075E+00
H1	Building	77.43	2000	-53.33	7.58	-15.20	0.73597E-01	0.27129E+00	0.89880E+01
G2	Grass	76.35	1800	-53.33	-26.37	-34.36	0.10099E-06	0.31778E-03	0.86654E+00
H2	Building	76.60	2000	-53.33	2.88	-21.45	0.39059E-02	0.62497E-01	0.87269E+01
H3	Building	78.33	2000	-53.33	3.01	-21.48	0.29121E-02	0.53964E-01	0.75796E+01
H4	Building	75.59	1200	-48.34	-2.52	-22.58	0.92553E-03	0.30423E-01	0.55109E+01
U1	Urban	55.14	10000	-53.33	3.15	-19.02	0.24927E-02	0.49927E-01	0.39804E+01
U2	Urban	68.21	10000	-41.80	1.78	-18.55	0.32617E-02	0.57111E-01	0.40870E+01
U3	Urban	74.41	5000	-43.88	0.21	-22.98	0.71330E-03	0.26708E-01	0.53029E+01
U4	Urban	76.44	5000	-45.31	6.69	-20.01	0.57059E-02	0.75538E-01	0.75740E+01
U13	Urban	76.31	5000	-53.33	4.42	-19.47	0.47427E-02	0.68868E-01	0.61006E+01
U17	Urban	78.26	5000	-53.33	6.56	-16.90	0.17514E-01	0.13234E+00	0.64759E+01
U18	Urban	74.23	5000	-45.91	-1.91	-23.38	0.54237E-03	0.23289E-01	0.50725E+01
U5	Urban	63.39	5000	-41.95	0.45	-19.94	0.13876E-02	0.37250E-01	0.36752E-01
U6	Urban	70.61	5000	-47.29	-2.84	-22.63	0.39308E-03	0.19826E-01	0.36334E+01
U7	Urban	73.16	5000	-48.53	-5.59	-24.73	0.12923E-03	0.11368E-01	0.33798E+01
G3	Grass	76.26	1200	-53.33	-25.06	-34.38	0.95224E-07	0.30858E-03	0.84507E+00
G4	Grass	73.27	1200	-44.54	-22.30	-32.60	0.22240E-06	0.47159E-03	0.85857E+00
H5	Terminal	78.85	2000	-53.33	10.72	-11.57	0.35902E+00	0.59918E+00	0.85993E+01
H6	Terminal	78.09	4000	-42.40	10.23	-11.93	0.20640E+00	0.45431E+00	0.70826E+01
H7	Terminal	74.82	2800	-53.33	-7.45	-25.07	0.10689E-03	0.10339E-01	0.33208E+01
G5	Grass	75.88	1800	-45.79	-16.88	-32.57	0.68132E-06	0.82542E-03	0.14912E+01
H8	Parking Lot	80.50	2500	-53.33	14.26	-7.87	0.18248E+01	0.13509E+01	0.82705E+01
H9	Parking Lot	79.36	2500	-53.33	10.78	-12.58	0.11479E+00	0.33880E+00	0.61302E+01
H10	Plane	74.82	200	-49.56	-11.09	-23.50	0.10054E-03	0.10027E-01	0.22433E+01
H11	Plane	77.67	200	-53.33	-4.43	-22.07	0.92692E-03	0.30445E-01	0.49088E+01
H12	Plane	75.90	225	-53.33	-29.52	-40.09	0.33291E-07	0.18246E-03	0.18640E+01
H13	Parking Lot	77.37	2500	-38.40	1.78	-15.91	0.51541E-02	0.71792E-01	0.28007E+01
G6	Grass	72.94	5000	-50.81	-7.17	-28.71	0.33424E-04	0.57813E-02	0.42958E+01
Ru1	Runway	75.90	1000	-53.33	-25.26	-37.85	0.50726E-07	0.22522E-03	0.13729E+01
Ru2	Runway	75.17	1000	-53.33	-28.22	-38.98	0.22505E-07	0.15002E-03	0.11859E+01
H14	Truck	72.68	25	-39.10	-7.17	-18.07	0.16857E-02	0.41057E-01	0.26305E+01
H15	Truck	66.98	25	-37.82	-18.26	-26.22	0.86225E-05	0.29364E-02	0.12290E+01
H16	Truck	77.44	25	-53.33	-14.91	-24.62	0.63287E-04	0.79553E-02	0.23041E+01
M1	Tree	70.16	49	-36.08	-1.67	-14.07	0.13142E-01	0.11464E+00	0.29256E+01
H17	Parking Lot	79.45	1200	-53.33	-2.28	-18.75	0.94226E-03	0.30696E-01	0.23025E+01
H18	Building	77.77	1200	-53.33	5.75	-12.94	0.68591E-01	0.26190E+00	0.51511E+01
H19	Plane	77.18	225	-53.33	-17.22	-31.67	0.44574E-05	0.21113E-02	0.31003E+01
H20	Plane	77.23	225	-53.33	-16.12	-30.65	0.63123E-05	0.25124E-02	0.29202E+01
H21	Plane	77.18	225	-53.33	-7.00	-28.23	0.16287E-03	0.13523E-01	0.89970E+01
H22	Parking Lot	81.13	2500	-53.33	11.73	-12.59	0.10886E+00	0.32994E+00	0.59858E+01
H23	Fence	76.44	1150	-53.33	-24.27	-33.39	0.19657E-06	0.44336E-03	0.96725E+00
Ru3	Runway	72.47	700	-49.47	-30.80	-37.38	0.18863E-07	0.13734E-03	0.75169E+00
W1	Water	61.41	400	-53.33	-35.35	-43.21	0.17210E-08	0.41485E-04	0.86957E+00
M2	Tree	55.63	300	-29.38	-11.61	-18.71	0.12870E-03	0.11344E-01	0.84242E+00
H125	Warehouse	46.51	400	-30.42	2.47	-11.68	0.37943E-01	0.19479E+00	0.28689E+01
H126	Warehouse	55.14	1600	-42.96	-0.54	-16.86	0.40846E-02	0.63911E-01	0.30982E-01
G7	Grass	71.91	400	-39.49	-20.99	-28.86	0.12927E-05	0.11370E-02	0.87460E+00
G8	Grass	74.85	400	-51.17	-23.96	-33.02	0.29009E-06	0.53860E-03	0.10793E+01
I3	Building	55.63	864	-42.62	-2.88	-15.70	0.29764E-02	0.54556E-01	0.20266E+01
I4	Building	64.60	750	-39.63	-4.17	-17.08	0.19845E-02	0.44547E-01	0.22753E+01
U8	Urban	74.27	3750	-46.17	-4.28	-24.32	0.19348E-03	0.13910E-01	0.37583E+01
U9	Urban	66.22	3750	-41.52	1.96	-18.17	0.33493E-02	0.57873E-01	0.37965E+01
U10	Urban	53.28	3750	-45.46	-1.75	-20.91	0.55599E-03	0.23579E-01	0.29076E+01
M3	Tree	66.66	1000	-42.67	-1.19	-18.83	0.21569E-02	0.46442E-01	0.35477E+01

Table A-2. Cont.

W2	Water	59.48	1000	-53.33	-29.94	-38.31	0.18824E-07	0.13720E-03	0.93048E+00
W3	Water	60.39	1000	-53.33	-23.13	-37.36	0.11918E-06	0.34522E-03	0.18807E+01
H25	Building	64.34	2000	-53.33	-5.72	-25.81	0.54587E-04	0.73883E-02	0.28125E+01
G9	Grass	66.16	5000	-43.84	-17.97	-27.01	0.25832E-05	0.16072E-02	0.80652E+00
G10	Grass	73.19	5000	-48.39	-17.03	-30.07	0.17936E-05	0.13393E-02	0.13626E+01
H26	Building	50.88	1000	-41.29	8.09	-17.35	0.44922E-01	0.21195E+00	0.11526E+02
G11	Grass	71.18	5000	-50.07	-4.90	-29.09	0.45387E-04	0.67370E-02	0.54637E+01
G12	Grass	65.47	5000	-53.33	-19.49	-26.97	0.24755E-05	0.15734E-02	0.78389E+00
M4	Tree	51.67	1950	-41.23	-13.55	-22.65	0.29423E-04	0.54243E-02	0.99957E+00
G13	Grass	74.46	1500	-47.67	-21.87	-31.44	0.50635E-06	0.71158E-03	0.99115E+00
G14	Grass	71.62	1500	-48.19	-20.50	-28.72	0.12942E-05	0.11376E-02	0.84798E+00
Ru4	Runway	73.02	450	-49.43	-29.95	-37.72	0.18219E-07	0.13498E-03	0.79757E+00
Ru5	Runway	73.54	450	-53.33	-30.47	-39.75	0.12386E-07	0.11129E-03	0.10510E+01
Ru6	Runway	73.54	450	-52.82	-31.38	-39.61	0.10770E-07	0.10378E-03	0.94961E+00
Ru7	Runway	75.84	450	-53.33	-31.04	-43.28	0.35479E-08	0.59564E-04	0.12678E+01
G15	Grass	74.89	10000	-53.33	-8.41	-32.96	0.28910E-05	0.17003E-02	0.33600E+01
G16	Grass	75.77	10000	-53.33	-10.08	-28.92	0.37109E-05	0.19264E-02	0.15019E+01
G17	Grass	75.11	10000	-53.33	-2.00	-30.48	0.43481E-04	0.65940E-02	0.73568E+01
G18	Grass	72.99	10000	-46.23	-16.49	-29.29	0.10995E-05	0.10486E-02	0.89105E+00
G19	Grass	78.93	2500	-53.33	-24.12	-32.34	0.25840E-06	0.50833E-03	0.87121E+00
M5	Tree	74.00	900	-43.23	-14.41	-26.16	0.14870E-04	0.38562E-02	0.15919E+01
I5	Industrial	66.27	3600	-41.32	3.55	-19.71	0.41874E-02	0.64710E-01	0.60570E+01
I6	Industrial	54.50	900	-38.64	1.58	-15.77	0.57454E-02	0.75798E-01	0.28611E+01
I7	Industrial	55.39	450	-38.53	-1.49	-13.19	0.64097E-02	0.80060E-01	0.16673E+01
Ru8	Runway	70.89	500	-47.40	-20.36	-31.75	0.78445E-06	0.88569E-03	0.13239E+01
Ru9	Runway	72.13	500	-50.81	-25.94	-36.15	0.75531E-07	0.27483E-03	0.11327E+01
Ru10	Runway	77.11	500	-53.33	-33.76	-44.50	0.31177E-08	0.55836E-04	0.15731E+01
Ru11	Runway	63.95	500	-53.33	-20.58	-31.32	0.11352E-05	0.10655E-02	0.14433E+01
H27	Parking Lot	79.57	5000	-53.33	5.96	-13.94	0.25679E-01	0.16025E+00	0.39727E+01
H28	Building	81.77	450	-53.33	1.69	-15.10	0.12370E-01	0.11122E+00	0.35959E+01
U11	Urban	81.15	5000	-53.33	17.02	-11.00	0.87110E+00	0.93333E+00	0.11746E+02
H29	Building	82.81	600	-53.33	17.00	-1.86	0.11118E+02	0.33344E+01	0.51226E+01
H108	Building	79.56	1250	-53.33	-3.36	-22.94	0.40535E-03	0.20133E-01	0.39587E+01
U12	Urban	81.11	1250	-53.33	1.09	-20.94	0.42683E-02	0.65332E-01	0.81201E+01
H127	Building	83.81	1000	-53.33	38.17	19.82	0.23264E+06	0.48233E+03	0.50251E+01
H30	Building	82.91	1250	-53.33	23.19	2.63	0.12751E+03	0.11292E+02	0.61574E+01
H31	Building	82.05	300	-53.33	12.07	-8.60	0.10719E+01	0.10353E+01	0.75014E+01
H32	Building	81.88	450	-53.33	13.75	-4.57	0.27612E+01	0.16617E+01	0.47599E+01
H33	Building	82.82	1000	-53.33	23.19	3.59	0.15836E+03	0.12584E+02	0.55073E+01
H34	Building	82.88	400	-53.33	8.18	-10.15	0.30841E+00	0.55534E+00	0.57440E+01
C1	City	81.71	1800	-53.33	16.49	-4.81	0.49974E+01	0.22355E+01	0.67646E+01
U14	Urban	81.69	800	-53.33	12.18	-8.31	0.55254E+00	0.74333E+00	0.50334E+01
H35	Building	80.09	2500	-53.33	17.74	0.83	0.19623E+02	0.44297E+01	0.36623E+01
U15	Urban	82.44	1200	-53.33	14.06	-7.00	0.11961E+01	0.10937E+01	0.54848E-01
H36	Building	83.38	450	-53.33	6.02	-13.52	0.55043E-01	0.23461E+00	0.52802E+01
U16	Urban	81.09	2400	-53.33	3.11	-16.17	0.14156E-01	0.11898E+00	0.49245E+01
H109	Building	80.38	680	-53.33	-2.04	-26.15	0.99274E-03	0.31508E-01	0.12979E+02
I8	Industrial	82.91	1800	-53.33	12.70	-8.03	0.74094E+00	0.86078E+00	0.54744E+01
H37	Building	83.81	1200	-53.33	20.34	0.98	0.39557E+02	0.62895E+01	0.50203E+01
H38	Building	84.83	400	-53.33	23.16	6.10	0.39389E+03	0.19847E+02	0.48688E+01
H39	Building	85.09	400	-53.33	15.90	-1.63	0.10656E+02	0.32644E+01	0.47551E+01
H40	Building	84.09	300	-53.33	19.18	3.02	0.59951E+02	0.77428E+01	0.38638E+01
H41	Building	84.31	300	-53.33	22.71	6.28	0.30167E+03	0.17369E+02	0.40942E+01
H42	Building	83.37	100	-53.33	13.57	1.00	0.14053E+02	0.37487E+01	0.29776E+01
H43	Building	83.58	450	-53.33	15.92	-1.65	0.70665E+01	0.26583E+01	0.38849E+01
H44	Building	83.61	125	-53.33	19.56	9.85	0.27985E+03	0.16729E+02	0.17332E+01
H45	Building	84.16	140	-53.33	15.13	2.44	0.19995E+02	0.44716E+01	0.25522E+01
H46	Building	84.88	210	-53.33	24.13	10.65	0.14533E+04	0.38122E+02	0.32834E+01
H47	Building	84.93	1120	-53.33	23.26	3.61	0.14795E+03	0.12164E+02	0.52920E+01
H48	Building	85.09	200	-53.33	25.87	9.48	0.14666E+04	0.38296E+02	0.43170E+01
H49	Building	85.97	3200	-53.33	31.41	5.64	0.15576E+04	0.39466E+02	0.10769E+02
H50	Building	85.51	150	-53.33	9.75	-1.43	0.31605E+01	0.17778E+01	0.24738E+01
H51	Building	86.06	129	-53.33	3.62	-9.84	0.16044E+00	0.40055E+00	0.38610E+01
H52	Building	85.96	159	-53.33	10.72	-1.40	0.33056E+01	0.18181E+01	0.25090E+01

Table A-2. Cont.

H53	Building	86.29	120	-53.33	4.20	-5.01	0.45315E+00	0.67317E+00	0.21354E+01
H54	Building	85.83	200	-53.33	12.29	1.33	0.90661E+01	0.30110E+01	0.22166E+01
H55	Building	86.29	6000	-53.33	26.80	-0.54	0.97952E+02	0.98971E+01	0.11219E+02
H56	Building	85.47	1050	-53.33	23.23	2.55	0.10400E+03	0.10198E+02	0.56702E+01
H57	Building	85.10	350	-53.33	17.88	0.24	0.20848E+02	0.45659E+01	0.43241E+01
H58	Building	85.36	700	-53.33	21.89	5.27	0.19973E+03	0.14133E+02	0.42009E+01
H59	Building	85.58	200	-53.33	29.83	14.66	0.71726E+04	0.84691E+02	0.28976E+01
H60	Building	85.71	1225	-53.33	17.88	-1.46	0.83436E+01	0.28885E+01	0.40472E+01
H61	Building	85.09	500	-53.33	16.27	2.70	0.27447E+02	0.52390E+01	0.28105E+01
H62	Building	84.76	2400	-53.33	19.77	-0.16	0.14126E+02	0.37584E+01	0.39035E+01
H63	Building	83.92	225	-53.33	8.42	-7.02	0.45979E+00	0.67808E+00	0.34160E+01
H64	Building	85.29	750	-53.33	31.82	11.84	0.10157E+05	0.10078E+03	0.65923E+01
H65	Building	86.04	500	-53.33	35.33	16.42	0.72120E+05	0.26855E+03	0.61264E+01
H66	Building	86.04	200	-53.33	16.41	3.05	0.39239E+02	0.62641E+01	0.31062E+01
H67	Building	86.95	540	-53.33	20.02	3.82	0.11924E+03	0.10920E+02	0.45333E+01
H68	Building	86.95	75	-53.33	33.14	19.81	0.11844E+06	0.34415E+03	0.35933E+01
H69	Building	86.76	120	-53.33	22.66	13.00	0.13363E+04	0.36556E+02	0.18333E+01
H70	Building	86.02	559	-53.33	20.38	4.46	0.84268E+02	0.91798E+01	0.32909E+01
H71	Building	86.12	825	-53.33	14.46	-2.10	0.82010E+01	0.28637E+01	0.46472E+01
H72	Building	84.09	500	-53.33	23.23	5.26	0.25940E+03	0.16106E+02	0.47943E+01
C2	City	83.31	5000	-53.33	16.40	-10.93	0.11014E+01	0.10495E+01	0.12987E+02
H73	Plane	77.40	420	-53.33	-0.52	-20.61	0.30728E-02	0.55433E-01	0.63744E+01
H74	Plane	76.87	420	-53.33	-5.60	-24.67	0.42882E-03	0.20708E-01	0.60735E+01
H75	Plane	78.12	420	-53.33	3.04	-16.63	0.26841E-01	0.16383E+00	0.75355E+01
H76	Truck	74.62	144	-45.30	-15.36	-27.64	0.17079E-04	0.41327E-02	0.24007E+01
H77	Truck	74.07	144	-45.46	-16.02	-28.48	0.11459E-04	0.33851E-02	0.23863E+01
G20	Grass	42.90	1600	-53.33	-15.11	-24.34	0.10347E-04	0.32166E-02	0.87332E+00
G21	Grass	53.56	1600	-45.09	-18.88	-28.11	0.21223E-05	0.14568E-02	0.94195E+00
G23	Grass	63.11	1600	-39.88	-17.56	-25.38	0.49802E-05	0.22316E-02	0.77068E+00
G24	Grass	66.50	1600	-53.33	-17.19	-27.14	0.34191E-05	0.18491E-02	0.95746E+00
G25	Grass	69.53	1600	-45.91	-19.94	-28.09	0.17432E-05	0.13203E-02	0.85006E+00
G26	Grass	71.79	1600	-43.73	-22.26	-28.81	0.85981E-06	0.92726E-03	0.70521E+00
G27	Grass	71.46	1600	-43.57	-22.04	-29.33	0.75642E-06	0.86972E-03	0.74479E+00
G28	Grass	74.39	1600	-49.58	-24.81	-33.94	0.13156E-06	0.36271E-03	0.89822E+00
C3	City	82.91	5000	-53.33	18.46	-8.59	0.26206E+01	0.16188E+01	0.11714E+02
G30	Grass	77.75	1600	-53.33	-29.12	-39.89	0.12329E-07	0.11103E-03	0.10821E+01
G31	Grass	69.36	1600	-41.37	-19.16	-28.46	0.12883E-05	0.11350E-02	0.79590E+00
G32	Grass	72.35	1600	-41.36	-19.91	-29.45	0.88145E-06	0.93886E-03	0.82793E+00
G33	Grass	74.24	1600	-46.58	-24.20	-31.12	0.33793E-06	0.58132E-03	0.75215E+00
G34	Grass	75.65	1600	-44.01	-20.58	-29.69	0.77797E-06	0.88203E-03	0.82066E+00
G35	Grass	76.54	1600	-45.41	-22.47	-30.41	0.50435E-06	0.71018E-03	0.78015E+00
G36	Grass	77.52	1600	-53.33	-24.24	-31.91	0.24834E-06	0.49834E-03	0.77417E+00
G37	Grass	78.12	1600	-53.33	-20.22	-32.44	0.27014E-06	0.51975E-03	0.91156E+00
G38	Grass	78.67	1600	-53.33	-24.09	-32.13	0.26556E-06	0.51532E-03	0.84135E+00
G39	Grass	79.16	1600	-53.33	-24.79	-35.70	0.13615E-06	0.36899E-03	0.13718E+01
G40	Grass	80.35	1600	-53.33	-23.93	-37.04	0.20234E-06	0.44982E-03	0.22733E+01
G41	Grass	69.36	1800	-41.71	-13.62	-24.68	0.96855E-05	0.31121E-02	0.91437E+00
G42	Grass	71.52	1800	-46.74	-11.65	-28.08	0.58961E-05	0.24282E-02	0.15600E+01
G43	Grass	73.27	1800	-47.12	-20.11	-30.42	0.62695E-06	0.79180E-03	0.87272E+00
G44	Grass	76.68	1800	-53.33	-20.69	-34.89	0.16113E-06	0.40141E-03	0.12386E+01
G45	Grass	79.23	1800	-53.33	-22.07	-41.13	0.78621E-07	0.28039E-03	0.36391E+01
Re5	Residential	50.55	4000	-53.33	4.69	-16.55	0.69885E-02	0.83597E-01	0.37781E+01
Re6	Residential	59.67	4000	-40.78	0.37	-17.36	0.31757E-02	0.56353E-01	0.30678E+01
Re7	Residential	66.71	4000	-39.94	2.76	-17.29	0.40174E-02	0.63383E-01	0.33980E+01
Re8	Residential	72.17	4000	-45.23	-1.80	-23.33	0.54342E-03	0.23311E-01	0.50134E+01
Re9	Residential	74.24	4000	-45.16	0.21	-23.86	0.48206E-03	0.21956E-01	0.53366E+01
Re10	Residential	76.40	4000	-45.31	6.69	-20.21	0.69677E-02	0.83473E-01	0.87701E+01
Re11	Residential	77.81	4000	-53.33	9.01	-16.68	0.51935E-01	0.22789E+00	0.10600E+02
Re12	Residential	79.41	4000	-53.33	2.33	-19.84	0.43862E-02	0.66228E-01	0.63781E+01
Re13	Residential	80.08	4000	-53.33	4.21	-18.27	0.96979E-02	0.98478E-01	0.66056E+01
Re14	Residential	81.13	4000	-53.33	4.50	-18.54	0.10898E-01	0.10440E+00	0.74660E+01
Re15	Residential	81.52	4000	-53.33	10.12	-18.64	0.34106E-01	0.18468E+00	0.13501E+02
H78	Building	49.54	1200	-40.05	-0.54	-19.25	0.23983E-02	0.48973E-01	0.41207E+01
H79	Building	67.23	1200	-38.24	2.39	-16.07	0.94986E-02	0.97461E-01	0.39438E+01

Table A-2. Cont.

H80	Building	58.30	1200	-40.83	1.20	-13.20	0.15183E-01	0.12322E+00	0.25721E+01
C4	City	82.35	5000	-53.33	12.37	-11.02	0.40563E+00	0.63689E+00	0.80598E+01
H82	Building	86.14	196	-53.33	20.95	5.07	0.23037E+03	0.15178E+02	0.47253E+01
H83	Building	78.01	4000	-43.57	8.76	-12.93	0.70635E-01	0.26577E+00	0.52139E+01
H84	Building	79.62	4000	-53.33	18.88	-6.52	0.51649E+01	0.22726E+01	0.10192E+02
H85	Building	78.56	225	-41.60	8.09	-10.08	0.28617E+00	0.53495E+00	0.54511E+01
H86	Building	78.23	400	-37.97	3.07	-13.42	0.30280E-01	0.17401E+00	0.38269E+01
H87	Building	74.05	405	-42.68	0.69	-17.23	0.72259E-02	0.85005E-01	0.44939E+01
H88	Building	76.75	2000	-53.33	6.41	-18.78	0.25765E-01	0.16052E+00	0.12107E+02
H89	Building	74.36	2000	-45.65	-8.28	-27.50	0.51898E-04	0.72040E-02	0.40526E+01
H90	Building	75.75	500	-53.33	1.13	-18.45	0.75252E-02	0.86748E-01	0.60649E+01
H91	Building	76.72	1200	-53.33	-9.71	-28.17	0.31938E-04	0.56514E-02	0.37067E+01
H92	Building	79.74	525	-53.33	8.07	-9.18	0.20086E+00	0.44817E+00	0.37102E+01
H93	Building	78.89	525	-53.33	5.43	-11.91	0.76658E-01	0.27687E+00	0.42976E+01
H94	Building	77.78	500	-34.96	16.03	-9.40	0.32907E+01	0.18140E+01	0.15808E+02
H95	Building	65.70	595	-36.64	6.60	-12.24	0.80719E-01	0.28411E+00	0.47597E+01
H96	Building	65.82	864	-37.97	0.46	-17.36	0.55101E-02	0.74230E-01	0.40429E+01
H97	Building	66.27	416	-35.69	1.69	-13.00	0.24284E-01	0.15583E+00	0.31085E+01
H98	Building	67.49	416	-37.16	-0.48	-17.56	0.35925E-02	0.59937E-01	0.34147E+01
C5	City	83.16	3750	-53.33	16.78	-5.75	0.41799E+01	0.20445E+01	0.76763E+01
H100	Building	80.91	600	-53.33	14.26	-8.49	0.22633E+01	0.15044E+01	0.10625E+02
H101	Building	82.56	900	-53.33	16.99	-5.73	0.45035E+01	0.21222E+01	0.79438E+01
H102	Building	81.92	675	-53.33	14.29	-2.97	0.43438E+01	0.20842E+01	0.41345E+01
H103	Building	81.56	450	-53.33	14.15	-2.76	0.41527E+01	0.20378E+01	0.38502E+01
H104	Building	82.72	450	-53.33	15.59	-5.35	0.47262E+01	0.21740E+01	0.74545E+01
H105	Building	82.03	600	-53.33	12.54	-5.28	0.16556E+01	0.12867E+01	0.43351E+01
H106	Building	82.43	600	-53.33	14.06	-4.63	0.22885E+01	0.15128E+01	0.43906E+01
H107	Building	82.74	600	-53.33	16.31	-4.85	0.62281E+01	0.24956E+01	0.76208E+01
G46	Grass	82.47	800	-53.33	-53.33	-53.33	0.72430E-18	0.85106E-09	0.18313E-03
G47	Grass	81.82	800	-53.33	-24.10	-50.22	0.18860E-07	0.13733E-03	0.14447E+02
G48	Grass	46.10	5000	-53.33	-12.50	-24.18	0.18168E-04	0.42624E-02	0.11170E+01
G49	Grass	65.17	5000	-41.99	-11.73	-23.60	0.22167E-04	0.47082E-02	0.10795E+01
G50	Grass	83.89	3000	-53.33	-3.86	-33.27	0.10976E-03	0.10477E-01	0.22240E+02
H110	Terminal	78.37	3500	-53.33	7.60	-13.52	0.64508E-01	0.25398E+00	0.57165E+01
I9	Industrial	81.25	7500	-53.33	21.02	-7.90	0.47437E+01	0.21780E+01	0.13429E+02
I10	Industrial	82.17	7500	-53.33	11.57	-13.26	0.15603E+00	0.39501E+00	0.83723E+01
I11	Industrial	82.62	7500	-53.33	16.31	-9.05	0.89743E+00	0.94733E+00	0.76134E+01
I12	Industrial	82.96	7500	-53.33	18.02	-9.76	0.13398E+01	0.11575E+01	0.10941E+02
I13	Industrial	83.40	7500	-53.33	20.87	-7.48	0.76310E+01	0.27624E+01	0.15468E+02
I14	Industrial	44.57	7500	-40.74	6.14	-14.71	0.15794E-01	0.12567E+00	0.37139E-01
I15	Industrial	61.82	7500	-44.49	4.32	-18.74	0.39708E-02	0.63014E-01	0.47142E+01
I16	Industrial	59.00	7500	-43.39	2.44	-20.19	0.22621E-02	0.47562E-01	0.49674E+01
Re16	Residential	81.81	5000	-53.33	-2.36	-24.63	0.56281E-03	0.23724E-01	0.68822E+01
U19	Urban	82.07	5000	-53.33	12.07	-17.74	0.79013E-01	0.28109E+00	0.16706E+02
U20	Urban	82.38	5000	-53.33	2.43	-21.13	0.32728E-02	0.57208E-01	0.74223E+01
U21	Urban	82.61	5000	-53.33	1.40	-29.34	0.72467E-03	0.26920E-01	0.23105E+02
U22	Urban	82.33	5000	-53.33	4.21	-19.27	0.67669E-02	0.82261E-01	0.69524E+01
U23	Urban	81.43	3750	-53.33	0.30	-23.78	0.12487E-02	0.35336E-01	0.84384E+01
U24	Urban	49.71	5000	-53.33	6.15	-16.89	0.79904E-02	0.89389E-01	0.43631E+01
C6	City	81.32	7500	-53.33	22.60	-6.30	0.11627E+02	0.34099E+01	0.14552E+02
C7	City	81.91	7500	-53.33	17.32	-8.09	0.17343E+01	0.13169E+01	0.84870E+01
C8	City	82.40	7500	-53.33	28.52	-6.38	0.79656E+02	0.89250E+01	0.38774E+02
C9	City	82.39	5000	-53.33	16.71	-8.52	0.14636E+01	0.12098E+01	0.85958E+01
G51	Grass	69.69	400	-41.72	-21.21	-28.65	0.10699E-05	0.10344E-02	0.75752E+00
G52	Grass	71.04	400	-42.37	-22.99	-29.78	0.65476E-06	0.80917E-03	0.76928E+00
G53	Grass	72.29	400	-40.85	-20.70	-28.44	0.12477E-05	0.11170E-02	0.77922E+00
G54	Grass	74.27	400	-47.77	-23.53	-33.27	0.26047E-06	0.51036E-03	0.10832E+01
G55	Grass	73.77	400	-43.88	-25.74	-31.67	0.20402E-06	0.45169E-03	0.66409E+00
G56	Grass	74.62	400	-39.94	-22.83	-31.32	0.30954E-06	0.55637E-03	0.75333E+00
G57	Grass	75.36	225	-42.23	-26.20	-32.27	0.18225E-06	0.42690E-03	0.71975E+00
G58	Grass	75.94	100	-53.33	-29.33	-34.38	0.62925E-07	0.25085E-03	0.68711E+00
G59	Grass	75.80	100	-43.01	-27.62	-34.08	0.79581E-07	0.28210E-03	0.72188E+00
G60	Grass	75.26	100	-42.50	-28.33	-33.47	0.79250E-07	0.28151E-03	0.62651E+00
G61	Grass	76.42	100	-53.33	-30.10	-35.84	0.30411E-07	0.17439E-03	0.66869E+00

Table A-2. Cont.

G62	Grass	76.79	100	-53.33	-29.15	-35.48	0.48161E-07	0.21946E-03	0.77566E+00
G63	Grass	76.63	100	-45.77	-28.89	-34.69	0.56325E-07	0.23733E-03	0.69839E+00
G64	Grass	76.54	400	-53.33	-27.33	-34.37	0.10283E-06	0.32068E-03	0.87711E+00
G65	Grass	77.15	400	-53.33	-27.69	-35.26	0.74412E-07	0.27279E-03	0.91504E+00
G66	Grass	77.68	400	-53.33	-29.95	-37.46	0.27052E-07	0.16447E-03	0.91727E+00
G67	Grass	78.29	400	-53.33	-29.26	-36.32	0.35268E-07	0.18780E-03	0.80566E+00
G68	Grass	78.79	400	-53.33	-27.75	-37.30	0.49878E-07	0.22333E-03	0.11998E+01
G69	Grass	78.94	400	-53.33	-28.21	-37.70	0.42897E-07	0.20711E-03	0.12200E+01
G70	Grass	79.69	400	-53.33	-30.41	-41.67	0.19630E-07	0.14011E-03	0.20584E+01
G71	Grass	79.65	400	-53.33	-28.58	-38.30	0.66764E-07	0.25839E-03	0.17456E+01
G72	Grass	80.09	400	-53.33	-29.23	-41.86	0.35854E-07	0.18935E-03	0.29030E+01
G73	Grass	80.34	400	-53.33	-29.05	-44.13	0.26369E-07	0.16238E-03	0.42001E+01
G74	Grass	80.57	400	-53.33	-29.18	-44.72	0.25636E-07	0.16011E-03	0.47496E+01
G75	Grass	81.06	400	-53.33	-25.52	-40.88	0.14924E-06	0.38632E-03	0.47291E+01
G76	Grass	82.15	400	-53.33	-22.81	-44.32	0.14125E-06	0.37583E-03	0.10174E+02
G77	Grass	82.72	400	-53.33	-20.99	-46.10	0.15805E-06	0.39755E-03	0.16194E+02
G78	Grass	83.00	400	-53.33	-17.88	-43.43	0.66187E-06	0.81356E-03	0.17929E+02
G79	Grass	83.04	400	-53.33	-53.33	-53.33	0.72430E-18	0.85106E-09	0.18313E-03
G80	Grass	83.38	400	-53.33	-53.33	-53.33	0.72430E-18	0.85106E-09	0.18313E-03
G81	Grass	83.39	400	-53.33	-53.33	-53.33	0.72430E-18	0.85106E-09	0.18313E-03
G82	Grass	83.54	400	-53.33	-53.33	-53.33	0.72430E-18	0.85106E-09	0.18313E-03
G83	Grass	83.79	400	-53.33	-53.33	-53.33	0.72430E-18	0.85106E-09	0.18313E-03
G84	Grass	83.73	400	-53.33	-53.33	-53.33	0.72430E-18	0.85106E-09	0.18313E-03
G85	Grass	83.96	200	-53.33	-53.33	-53.33	0.72430E-18	0.85106E-09	0.18313E-03
G86	Grass	84.11	400	-53.33	-53.33	-53.33	0.72430E-18	0.85106E-09	0.18313E-03
U25	Urban	59.85	1800	-44.25	0.03	-17.99	0.33033E-02	0.57475E-01	0.36212E+01
U26	Urban	62.82	1800	-39.84	-0.88	-19.70	0.13927E-02	0.37318E-01	0.34836E+01
U27	Urban	63.95	1800	-39.63	-5.06	-21.35	0.32050E-03	0.17903E-01	0.24403E+01
U28	Urban	70.39	1800	-40.59	-3.48	-21.21	0.71103E-03	0.26665E-01	0.35196E+01
U29	Urban	71.52	1800	-45.28	-6.37	-24.42	0.15038E-03	0.12263E-01	0.33938E+01
H111	Structure	58.20	81	-39.25	-12.81	-23.12	0.81104E-04	0.90058E-02	0.18464E+01
H112	Structure	65.94	81	-34.07	-4.91	-17.78	0.23250E-02	0.48219E-01	0.28922E+01
H113	Structure	69.69	81	-37.90	-8.19	-20.03	0.54473E-03	0.23339E-01	0.23476E+01
H114	Structure	71.79	81	-36.10	-5.34	-18.48	0.15402E-02	0.39245E-01	0.27651E+01
H115	Structure	73.43	81	-39.59	-7.22	-19.31	0.10745E-02	0.32780E-01	0.27980E+01
H116	Structure	75.00	81	-53.33	-8.41	-22.87	0.30983E-03	0.17602E-01	0.34119E+01
H117	Structure	75.86	81	-41.63	-4.86	-20.52	0.13961E-02	0.37365E-01	0.42086E+01
H118	Structure	76.82	81	-53.33	-1.21	-16.37	0.83245E-02	0.91239E-01	0.39534E+01
H119	Structure	77.59	81	-53.33	-5.83	-20.14	0.12884E-02	0.35894E-01	0.37044E+01
H120	Structure	78.15	81	-53.33	3.09	-13.50	0.54346E-01	0.23312E+00	0.52177E+01
H121	Structure	79.15	81	-53.33	-1.00	-15.56	0.14461E-01	0.12025E+00	0.43254E+01
H122	Structure	79.72	81	-53.33	-5.69	-19.18	0.16708E-02	0.40876E-01	0.33822E+01
H123	Structure	80.21	81	-53.33	-0.19	-16.73	0.12350E-01	0.11113E+00	0.52308E+01
H124	Structure	80.57	81	-53.33	-10.78	-25.81	0.11564E-03	0.10754E-01	0.40944E+01
U30	Urban	73.32	1800	-43.84	-6.05	-24.70	0.15005E-03	0.12249E-01	0.36177E+01
U31	Urban	77.78	1800	-53.33	5.56	-16.79	0.16008E-01	0.12652E+00	0.60484E+01
U32	Urban	80.39	1800	-53.33	6.18	-18.55	0.17257E-01	0.13137E+00	0.94028E+01

Table A-3. Clutter Statistics for the Denver Low Altitude Image, X-VV

ID	Reginal Type	Incidence Angle	# Pts	Min (dB)	Max(dB)	Mean (dB)	Variance	SDEV	Variation
Re1	Residential	49.36	5000	-47.22	0.19	-19.68	0.70035E-03	0.26464E-01	0.24604E+01
Re2	Residential	62.96	5000	-47.22	-1.62	-19.48	0.48895E-03	0.22112E-01	0.19604E+01
Re3	Residential	54.50	5000	-40.38	1.37	-18.28	0.15729E-02	0.39659E-01	0.26666E+01
Re4	Residential	61.91	5000	-47.22	8.21	-17.70	0.11935E-01	0.10925E+00	0.64333E+01
G1	Grass	75.11	1000	-47.22	-25.73	-33.78	0.10639E-06	0.32617E-03	0.77878E+00
H1	Building	77.43	2000	-47.22	7.47	-16.81	0.36091E-01	0.18998E+00	0.91115E+01
G2	Grass	76.35	1800	-47.22	-23.62	-34.04	0.25065E-06	0.50065E-03	0.12701E+01
H2	Building	76.60	2000	-47.22	2.08	-22.24	0.29740E-02	0.54534E-01	0.91369E+01
H3	Building	78.33	2000	-47.22	2.45	-20.41	0.36516E-02	0.60429E-01	0.66401E+01
H4	Building	75.59	1200	-47.22	-2.77	-22.97	0.72341E-03	0.26896E-01	0.53333E+01
U1	Urban	55.14	10000	-47.22	-0.13	-20.20	0.70586E-03	0.26568E-01	0.27805E+01
U2	Urban	68.21	10000	-47.22	2.60	-18.43	0.15977E-02	0.39971E-01	0.27862E+01
U3	Urban	74.41	5000	-47.22	-4.83	-21.15	0.26943E-03	0.16414E-01	0.21388E+01
U4	Urban	76.44	5000	-47.22	-3.82	-20.81	0.29895E-03	0.17290E-01	0.20817E+01
U13	Urban	76.31	5000	-47.22	8.71	-20.19	0.13871E-01	0.11778E+00	0.12308E+02
U17	Urban	78.26	5000	-47.22	4.50	-19.05	0.42138E-02	0.64914E-01	0.52216E+01
U18	Urban	74.23	5000	-47.22	-3.37	-22.84	0.16271E-03	0.12756E-01	0.24550E+01
U5	Urban	63.39	5000	-47.22	-0.42	-19.89	0.73172E-03	0.27050E-01	0.26348E+01
U6	Urban	70.61	5000	-47.22	-4.68	-20.65	0.25660E-03	0.16019E-01	0.18602E+01
U7	Urban	73.16	5000	-47.22	0.54	-20.69	0.91094E-03	0.30182E-01	0.35368E+01
G3	Grass	76.26	1200	-47.22	-25.66	-36.51	0.14986E-06	0.38712E-03	0.17346E+01
G4	Grass	73.27	1200	-47.22	-22.29	-32.48	0.29531E-06	0.54342E-03	0.96168E+00
H5	Terminal	78.85	2000	-47.22	7.46	-15.11	0.45020E-01	0.21218E+00	0.68842E+01
H6	Terminal	78.09	4000	-47.22	19.22	-5.51	0.78797E+01	0.28071E+01	0.99846E+01
H7	Terminal	74.82	2800	-47.22	-16.89	-33.13	0.14871E-05	0.12195E-02	0.25093E+01
G5	Grass	75.88	1800	-47.22	-21.14	-31.82	0.29393E-06	0.54215E-03	0.82359E+00
H8	Parking Lot	80.50	2500	-47.22	13.84	-11.38	0.70655E+00	0.84057E+00	0.11553E+02
H9	Parking Lot	79.36	2500	-47.22	-2.39	-18.53	0.95079E-03	0.30835E-01	0.21965E+01
H10	Plane	74.82	200	-47.22	-24.26	-35.57	0.27347E-06	0.52294E-03	0.18867E+01
H11	Plane	77.67	200	-47.22	-6.90	-23.88	0.32102E-03	0.17917E-01	0.43787E+01
H12	Plane	75.90	225	-47.22	-19.19	-32.79	0.23307E-05	0.15267E-02	0.29008E-01
H13	Parking Lot	77.37	2500	-47.22	6.16	-15.59	0.95700E-02	0.97826E-01	0.35467E-01
G6	Grass	72.94	5000	-47.22	-2.33	-28.37	0.83744E-04	0.91512E-02	0.62894E+01
Ru1	Runway	75.90	1000	-47.22	-31.66	-44.98	0.27555E-08	0.52493E-04	0.16514E+01
Ru2	Runway	75.17	1000	-47.22	-27.60	-42.92	0.14613E-07	0.12088E-03	0.23670E+01
H14	Truck	72.68	25	-44.90	-8.49	-19.17	0.87281E-03	0.29543E-01	0.24392E+01
H15	Truck	66.98	25	-47.22	-14.88	-26.29	0.41766E-04	0.64627E-02	0.27499E+01
H16	Truck	77.44	25	-47.22	-17.14	-23.71	0.35229E-04	0.59354E-02	0.13961E+01
M1	Tree	70.16	49	-38.74	-6.68	-18.08	0.12075E-02	0.34749E-01	0.22322E-01
H17	Parking Lot	79.45	1200	-47.22	3.67	-14.35	0.11968E-01	0.10940E+00	0.29811E+01
H18	Building	77.77	1200	-47.22	7.63	-10.89	0.12263E+00	0.35019E+00	0.42996E+01
H19	Plane	77.18	225	-47.22	-7.75	-22.68	0.34083E-03	0.18462E-01	0.34193E+01
H20	Plane	77.23	225	-47.22	-6.93	-22.32	0.50870E-03	0.22554E-01	0.38512E+01
H21	Plane	77.18	225	-47.22	2.12	-18.78	0.12449E-01	0.11157E+00	0.84256E+01
H22	Parking Lot	81.13	2500	-47.22	4.84	-19.82	0.49309E-02	0.70221E-01	0.67363E+01
H23	Fence	76.44	1150	-47.22	-23.28	-32.29	0.48913E-06	0.69938E-03	0.11861E+01
Ru3	Runway	72.47	700	-47.22	-34.85	-44.83	0.11197E-08	0.33462E-04	0.10171E+01
W1	Water	61.41	400	-47.22	-32.23	-42.28	0.49307E-08	0.70219E-04	0.11874E+01
M2	Tree	55.63	300	-28.60	-9.64	-17.86	0.18374E-03	0.13555E-01	0.82839E+00
H125	Warehouse	46.51	400	-31.77	-2.96	-15.55	0.26415E-02	0.51395E-01	0.18462E+01
H126	Warehouse	55.14	1600	-42.57	-4.90	-19.36	0.69782E-03	0.26416E-01	0.22794E+01
G7	Grass	71.91	400	-41.49	-18.69	-28.34	0.22492E-05	0.14997E-02	0.10239E+01
G8	Grass	74.85	400	-47.22	-25.35	-33.12	0.24521E-06	0.49519E-03	0.10165E+01
I3	Building	55.63	864	-37.94	3.85	-10.46	0.51623E-01	0.22721E+00	0.25257E+01
I4	Building	64.60	750	-39.77	-0.28	-15.77	0.62966E-02	0.79351E-01	0.29985E+01
U8	Urban	74.27	3750	-47.22	-6.12	-22.39	0.12471E-03	0.11167E-01	0.19371E+01
U9	Urban	66.22	3750	-41.65	5.65	-17.84	0.63613E-02	0.79758E-01	0.48473E+01
U10	Urban	53.28	3750	-41.76	0.75	-18.86	0.17943E-02	0.42359E-01	0.32580E+01
M3	Tree	66.66	1000	-47.22	-1.14	-17.68	0.38272E-02	0.61864E-01	0.36242E+01

Table A-3. Cont.

W2	Water	59.48	1000	-47.22	-33.47	-43.14	0.34932E-08	0.59103E-04	0.12186E+01
W3	Water	60.39	1000	-47.22	-28.03	-40.63	0.22080E-07	0.14859E-03	0.17190E+01
H25	Building	64.34	2000	-47.22	-6.42	-22.63	0.20500E-03	0.14318E-01	0.26233E+01
G9	Grass	66.16	5000	-47.22	-17.90	-26.26	0.34867E-05	0.18673E-02	0.78865E+00
G10	Grass	73.19	5000	-47.22	-15.28	-28.79	0.34203E-05	0.18494E-02	0.13986E+01
H26	Building	50.88	1000	-41.57	1.68	-20.14	0.25977E-02	0.50968E-01	0.52631E+01
G11	Grass	71.18	5000	-47.22	-3.48	-28.22	0.86880E-04	0.93209E-02	0.61901E+01
G12	Grass	65.47	5000	-47.22	-18.01	-26.54	0.31942E-05	0.17872E-02	0.80591E+00
M4	Tree	51.67	1950	-42.09	-11.25	-22.23	0.50483E-04	0.71052E-02	0.11860E+01
G13	Grass	74.46	1500	-47.22	-19.81	-31.09	0.66276E-06	0.81410E-03	0.10465E+01
G14	Grass	71.62	1500	-47.22	-19.29	-27.53	0.28530E-05	0.16891E-02	0.95559E+00
Ru4	Runway	73.02	450	-47.22	-36.92	-44.58	0.75174E-09	0.27418E-04	0.78735E+00
Ru5	Runway	73.54	450	-47.22	-36.91	-45.62	0.57423E-09	0.23963E-04	0.87421E+00
Ru6	Runway	73.54	450	-47.22	-37.83	-46.96	0.84603E-10	0.91980E-05	0.45719E+00
Ru7	Runway	75.84	450	-47.22	-37.35	-46.87	0.23190E-09	0.15228E-04	0.73996E+00
G15	Grass	74.89	10000	-47.22	-8.45	-30.73	0.54958E-05	0.23443E-02	0.27719E+01
G16	Grass	75.77	10000	-47.22	-9.21	-27.61	0.10119E-04	0.31810E-02	0.18334E+01
G17	Grass	75.11	10000	-47.22	-7.13	-29.37	0.11275E-04	0.33579E-02	0.29058E+01
G18	Grass	72.99	10000	-47.22	-11.32	-28.36	0.28776E-05	0.16963E-02	0.11619E+01
G19	Grass	78.93	2500	-47.22	-18.96	-32.44	0.22433E-05	0.14978E-02	0.26254E+01
M5	Tree	74.00	900	-47.22	-8.84	-22.15	0.15105E-03	0.12290E-01	0.20166E+01
I5	Industrial	66.27	3600	-47.22	2.89	-20.01	0.19534E-02	0.44197E-01	0.44324E+01
I6	Industrial	54.50	900	-36.85	0.43	-18.60	0.29032E-02	0.53881E-01	0.39024E+01
I7	Industrial	55.39	450	-40.49	-4.60	-18.32	0.83152E-03	0.28836E-01	0.19569E+01
Ru8	Runway	70.89	500	-47.22	-30.12	-40.01	0.18889E-07	0.13744E-03	0.13777E+01
Ru9	Runway	72.13	500	-47.22	-23.32	-41.10	0.84093E-07	0.28999E-03	0.37363E+01
Ru10	Runway	77.11	500	-47.22	-32.30	-46.56	0.13582E-08	0.36854E-04	0.16687E+01
Ru11	Runway	63.95	500	-47.22	-28.84	-38.39	0.26544E-07	0.16292E-03	0.11253E+01
H27	Parking Lot	79.57	5000	-47.22	7.12	-16.79	0.14675E-01	0.12114E+00	0.57838E+01
H28	Building	81.77	450	-47.22	5.91	-11.00	0.95402E-01	0.30887E+00	0.38842E+01
U11	Urban	81.15	5000	-47.22	4.84	-20.65	0.48946E-02	0.69962E-01	0.81189E+01
H29	Building	82.81	600	-47.22	17.72	-2.03	0.13300E+02	0.36469E+01	0.58158E+01
H108	Building	79.56	1250	-47.22	-5.25	-24.28	0.15424E-03	0.12419E-01	0.33309E+01
U12	Urban	81.11	1250	-47.22	-2.42	-25.72	0.36650E-03	0.19144E-01	0.71538E+01
H127	Building	83.81	1000	-47.22	37.66	19.04	0.15432E+06	0.39294E+03	0.49017E+01
H30	Building	82.81	1250	-47.22	16.92	-1.88	0.11168E+02	0.33419E+01	0.51528E+01
H31	Building	82.05	300	-47.22	12.03	-8.38	0.12258E+01	0.11072E+01	0.76269E+01
H32	Building	81.88	450	-47.22	7.67	-11.30	0.18525E+00	0.43041E+00	0.58095E+01
H33	Building	82.82	1000	-47.22	16.92	-1.22	0.13388E+02	0.36590E+01	0.48419E+01
H34	Building	82.88	400	-47.22	2.83	-17.35	0.18793E-01	0.13709E+00	0.74387E+01
C1	City	81.71	1800	-47.22	13.69	-9.50	0.55605E+00	0.74569E+00	0.66418E+01
U14	Urban	81.69	800	-47.22	4.17	-12.25	0.40532E-01	0.20133E+00	0.33813E+01
H35	Building	80.09	2500	-47.22	16.31	-2.97	0.49827E+01	0.22322E+01	0.44182E+01
U15	Urban	82.44	1200	-47.22	10.52	-8.83	0.46365E+00	0.68092E+00	0.51987E+01
H36	Building	83.38	450	-47.22	20.77	3.85	0.11674E+03	0.10804E+02	0.44538E+01
U16	Urban	81.09	2400	-47.22	-0.59	-19.13	0.23687E-02	0.48670E-01	0.39841E+01
H109	Building	80.38	680	-47.22	-1.36	-26.58	0.10169E-02	0.31888E-01	0.14522E+02
I8	Industrial	82.91	1800	-47.22	7.59	-11.90	0.91205E-01	0.30200E+00	0.46810E+01
H37	Building	83.81	1200	-47.22	21.42	0.45	0.43115E+02	0.65662E+01	0.59180E+01
H38	Building	84.83	400	-47.22	22.45	5.05	0.25142E+03	0.15856E+02	0.49578E+01
H39	Building	85.09	400	-47.22	18.96	2.56	0.49581E+02	0.70414E+01	0.39062E+01
H40	Building	84.09	300	-47.22	16.05	-0.84	0.12869E+02	0.35873E+01	0.43550E+01
H41	Building	84.31	300	-47.22	21.17	4.12	0.13205E+03	0.11491E+02	0.44475E+01
H42	Building	83.37	100	-47.22	12.19	-0.72	0.64569E+01	0.25410E+01	0.29998E+01
H43	Building	83.58	450	-47.22	10.33	-7.70	0.73445E+00	0.85700E+00	0.50429E+01
H44	Building	83.61	125	-47.22	18.59	6.87	0.11543E+03	0.10744E+02	0.22101E+01
H45	Building	84.16	140	-47.22	9.61	-1.82	0.28338E+01	0.16834E+01	0.25606E+01
H46	Building	84.88	210	-47.22	22.54	8.96	0.67787E+03	0.26036E+02	0.33089E+01
H47	Building	84.93	1120	-47.22	19.69	-0.44	0.32084E+02	0.56643E+01	0.62685E+01
H48	Building	85.09	200	-47.22	19.78	3.43	0.11476E+03	0.10713E+02	0.48655E+01
H49	Building	85.97	3200	-47.22	24.76	1.55	0.16051E+03	0.12669E+02	0.88741E+01
H50	Building	85.51	150	-47.22	-47.22	-47.22	-0.52693E-17	0.00000E+00	0.00000E+00
H51	Building	86.06	129	-47.22	10.38	-10.73	0.91434E+00	0.95621E+00	0.11311E+02
H52	Building	85.96	159	-47.22	14.90	1.18	0.22125E+02	0.47038E+01	0.35819E+01

Table A-3. Cont.

H53	Building	86.29	120	-47.22	-47.22	-47.22	-0.52693E-17	0.00000E+00	0.00000E+00
H54	Building	85.83	200	-47.22	12.04	-1.03	0.77346E+01	0.27811E+01	0.35230E+01
H55	Building	86.29	6000	-47.22	22.93	-6.62	0.14027E+02	0.37452E+01	0.17179E+02
H56	Building	85.47	1050	-47.22	19.20	-0.85	0.24022E+02	0.49013E+01	0.59612E+01
H57	Building	85.10	350	-47.22	16.86	-1.06	0.17431E+02	0.41751E+01	0.53353E+01
H58	Building	85.36	700	-47.22	22.39	4.57	0.21058E+03	0.14512E+02	0.50655E+01
H59	Building	85.58	200	-47.22	28.45	12.41	0.33214E+04	0.57631E+02	0.33070E+01
H60	Building	85.71	1225	-47.22	16.86	0.48	0.21912E+02	0.46810E+01	0.41882E+01
H61	Building	85.09	500	-47.22	15.54	1.78	0.23915E+02	0.48903E+01	0.32492E+01
H62	Building	84.76	2400	-47.22	22.01	-1.87	0.25274E-02	0.50273E+01	0.77376E+01
H63	Building	83.92	225	-47.22	25.93	9.25	0.13037E+04	0.36107E+02	0.42924E+01
H64	Building	85.29	750	-47.22	27.64	8.07	0.16071E+04	0.40088E+02	0.62579E+01
H65	Building	86.04	500	-47.22	33.58	14.18	0.27438E+05	0.16565E+03	0.63255E+01
H66	Building	86.04	200	-47.22	16.10	2.45	0.41564E+02	0.64470E+01	0.36698E+01
H67	Building	86.95	540	-47.22	25.23	4.74	0.44339E+03	0.21057E+02	0.70724E+01
H68	Building	86.95	75	-47.22	32.89	19.39	0.85956E+05	0.29318E+03	0.33727E+01
H69	Building	86.76	120	-47.22	26.15	12.75	0.28227E-04	0.53129E+02	0.28189E+01
H70	Building	86.02	559	-47.22	13.58	-5.74	0.37553E+01	0.19379E+01	0.72733E+01
H71	Building	86.12	825	-47.22	22.86	0.61	0.11250E+03	0.10606E+02	0.92203E+01
H72	Building	84.09	500	-47.22	20.10	2.59	0.76821E+02	0.87648E+01	0.48321E+01
C2	City	83.31	5000	-47.22	8.81	-15.28	0.84660E-01	0.29096E+00	0.98124E+01
H73	Plane	77.40	420	-47.22	-5.37	-21.22	0.97301E-03	0.31193E-01	0.41269E+01
H74	Plane	76.87	420	-47.22	-9.07	-28.63	0.68618E-04	0.82836E-02	0.60395E+01
H75	Plane	78.12	420	-47.22	3.15	-17.54	0.15442E-01	0.12427E+00	0.70484E+01
H76	Truck	74.62	144	-47.22	-10.54	-24.62	0.11873E-03	0.10896E-01	0.31545E+01
H77	Truck	74.07	144	-47.22	-11.85	-23.92	0.11571E-03	0.10757E-01	0.26522E+01
G20	Grass	42.90	1600	-47.22	-11.25	-22.83	0.27162E-04	0.52117E-02	0.10009E+01
G21	Grass	53.56	1600	-47.22	-19.73	-28.61	0.15872E-05	0.12598E-02	0.91447E+00
G23	Grass	63.11	1600	-41.03	-17.53	-25.60	0.50700E-05	0.22517E-02	0.81788E+00
G24	Grass	66.50	1600	-47.22	-19.54	-29.38	0.16811E-05	0.12966E-02	0.11246E+01
G25	Grass	69.53	1600	-47.22	-20.14	-30.75	0.73839E-06	0.85930E-03	0.10204E+01
G26	Grass	71.79	1600	-39.61	-17.49	-28.42	0.18299E-05	0.13528E-02	0.94098E+00
G27	Grass	71.46	1600	-43.61	-19.30	-28.24	0.15963E-05	0.12635E-02	0.84176E+00
G28	Grass	74.39	1600	-47.22	-21.16	-31.80	0.62173E-06	0.78850E-03	0.11929E+01
C3	City	82.91	5000	-47.22	11.31	-14.05	0.15808E+00	0.39759E+00	0.10113E+02
G30	Grass	77.75	1600	-47.22	-21.47	-35.06	0.46806E-06	0.68415E-03	0.21958E+01
G31	Grass	69.36	1600	-47.22	-20.82	-30.64	0.45878E-06	0.67733E-03	0.78505E+00
G32	Grass	72.35	1600	-47.22	-18.86	-28.66	0.12759E-05	0.11296E-02	0.82915E+00
G33	Grass	74.24	1600	-47.22	-22.41	-30.07	0.63229E-06	0.79516E-03	0.80731E+00
G34	Grass	75.65	1600	-47.22	-19.53	-29.15	0.10618E-05	0.10304E-02	0.84707E+00
G35	Grass	76.54	1600	-47.22	-18.73	-29.24	0.99661E-06	0.99830E-03	0.83844E+00
G36	Grass	77.52	1600	-47.22	-18.08	-28.26	0.27486E-05	0.16579E-02	0.11095E+01
G37	Grass	78.12	1600	-47.22	-19.81	-30.32	0.25100E-05	0.15843E-02	0.17071E+01
G38	Grass	78.67	1600	-47.22	-19.58	-30.59	0.28526E-05	0.16890E-02	0.19358E+01
G39	Grass	79.16	1600	-47.22	-19.30	-35.87	0.10869E-05	0.10425E-02	0.40249E+01
G40	Grass	80.35	1600	-47.22	-21.80	-42.96	0.17818E-06	0.42211E-03	0.83496E+01
G41	Grass	69.36	1800	-47.22	-15.94	-25.53	0.59982E-05	0.24491E-02	0.87599E+00
G42	Grass	71.52	1800	-42.55	-14.10	-27.43	0.33108E-05	0.18196E-02	0.10073E+01
G43	Grass	73.27	1800	-47.22	-20.92	-29.95	0.70685E-06	0.84074E-03	0.83102E+00
G44	Grass	76.68	1800	-47.22	-18.93	-36.47	0.24880E-06	0.49880E-03	0.22110E+01
G45	Grass	79.23	1800	-47.22	-18.75	-42.13	0.31552E-06	0.56171E-03	0.91819E+01
Re5	Residential	50.55	4000	-39.33	2.15	-20.13	0.20623E-02	0.45412E-01	0.46821E+01
Re6	Residential	59.67	4000	-47.22	-4.33	-18.89	0.51188E-03	0.22625E-01	0.17541E+01
Re7	Residential	66.71	4000	-40.43	0.98	-17.63	0.17797E-02	0.42187E-01	0.24465E+01
Re8	Residential	72.17	4000	-43.70	-1.01	-21.01	0.47982E-03	0.21905E-01	0.27672E+01
Re9	Residential	74.24	4000	-47.22	-4.83	-21.28	0.23557E-03	0.15348E-01	0.20623E+01
Re10	Residential	76.40	4000	-47.22	4.16	-19.97	0.28418E-02	0.53309E-01	0.52961E+01
Re11	Residential	77.81	4000	-47.22	1.80	-19.48	0.14317E-02	0.37838E-01	0.33532E+01
Re12	Residential	79.41	4000	-47.22	-4.35	-24.52	0.14247E-03	0.11936E-01	0.33796E+01
Re13	Residential	80.08	4000	-47.22	-5.63	-25.58	0.10869E-03	0.10426E-01	0.37688E+01
Re14	Residential	81.13	4000	-47.22	-3.40	-24.88	0.32310E-03	0.17975E-01	0.55356E+01
Re15	Residential	81.52	4000	-47.22	-0.54	-24.12	0.84680E-03	0.29100E-01	0.75201E+01
H78	Building	49.54	1200	-43.59	0.50	-20.58	0.20903E-02	0.45720E-01	0.52300E+01
H79	Building	67.23	1200	-47.22	-3.92	-19.47	0.88610E-03	0.29767E-01	0.26367E+01

Table A-3. Cont.

H80	Building	58.30	1200	-47.22	3.40	-13.75	0.14061E-01	0.11858E+00	0.28123E+01
C4	City	82.35	5000	-47.22	5.82	-17.17	0.21465E-01	0.14651E+00	0.76328E+01
H82	Building	86.14	196	-47.22	16.12	-0.82	0.32859E+02	0.57322E+01	0.69282E+01
H83	Building	78.01	4000	-47.22	9.76	-11.84	0.81149E-01	0.28487E+00	0.43473E+01
H84	Building	79.62	4000	-47.22	17.67	-7.90	0.27971E+01	0.16725E+01	0.10315E+02
H85	Building	78.56	225	-47.22	6.52	-10.68	0.21970E+00	0.46872E+00	0.54869E+01
H86	Building	78.23	400	-47.22	-2.64	-14.84	0.67303E-02	0.82039E-01	0.24987E+01
H87	Building	74.05	405	-47.22	-4.83	-20.35	0.96784E-03	0.31110E-01	0.33703E+01
H88	Building	76.75	2000	-47.22	9.80	-17.80	0.67824E-01	0.26043E+00	0.15687E+02
H89	Building	74.36	2000	-47.22	1.89	-22.69	0.16196E-02	0.40244E-01	0.74795E+01
H90	Building	75.75	500	-47.22	-1.07	-21.13	0.15145E-02	0.38916E-01	0.50433E+01
H91	Building	76.72	1200	-47.22	-10.90	-25.08	0.58601E-04	0.76551E-02	0.24665E+01
H92	Building	79.74	525	-47.22	0.04	-15.44	0.65115E-02	0.80694E-01	0.28209E+01
H93	Building	78.89	525	-47.22	2.36	-17.31	0.87200E-02	0.93381E-01	0.50250E+01
H94	Building	77.78	500	-47.22	7.46	-10.35	0.15260E+00	0.39064E+00	0.42351E+01
H95	Building	65.70	595	-39.19	3.95	-13.56	0.30159E-01	0.17366E+00	0.39409E+01
H96	Building	65.82	864	-47.22	3.23	-14.69	0.23794E-01	0.15425E+00	0.45424E+01
H97	Building	66.27	416	-47.22	-3.42	-16.83	0.19570E-02	0.44238E-01	0.21303E+01
H98	Building	67.49	416	-47.22	0.24	-17.06	0.56840E-02	0.75392E-01	0.38288E+01
C5	City	83.16	3750	-47.22	13.88	-9.92	0.82322E+00	0.90732E+00	0.89014E+01
H100	Building	80.91	600	-47.22	12.42	-7.47	0.12677E+01	0.11259E+01	0.62915E+01
H101	Building	82.56	900	-47.22	7.52	-10.23	0.23096E+00	0.48058E+00	0.50617E+01
H102	Building	81.92	675	-47.22	6.07	-12.15	0.66189E-01	0.25727E+00	0.42182E+01
H103	Building	81.56	450	-47.22	1.15	-14.28	0.17306E-01	0.13155E+00	0.35275E+01
H104	Building	82.72	450	-47.22	9.40	-7.11	0.77066E+00	0.87787E+00	0.45097E+01
H105	Building	82.03	600	-47.22	5.98	-12.54	0.55162E-01	0.23487E+00	0.42120E+01
H106	Building	82.43	600	-47.22	10.52	-6.02	0.89384E+00	0.94543E+00	0.37837E+01
H107	Building	82.74	600	-47.22	12.63	-5.87	0.19250E+01	0.13875E+01	0.53658E+01
G46	Grass	82.47	800	-47.22	-47.22	-47.22	-0.52693E-17	0.00000E+00	0.00000E+00
G47	Grass	81.82	800	-47.22	-47.22	-47.22	-0.52693E-17	0.00000E+00	0.00000E+00
G48	Grass	46.10	5000	-47.22	-14.09	-24.21	0.16001E-04	0.40001E-02	0.10536E+01
G49	Grass	65.17	5000	-47.22	-8.99	-21.53	0.69687E-04	0.83479E-02	0.11873E+01
G50	Grass	83.89	3000	-47.22	-47.22	-47.22	-0.52693E-17	0.00000E+00	0.00000E+00
H110	Terminal	78.37	3500	-47.22	9.07	-14.63	0.66695E-01	0.25825E+00	0.74930E+01
I9	Industrial	81.25	7500	-47.22	7.73	-15.59	0.32387E-01	0.17996E+00	0.65198E+01
I10	Industrial	82.17	7500	-47.22	4.51	-19.54	0.89311E-02	0.94505E-01	0.85049E+01
I11	Industrial	82.62	7500	-47.22	12.63	-12.32	0.22391E+00	0.47319E+00	0.80672E+01
I12	Industrial	82.96	7500	-47.22	13.36	-14.32	0.17946E+00	0.42362E+00	0.11442E+02
I13	Industrial	83.40	7500	-47.22	20.97	-10.00	0.55599E+01	0.23579E+01	0.23580E+02
I14	Industrial	44.57	7500	-47.22	9.82	-12.55	0.88476E-01	0.29745E+00	0.53446E+01
I15	Industrial	61.82	7500	-47.22	2.39	-20.64	0.13231E-02	0.36375E-01	0.42168E+01
I16	Industrial	59.00	7500	-47.22	0.56	-19.88	0.17710E-02	0.42084E-01	0.40942E+01
Re16	Residential	81.81	5000	-47.22	-4.24	-27.81	0.18983E-03	0.13778E-01	0.83130E+01
U19	Urban	82.07	5000	-47.22	12.03	-19.47	0.76236E-01	0.27611E+00	0.24442E+02
U20	Urban	82.38	5000	-47.22	-4.21	-29.29	0.19497E-03	0.13963E-01	0.11862E+02
U21	Urban	82.61	5000	-47.22	4.58	-25.12	0.46895E-02	0.68480E-01	0.22260E+02
U22	Urban	82.33	5000	-47.22	-5.25	-30.79	0.12786E-03	0.11308E-01	0.13571E+02
U23	Urban	81.43	3750	-47.22	-9.82	-29.79	0.41712E-04	0.64585E-02	0.61578E+01
U24	Urban	49.71	5000	-47.22	2.72	-18.80	0.19965E-02	0.44682E-01	0.33886E+01
C6	City	81.32	7500	-47.22	15.88	-13.50	0.40367E+00	0.63535E+00	0.14225E+02
C7	City	81.91	7500	-47.22	14.88	-14.42	0.19346E+00	0.43984E+00	0.12169E+02
C8	City	82.40	7500	-47.22	20.18	-8.87	0.41121E+01	0.20278E+01	0.15638E+02
C9	City	82.39	5000	-47.22	6.60	-16.16	0.37160E-01	0.19277E+00	0.79678E+01
G51	Grass	69.69	400	-39.25	-21.40	-28.77	0.10469E-05	0.10232E-02	0.77117E+00
G52	Grass	71.04	400	-44.49	-23.18	-30.75	0.61920E-06	0.78689E-03	0.93513E+00
G53	Grass	72.29	400	-39.25	-21.18	-28.73	0.87969E-06	0.93792E-03	0.70004E+00
G54	Grass	74.27	400	-47.22	-22.58	-33.31	0.36898E-06	0.60743E-03	0.13022E+01
G55	Grass	73.77	400	-47.22	-22.36	-30.29	0.61780E-06	0.78600E-03	0.84075E+00
G56	Grass	74.62	400	-47.22	-23.38	-31.21	0.35992E-06	0.59994E-03	0.79329E+00
G57	Grass	75.36	225	-47.22	-25.67	-31.48	0.30384E-06	0.55122E-03	0.77506E+00
G58	Grass	75.94	100	-47.22	-27.13	-33.74	0.16735E-06	0.40909E-03	0.96727E+00
G59	Grass	75.80	100	-47.22	-24.98	-32.62	0.28141E-06	0.53048E-03	0.96994E+00
G60	Grass	75.26	100	-47.22	-26.99	-32.64	0.15564E-06	0.39451E-03	0.72421E+00
G61	Grass	76.42	100	-47.22	-29.21	-36.04	0.87449E-07	0.29572E-03	0.11873E+01

Table A-3. Cont.

G62	Grass	76.79	100	-47.22	-25.93	-32.54	0.31579E-06	0.56195E-03	0.10086E+01
G63	Grass	76.63	100	-47.22	-25.99	-32.34	0.31913E-06	0.56492E-03	0.96767E+00
G64	Grass	76.54	400	-47.22	-24.93	-35.34	0.15107E-06	0.38867E-03	0.13289E+01
G65	Grass	77.15	400	-47.22	-23.77	-35.32	0.34029E-06	0.58334E-03	0.19865E+01
G66	Grass	77.68	400	-47.22	-25.29	-37.74	0.21121E-06	0.45958E-03	0.27306E+01
G67	Grass	78.29	400	-47.22	-21.86	-33.24	0.92049E-06	0.95942E-03	0.20242E+01
G68	Grass	78.79	400	-47.22	-24.37	-41.81	0.12837E-06	0.35828E-03	0.54327E+01
G69	Grass	78.94	400	-47.22	-25.55	-40.88	0.14104E-06	0.37555E-03	0.46007E+01
G70	Grass	79.69	400	-47.22	-22.81	-41.91	0.20683E-06	0.45479E-03	0.70530E+01
G71	Grass	79.65	400	-47.22	-22.78	-43.13	0.12279E-06	0.35041E-03	0.72042E+01
G72	Grass	80.09	400	-47.22	-47.22	-47.22	-0.52693E-17	0.00000E+00	0.00000E+00
G73	Grass	80.34	400	-47.22	-47.22	-47.22	-0.52693E-17	0.00000E+00	0.00000E+00
G74	Grass	80.57	400	-47.22	-19.25	-43.13	0.35064E-06	0.59215E-03	0.12177E+02
G75	Grass	81.06	400	-47.22	-47.22	-47.22	-0.52693E-17	0.00000E+00	0.00000E+00
G76	Grass	82.15	400	-47.22	-10.67	-36.32	0.18311E-04	0.42792E-02	0.18349E+02
G77	Grass	82.72	400	-47.22	-47.22	-47.22	-0.52693E-17	0.00000E+00	0.00000E+00
G78	Grass	83.00	400	-47.22	-47.22	-47.22	-0.52693E-17	0.00000E+00	0.00000E+00
G79	Grass	83.04	400	-47.22	-47.22	-47.22	-0.52693E-17	0.00000E+00	0.00000E+00
G80	Grass	83.38	400	-47.22	-47.22	-47.22	-0.52693E-17	0.00000E+00	0.00000E+00
G81	Grass	83.39	400	-47.22	-47.22	-47.22	-0.52693E-17	0.00000E+00	0.00000E+00
G82	Grass	83.54	400	-47.22	-47.22	-47.22	-0.52693E-17	0.00000E+00	0.00000E+00
G83	Grass	83.79	400	-47.22	-47.22	-47.22	-0.52693E-17	0.00000E+00	0.00000E+00
G84	Grass	83.73	400	-47.22	-47.22	-47.22	-0.52693E-17	0.00000E+00	0.00000E+00
G85	Grass	83.96	200	-47.22	-47.22	-47.22	-0.52693E-17	0.00000E+00	0.00000E+00
G86	Grass	84.11	400	-47.22	-47.22	-47.22	-0.52693E-17	0.00000E+00	0.00000E+00
U25	Urban	59.85	1800	-40.27	-7.48	-19.67	0.26661E-03	0.16328E-01	0.15145E+01
U26	Urban	62.82	1800	-39.82	-4.94	-19.93	0.40430E-03	0.20107E-01	0.19806E+01
U27	Urban	63.95	1800	-40.18	-7.91	-21.13	0.11951E-03	0.10932E-01	0.14169E+01
U28	Urban	70.39	1800	-47.22	-6.15	-20.39	0.28742E-03	0.16954E-01	0.18563E+01
U29	Urban	71.52	1800	-43.44	-4.84	-21.39	0.23572E-03	0.15353E-01	0.21124E+01
H111	Structure	58.20	81	-39.12	-15.42	-24.40	0.30499E-04	0.55226E-02	0.15196E+01
H112	Structure	65.94	81	-36.66	-5.32	-18.92	0.16102E-02	0.40128E-01	0.31276E+01
H113	Structure	69.69	81	-38.52	-7.64	-19.06	0.83987E-03	0.28981E-01	0.23332E+01
H114	Structure	71.79	81	-32.88	-4.00	-16.12	0.51589E-02	0.71826E-01	0.29414E+01
H115	Structure	73.43	81	-40.10	-7.00	-18.96	0.10432E-02	0.32298E-01	0.25422E+01
H116	Structure	75.00	81	-47.22	-8.45	-20.20	0.52354E-03	0.22881E-01	0.23959E+01
H117	Structure	75.86	81	-47.22	-6.93	-18.51	0.11207E-02	0.33476E-01	0.23736E+01
H118	Structure	76.82	81	-47.22	-10.38	-21.29	0.20394E-03	0.14281E-01	0.19214E+01
H119	Structure	77.59	81	-47.22	-7.16	-19.06	0.61512E-03	0.24802E-01	0.19955E+01
H120	Structure	78.15	81	-47.22	-2.66	-17.72	0.48304E-02	0.69501E-01	0.41088E+01
H121	Structure	79.15	81	-47.22	-6.54	-19.77	0.14393E-02	0.37939E-01	0.35983E+01
H122	Structure	79.72	81	-47.22	-8.71	-23.79	0.38998E-03	0.19748E-01	0.47239E+01
H123	Structure	80.21	81	-47.22	-4.76	-22.22	0.14381E-02	0.37923E-01	0.63244E+01
H124	Structure	80.57	81	-47.22	-11.27	-27.44	0.12571E-03	0.11212E-01	0.62224E+01
U30	Urban	73.32	1800	-41.81	-4.92	-21.16	0.30294E-03	0.17405E-01	0.22756E+01
U31	Urban	77.78	1800	-47.22	-4.27	-18.93	0.98831E-03	0.31437E-01	0.24557E+01
U32	Urban	80.39	1800	-47.22	5.95	-19.17	0.16140E-01	0.12704E+00	0.10499E+02

APPENDIX B

Processing and Calibration of SAR Data

APPENDIX B

Processing and calibration proceeded in much the same manner as the other Denver images. The phase histories of the images were focused in azimuth and range. This was achieved by convolving the data with a match filter of the transmitted chirp in azimuth and range. The images were processed to remove the effects of system noise and were then radiometrically corrected to compensate for the effects of range fall-off, the antenna gain pattern, and resolution cell power. The radiometrically corrected images were then converted to normalized radar scattering coefficients (NRSC) by normalizing the magnitude of the radar cross section by the resolution area.

The absolute calibration of the Denver images was performed based on data obtained from a calibration array positioned at Denver Stapleton International Airport and Lowry AFB. This array is described in Volume III report Appendix A. For a radar operating in its linear region, a linear relationship will exist between the measured intensity of a point target in an image and the expected value of the backscattering cross section of the target. The slope of the function is unity and the y-intercept of the function is a measure of the system gain function. Groups of three 60 cm trihedral corner reflectors were placed in grassy fields around the Denver Airport. The returns from these reflectors were used to calibrate the images. In images with no corner reflectors, such as the Rocky Mountains image, measured intensities from corner reflectors in other Denver images were used to determine the absolute system gain function. This gain function was then adjusted for differences in attenuation and transmitted power between the images under analysis and the calibrating image, and the adjusted gain function was then applied to the image under analysis.

APPENDIX C

Discussion of Statistical Analysis Performed

APPENDIX C

Two analyses were performed in this additional work. One analysis employed clutter analysis techniques similar to those performed on previous data. The second analysis employed complex polarimetric analysis of the full-polarization data set. Statistical clutter analysis was performed on the pair of X-HH and X-VV low altitude images and on the Rocky Mountain image. The purpose of the low altitude analysis was twofold. First, the low altitude images provided clutter information at incidence angles larger than any that have been analyzed before. These images would provide needed information about the returns from depression angle which are almost identical to that of the glide slope of incoming aircraft. Second, analysis of this data would provide more information to the database of clutter which has been developed over the course of the NASA LaRC windshear analysis. The Rocky Mountain image was analyzed in order to focus upon an aspect of clutter indigenous to the Denver area. First and foremost, an attempt to analyze and quantify the effect of range ambiguity caused by the mountains was necessary. Secondly, an analysis of the normalized scattering coefficients of the mountains and their relation to geological slope and position was performed to characterize the effects of such topography and to determine when mountain topography represents a potential hazard to windshear detection.

The analyses of these images were performed on a 4096 element by 4096 record slant range image of normalized scattering coefficients with the finest resolution possible. The images have one independent sample per resolution cell. Statistical analyses were performed to characterize the returns from different clutter types in the images. A thresholding analysis, which separated the normalized scattering coefficient into bins of 5 dB, was also performed in order to locate and quantify sources which produced similar absolute backscatter levels.

Regions of critical clutter types were located and extracted and the mean, standard deviation, and coefficient of variation for each of these subregions were calculated using techniques described in Appendix

C of Volume II. During Phase I, probability density function analysis indicated that most clutter types were well described using a gamma density function. These regions of similar type were then employed in general clutter characterization and in the examination of the change in response with incidence angle. Areas of similar clutter types and incidence angles were merged. Histograms, means, standard deviations, and coefficients of variation were calculated. The general shape of the histograms was also examined. It should be noted that in order to compare the expected scattering cross sections from point and man-made targets to normalized scattering cross sections the area extent of the target must be taken into account. Incidence angle effects in the data were examined by plotting the mean return of each sub-region as a function of the mean incidence angle. Clutter types common with the other Denver images were also compared to previous analysis results.

For the polarimetric analysis, previously analyzed amplitude data was reprocessed complexly and phase calibrated using a polarimetric array set up at the Denver Stapleton International Airport. The phase characteristics of different clutter types were then calculated and compared. In addition, spans, depolarization ratios, correlation coefficient magnitudes and phase differences were calculated.

APPENDIX D

Polarization Properties of Hydrospheres and Ground Clutter

APPENDIX D
POLARIMETRIC DISCRIMINANTS

Given a scattering matrix of the form

$$[S] = \begin{bmatrix} S_{HH} & S_{HV} \\ S_{VH} & S_{VV} \end{bmatrix}$$

the covariance matrix may be defined as

$$[C] = \begin{bmatrix} \langle S_{HH}S_{HH}^{*}\rangle & \langle S_{HH}S_{VH}^{*}\rangle & \langle S_{HH}S_{VV}^{*}\rangle \\ \langle S_{VH}S_{HH}^{*}\rangle & \langle S_{VH}S_{VH}^{*}\rangle & \langle S_{VH}S_{VV}^{*}\rangle \\ \langle S_{VV}S_{HH}^{*}\rangle & \langle S_{VV}S_{VH}^{*}\rangle & \langle S_{VV}S_{VV}^{*}\rangle \end{bmatrix} \qquad (2)$$

if reciprocity is assumed. The elements along the diagonal of the covariance matrix are related to the real scattering coefficients

$\sigma^{\circ}_{VV} = 4\pi\langle S_{VV}S_{VV}^{*}\rangle$, and
$\sigma^{\circ}_{HH} = 4\pi\langle S_{HH}S_{HH}^{*}\rangle$, and
$\sigma^{\circ}_{VH} = 4\pi\langle S_{VH}S_{VH}^{*}\rangle$.

The polarimetric discriminants utilized in this study are defined in terms of the elements of the covariance matrix and will be presented here.

Phase Difference

One of the new pieces of new information provided by a polarimetric radar and its coherent properties is the difference between the phase at HH and VV polarizations. This phase difference may be retrieved from the covariance matrix by performing the calculation where

$$\theta_{VVHH} = \tan^{-1}\left|\frac{(\mathrm{Im}\langle S_{HH}S_{VV}^{*}\rangle)}{(\mathrm{Re}\langle S_{HH}S_{VV}^{*}\rangle)}\right| \tag{3}$$

A simple man-made target made of a conducting material will produce a mean phase difference of 0 and a probability distribution that is very narrow, if not a delta function. Complex shapes and multiple reflections have been observed which produce non-zero phase difference values. The phase differences for plane dielectric surface is shown to increase with increasing angle.

Total Power or Span

Span is the terminology used to represent the total power of the scattered field. It may be calculated accordingly

$$\mathrm{SPAN} = \langle S_{HH}S_{HH}^{*}\rangle + \langle S_{VH}S_{VH}^{*}\rangle + \langle S_{HV}S_{HV}^{*}\rangle + \langle S_{VV}S_{VV}^{*}\rangle \tag{4}$$

Depolarization Ratio

The depolarization ratio has been defined here as the ratio of the power associated with the copolarization elements of the scattering matrix and the cross polarization elements. It is defined as

$$Pd = \frac{\langle S_{HH}S_{HH}^{*}\rangle + \langle S_{VV}S_{VV}^{*}\rangle}{\langle S_{HV}S_{HV}^{*}\rangle + \langle S_{VH}S_{VH}^{*}\rangle} \tag{5}$$

One of the advantages of this definition for depolarization ratio is that it allows for an intuitive understanding and provides a reduction in the variance since it is composed of four elements rather than just two.

Correlation Coefficient

The correlation between the copolarization elements (VV and HH) is defined as

$$\rho_{HHVV} = \left| \frac{\langle S_{HH} S_{VV}^{*} \rangle}{\langle S_{HH} S_{HH}^{*} \rangle \ \langle S_{VV} S_{VV}^{*} \rangle} \right|$$

Table D-1. Clutter Statistics for Polarimetric Image Set at HH and HV Polarizations

ID	LANDUSE	PTS.	INCIDENCE ANGLE	MIN(dB)	MAX(dB)	MEAN(dB)	VARIANCE	STANDARD DEVIATION
U5	URBAN	90000	73.44	-44.00	21.17	-9.67	1.44676	1.20281
U6	URBAN	90000	74.45	-44.00	23.58	-7.65	4.47093	2.11446
U7	URBAN	90000	75.24	-44.00	22.52	-9.33	2.74041	1.65542
U8	URBAN	90000	75.76	-44.00	22.77	-9.47	3.07333	1.75309
U9	URBAN	90000	76.82	-44.00	24.50	-10.39	3.94631	1.98653
U10	URBAN	90000	77.23	-44.00	25.41	-9.11	6.62017	2.57297
U11	URBAN	90000	77.62	-44.00	22.67	-12.26	0.88836	0.94253
G4	GRASS	20000	51.33	-44.00	-1.68	-15.52	0.00130	0.03606
G5	GRASS	11250	55.72	-44.00	-4.88	-17.11	0.00048	0.02189
G14	GRASS	11250	59.97	-44.00	-3.15	-22.77	0.00008	0.00913
RE6	RESIDENTIAL	90000	64.92	-44.00	25.83	-6.48	7.51306	2.74100
RE7	RESIDENTIAL	90000	68.14	-44.00	23.80	-6.20	4.03536	2.00882
RE23	RESIDENTIAL	120000	51.25	-44.00	24.75	-6.03	4.93246	2.22091
RE24	RESIDENTIAL	60000	62.64	-44.00	23.91	-10.32	2.04869	1.43133
H2	TERMINAL	4800	77.65	-44.00	25.70	6.48	296.02515	17.20538
H3	TERMINAL	4800	78.04	-44.00	25.35	5.19	206.36307	14.36534
H4	BUILDING	2500	80.23	-44.00	24.37	3.51	195.87170	13.99542
H5	BUILDING	4000	80.37	-44.00	26.25	0.27	214.81818	14.65668

ID	LANDUSE	PTS.	INCIDENCE ANGLE	MIN(dB)	MAX(dB)	MEAN(dB)	VARIANCE	STANDARD DEVIATION
U5	URBAN	90000	73.44	-44.00	8.21	-19.05	0.00606	0.07782
U6	URBAN	90000	74.45	-44.00	12.11	-16.45	0.03742	0.19344
U7	URBAN	90000	75.24	-44.00	9.82	-17.45	0.01544	0.12427
U8	URBAN	90000	75.76	-44.00	12.61	-16.82	0.03073	0.17530
U9	URBAN	90000	76.82	-44.00	17.57	-15.22	0.13561	0.36825
U10	URBAN	90000	77.23	-44.00	17.41	-14.07	0.22946	0.47902
U11	URBAN	90000	77.62	-44.00	14.96	-16.29	0.05955	0.24403
G4	GRASS	20000	51.33	-44.00	-11.70	-28.19	0.00001	0.00251
G5	GRASS	11250	55.72	-44.00	-16.96	-26.93	0.00000	0.00222
G14	GRASS	11250	59.97	-44.00	-16.76	-29.49	0.00000	0.00130
RE6	RESIDENTIAL	90000	64.92	-44.00	4.86	-22.16	0.00118	0.03437
RE7	RESIDENTIAL	90000	68.14	-44.00	13.03	-19.81	0.01807	0.13444
RE23	RESIDENTIAL	120000	51.25	-44.00	16.45	-16.35	0.08467	0.29099
RE24	RESIDENTIAL	60000	62.64	-44.00	8.41	-19.93	0.00533	0.07300
H2	TERMINAL	4800	77.65	-44.00	17.49	-0.36	10.47340	3.23626
H3	TERMINAL	4800	78.04	-44.00	17.33	-1.83	6.75839	2.59969
H4	BUILDING	2500	80.23	-44.00	17.49	-3.30	5.97209	2.44379
H5	BUILDING	4000	80.37	-44.00	21.41	-5.29	12.74261	3.56968

Table D-2. Clutter Statistics for Polarimetric Image Set at VH and VV Polarizations

ID	LANDUSE	PTS.	INCIDENCE ANGLE	MIN(dB)	MAX(dB)	MEAN(dB)	VARIANCE	STANDARD DEVIATION
U5	URBAN	90000	73.44	-44.00	-5.23	-26.30	0.00003	0.00587
U6	URBAN	90000	74.45	-44.00	2.78	-25.97	0.00045	0.02110
U7	URBAN	90000	75.24	-44.00	-4.95	-27.90	0.00002	0.00462
U8	URBAN	90000	75.76	-44.00	-5.06	-28.32	0.00002	0.00466
U9	URBAN	90000	76.82	-44.00	-1.84	-28.72	0.00006	0.00795
U10	URBAN	90000	77.23	-44.00	0.03	-28.68	0.00009	0.00970
U11	URBAN	90000	77.62	-44.00	9.23	-28.28	0.00159	0.03986
G4	GRASS	20000	51.33	-44.00	-13.65	-31.12	0.00000	0.00122
G5	GRASS	11250	55.72	-44.00	-18.61	-29.91	0.00000	0.00116
G14	GRASS	11250	59.97	-44.00	-10.27	-34.34	0.00000	0.00152
RE6	RESIDENTIAL	90000	64.92	-44.00	-1.56	-26.05	0.00004	0.00645
RE7	RESIDENTIAL	90000	68.14	-44.00	1.95	-23.82	0.00025	0.01594
RE23	RESIDENTIAL	120000	51.25	-44.00	15.63	-20.59	0.02933	0.17127
RE24	RESIDENTIAL	60000	62.64	-44.00	3.85	-25.07	0.00021	0.01439
H2	TERMINAL	4800	77.65	-44.00	3.69	-14.29	0.02096	0.14477
H3	TERMINAL	4800	78.04	-44.00	1.60	-17.80	0.00404	0.06357
H4	BUILDING	2500	80.23	-44.00	-5.15	-24.95	0.00027	0.01656
H5	BUILDING	4000	80.37	-44.00	0.95	-25.02	0.00135	0.03671

ID	LANDUSE	PTS.	INCIDENCE ANGLE	MIN(dB)	MAX(dB)	MEAN(dB)	VARIANCE	STANDARD DEVIATION
U5	URBAN	90000	73.44	-44.00	-5.60	-26.62	0.00003	0.00539
U6	URBAN	90000	74.45	-44.00	2.56	-25.98	0.00039	0.01979
U7	URBAN	90000	75.24	-44.00	-4.76	-27.67	0.00002	0.00485
U8	URBAN	90000	75.76	-44.00	-4.67	-27.98	0.00003	0.00503
U9	URBAN	90000	76.82	-44.00	-1.39	-28.36	0.00008	0.00868
U10	URBAN	90000	77.23	-44.00	0.49	-28.25	0.00012	0.01074
U11	URBAN	90000	77.62	-44.00	9.62	-27.86	0.00189	0.04345
G4	GRASS	20000	51.33	-44.00	-14.60	-31.19	0.00000	0.00119
G5	GRASS	11250	55.72	-44.00	-18.69	-29.67	0.00000	0.00122
G14	GRASS	11250	59.97	-44.00	-10.10	-33.98	0.00000	0.00165
RE6	RESIDENTIAL	90000	64.92	-44.00	-1.57	-26.05	0.00004	0.00642
RE7	RESIDENTIAL	90000	68.14	-44.00	1.67	-23.97	0.00023	0.01514
RE23	RESIDENTIAL	120000	51.25	-44.00	9.55	-21.81	0.00475	0.06891
RE24	RESIDENTIAL	60000	62.64	-44.00	3.71	-25.01	0.00020	0.01422
H2	TERMINAL	4800	77.65	-44.00	3.68	-14.23	0.02143	0.14640
H3	TERMINAL	4800	78.04	-44.00	1.59	-17.57	0.00424	0.06511
H4	BUILDING	2500	80.23	-44.00	-4.78	-24.42	0.00035	0.01868
H5	BUILDING	4000	80.37	-44.00	0.68	-25.07	0.00124	0.03524

Table D-3. Clutter Statistics for Polarimetric Image Set at LL and RL Polarizations

ID	LANDUSE	PTS.	INCIDENCE ANGLE	MIN(dB)	MAX(dB)	MEAN(dB)	VARIANCE	STANDARD DEVIATION
U5	URBAN	90000	73.44	-44.00	14.95	-15.37	0.08862	0.29769
U6	URBAN	90000	74.45	-44.00	15.96	-13.88	0.22862	0.47815
U7	URBAN	90000	75.24	-44.00	15.95	-15.60	0.12586	0.35477
U8	URBAN	90000	75.76	-44.00	15.96	-15.51	0.16540	0.40669
U9	URBAN	90000	76.82	-44.00	17.75	-16.72	0.14099	0.37549
U10	URBAN	90000	77.23	-44.00	17.29	-15.71	0.19960	0.44677
U11	URBAN	90000	77.62	-44.00	18.33	-18.04	0.09817	0.31332
G4	GRASS	20000	51.33	-44.00	-7.26	-20.79	0.00012	0.01096
G5	GRASS	11250	55.72	-44.00	-10.07	-22.62	0.00004	0.00621
G14	GRASS	11250	59.97	-44.00	-8.39	-27.97	0.00001	0.00256
RE6	RESIDENTIAL	90000	64.92	-44.00	20.29	-12.01	0.58274	0.76338
RE7	RESIDENTIAL	90000	68.14	-44.00	15.67	-11.77	0.24975	0.49975
RE23	RESIDENTIAL	120000	51.25	-44.00	15.37	-12.47	0.16517	0.40641
RE24	RESIDENTIAL	60000	62.64	-44.00	17.95	-16.06	0.13278	0.36439
H2	TERMINAL	4800	77.65	-41.67	20.23	0.59	19.51025	4.41704
H3	TERMINAL	4800	78.04	-44.00	18.91	-1.05	9.22339	3.03700
H4	BUILDING	2500	80.23	-44.00	17.59	-3.36	7.76472	2.78653
H5	BUILDING	4000	80.37	-44.00	18.06	-8.26	3.83802	1.95909

ID	LANDUSE	PTS.	INCIDENCE ANGLE	MIN(dB)	MAX(dB)	MEAN(dB)	VARIANCE	STANDARD DEVIATION
U5	URBAN	90000	73.44	-44.00	15.24	-14.84	0.10401	0.32251
U6	URBAN	90000	74.45	-44.00	18.82	-12.40	0.44393	0.66628
U7	URBAN	90000	75.24	-44.00	17.16	-13.86	0.26537	0.51514
U8	URBAN	90000	75.76	-44.00	17.95	-13.99	0.31376	0.56014
U9	URBAN	90000	76.82	-44.00	20.89	-13.83	0.66870	0.81774
U10	URBAN	90000	77.23	-44.00	21.72	-12.46	1.17477	1.08387
U11	URBAN	90000	77.62	-44.00	18.45	-15.54	0.15518	0.39393
G4	GRASS	20000	51.33	-44.00	-8.35	-21.66	0.00008	0.00875
G5	GRASS	11250	55.72	-44.00	-10.68	-22.04	0.00005	0.00672
G14	GRASS	11250	59.97	-44.00	-8.25	-27.06	0.00001	0.00295
RE6	RESIDENTIAL	90000	64.92	-44.00	19.65	-12.34	0.44721	0.66874
RE7	RESIDENTIAL	90000	68.14	-44.00	19.61	-11.76	0.36816	0.60676
RE23	RESIDENTIAL	120000	51.25	-44.00	22.22	-11.01	0.83390	0.91318
RE24	RESIDENTIAL	60000	62.64	-44.00	17.35	-15.60	0.10863	0.32960
H2	TERMINAL	4800	77.65	-58.45	20.47	2.13	36.30901	6.02570
H3	TERMINAL	4800	78.04	-44.00	20.88	1.01	32.29857	5.68318
H4	BUILDING	2500	80.23	-44.00	20.12	-0.40	29.31904	5.41471
H5	BUILDING	4000	80.37	-44.00	23.13	-2.57	53.92784	7.34356

Table D-4. Clutter Statistics for Polarimetric Image Set at LR and RR Polarizations

ID	LANDUSE	PTS.	INCIDENCE ANGLE	MIN(dB)	MAX(dB)	MEAN(dB)	VARIANCE	STANDARD DEVIATION
U5	URBAN	90000	73.44	-44.00	15.26	-14.74	0.10777	0.32829
U6	URBAN	90000	74.45	-44.00	19.04	-12.26	0.48770	0.69835
U7	URBAN	90000	75.24	-44.00	17.18	-13.78	0.27183	0.52137
U8	URBAN	90000	75.76	-44.00	17.96	-13.92	0.32086	0.56644
U9	URBAN	90000	76.82	-44.00	20.97	-13.78	0.69165	0.83165
U10	URBAN	90000	77.23	-44.00	21.82	-12.38	1.23397	1.11084
U11	URBAN	90000	77.62	-44.00	18.24	-15.52	0.14874	0.38567
G4	GRASS	20000	51.33	-44.00	-8.58	-21.63	0.00008	0.00879
G5	GRASS	11250	55.72	-44.00	-10.47	-22.06	0.00005	0.00676
G14	GRASS	11250	59.97	-44.00	-8.21	-26.99	0.00001	0.00295
RE6	RESIDENTIAL	90000	64.92	-44.00	19.62	-12.33	0.44320	0.66573
RE7	RESIDENTIAL	90000	68.14	-44.00	19.60	-11.70	0.37472	0.61214
RE23	RESIDENTIAL	120000	51.25	-44.00	20.60	-11.56	0.47869	0.69187
RE24	RESIDENTIAL	60000	62.64	-44.00	17.44	-15.55	0.11271	0.33572
H2	TERMINAL	4800	77.65	-58.45	20.48	2.15	35.90646	5.99220
H3	TERMINAL	4800	78.04	-44.00	20.82	1.00	32.06829	5.66289
H4	BUILDING	2500	80.23	-44.00	19.99	-0.48	28.11340	5.30221
H5	BUILDING	4000	80.37	-44.00	23.13	-2.59	53.54621	7.31753

ID	LANDUSE	PTS.	INCIDENCE ANGLE	MIN(dB)	MAX(dB)	MEAN(dB)	VARIANCE	STANDARD DEVIATION
U5	URBAN	90000	73.44	-44.00	15.16	-15.33	0.09654	0.31071
U6	URBAN	90000	74.45	-44.00	16.50	-13.81	0.24102	0.49093
U7	URBAN	90000	75.24	-44.00	15.82	-15.61	0.12737	0.35689
U8	URBAN	90000	75.76	-44.00	15.08	-15.49	0.15240	0.39038
U9	URBAN	90000	76.82	-44.00	16.87	-17.08	0.08435	0.29043
U10	URBAN	90000	77.23	-44.00	16.12	-16.32	0.12293	0.35062
U11	URBAN	90000	77.62	-44.00	12.16	-18.41	0.02319	0.15228
G4	GRASS	20000	51.33	-44.00	-6.57	-20.42	0.00014	0.01167
G5	GRASS	11250	55.72	-44.00	-10.29	-22.48	0.00004	0.00643
G14	GRASS	11250	59.97	-44.00	-5.97	-27.91	0.00002	0.00437
RE6	RESIDENTIAL	90000	64.92	-44.00	19.68	-12.51	0.44269	0.66535
RE7	RESIDENTIAL	90000	68.14	-44.00	16.05	-12.40	0.18359	0.42847
RE23	RESIDENTIAL	120000	51.25	-44.00	18.63	-10.85	0.44871	0.66986
RE24	RESIDENTIAL	60000	62.64	-44.00	18.77	-15.36	0.18915	0.43491
H2	TERMINAL	4800	77.65	-49.59	19.36	0.12	15.03290	3.87723
H3	TERMINAL	4800	78.04	-44.00	18.80	-1.62	7.20784	2.68474
H4	BUILDING	2500	80.23	-44.00	17.46	-3.45	7.62657	2.76163
H5	BUILDING	4000	80.37	-44.00	15.83	-9.50	1.74205	1.31987

Table D-5. Clutter Statistics for Polarimetric Image Set at LL_e and RL_e for a Canted Oblate Spheroid Case

ID	LANDUSE	PTS.	INCIDENCE ANGLE	MIN(dB)	MAX(dB)	MEAN(dB)	VARIANCE	STANDARD DEVIATION
U5	URBAN	90000	73.44	-44.00	15.05	-15.57	0.09151	0.30251
U6	URBAN	90000	74.45	-44.00	16.31	-13.93	0.23472	0.48448
U7	URBAN	90000	75.24	-44.00	16.06	-15.63	0.13653	0.36950
U8	URBAN	90000	75.76	-44.00	15.83	-15.53	0.17095	0.41346
U9	URBAN	90000	76.82	-44.00	17.65	-16.80	0.13186	0.36313
U10	URBAN	90000	77.23	-44.00	17.20	-15.80	0.18004	0.42431
U11	URBAN	90000	77.62	-44.00	15.38	-18.29	0.04057	0.20141
G4	GRASS	20000	51.33	-44.00	-7.07	-21.06	0.00010	0.01006
G5	GRASS	11250	55.72	-44.00	-11.23	-23.54	0.00003	0.00514
G14	GRASS	11250	59.97	-44.00	-9.76	-28.73	0.00000	0.00219
RE6	RESIDENTIAL	90000	64.92	-44.00	20.02	-12.36	0.51225	0.71572
RE7	RESIDENTIAL	90000	68.14	-44.00	16.27	-12.25	0.22119	0.47031
RE23	RESIDENTIAL	120000	51.25	-44.00	15.96	-11.99	0.22852	0.47803
RE24	RESIDENTIAL	60000	62.64	-44.00	18.28	-16.22	0.15049	0.38793
H2	TERMINAL	4800	77.65	-41.23	20.28	0.52	19.30264	4.39348
H3	TERMINAL	4800	78.04	-44.00	19.44	-1.06	9.72018	3.11772
H4	BUILDING	2500	80.23	-44.00	17.91	-2.94	9.33135	3.05473
H5	BUILDING	4000	80.37	-44.00	17.17	-8.48	3.09488	1.75923

ID	LANDUSE	PTS.	INCIDENCE ANGLE	MIN(dB)	MAX(dB)	MEAN(dB)	VARIANCE	STANDARD DEVIATION
U5	URBAN	90000	73.44	-44.00	15.79	-14.00	0.14557	0.38153
U6	URBAN	90000	74.45	-44.00	19.88	-11.48	0.75584	0.86939
U7	URBAN	90000	75.24	-44.00	17.52	-13.17	0.34017	0.58324
U8	URBAN	90000	75.76	-44.00	18.40	-13.34	0.39243	0.62644
U9	URBAN	90000	76.82	-44.00	21.63	-13.39	0.86869	0.93204
U10	URBAN	90000	77.23	-44.00	22.27	-11.95	1.58566	1.25923
U11	URBAN	90000	77.62	-44.00	18.42	-15.16	0.16850	0.41049
G4	GRASS	20000	51.33	-44.00	-7.01	-20.67	0.00012	0.01116
G5	GRASS	11250	55.72	-44.00	-10.36	-21.23	0.00007	0.00811
G14	GRASS	11250	59.97	-44.00	-7.75	-26.12	0.00001	0.00367
RE6	RESIDENTIAL	90000	64.92	-44.00	20.00	-11.89	0.51442	0.71723
RE7	RESIDENTIAL	90000	68.14	-44.00	19.55	-11.05	0.44273	0.66538
RE23	RESIDENTIAL	120000	51.25	-44.00	20.38	-12.23	0.45690	0.67594
RE24	RESIDENTIAL	60000	62.64	-44.00	18.30	-14.63	0.16632	0.40783
H2	TERMINAL	4800	77.65	-43.16	20.64	2.40	37.63950	6.13510
H3	TERMINAL	4800	78.04	-44.00	20.80	1.12	32.82498	5.72931
H4	BUILDING	2500	80.23	-44.00	19.74	-0.69	25.44712	5.04451
H5	BUILDING	4000	80.37	-44.00	22.73	-2.82	47.09010	6.86222

Table D-6. Clutter Statistics for Polarimetric Image Set at LR_e and RR_e for a Canted Oblate Spheroid Case

ID	LANDUSE	PTS.	INCIDENCE ANGLE	MIN(dB)	MAX(dB)	MEAN(dB)	VARIANCE	STANDARD DEVIATION
U5	URBAN	90000	73.44	-44.00	15.07	-15.57	0.09259	0.30429
U6	URBAN	90000	74.45	-44.00	16.38	-13.94	0.23606	0.48586
U7	URBAN	90000	75.24	-44.00	16.03	-15.67	0.13498	0.36740
U8	URBAN	90000	75.76	-44.00	15.72	-15.56	0.16697	0.40862
U9	URBAN	90000	76.82	-44.00	17.53	-16.86	0.12337	0.35124
U10	URBAN	90000	77.23	-44.00	17.02	-15.90	0.16718	0.40887
U11	URBAN	90000	77.62	-44.00	14.78	-18.32	0.03628	0.19047
G4	GRASS	20000	51.33	-44.00	-7.03	-21.02	0.00010	0.01013
G5	GRASS	11250	55.72	-44.00	-11.12	-23.54	0.00003	0.00515
G14	GRASS	11250	59.97	-44.00	-10.18	-28.76	0.00001	0.00224
RE6	RESIDENTIAL	90000	64.92	-44.00	19.95	-12.42	0.49763	0.70543
RE7	RESIDENTIAL	90000	68.14	-44.00	16.30	-12.32	0.21555	0.46428
RE23	RESIDENTIAL	120000	51.25	-44.00	17.28	-11.75	0.29825	0.54613
RE24	RESIDENTIAL	60000	62.64	-44.00	18.37	-16.17	0.15693	0.39614
H2	TERMINAL	4800	77.65	-44.40	20.18	0.49	18.81848	4.33803
H3	TERMINAL	4800	78.04	-44.00	19.42	-1.08	9.59202	3.09710
H4	BUILDING	2500	80.23	-44.00	17.89	-2.93	9.43305	3.07133
H5	BUILDING	4000	80.37	-44.00	17.04	-8.55	2.95883	1.72013

ID	LANDUSE	PTS.	INCIDENCE ANGLE	MIN(dB)	MAX(dB)	MEAN(dB)	VARIANCE	STANDARD DEVIATION
U5	URBAN	90000	73.44	-44.00	14.62	-15.30	0.07230	0.26889
U6	URBAN	90000	74.45	-44.00	17.52	-13.23	0.24607	0.49606
U7	URBAN	90000	75.24	-44.00	16.50	-14.52	0.18542	0.43060
U8	URBAN	90000	75.76	-44.00	17.37	-14.60	0.21971	0.46873
U9	URBAN	90000	76.82	-44.00	20.03	-14.34	0.45609	0.67535
U10	URBAN	90000	77.23	-44.00	20.85	-13.10	0.79912	0.89394
U11	URBAN	90000	77.62	-44.00	18.98	-15.84	0.16406	0.40504
G4	GRASS	20000	51.33	-44.00	-8.63	-21.67	0.00008	0.00888
G5	GRASS	11250	55.72	-44.00	-9.15	-21.42	0.00006	0.00790
G14	GRASS	11250	59.97	-44.00	-6.99	-26.85	0.00002	0.00390
RE6	RESIDENTIAL	90000	64.92	-44.00	19.26	-12.54	0.39158	0.62576
RE7	RESIDENTIAL	90000	68.14	-44.00	19.27	-12.11	0.28785	0.53652
RE23	RESIDENTIAL	120000	51.25	-44.00	22.46	-10.08	0.99100	0.99549
RE24	RESIDENTIAL	60000	62.64	-44.00	16.41	-15.72	0.07623	0.27609
H2	TERMINAL	4800	77.65	-52.80	20.27	1.64	29.82462	5.46119
H3	TERMINAL	4800	78.04	-44.00	20.41	0.56	26.21430	5.11999
H4	BUILDING	2500	80.23	-44.00	19.65	-0.70	25.68318	5.06786
H5	BUILDING	4000	80.37	-44.00	23.17	-2.50	56.08040	7.48869

Table D-7. Clutter Statistics for Polarimetric Image Set at LL_e and RL_e for a Case of Propagating Thru a Rain Filled Medium

ID	LANDUSE	PTS.	INCIDENCE ANGLE	MIN(dB)	MAX(dB)	MEAN(dB)	VARIANCE	STANDARD DEVIATION
U5	URBAN	90000	73.44	-44.00	16.42	-13.50	0.19121	0.43727
U6	URBAN	90000	74.45	-44.00	20.39	-11.00	0.95878	0.97918
U7	URBAN	90000	75.24	-44.00	18.16	-12.70	0.44119	0.66422
U8	URBAN	90000	75.76	-44.00	18.93	-12.90	0.50817	0.71286
U9	URBAN	90000	76.82	-44.00	21.98	-13.03	1.05882	1.02899
U10	URBAN	90000	77.23	-44.00	22.71	-11.59	1.90456	1.38006
U11	URBAN	90000	77.62	-44.00	18.98	-14.83	0.20561	0.45344
G4	GRASS	20000	51.33	-44.00	-6.62	-20.19	0.00016	0.01246
G5	GRASS	11250	55.72	-44.00	-10.01	-20.89	0.00008	0.00881
G14	GRASS	11250	59.97	-44.00	-7.13	-25.73	0.00002	0.00398
RE6	RESIDENTIAL	90000	64.92	-44.00	20.69	-11.26	0.70298	0.83844
RE7	RESIDENTIAL	90000	68.14	-44.00	20.10	-10.47	0.58271	0.76336
RE23	RESIDENTIAL	120000	51.25	-44.00	20.79	-11.64	0.56883	0.75421
RE24	RESIDENTIAL	60000	62.64	-44.00	18.94	-14.18	0.22026	0.46932
H2	TERMINAL	4800	77.65	-47.56	21.15	2.89	48.62994	6.97352
H3	TERMINAL	4800	78.04	-44.00	21.33	1.62	41.59822	6.44967
H4	BUILDING	2500	80.23	-44.00	20.30	-0.15	33.08904	5.75231
H5	BUILDING	4000	80.37	-44.00	23.02	-2.49	55.66404	7.46083

ID	LANDUSE	PTS.	INCIDENCE ANGLE	MIN(dB)	MAX(dB)	MEAN(dB)	VARIANCE	STANDARD DEVIATION
U5	URBAN	90000	73.44	-44.00	14.96	-15.75	0.08583	0.29296
U6	URBAN	90000	74.45	-44.00	16.01	-14.20	0.20553	0.45336
U7	URBAN	90000	75.24	-44.00	15.85	-15.89	0.12235	0.34979
U8	URBAN	90000	75.76	-44.00	15.58	-15.75	0.15403	0.39246
U9	URBAN	90000	76.82	-44.00	17.34	-17.12	0.11062	0.33260
U10	URBAN	90000	77.23	-44.00	16.68	-16.16	0.15425	0.39275
U11	URBAN	90000	77.62	-44.00	15.27	-18.57	0.03776	0.19433
G4	GRASS	20000	51.33	-44.00	-7.01	-21.04	0.00010	0.01011
G5	GRASS	11250	55.72	-44.00	-11.00	-23.47	0.00003	0.00522
G14	GRASS	11250	59.97	-44.00	-9.93	-28.95	0.00000	0.00214
RE6	RESIDENTIAL	90000	64.92	-44.00	19.96	-12.44	0.49892	0.70634
RE7	RESIDENTIAL	90000	68.14	-44.00	15.91	-12.39	0.20457	0.45229
RE23	RESIDENTIAL	120000	51.25	-44.00	15.96	-11.98	0.22834	0.47785
RE24	RESIDENTIAL	60000	62.64	-44.00	18.19	-16.33	0.14441	0.38001
H2	TERMINAL	4800	77.65	-46.00	19.97	0.28	17.02716	4.12640
H3	TERMINAL	4800	78.04	-44.00	19.00	-1.34	8.25210	2.87265
H4	BUILDING	2500	80.23	-44.00	17.60	-3.31	7.98735	2.82619
H5	BUILDING	4000	80.37	-44.00	17.10	-8.78	2.76478	1.66276

Table D-8. Clutter Statistics for Polarimetric Image Set at LR_e and RR_e for a Case of Propagating Thru a Rain Filled Medium

ID	LANDUSE	PTS.	INCIDENCE ANGLE	MIN(dB)	MAX(dB)	MEAN(dB)	VARIANCE	STANDARD DEVIATION
U5	URBAN	90000	73.44	-44.00	14.97	-15.75	0.08708	0.29510
U6	URBAN	90000	74.45	-44.00	16.11	-14.19	0.20830	0.45640
U7	URBAN	90000	75.24	-44.00	15.83	-15.92	0.12120	0.34814
U8	URBAN	90000	75.76	-44.00	15.47	-15.77	0.15071	0.38821
U9	URBAN	90000	76.82	-44.00	17.21	-17.18	0.10342	0.32159
U10	URBAN	90000	77.23	-44.00	16.50	-16.25	0.14369	0.37906
U11	URBAN	90000	77.62	-44.00	14.64	-18.60	0.03355	0.18316
G4	GRASS	20000	51.33	-44.00	-6.98	-21.00	0.00010	0.01018
G5	GRASS	11250	55.72	-44.00	-10.88	-23.47	0.00003	0.00524
G14	GRASS	11250	59.97	-44.00	-10.27	-28.95	0.00000	0.00222
RE6	RESIDENTIAL	90000	64.92	-44.00	19.89	-12.50	0.48435	0.69595
RE7	RESIDENTIAL	90000	68.14	-44.00	15.94	-12.46	0.19943	0.44658
RE23	RESIDENTIAL	120000	51.25	-44.00	16.95	-11.79	0.28262	0.53162
RE24	RESIDENTIAL	60000	62.64	-44.00	18.29	-16.27	0.15099	0.38857
H2	TERMINAL	4800	77.65	-49.69	19.86	0.24	16.56062	4.06947
H3	TERMINAL	4800	78.04	-44.00	18.97	-1.37	8.12680	2.85075
H4	BUILDING	2500	80.23	-44.00	17.57	-3.31	8.05174	2.83756
H5	BUILDING	4000	80.37	-44.00	16.96	-8.86	2.62884	1.62137

ID	LANDUSE	PTS.	INCIDENCE ANGLE	MIN(dB)	MAX(dB)	MEAN(dB)	VARIANCE	STANDARD DEVIATION
U5	URBAN	90000	73.44	-44.00	13.89	-15.71	0.05444	0.23333
U6	URBAN	90000	74.45	-44.00	17.13	-13.57	0.20459	0.45231
U7	URBAN	90000	75.24	-44.00	15.96	-14.82	0.15038	0.38778
U8	URBAN	90000	75.76	-44.00	16.92	-14.89	0.18129	0.42579
U9	URBAN	90000	76.82	-44.00	19.70	-14.46	0.40558	0.63685
U10	URBAN	90000	77.23	-44.00	20.61	-13.23	0.70501	0.83965
U11	URBAN	90000	77.62	-44.00	18.53	-15.93	0.14250	0.37749
G4	GRASS	20000	51.33	-44.00	-9.63	-22.41	0.00006	0.00750
G5	GRASS	11250	55.72	-44.00	-9.84	-21.91	0.00005	0.00703
G14	GRASS	11250	59.97	-44.00	-7.26	-27.07	0.00001	0.00366
RE6	RESIDENTIAL	90000	64.92	-44.00	18.45	-13.20	0.27421	0.52365
RE7	RESIDENTIAL	90000	68.14	-44.00	18.99	-12.68	0.23257	0.48225
RE23	RESIDENTIAL	120000	51.25	-44.00	22.28	-10.46	0.88255	0.93944
RE24	RESIDENTIAL	60000	62.64	-44.00	15.53	-16.16	0.05357	0.23146
H2	TERMINAL	4800	77.65	-43.22	20.07	1.39	26.45762	5.14370
H3	TERMINAL	4800	78.04	-44.00	20.22	0.34	23.69230	4.86747
H4	BUILDING	2500	80.23	-44.00	19.62	-0.86	23.39676	4.83702
H5	BUILDING	4000	80.37	-44.00	23.15	-2.68	51.26156	7.15972

Table D-9. Table of Polarimetric Discriminants for the Polarimetric Image Set at Linear Polarization

IMAGE: P3T626
TARGET: DENVER

LABEL	σ^oHH HH HH* (dB)	σ^oVH VH VH* (dB)	σ^oHV HV HV* (dB)	σ^oVV VV VV* (dB)	(VV VV*)/ (HH HH*) (dB)	SPAN (dB)	DEPOL (dB)	RHO HHVV (dB)	THETA HHVV (deg)
URBAN	-11.184	-26.900	-26.551	-19.682	-8.498	-10.402	13.101	-4.584	-52.942
URBAN	-9.745	-27.206	-27.357	-18.285	-8.540	-9.044	15.094	-3.607	-33.876
URBAN	-9.502	-27.545	-27.819	-17.540	-8.038	-8.755	15.801	-2.918	-25.597
URBAN	-7.113	-27.235	-27.569	-15.085	-7.972	-6.401	17.918	-5.125	-34.392
URBAN	-9.727	-27.574	-27.990	-14.253	-4.526	-8.315	16.352	-2.011	-20.509
URBAN	-9.066	-28.537	-29.016	-13.952	-4.887	-7.775	17.915	-2.282	-37.004
URBAN	-11.108	-25.649	-26.063	-15.169	-4.061	-9.466	13.171	-2.078	-30.958
GRASS	-15.517	-31.186	-31.123	-28.192	-12.675	-15.069	12.855	-4.134	119.281
GRASS	-17.106	-29.674	-29.910	-26.929	-9.823	-16.271	10.104	-3.893	49.429
GRASS	-22.766	-33.983	-34.345	-29.491	-6.725	-21.438	9.221	-3.902	-44.649
RESIDENTIA	-5.484	-25.873	-25.911	-21.187	-15.703	-5.293	17.513	-8.527	-93.253
RESIDENTIA	-7.259	-24.206	-24.054	-21.265	-14.006	-6.921	14.029	-6.606	-62.894
RESIDENTIA	-6.705	-24.403	-23.757	-18.372	-11.667	-6.272	14.638	-10.426	-96.154
RESIDENTIA	-11.833	-25.140	-25.213	-20.917	-9.084	-10.983	10.839	-7.496	-26.944
TERMINAL	6.482	-14.227	-14.286	-0.358	-6.840	7.360	18.545	-3.031	-54.423
TERMINAL	5.192	-17.575	-17.796	-1.828	-7.020	6.016	20.652	-2.288	-51.656
BUILDING	3.515	-24.424	-24.950	-3.296	-6.811	4.348	26.006	-1.316	-53.544
BUILDING	0.270	-25.068	-25.023	-5.290	-5.559	1.355	23.371	-1.072	-14.569

Table D-10. Table of Polarimetric Discriminants for the Polarimetric Image Set at Circular Polarization

IMAGE: p3t626
TARGET: DENVER

LABEL	RR RR* (dB)	LR LR* (dB)	RL RL* (dB)	LL LL* (dB)	(LL LL*)/(RR RR*) (dB)	SPAN (dB)	DEPOL (dB)	RHO RRLL (dB)	THETA RRLL (deg)
URBAN	-16.784	-16.088	-16.032	-16.855	-0.070	-10.402	-0.760	-0.952	4.929
URBAN	-15.815	-14.298	-14.238	-16.279	-0.464	-9.044	-1.773	-0.670	5.276
URBAN	-16.071	-13.723	-13.667	-16.373	-0.301	-8.755	-2.525	-0.639	4.747
URBAN	-13.037	-11.818	-11.761	-13.288	-0.252	-6.401	-1.371	-0.322	3.821
URBAN	-17.314	-12.637	-12.604	-17.112	0.202	-8.315	-4.592	-0.813	1.655
URBAN	-16.133	-12.401	-12.362	-15.691	0.442	-7.775	-3.525	-0.452	0.396
URBAN	-18.817	-13.972	-14.000	-16.971	1.846	-9.466	-3.810	-1.401	-11.184
GRASS	-20.419	-21.655	-21.629	-20.789	-0.370	-15.069	1.042	-0.753	0.389
GRASS	-22.481	-22.037	-22.056	-22.624	-0.143	-16.271	-0.506	-1.968	-3.406
GRASS	-27.908	-27.060	-26.992	-27.973	-0.065	-21.438	-0.915	-2.545	2.611
RESIDENTIA	-11.384	-11.399	-11.381	-11.096	0.288	-5.293	0.153	-0.284	0.580
RESIDENTIA	-13.199	-12.976	-12.886	-12.719	0.480	-6.921	-0.022	-0.662	4.042
RESIDENTIA	-11.602	-12.228	-12.659	-12.782	-1.180	-6.272	0.286	-0.440	-10.378
RESIDENTIA	-16.751	-16.939	-16.889	-17.469	-0.718	-10.983	-0.181	-1.522	4.481
TERMINAL	0.120	2.129	2.147	0.585	0.465	7.359	-1.779	-0.289	-3.878
TERMINAL	-1.616	1.014	0.997	-1.049	0.567	6.016	-2.329	-0.184	-3.660
BUILDING	-3.454	-0.398	-0.478	-3.355	0.099	4.348	-2.966	-0.035	-5.929
BUILDING	-9.503	-2.566	-2.590	-8.256	1.247	1.355	-6.257	-0.112	-8.014

Table D-11. Table of Polarimetric Discriminants for the Polarimetric Image Set at Elliptical Polarization for the Canted Oblate Spheroid Case

IMAGE: P3T626
TARGET: DENVER

LABEL	RRe RRe* (dB)	Re LRe* (dB)	RLe RLe* (dB)	LLe LLe* (dB)	(LLe LLe*)/ (RRe RRe*) (dB)	SPAN (dB)	DEPOL (dB)	RHO RReLLe (dB)	THETA RReLLe (deg)
URBAN	-16.396	-17.136	-17.127	-15.301	1.094	-10.402	1.317	-0.757	-0.888
URBAN	-14.819	-16.241	-16.223	-13.562	1.257	-9.044	2.087	-0.426	2.072
URBAN	-14.245	-16.373	-16.374	-13.057	1.188	-8.755	2.763	-0.336	0.353
URBAN	-12.445	-13.231	-13.228	-11.134	1.311	-6.401	1.490	-0.222	-1.230
URBAN	-13.027	-17.247	-17.283	-12.215	0.812	-8.315	4.663	-0.246	-3.536
URBAN	-12.926	-15.712	-15.767	-12.035	0.891	-7.775	3.282	-0.177	-3.725
URBAN	-14.064	-17.969	-18.112	-13.721	0.343	-9.466	4.151	-0.429	-13.121
GRASS	-21.673	-21.057	-21.019	-20.669	1.003	-15.069	-0.104	-0.865	2.357
GRASS	-21.421	-23.541	-23.537	-21.230	0.191	-16.271	2.214	-1.394	2.040
GRASS	-26.847	-28.734	-28.757	-26.119	0.728	-21.438	2.278	-1.658	2.209
RESIDENTIA	-11.719	-11.324	-11.373	-10.878	0.842	-5.293	0.070	-0.292	-1.514
RESIDENTIA	-13.275	-13.179	-13.273	-12.147	1.129	-6.921	0.551	-0.637	-2.994
RESIDENTIA	-11.780	-12.452	-12.237	-12.763	-0.983	-6.272	0.099	-0.424	9.531
RESIDENTIA	-16.862	-17.771	-17.732	-15.920	0.942	-10.983	1.386	-1.269	5.949
TERMINAL	1.644	0.521	0.486	2.401	0.756	7.359	1.535	-0.146	-6.976
TERMINAL	0.564	-1.057	-1.082	1.118	0.554	6.016	1.919	-0.078	-6.317
BUILDING	-0.702	-2.944	-2.932	-0.687	0.015	4.348	2.244	-0.017	-1.247
BUILDING	-2.499	-8.483	-8.549	-2.821	-0.322	1.355	5.859	-0.018	-4.600

Table D-12. Table of Polarimetric Discriminants for the Polarimetric Image Set at Elliptical Polarization for the Case of Propagating Thru a Rain Filled Medium

IMAGE: P3T626
TARGET: DENVER

LABEL	RRe RRe* (dB)	LRe LRe* (dB)	RLe RLe* (dB)	LLe LLe* (dB)	(LLe LLe*)/ (RRe RRe*) (dB)	SPAN (dB)	DEPOL (dB)	RHO RReLLe (dB)	THETA RReLLe (deg)
URBAN	-16.738	-17.333	-17.323	-14.821	1.917	-10.402	1.654	-0.796	0.979
URBAN	-15.153	-16.453	-16.427	-13.125	2.028	-9.044	2.418	-0.448	3.474
URBAN	-14.554	-16.595	-16.589	-12.651	1.902	-8.755	3.093	-0.353	1.561
URBAN	-12.813	-13.401	-13.392	-10.694	2.120	-6.401	1.771	-0.256	-0.111
URBAN	-13.155	-17.567	-17.596	-11.929	1.226	-8.315	5.083	-0.264	-2.293
URBAN	-13.045	-16.059	-16.111	-11.673	1.372	-7.775	3.780	-0.200	-1.590
URBAN	-14.178	-18.270	-18.421	-13.410	0.767	-9.466	4.568	-0.432	-11.132
GRASS	-22.414	-21.041	-21.003	-20.186	2.228	-15.069	-0.137	-0.911	0.807
GRASS	-21.907	-23.473	-23.466	-20.886	1.022	-16.271	2.103	-1.439	0.186
GRASS	-27.071	-28.946	-28.955	-25.733	1.337	-21.438	2.600	-1.647	4.251
RESIDENTIA	-12.395	-11.410	-11.459	-10.256	2.140	-5.293	0.239	-0.309	-1.050
RESIDENTIA	-13.874	-13.302	-13.394	-11.569	2.305	-6.921	0.777	-0.669	-2.059
RESIDENTIA	-12.281	-12.457	-12.271	-12.167	0.114	-6.272	0.139	-0.448	9.259
RESIDENTIA	-17.257	-17.881	-17.837	-15.499	1.758	-10.983	1.569	-1.314	6.664
TERMINAL	1.390	0.278	0.243	2.885	1.495	7.359	1.941	-0.161	-4.565
TERMINAL	0.336	-1.344	-1.371	1.621	1.285	6.016	2.383	-0.100	-3.717
BUILDING	-0.858	-3.310	-3.306	-0.147	0.711	4.348	2.820	-0.029	1.753
BUILDING	-2.675	-8.784	-8.861	-2.489	0.187	1.355	6.242	-0.031	-3.777

Denver X-VH P3T642
Pass 37 November 16, 1988
Slant Range Image

Line Length = 2048 Margin = 0 Line Reps = 1 Pixel Width = 1 Text Size = 2 White = 255 b=7 g=8 c=8 7774

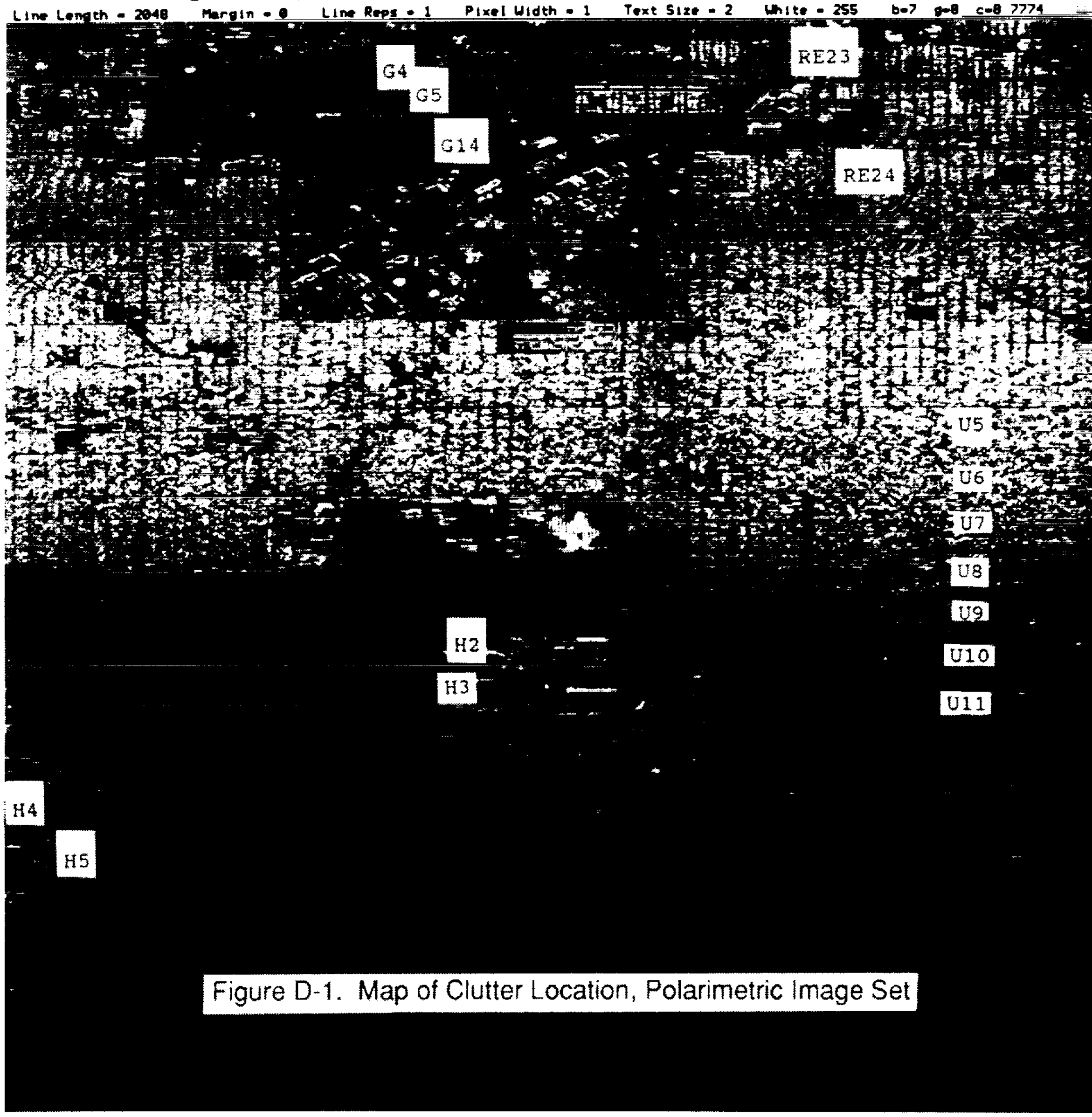

Figure D-1. Map of Clutter Location, Polarimetric Image Set

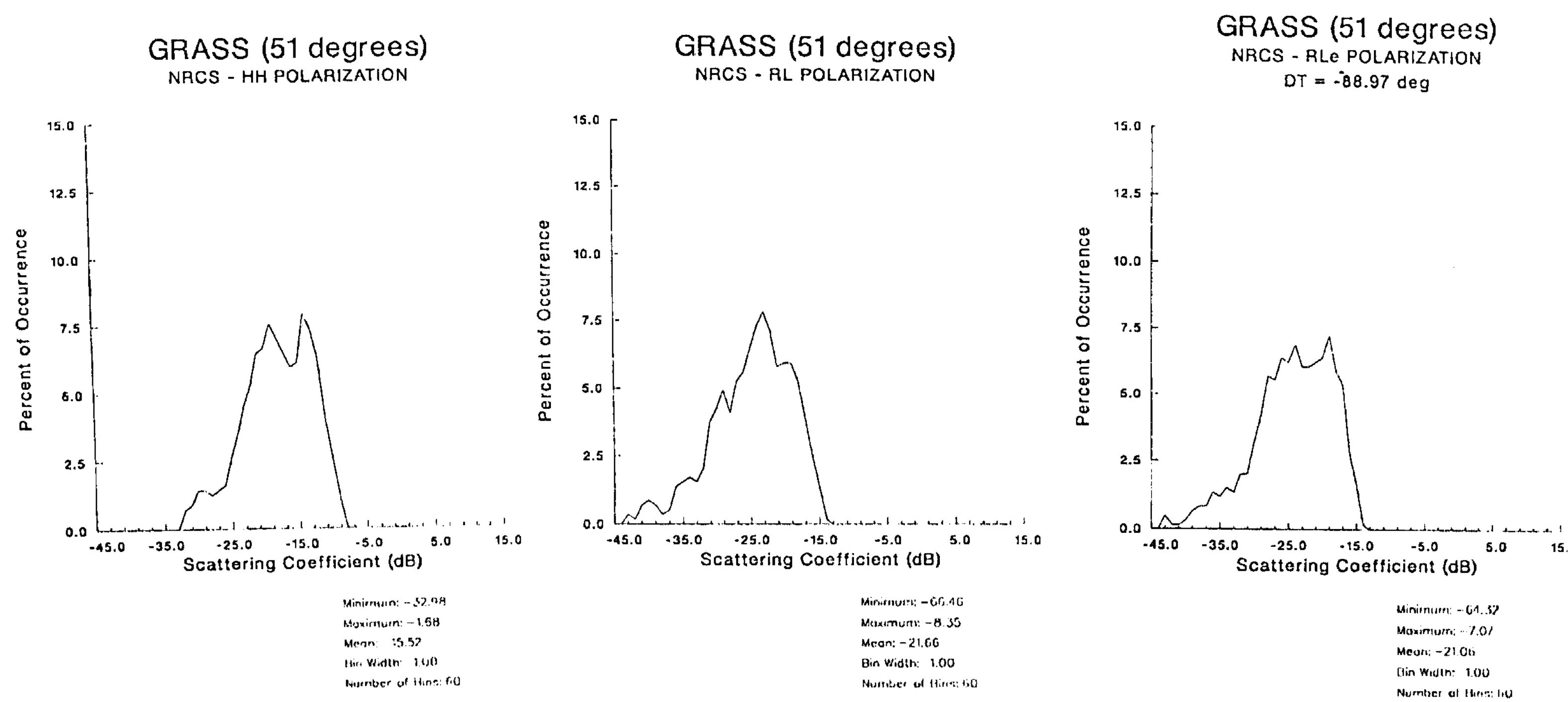

Figure D-2. Histogram at Linear-HH, Circular-RL, and Elliptical-RL for a Grass Area at an Incidence Angle of 51 Degrees.

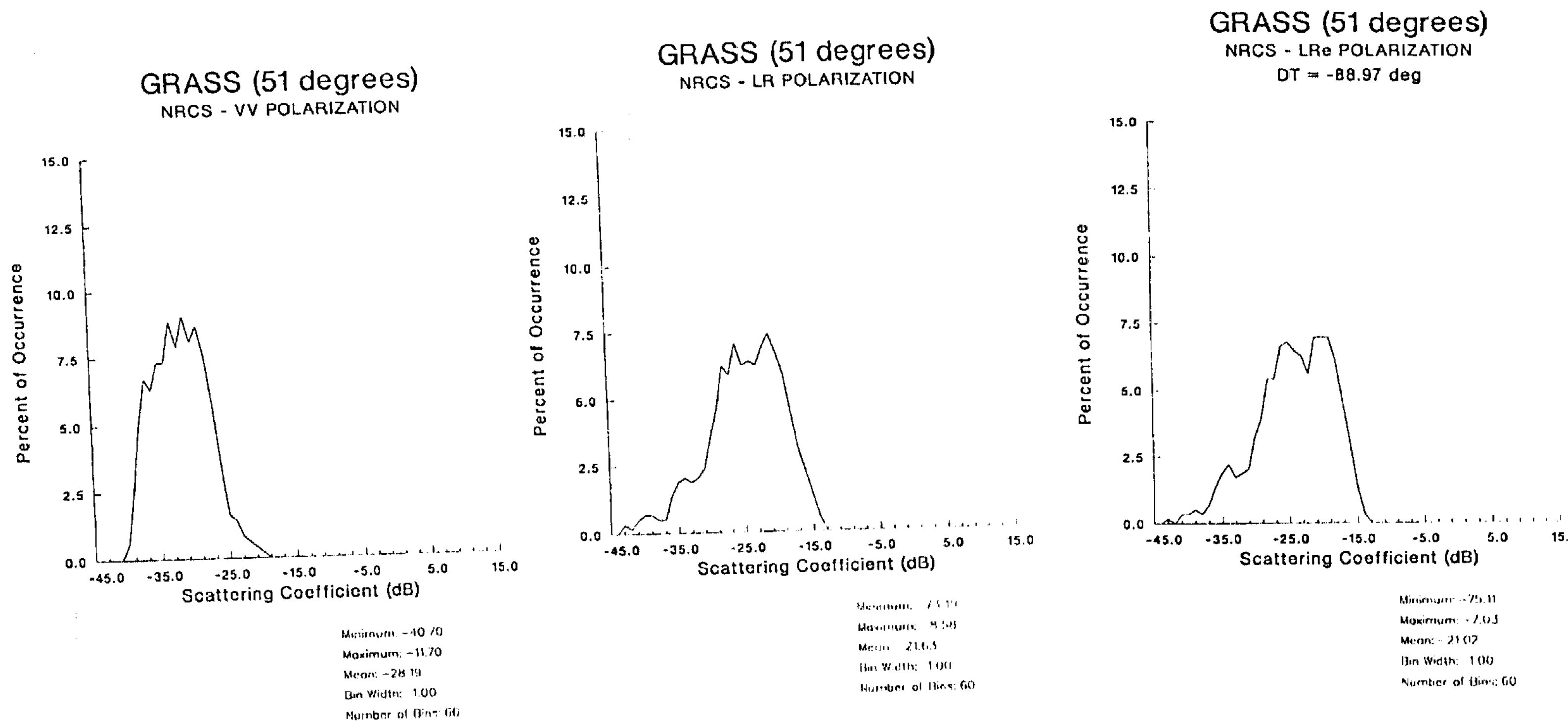

Figure D-3. Histogram at Linear-VV, Circular-LR, and Elliptical-LRe for Grass Area at an Incidence Angle of 51 Degrees.

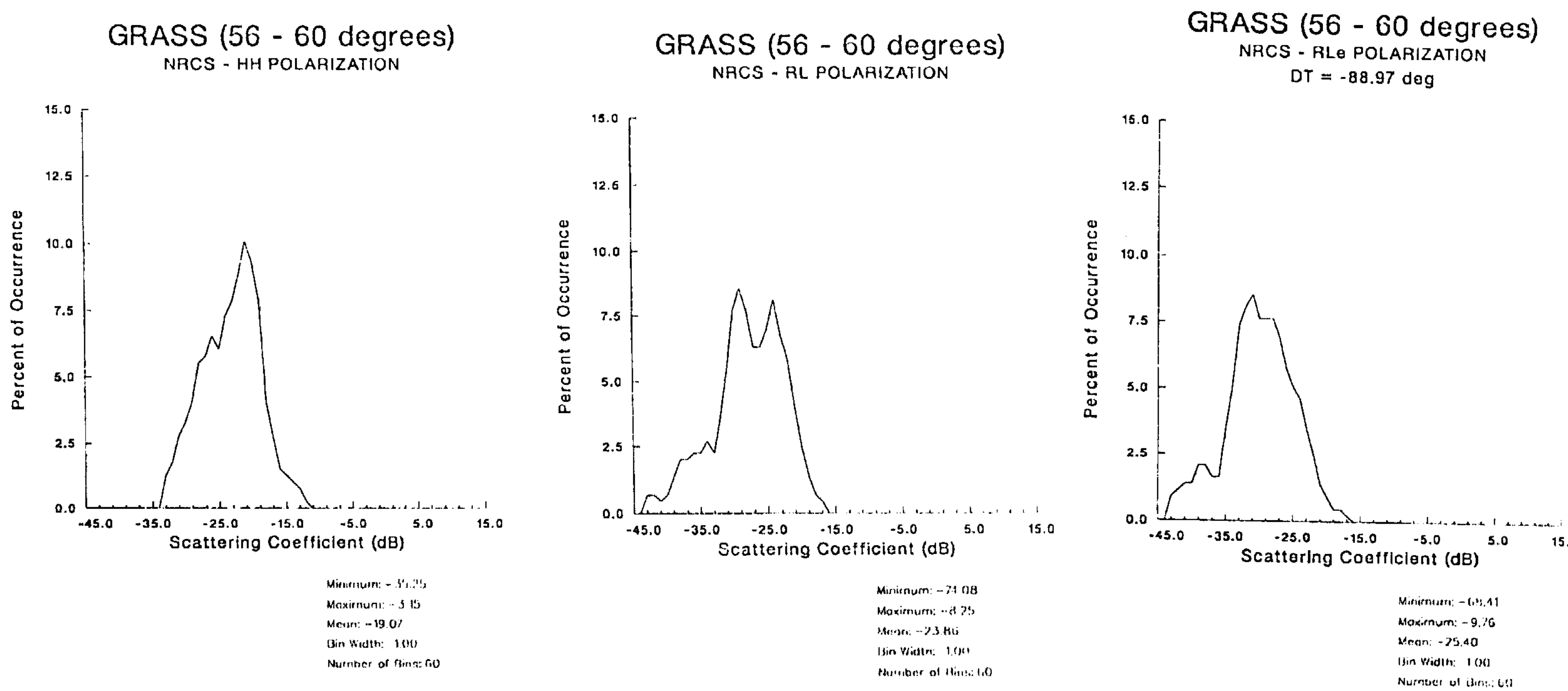

Figure D-4. Histogram at Linear-HH, Circular-RL, and Elliptical-RL for a Grass Area at an Incidence Angle of 56-60 Degrees.

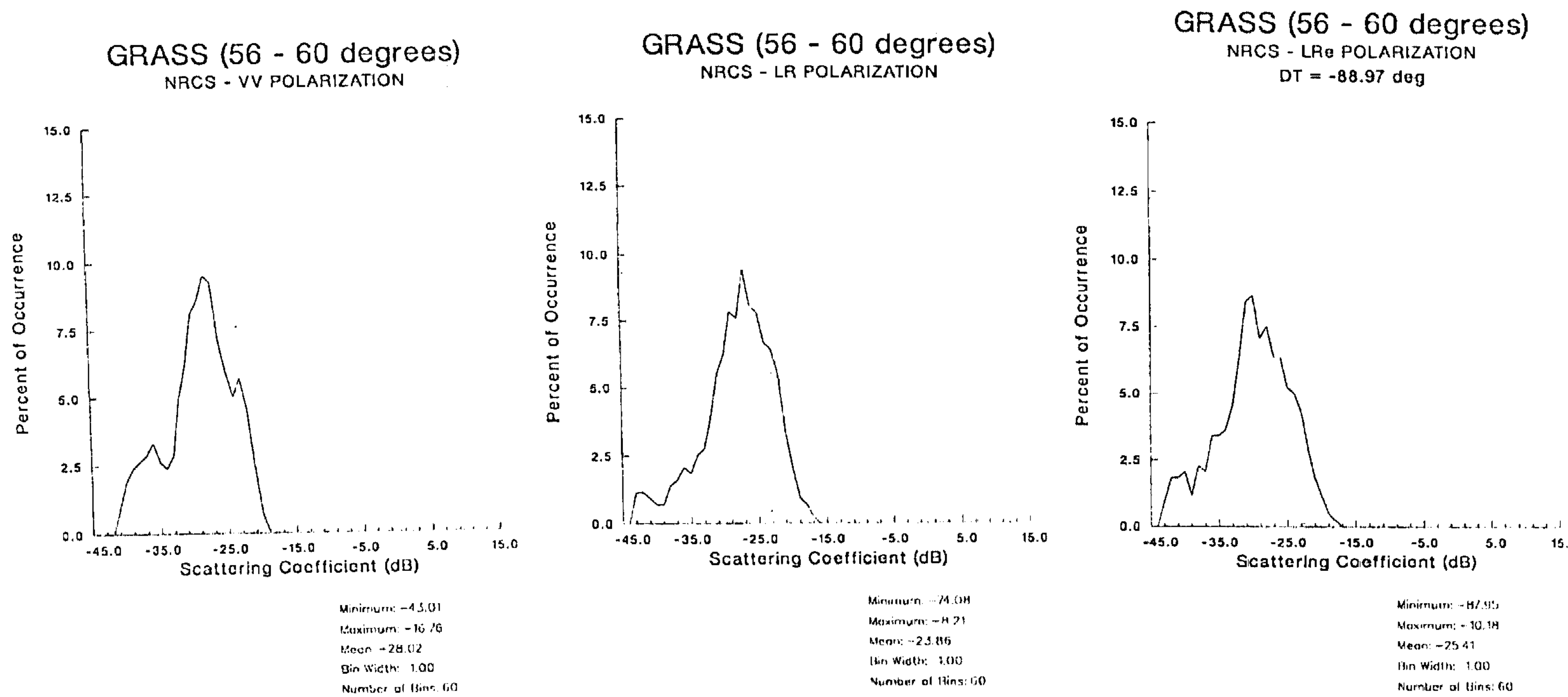

Figure D-5. Histogram at Linear-VV, Circular-LR, and Elliptical-LR for Grass Area at an Incidence Angle of 56-60 Degrees.

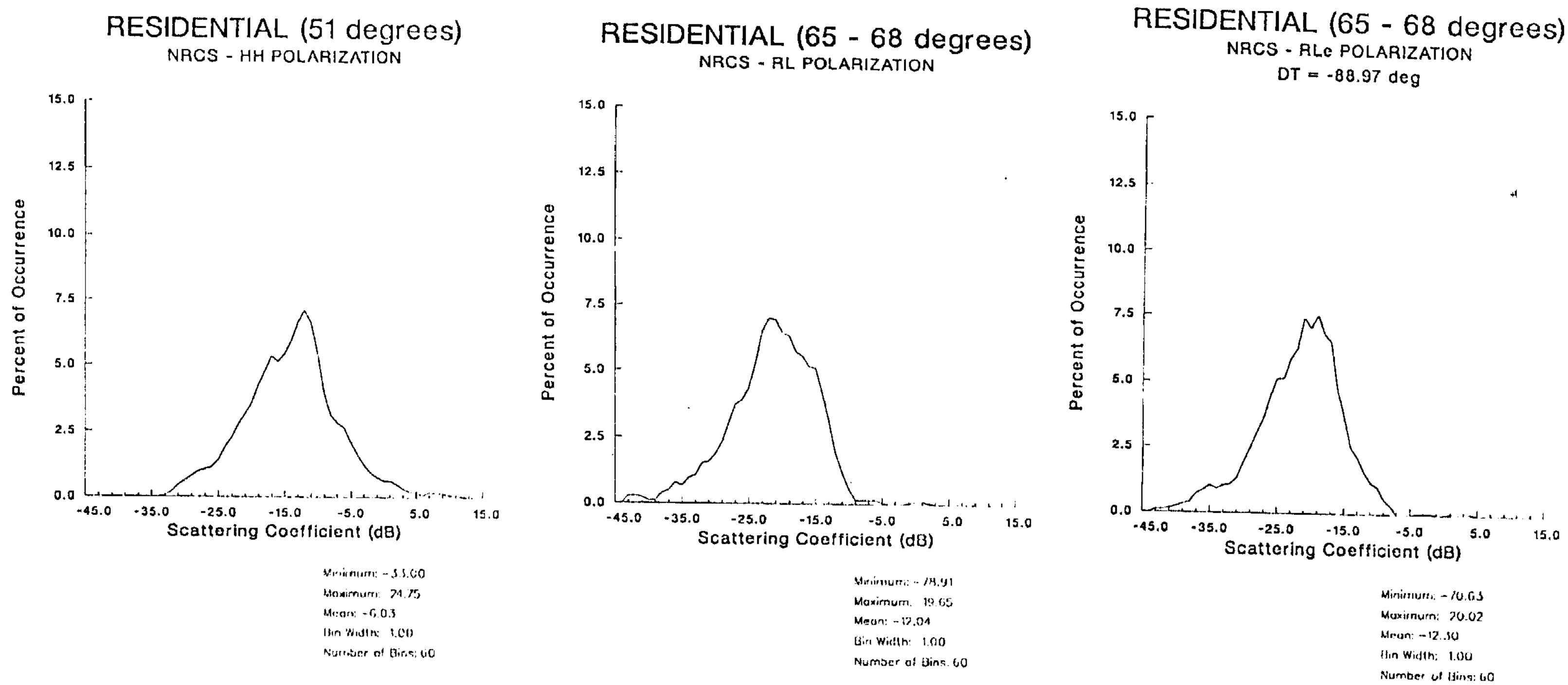

Figure D-6. Histogram at Linear-HH, Circular-RL, and Elliptical-RL for a Residential Area at an Incidence Angle of 51 Degrees.

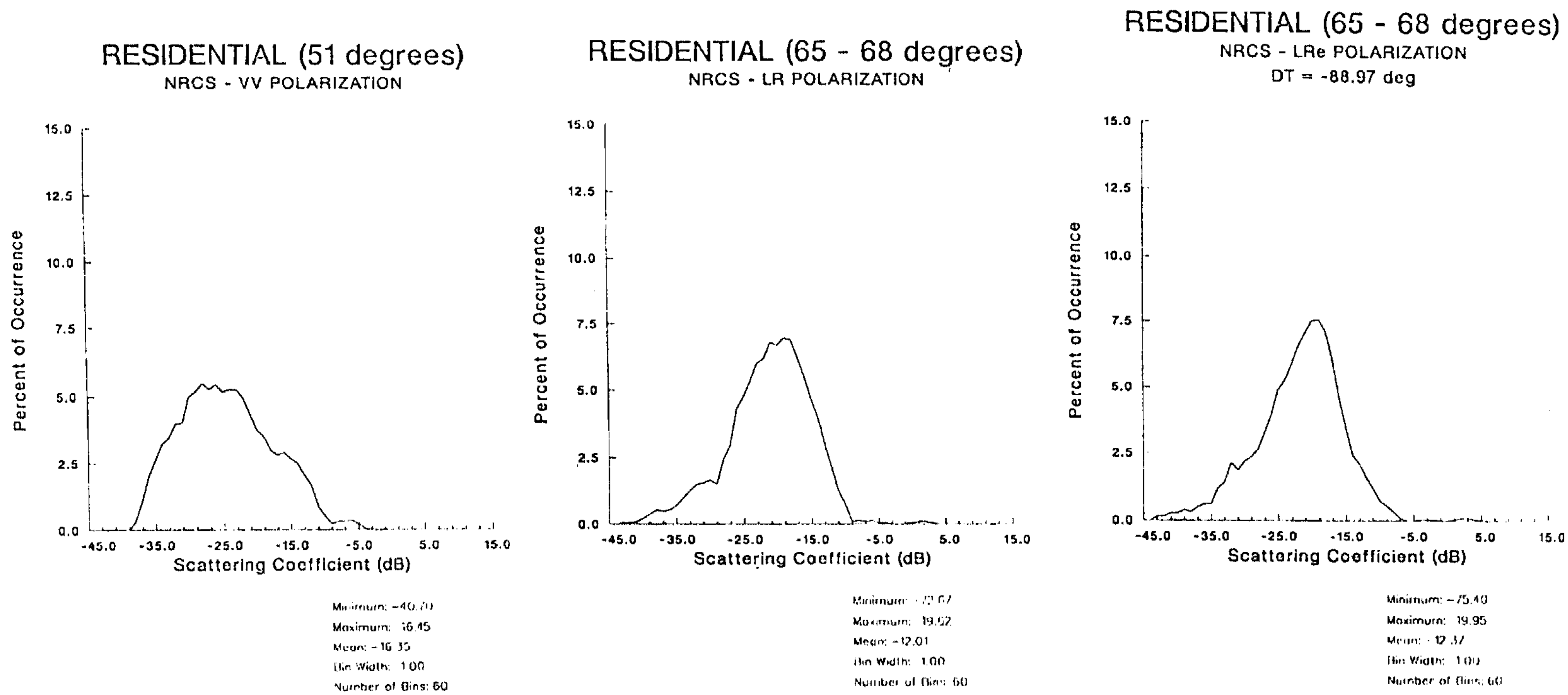

Figure D-7. Histogram at Linear-VV, Circular-LR, and Elliptical-LR for a Residential Area at an Incidence Angle of 51 Degrees.

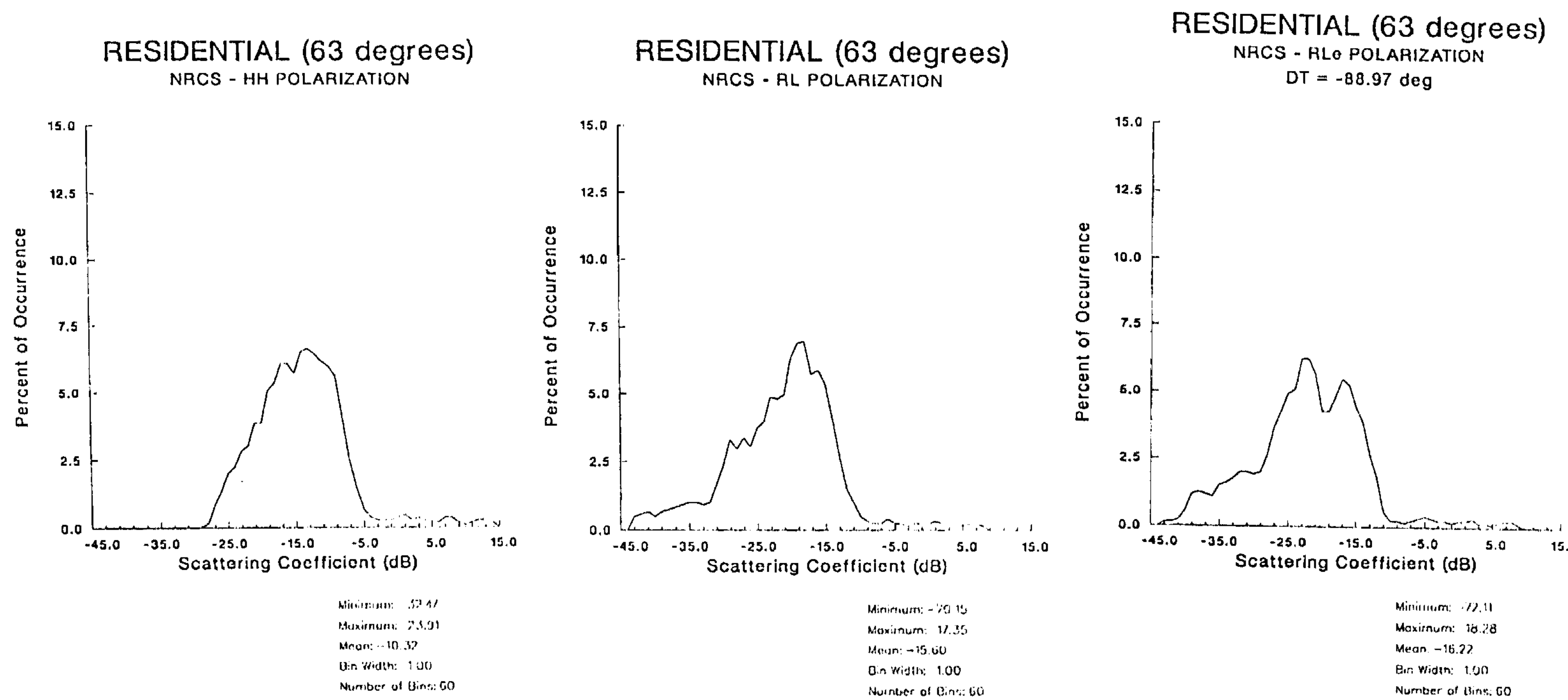

Figure D-8. Histogram at Linear-HH, Circular-RL, and Elliptical-RL for a Residential Area at an Incidence Angle of 63 Degrees.

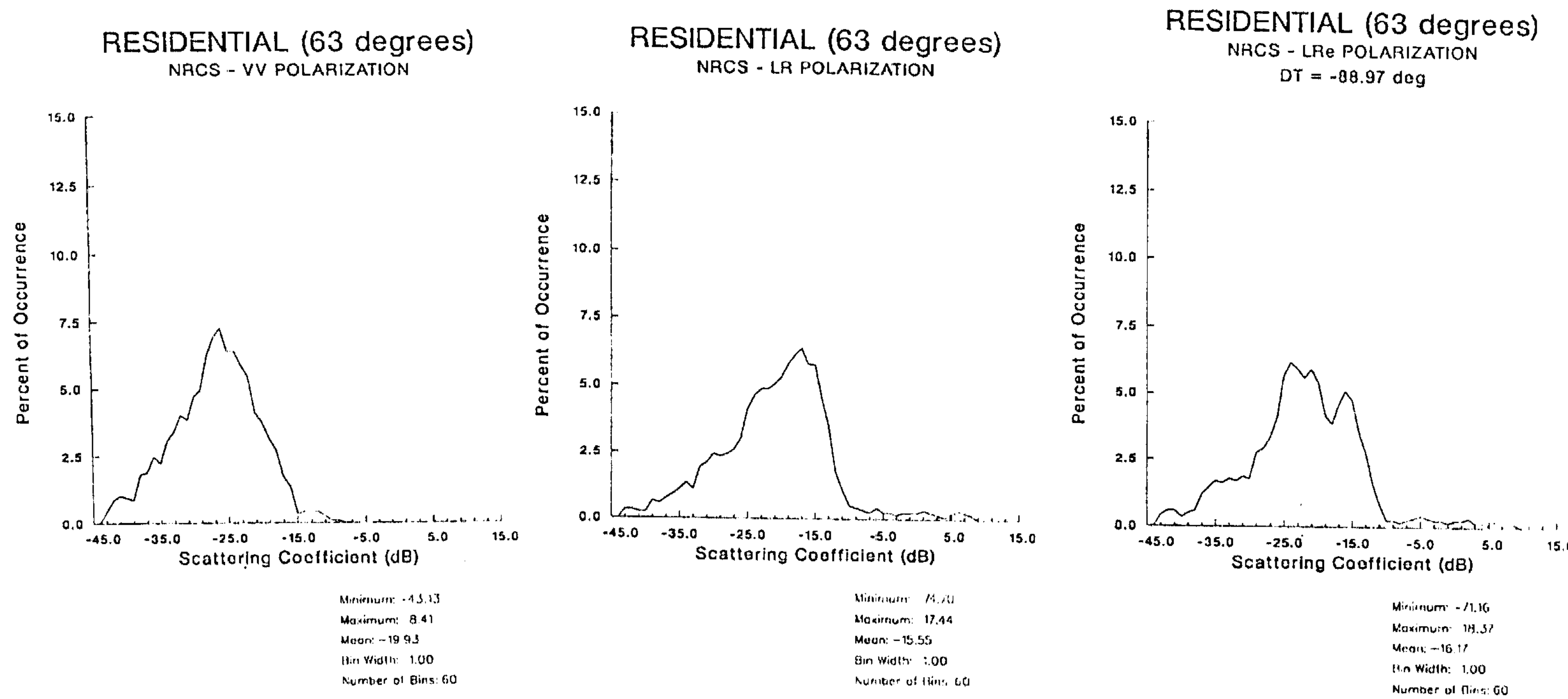

Figure D-9. Histogram at Linear-VV, Circular-LR, and Elliptical-LR for a Residential Area at an Incidence Angle of 63 Degrees.

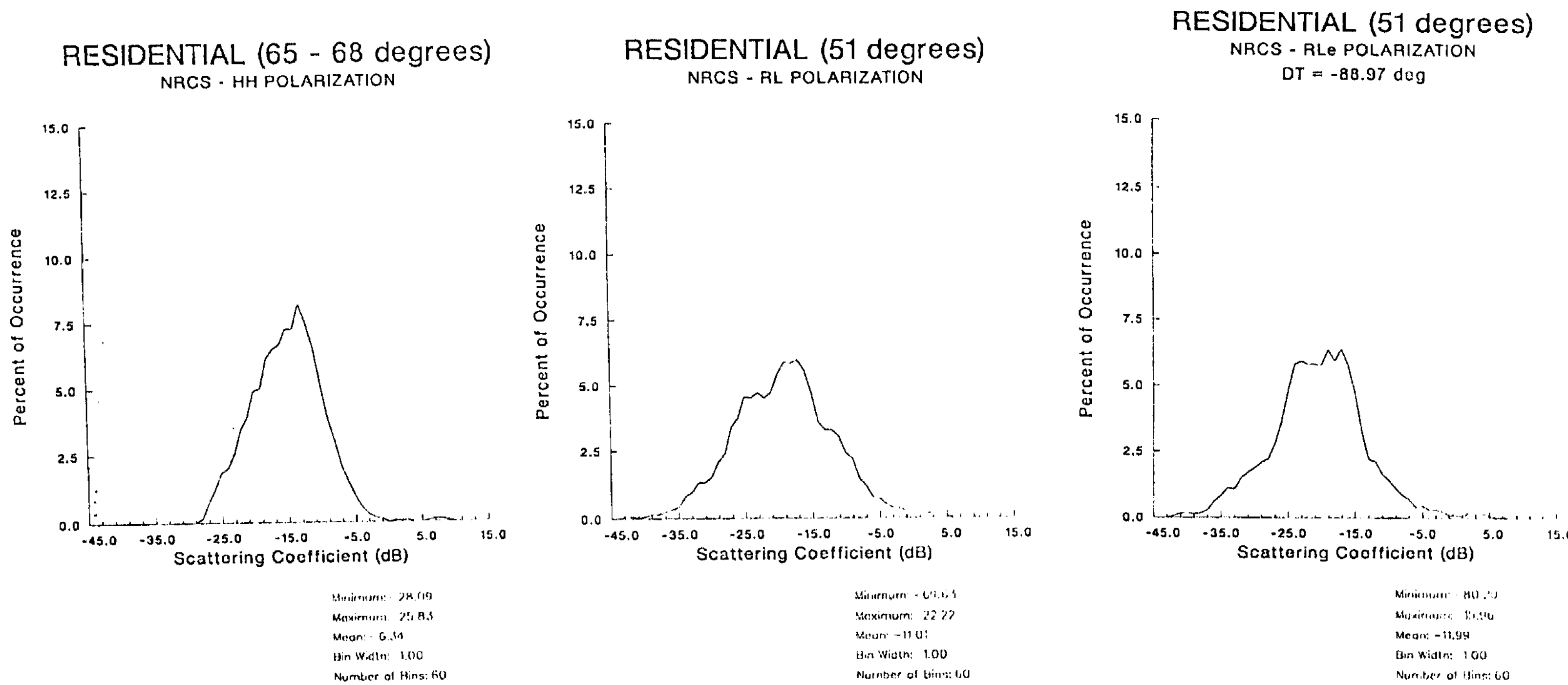

Figure D-10. Histogram at Linear-HH, Circular-RL, and Elliptical-RL for a Residential Area at an Incidence Angle of 65-68 Degrees.

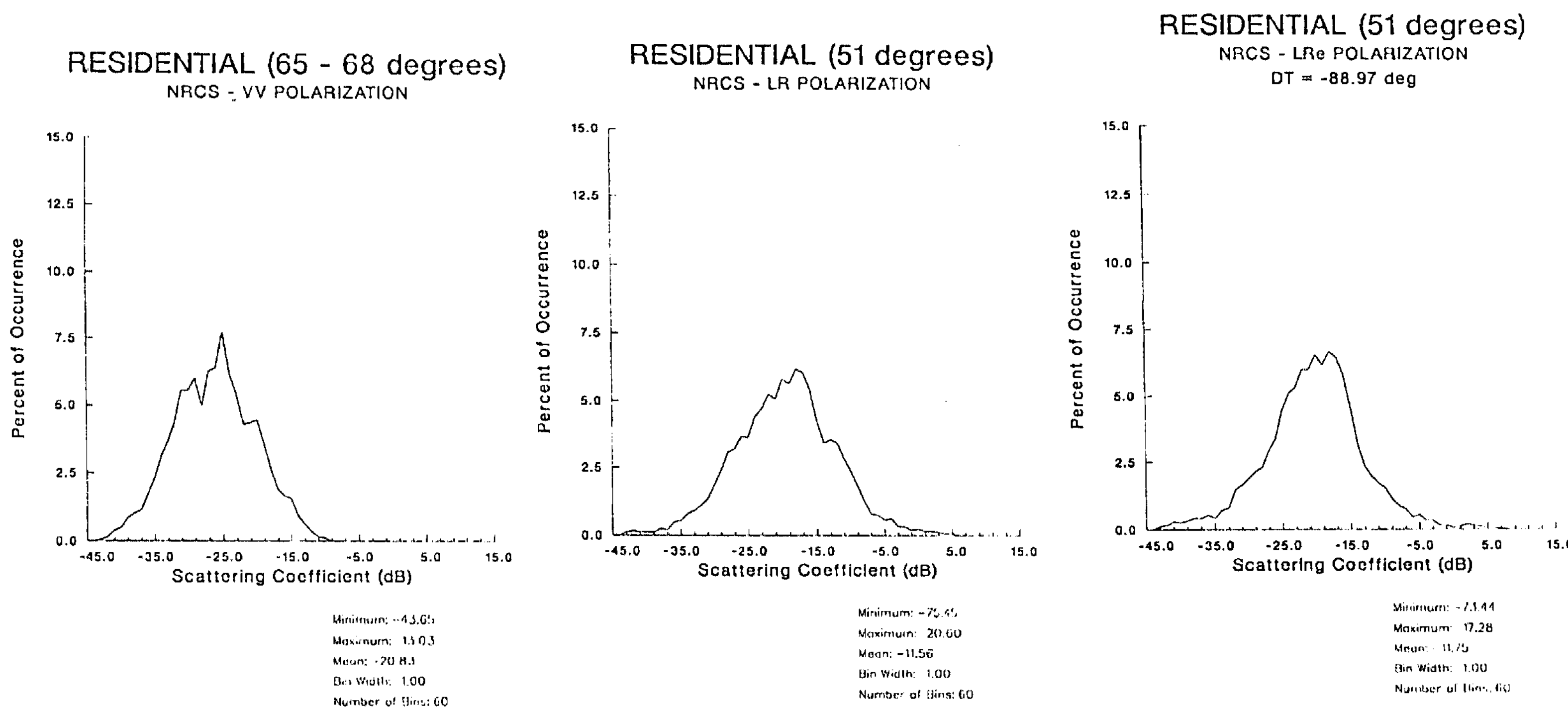

Figure D-11. Histogram at Linear-VV, Circular-LR, and Elliptical-LR for a Residential Area at an Incidence Angle of 65-68 Degrees.

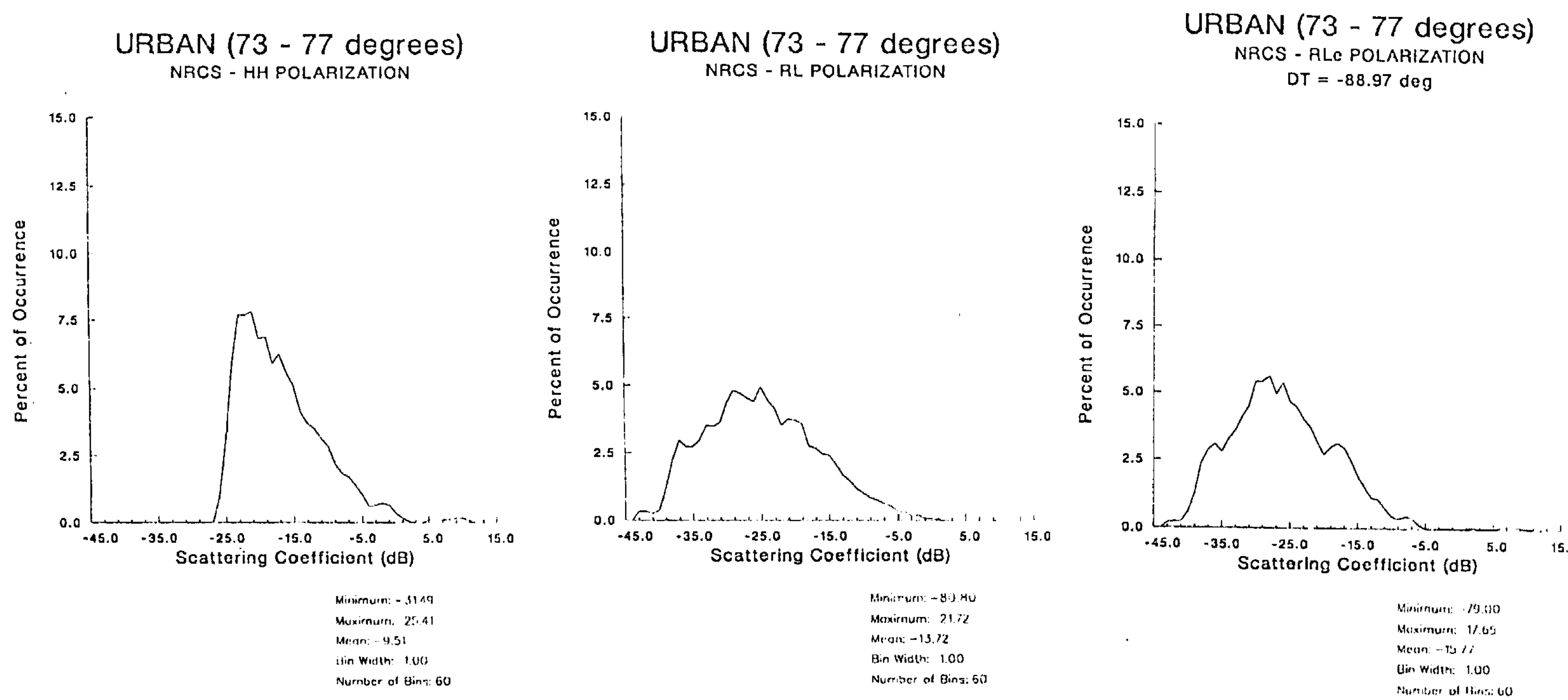

Figure D-12. Histogram at Linear-HH, Circular-RL, and Elliptical-RL for an Urban Area at an Incidence Angle of 73-77 Degrees.

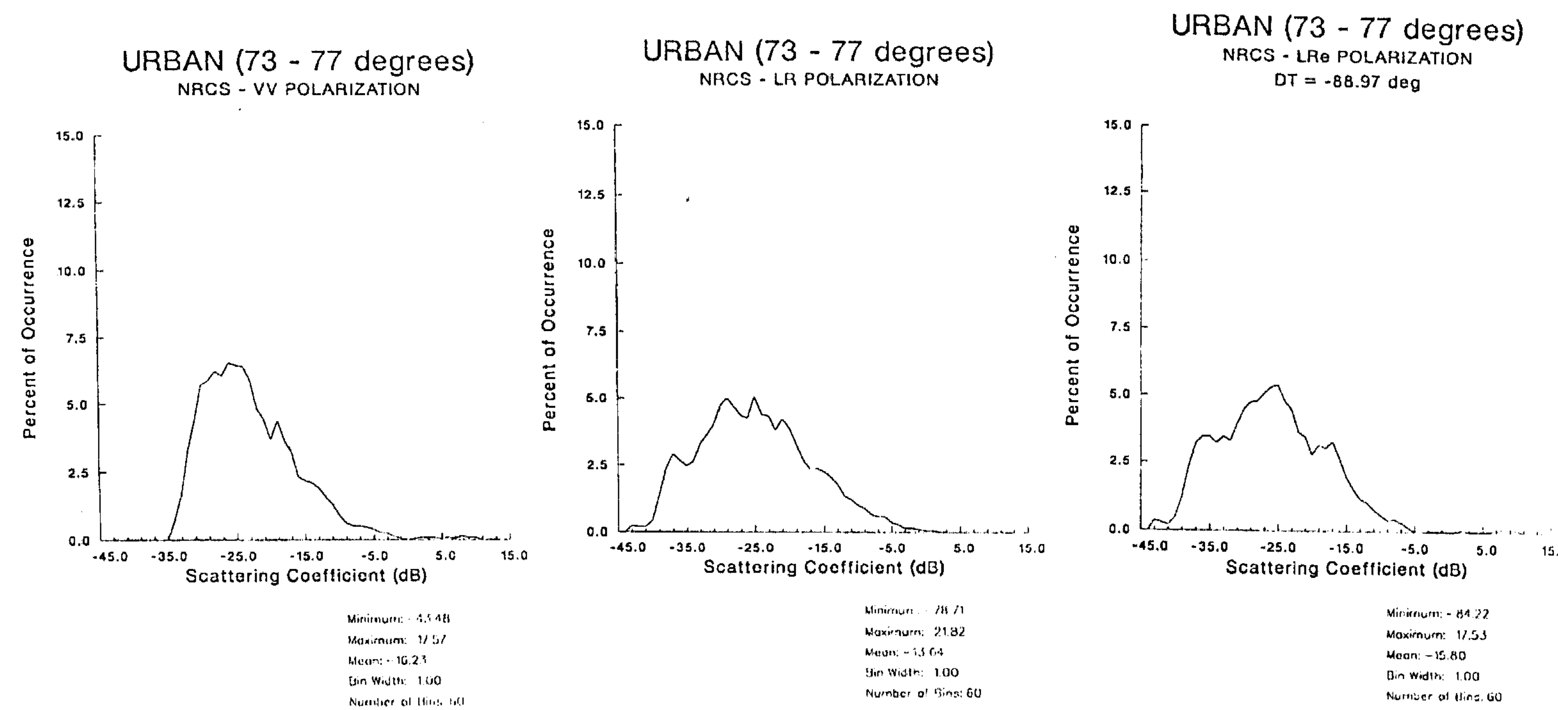

Figure D-13. Histogram at Linear-VV, Circular-LR, and Elliptical-LR for an Urban Area at an Incidence Angle of 73-77 Degrees.

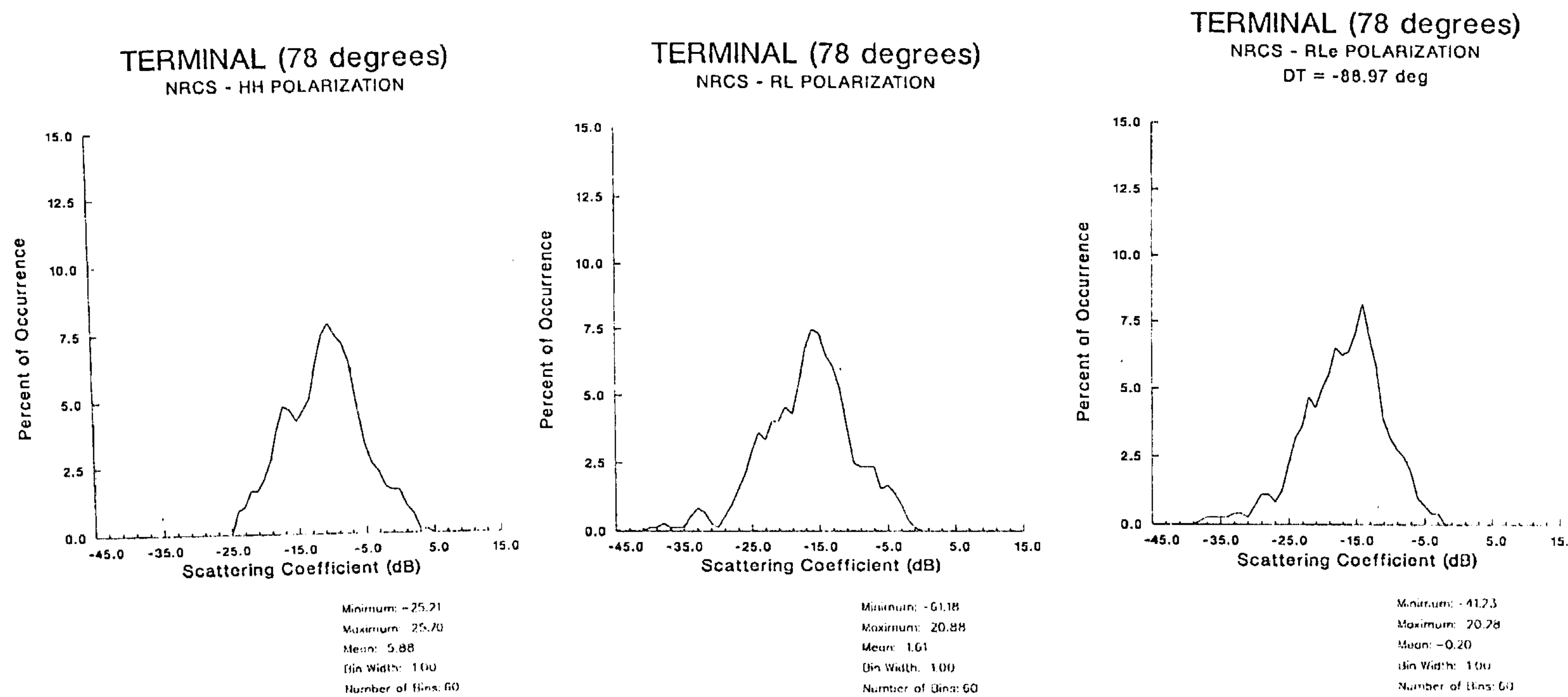

Figure D-14. Histogram at Linear-HH, Circular-RL, and Elliptical-RL for a Terminal Area at an Incidence Angle of 78 Degrees.

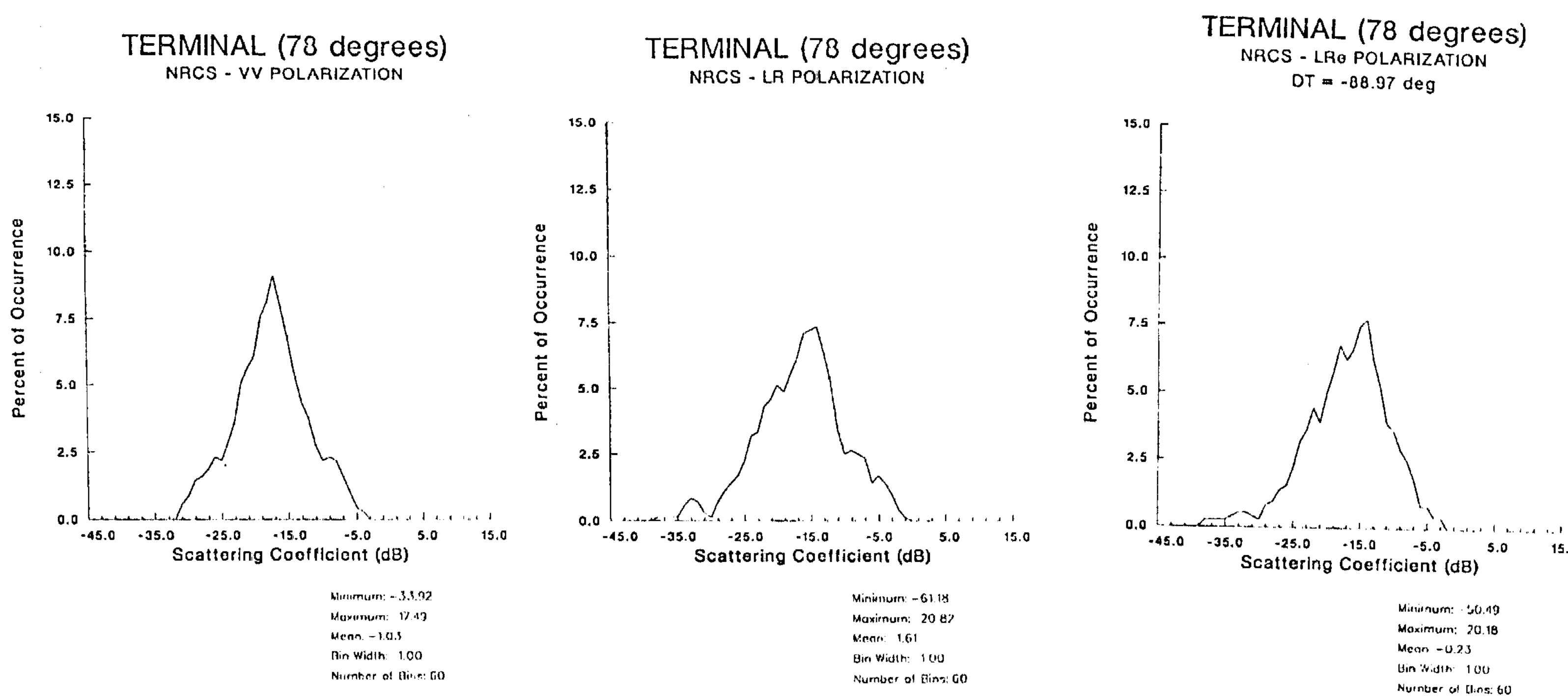

Figure D-15. Histogram at Linear-VV, Circular-LR, and Elliptical-LR for a Terminal Area at an Incidence Angle of 78 Degrees.

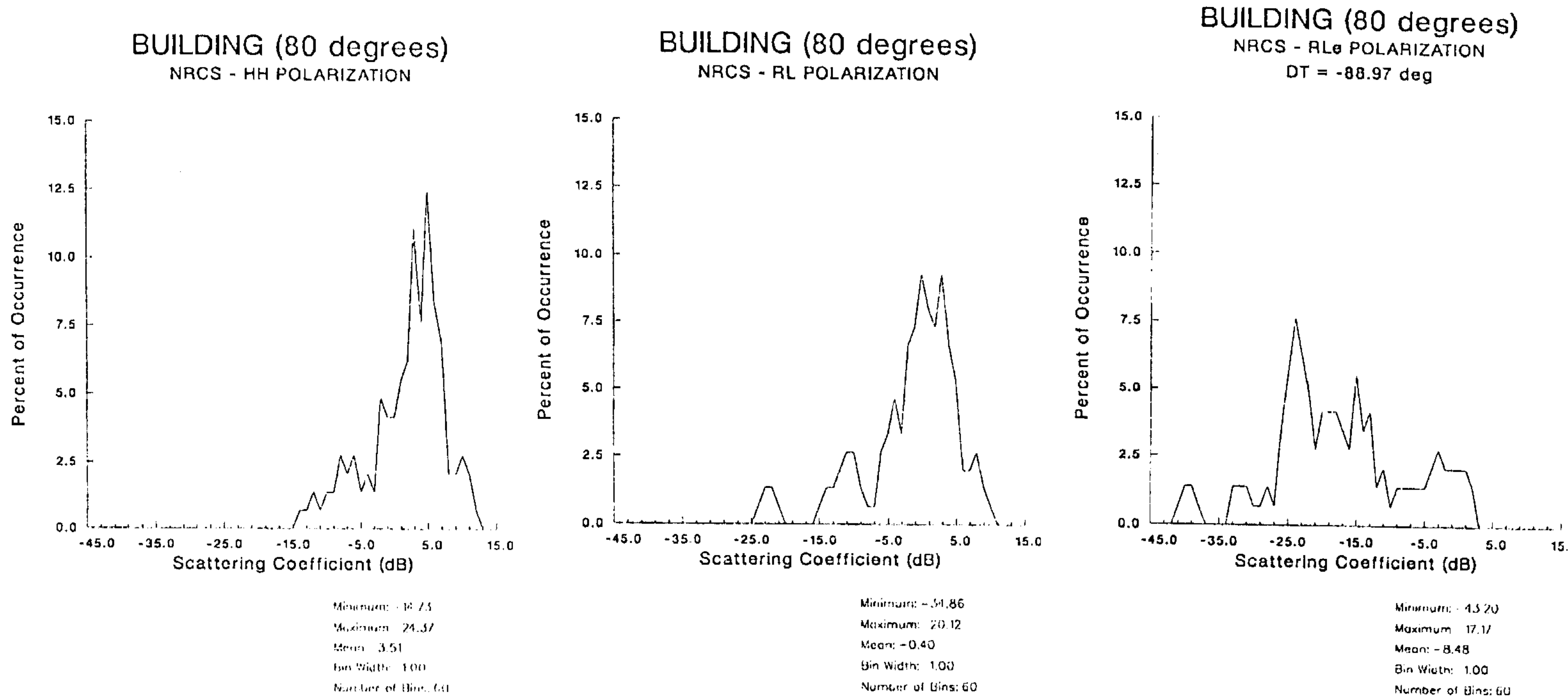

Figure D-16. Histogram at Linear-HH, Circular-RL, and Elliptical-RL for a Building Area at an Incidence Angle of 80 Degrees.

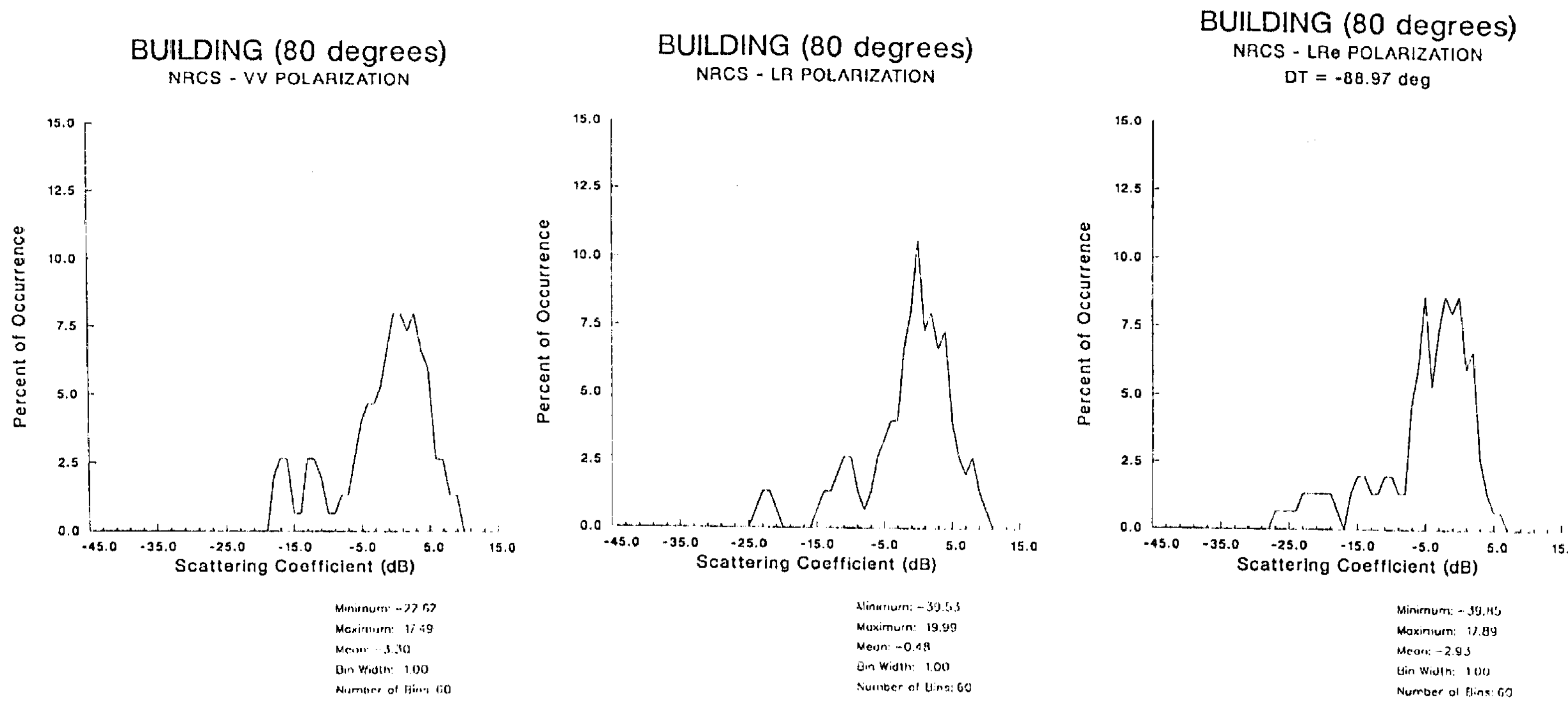

Figure D-17. Histogram at Linear-VV, Circular-LR, and Elliptical-LR for a Building Area at an Incidence Angle of 80 Degrees.

C-3

ORIGINAL PAGE IS
OF POOR QUALITY

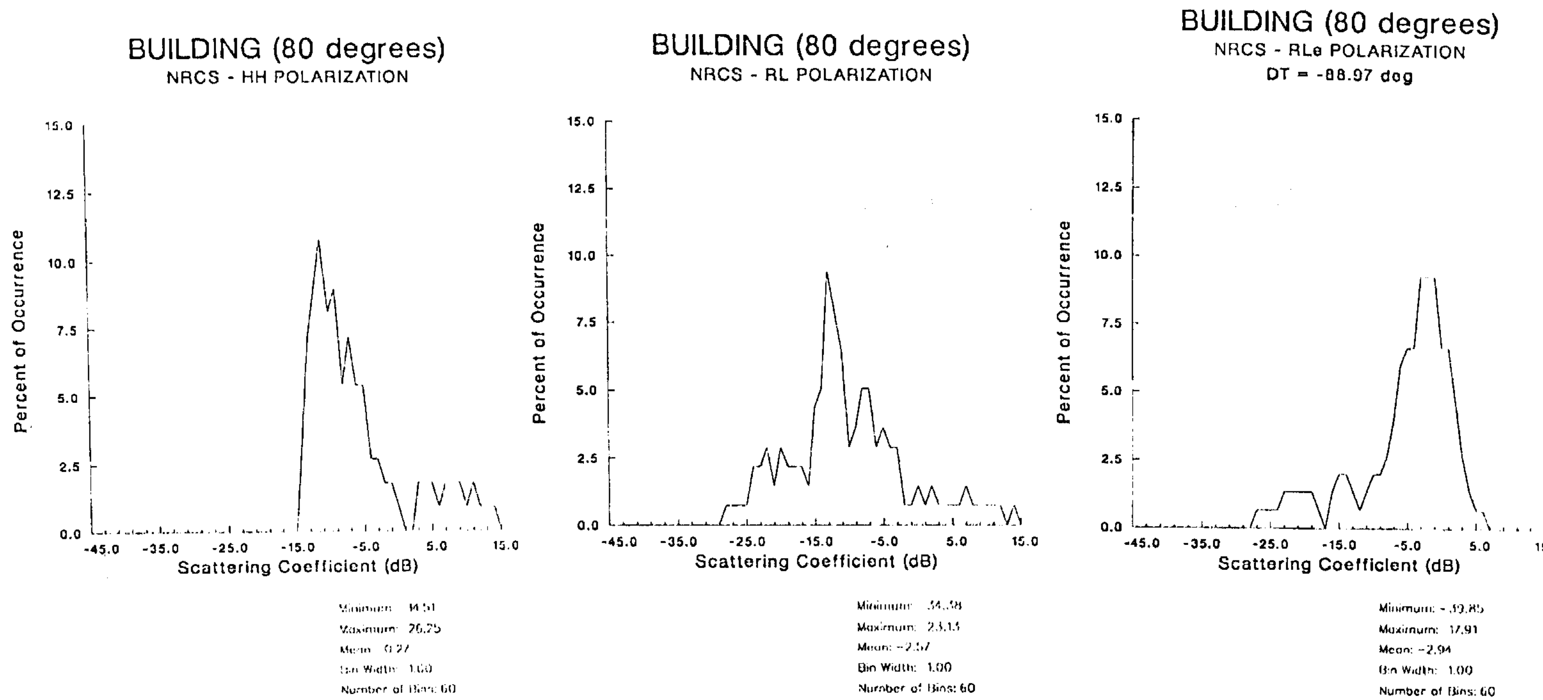

Figure D-18. Histogram at Linear-HH, Circular-RL, and Elliptical-RL for a Building Area at an Incidence Angle of 80 Degrees.

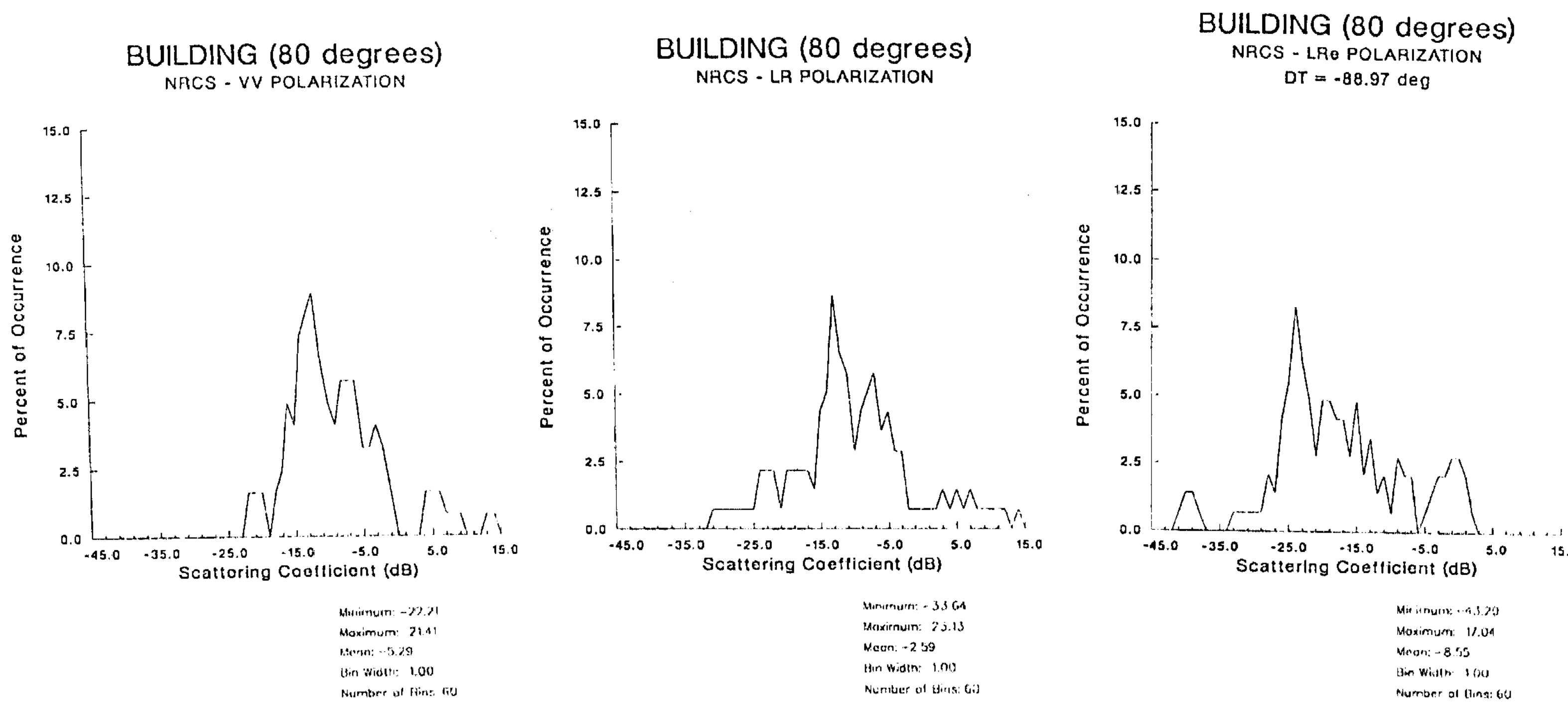

Figure D-19. Histogram at Linear-VV, Circular-LR, and Elliptical-LR for a Building Area at an Incidence Angle of 80 Degrees.

ORIGINAL PAGE IS
OF POOR QUALITY

APPENDIX E

Examination of the Calibration of the Polarimetric Image Set

APPENDIX E

Calibration Targets

Trihedral calibration targets were utilized in the calibration of the VV and HH channels. These targets will be used to demonstrate balance between the VV and HH channels. The scattering matrices for these targets after calibration are provided here.

$$[S]_{TRI1} = \begin{bmatrix} 1.000/+12.2^\circ & 0.055/-89.1^\circ \\ 0.054/-89.1^\circ & 0.956/+14.7^\circ \end{bmatrix}$$

$$[S]_{TRI2} = \begin{bmatrix} 1.000/-157.3^\circ & 0.053/+95.7 \\ 0.057/+95.7^\circ & 1.010/-158.4^\circ \end{bmatrix}$$

$$[S]_{TRI3} = \begin{bmatrix} 1.000/-32.4^\circ & 0.045/-120.4^\circ \\ 0.020/-117.5^\circ & 1.010/-7.60^\circ \end{bmatrix}$$

$$[S]_{TRIavg} = \begin{bmatrix} 1.000/0.000^\circ & 0.051/-85.7^\circ \\ 0.044/-85.8^\circ & 0.994/+24.3^\circ \end{bmatrix}$$

$$[|P|]_{TRIavg} = \begin{bmatrix} 0.0\ \mathrm{dB} & -25.85\ \mathrm{dB} \\ -27.13\ \mathrm{dB} & -0.05\ \mathrm{dB} \end{bmatrix}$$

These results show that the VV and HH channels were well balanced, the standard deviation is 0.003 dB. The dihedral data also showed similar results.

NASA
National Aeronautics and Space Administration

Report Documentation Page

1. Report No. NASA CR-4398 DOT/FAA/RD-91/14	2. Government Accession No.	3. Recipient's Catalog No.
4. Title and Subtitle Synthetic Aperture Radar Imagery of Airports and Surrounding Areas - Study of Clutter at Grazing Angles and Their Polarimetric Properties		5. Report Date October 1991
		6. Performing Organization Code
7. Author(s) Robert G. Onstott, Denise J. Gineris, and James T. Clinthorne		8. Performing Organization Report No.
		10. Work Unit No. 505-64-12-51
9. Performing Organization Name and Address Environmental Research Institute of Michigan 1975 Green Road Ann Arbor, MI 48105		11. Contract or Grant No. NAS1-18465
12. Sponsoring Agency Name and Address National Aeronautics and Space Administration Langley Research Center Hampton, VA 23665-5225		13. Type of Report and Period Covered Contractor Report 31 Aug. 87 - 30 Dec. 90
		14. Sponsoring Agency Code

15. Supplementary Notes
Langley Technical Monitor: E.M. Bracalente
Phase III Extension Final Report

16. Abstract
This report is the fourth in a series of four which address the statistical description of ground clutter at an airport and in the surrounding area. These data are being utilized in a program to detect microbursts. Synthetic aperture radar (SAR) data were collected at the Denver Stapleton Airport. Mountain terrain data were examined to determine if they may potentially contribute to range ambiguity problems and degrade microburst detection. Results suggest that mountain clutter may not present a special problem source. The examination of clutter at small grazing angles was continued by examining data collected at especially low altitudes. Cultural objects such as buildings produce strong sources of backscatter at angles of about 85°, with responses of 30 dB to 60 dB above the background. Otherwise there are a few sources which produce significant scatter. The polarization properties of hydrospheres and clutter were examined with the intent of determining the optimum polarization. This polarization was determined to be dependent upon the ratio of VV and HH polarizations of both rain and ground clutter.

17. Key Words (Suggested by Author(s)) Clutter, Backscatter, SAR, Microbursts, Grazing, Polarimetrics	18. Distribution Statement Unclassified - Unlimited Subject Category 03

19. Security Classif. (of this report)	20. Security Classif. (of this page)	21. No. of pages	22. Price
Unclassified	Unclassified	216	A10

NASA FORM 1626 OCT 86

For sale by the National Technical Information Service, Springfield, Virginia 22161-2171

NASA-Langley, 1991